ab initio Quantum Chemical Analysis of Small Molecular Systems: Pushing and Expanding the Limits of Computational Capability

by

Mitchell Evan Lahm

(Under the Direction of Henry F. Schaefer III)

ABSTRACT

The Bismuth tetramer cluster (Bi_4) is studied using high level *ab initio* techniques. Dissociation and atomization energies are determined and visual analysis is performed on natural bonding orbitals (NBO). Substituted variants of *ortho*-benzyne are studied using density functional theory (DFT). The impact of differing sustituents on the triple-bond is elucidated via the analysis of several properties, as well as NBO analysis. A prototype of hydrocarbon combustion in *i*-propyl + O_2 is analyzed using high level *ab initio* techniques. Relevant stationary points are studied and categorized into reaction pathways and rich potential energy surface dynamics are elucidated. A novel approach for computing harmonic vibrational frequencies is formulated, the Concordant Mode Approach (CMA). Computing diagonal force constants under this approach yields a powerful approximation that scales linearly with respect to single point energy displacements as opposed to the quadratic scaling of standard finite difference computations of harmonic vibrational frequencies.

Index Words: Bismuth, Focal Point Analysis, Quantum Chemistry, Electron Correlation, Benzyne, Harmonic Vibrational Analysis, Propane, Combustion, Harmonic Vibrational Frequencies, Normal Mode Basis, Approximation

ab initio Quantum Chemical Analysis of Small Molecular Systems: Pushing and Expanding the Limits of Computational Capability

by

Mitchell Evan Lahm

B.S. Bethel University, 2017

A Dissertation Submitted to the Graduate Faculty
of the University of Georgia in Partial Fulfillment
of the Requirements for the Degree

Doctor of Philosophy

Athens, Georgia

2021

ab initio Quantum Chemical Analysis of Small Molecular Systems: Pushing and Expanding the Limits of Computational Capability

by

Mitchell Evan Lahm

Major Professors:	Henry F Schaefer III
Committee:	Steven E Wheeler
	Gary E Douberly

Electronic version approved:

Ron Walcott

Vice Provost for Graduate Education and Dean of the Graduate School

The University of Georgia

December 2021

ACKNOWLEDGEMENTS

I would like to acknowledge my wife, the love of my life, Amber Cathey Lahm, as she has been a rock in supporting me in my PhD. I wouldn't be here without my parents who cultivated my love of science in profound manners as well as my siblings for never letting me settle for less. Along my scientific journey, Dr. Bollinger, Dr. Rollin King, Dr. Wesley Allen and of course Dr. Schaefer have been vital in developing me into the scientist I am today. A special thank you to all my friends who have supported me, there are too many of you to name here! Most importantly I would like to aknowledge the part God has played in this all. The death and resurrection of His son Jesus gives me hope for the resurrection of my own sinful, imperfect form. Research is very difficult, and the hope I have in Christ has been a light in even the darkest of circumstances. He has been my shepard through this whole journey.[1]

TABLE OF CONTENTS

CHAPTER 1

INTRODUCTION

1.1 The Schrödinger Equation

In order to describe the non-relativistic, quantum mechanical, electronic structure of an N-atom molecular system ($N \geq 1$), the Schrödinger equation must be employed.[0] The Schrödinger equation is defined as follows,

$$\mathrm{H}\psi = \mathrm{E}\psi. \tag{1.1}$$

Where ψ is a wavefunction describing the spatial location and spin of the electrons, H is the Hamiltonian that operates upon the wavefunction, and E is the energy of the system, dependent upon the form of the Hamiltonian and wavefunction. The electronic wavefunction and model Hamiltonian, ψ and H, must be constructed such that all physically observable properties of the electrons may be obtained via the operation of H and any other property operators. The electronic Hamiltonian of a molecular system is generally split into two contributions, the kinetic and potential energies (T and V). T describes the energy of motion of the electrons, whereas V introduces electrostatic terms. As such, V describes the electrostatic interactions between nuclei, nuclei and electrons, and between electrons. A uniquely quantum effect comes into play, a result of the electron's half integer spin, in the electron-electron interactions, wherein the electrons can 'exchange' positions by changing the sign of the wavefunction, the sign change being a consequence of the half-integer 'spin' of the electrons which labels them as fermions.

When the electrons experience the electrostatic potential from the nuclei they 'quantize' into orbitals, wherein the electrons occupy discrete energy levels and specific orbital patterns. This is a consequence of the wavelike nature of the electrons as quantum particles. Indeed the spin of the electron occupying an orbital must also be specified, as two electrons of opposite spin may occupy the same orbital. Such orbitals that contain information regarding the electron spin are referred to as spin-orbitals. A set of spin-orbitals

[0] Unless otherwise specified, all information contained in the introduction came from the same set of sources.[2,3]

that can describe any possible state of one or more electrons about a molecular system is deemed complete as it spans the whole space of electronic spin-orbital solutions. By this same linear algebra framework, a Hamiltonian matrix containing the expectation value between all spin-orbitals can be diagonalized to yield spin-orbital energy eigenvalues and corresponding eigenvectors. The molecular spin-orbitals that describe the lowest energy configuration of electrons about the molecular system are determined by linear combinations of the chosen basis functions.

1.2 Hartree-Fock

The electronic Hamiltonian describes all pertinent electronic and nucleic interactions. $\mathrm{H}_{\mathrm{elec}}$ is mathematically described as follows,

$$\hat{\mathrm{H}}_{\mathrm{elec}} = -\sum_i \frac{1}{2}\nabla_i^2 - \sum_i \sum_A \frac{Z_A}{|\mathbf{R}_A - \mathbf{r}_i|} + \sum_{i<j} \frac{1}{\mathbf{r}_{ij}} + V_{nuc} \tag{1.2}$$

$$\hat{h}(i) = -\sum_i \frac{1}{2}\nabla_i^2 - \sum_i \sum_A \frac{Z_A}{|\mathbf{R}_A - \mathbf{r}_i|} \tag{1.3}$$

$$\hat{g}(i,j) = \sum_{i<j} \frac{1}{\mathbf{r}_{ij}} \tag{1.4}$$

where the first term refers to the electron kinetic energy, the second term the electron-nuclei attraction, the third term the electron-electron repulsion, and the fourth and final term refers to the nuclear-nuclear electrostatic repulsion. When using H_{HF}, the form of the wavefunction (ψ_{HF}) is profoundly important. If one simply assembles a Hartree product, a product of all the spin-orbital basis functions, the exchange will be neglected. Therefore, a determinant of the spin-orbital basis functions must be assembled in the following manner,

$$\Phi_0 = \frac{1}{\sqrt{N!}} \begin{vmatrix} \phi_1^1 & \phi_2^1 & \dots & \phi_N^1 \\ \phi_1^2 & \phi_2^2 & \dots & \phi_N^2 \\ \vdots & \vdots & \ddots & \vdots \\ \phi_1^N & \phi_2^N & \dots & \phi_N^N \end{vmatrix} \tag{1.5}$$

for an N-electron system where the superscript refers to the electron number and the subscript refers to the occupied orbital. Note that interchanging any two columns or rows will flip the sign of the determinant, a useful aspect of determinants that properly reflects the electron's fermionic character.

If one only wishes to describe the one-electron system of hydrogen, then analytic wavefunctions exist for this Hamiltonian which consist of a product an infinite series of spherical harmonics and a radial component.

Unfortunately, as soon as one moves from the one-electron system of hydrogen up to any two-electron or higher system, the hydrogenic wavefunctions are no longer analytic solutions due to the electron-electron repulsion term. A solution to this problem is to represent the spin-orbital basis in terms of atomic spin-orbitals. In principle these orbitals constitute a complete basis ... if the entire series of spherical harmonics is included in the basis and the radial component is properly described. Basis sets may be constructed for different atoms holding varying numbers of basis functions. The Dunning series of basis sets are described as correlation-consistent valence polarized X ζ (cc-pVXZ) basis sets, where X refers to the "cardinality" of the basis. The cardinality of a basis set conveys the size of the basis set and in fact these basis sets are specially constructed to extrapolate towards the complete basis set (CBS) limit, where all (infinite) spherical harmonic basis functions are included and the radial component is fully described..

Once an atomic basis set has been selected, this basis can be used to yield a set of canonical, molecular spin-orbitals. For an electronic system containing equal numbers of α and β electrons in spin-degenerate orbitals, commonly referred to a closed-shell system, the orbital optimization is mathematically represented as,

$$\delta \mathrm{E_{HF}} = 2\sum_{i}^{N/2} \langle \delta\phi_i | \hat{h}_i | \delta\phi_i \rangle + \sum_{i}^{N/2}\sum_{j}^{N/2} 2\,\langle \delta\phi_i \delta\phi_j | \hat{g}(i,j) | \delta\phi_i \delta\phi_j \rangle - \langle \delta\phi_i \delta\phi_j | \hat{g}(i,j) | \delta\phi_j \delta\phi_i \rangle. \tag{1.6}$$

This HF energy expression was constructed under the assumption of orthonormal orbitals, and so this process is a constrained minimization.

The most commonly utilized method for finding the HF solution is to employ the Roothaan-Hall equations as follows,

$$\mathbf{FC} = \mathbf{SC}\varepsilon \tag{1.7}$$

$$\mathbf{F} = \langle \chi_p | \hat{f} | \chi_q \rangle \tag{1.8}$$

$$\hat{f} = \hat{h} + \sum_{j}^{N/2} 2\hat{J}_j - \hat{K}_j \tag{1.9}$$

$$\hat{J}_j \left| \phi^\mu \right\rangle = \left\langle \phi_j^\nu \right| \hat{g}(\mu,\nu) \left| \phi_j^\nu \phi^\mu \right\rangle \tag{1.10}$$

$$\hat{K}_j \left| \phi^\mu \right\rangle = \left\langle \phi_j^\nu \right| \hat{g}(\mu,\nu) \left| \phi^\nu \phi_j^\mu \right\rangle \tag{1.11}$$

where $\mathbf{F}$ is the Fock matrix, $\mathbf{C}$ is the MO coefficients matrix, $\mathbf{S}$ is the overlap matrix, ε is a vector of the orbital energies, χ is an atomic orbital, and ϕ is a molecular orbital. These equations must be iteratively solved as at each point the MO coefficients are solved for, but the Fock operators that determine the Fock matrix are dependant upon the MO densities as shown in the equations above. A consequence of this

approach is that each electron's orbital will feel the average field of all other electrons. This is why HF is referred to as a mean-field optimization.

1.3 Basis Sets

The aforementioned cc-pVXZ basis sets have been constructed to extrapolate energies smoothly to the CBS limit based upon the cardinalities of the basis sets. Basis sets are generally constructed utilizing gaussian functions for the radial components and spherical harmonics for the angular. Larger cardinalities of basis sets contain successively more gaussian functions and spherical harmonics. Gaussian functions are utilized due to their ease of integration. However, they struggle to describe the wavefunction region near the nuclei, which takes the form of a cusp. This cusp can be approximately described by many gaussian functions in a linear combination. Basis sets can be predesigned with set proportions of these gaussian functions for each element of the periodic table. These predesigned basis sets seek to best describe the atomic orbitals used in Roothaan-Hall Hartree-Fock to generate molecular orbitals.

1.4 Electron Correlation

As discussed above, Hartree-Fock is a mean field method, which implies that instantaneous 2-electron interactions are neglected. These neglected 2-electron interactions are commonly referred to the "correlation" energy and are defined as follows,

$$\mathrm{E_{corr}} = \mathrm{E_{Exact}} - \mathrm{E_{HF}} \tag{1.12}$$

where the correlation energy is simply what the Hartree-Fock energy misses. Electron correlation may be partitioned into two classes, static and dynamic correlation. Static correlation is strongest when there are multiple degenerate or nearly degenerate reference configurations for HF to choose from. In such cases it is common to use wavefunctions with multiple reference configurations, also called multi-reference wavefunctions. Dynamic correlation seeks a description of how the electrons move around with respect to electron-electron interactions. Dynamic correlation is most commonly described atop single-reference wavefunctions. However, methods exist to describe dynamic correlation atop multi-reference wavefunctions. It should be noted that for this body of work, only single-reference methods were utilized and thus these will be the only methods discussed.

There are several available methods for describing the dynamic electron correlation Three of these meth-

ods utilized in this body of work are based on a Hartree-Fock reference, while others modify Hartree-Fock to attempt to describe electron correlation in a mean field manner. These methods for treating electron correlation are described in the following subsections.

1.4.1 Configuration Interaction Theory

The single-reference wavefunction obtained via the Hartree-Fock procedure may be expanded to include all possible excited determinants in the following manner,

$$\Psi = c_0 \left|\Phi_0\right\rangle + \left(\frac{1}{1!}\right)^2 \sum_{ar} c_a^r \left|\Phi_a^r\right\rangle + \left(\frac{1}{2!}\right)^2 \sum_{abrs} c_{ab}^{rs} \left|\Phi_{ab}^{rs}\right\rangle + \ldots, \tag{1.13}$$

where $abc\cdots$ and $rst\cdots$ refer to unoccupied and occupied orbitals, respectively and the number of indices considered determines how many orbital excitations occur from the reference to get to the new determinant. If all possible excited determinants are included in the wavefunction, one holds the full configuration interaction (FCI) wavefunction. The FCI wavefunction describes 100% of the correlation energy, dynamic and static. If the CI coefficients are optimized to obtain the exact FCI wavefunction, the exact correlation energy may be obtained via the following,

$$\langle \Phi_0 | \mathrm{H} - \mathrm{E}_0 | \Psi \rangle = \mathrm{E}_{\mathrm{corr}}. \tag{1.14}$$

After intermediate normalization ($\langle \Psi | \Phi_0 \rangle = 1$) and a variational optimization of the CI coefficients, the FCI wavefunction may be obtained via the following,

$$\left\langle \Phi_{abc\ldots}^{rst\ldots} \middle| \mathrm{H} - \mathrm{E}_0 \middle| \Psi \right\rangle = \mathrm{E}_{\mathrm{corr}} \left\langle \Phi_{abc\ldots}^{rst\ldots} \middle| \Psi \right\rangle \tag{1.15}$$

for any arbitrary coefficient, since

$$\left\langle \Phi_{abc\ldots}^{rst\ldots} \middle| \Psi \right\rangle = c_{abc\ldots}^{rst\ldots}. \tag{1.16}$$

Depending upon basis set size, the FCI expansion can very rapidly become untenable for computations, so CI is frequently truncated to include an arbitrary set of excitations. A common approach is to include the single and double excitations (CISD). The issue with this approach is that it is not size-extensive, which means that if two moieties of a molecular system being treated with CISD are separated to an infinite distance the resulting energy will differ from the energy obtained on the individual moieties.

1.4.2 Perturbation Theory

Another method for treating electron correlation comes in the form of perturbation theory. The goal is to lightly 'perturb' the reference system to describe a small physical effect. The Hamiltonian is split into two parts, typically an easy to compute and a hard to compute component, as follows,

$$\mathrm{H} = \mathrm{H}_0 + \mathrm{H}'. \tag{1.17}$$

Where H_0 is the easy part and H' is the hard part. After solving for the wavefunction under the influence of H_0, H' may be utilized according to an arbitrary order of perturbation theory to achieve an approximate description of the physics contained within H'. Only one example of perturbation theory will be provided here for electron correlation, as it is the most commonly utilized, and this is second order Møller-Plesset perturbation theory (MP2).

$$\mathrm{E}_n^{(2)} = \sum_{m \neq n} \frac{\left\langle \psi_m^{(0)} \middle| \hat{H}' \middle| \psi_n^{(0)} \right\rangle \left\langle \psi_n^{(0)} \middle| \hat{H}' \middle| \psi_m^{(0)} \right\rangle}{\mathrm{E}_n^{(0)} - \mathrm{E}_m^{(0)}}. \tag{1.18}$$

1.4.3 Coupled Cluster Theory

Coupled Cluster (CC) theory is a variant of CI that uses a different wavefunction ansatz to ensure size-extensivity is preserved upon truncation of included excitations. The ansatz is as follows,

$$|\Psi_{\mathrm{CC}}\rangle = \mathrm{e}^{\hat{T}} |\Psi_{\mathrm{HF}}\rangle \tag{1.19}$$

$$|\Psi_{\mathrm{CC}}\rangle = \mathrm{e}^{\hat{T}_1 + \hat{T}_2 + \ldots + \hat{T}_n} |\Psi_{\mathrm{HF}}\rangle \tag{1.20}$$

$$\hat{T}_k = \left(\frac{1}{k!}\right)^2 t_{a_1 \ldots a_k}^{i_1 \ldots i_k} \hat{a}_{i_1 \ldots i_k}^{a_1 \ldots a_k} \tag{1.21}$$

where t refers to an individual cluster amplitude and $\hat{a}$ is an excitation operator. Equations may constructed in a similar manner to CI in order to solve for the CC energy and amplitudes. The most commonly used CC procedure is CC with single, double, and perturbative triple excitations [CCSD(T)], wherein the singles and doubles amplitudes are solved for iteratively and explicitly. The triples contribution is solved for perturbatively using the singles and doubles amplitudes. CCSD(T) benefits from cancellation of error and so is even more accurate than CCSDT. Due to its balance of accuracy with relative computational efficiency, CCSD(T) is frequently referred to as the "gold standard" for describing electron correlation.

1.4.4 Density Functional Theory

Density Functional Theory (DFT) offers an intriguing promise of recovering electron correlation at a Hartree-Fock, or lower, cost. Unfortunately DFT comes with a greater level of variability as compared to CC and CI methods. Do to the variational principle, CC and CI methods will always recover successively more of the correlation energy as they approach FCI in a systematic and predictable manner. DFT on the other hand can under or overestimate the correlation energy. Nevertheless, DFT is a powerful and computationally tractable method for calculating the electronic structure of larger molecules. Kohn-Sham DFT (KS-DFT) is the most commonly used variation and it seeks to match the exact electron density of a fully correlated system using a functional. The general form of KS-DFT is as follows,

$$\hat{\mathrm{H}}_{\mathrm{KS}} = -\sum_{i} \frac{1}{2}\nabla_i^2 - \sum_{A} \frac{\rho(\mathbf{r})Z_A}{|\mathbf{R}_A - \mathbf{r}|} + \sum_{i<j} \frac{1}{\mathbf{r}_{ij}} + \int f(\rho(\mathbf{r}), \nabla\rho(\mathbf{r}))d\mathbf{r} + V_{nuc}. \tag{1.22}$$

The key differentiating point between this Hamiltonian and the Hartree-Fock Hamiltonian comes in how the exchange and correlation terms are described. While the KS Hamiltonian retains the coulombic two-electron term from Hartree-Fock, the exchange and correlation terms are grouped into a functional, f. The functional that exactly determines the electron density about a molecular system is unknown, but many approximate functionals have been formulated.

1.5 Focal Point Analysis

Focal Point Analysis[4–8] utilizes computations at the limits of current computational capibilities to push towards the FCI/CBS limit, AKA the exact correlation energy. The aforementioned Dunning series of basis sets have been constructed to extrapolate in energy towards the CBS limit, depending on the level of correlation utilized and the cardinalities of basis sets the energies have been computed at. For the FPA procedure, one first computes as many single point energies as are computationally feasible. Then the single point energies are extrapolated or added according to which cardinalities are available. One can construct an incremented Focal Point table moving from lower to higher levels of correlation to determine how well converged the correlation energy is. Fortuitously, the correlation energy converges rapidly with respect to basis set cardinality as one utilizes higher levels of correlation treatment, so addition is frequently a good approximation.

1.6 Molecular Vibrational Analysis

In addition to the electronic energy levels being quantized in a molecular system, the nuclear vibrational wavefunction is also quantized. The vibrational energy levels of the molecular system are solved for approximately, as harmonic oscillators. A Hamiltonian may be proposed that solves the second order differential equation in one dimension of a cartesian coordinate,

$$\alpha = \frac{2\pi\omega m}{\hbar} \tag{1.23}$$

$$\hat{\mathrm{H}}_{\mathrm{nuc}} = -\frac{\hbar^2}{2m}\left(\frac{d^2}{dx^2} - \alpha^2 x^2\right) \tag{1.24}$$

$$0 = \frac{d^2\psi}{dx^2} + \left(\frac{2mE}{\hbar^2} - \alpha^2 x^2\right)\psi. \tag{1.25}$$

The form of the wavefunction, ψ, may then be determined as,

$$\psi = e^{-\alpha x^2/2}(c_0 + c_2 x^2 + \ldots + c_\nu x^\nu) \text{ for } v \text{ even} \tag{1.26}$$

$$\psi = e^{-\alpha x^2/2}(c_1 x + c_3 x^3 + \ldots + c_\nu x^\nu) \text{ for } v \text{ odd} \tag{1.27}$$

and the energy takes the following, quantized form,

$$E = \left(v + \frac{1}{2}\right)h\omega \tag{1.28}$$

where v refers to the excitation level of the harmonic mode and it begins at 0.

1.7 Natural Bond Orbital Theory

After one has generated an electronic wavefunction, the electronic density can be transformed and analyzed. One well established analysis for qualitative insights is natural bond orbital (NBO) theory.[9,10] The density matrix of a closed shell species can be defined as follows,

$$\mathbf{D} = 2\sum_{i=1}^{\mathrm{occ}} \mathbf{c}_i \mathbf{c}_i\dagger \tag{1.29}$$

where $\mathbf{c}$ refers to the linear combination of atomic orbital (LCAO) coefficients. A series of matrix transformations on $\mathbf{D}$ transforms the MO density into NBO density. NBOs are localized bonds that correspond to the more qualitative understanding of bonding with σ, π and higher order bonds. Once NBOs have been

generated a slew of qualitative properties can be calculated and analysis can be performed. More information on these properties and analysis can be found in the proceeding chapters.

CHAPTER 2

The Bismuth Tetramer Bi_4: The ν_3 Key to Experimental Observation

Lahm, M. E.; Hoobler, P. R.; Turney, J. M.; Peterson, K. A.; Schaefer, H. F. *Phys. Chem. Chem. Phys.* **2018**, *20*, 21881−21889. Reproduced from Ref.[11] with permission from the PCCP Owner Societies. https://pubs.rsc.org/en/content/articlelanding/2018/cp/c8cp03529f

2.1 Abstract

The spectroscopic identification of Bi_4 has been very elusive. Two constitutional Bi_4 isomers of T_d and C_{2v} symmetry are investigated and each is found to be a local energetic minimum. The optimized geometries and fundamental vibrational frequencies of these two isomers are obtained at the CCSD(T)/cc-pVQZ-PP level of theory, utilizing the Stoll, Metz, and Dolg 78-electron effective core potential. The focal point analysis method, from a maximum basis set of cc-pV5Z-PP, and proceeding to a maximum correlation method of CCSDTQ, was employed to determine the dissociation energy of Bi_4 (T_d) into two Bi_2 and the adiabatic energy difference between the C_{2v} and T_d isomers of Bi_4. These quantities are predicted to be +78 kcal mol^{-1} and +43 kcal mol^{-1}, respectively. Two electron vertical excitation energies between the T_d and C_{2v} electronic configurations are computed to be 170 kcal mol^{-1} for the T_d isomer and 13 kcal mol^{-1} for the C_{2v} isomer. The most probable approach to laboratory spectroscopic identification of Bi_4 is via an infrared spectrum. The predicted fundamentals (cm^{-1}) with IR intensities in parentheses (km mol^{-1}) are 100(0), 130(0.20), and 175(0) for the T_d isomer. The moderate IR intensity for the only allowed fundamental may explain why Bi_4 has yet to be observed. Through natural bond orbital analysis, the C_{2v} isomer of Bi_4 was discovered to exhibit "long-bonding" between the furthest apart 'wing' atoms. This long-bonding is postulated to be facilitated by the σ-bonding orbital between the 'spine' atoms of the C_{2v} isomer.

2.2 Introduction

Given the remarkable stability of P_4, it is not unreasonable to search for its heavier valence isoelectronic species. Despite many attempts, it is unclear whether the Bi_4 molecule has been positively identified in the laboratory, apart from mass spectrometry in several studies,[12–16] most recently those of Duncan and coworkers.[17,18] As of yet, no vibronic spectra have been unambiguously assigned to this molecule, though many have tried.[19–23] Although Bi_4 has proven evasive to spectroscopists, it has been explored by theoretical chemists using several varieties of density functional theory (DFT). Various characteristics of Bi_4 have been studied, including its electronic structure,[24–27] electron affinity,[25,27–29] ionization potential,[25,27,29], and binding energy,[25,30]. The preferred geometry[24,25,27,29–32] and harmonic vibrational frequencies[25,30] of Bi_4 have been computed mostly by DFT studies, with one study[24] utilizing dynamical correlation methods. While DFT and static correlation methods have been fruitful in many endeavors, they are not the highest level of theory that may be utilized, and high precision is of the utmost importance for this system.

Several spectroscopic studies[19–23] initially claimed to have identified three vibronic emission bands of Bi_4. Arrington and Morse[33] later (2008) observed these same emission bands but identified the source as

Bi_3 via time-of-flight mass spectrometry. An excellent *ab initio* analysis of the electronic structure of Bi_4 at the MRCISD/CASSCF level of theory was provided by Zhang and Balasubramanian as early as 1992.[24] In the latter study, the authors give further evidence that these emission bands should not be assigned to Bi_4 on the grounds that only one of the low energy Bi_4 electronic excitations is formally dipole allowed, and its expected excitation energy is qualitatively different from the excitations observed. Additionally, Wakabayashi et al. analyzed small bismuth clusters using laser induced fluorescence spectroscopy and their results also support the reassignment of the supposed Bi_4 emission bands to Bi_3.[34,35]

Several theoretical studies have explored the energetically low-lying constitutional isomers of Bi_4 and their corresponding harmonic vibrational frequencies, although the highest level of theory used in these studies was MRCISD with a triple zeta basis set. From a Lewis-bonding perspective,[36] one would expect that the lowest energy isomer would be one that has three bonds per bismuth to find pairs for its three unpaired valence electrons. Jia et al. noted that due to the relativistic contraction of the bismuth 6s orbital,[25] covalent bonding in Bi_n species will be dominated by the 6p orbitals. While the Lewis-bonding perspective yields one constitutional isomer of Bi_4, other energetic local minima isomers are theoretically possible.

Lauher[37] lists four possible geometric isomers of metal cluster tetramers labeled as tetrahedral (T_d), butterfly (C_{2v} and D_{2h}), and square planar (D_{4h}). Yuan et al. predicted the three lowest energy isomers of Bi_4, utilizing the BPW functional with a relativisitic effective core potential (RECP) and a double numeric plus d polarization functions (DN+d) basis set, to be, T_d, C_{2v} (+27.4 kcal mol^{-1}), and D_{4h}(+39.9 kcal mol^{-1}).[29] Akola and co-workers mention only the T_d and C_{2v} structures as low energy isomers in their computations using the PBE functional with an RECP and a plane-wave basis ,[30] shedding some doubt on the existence of the square planar isomer. Several studies[38–41] have shown that the C_{2v} isomer can exist for P_4 analogues if a ligand is inserted into a bond, thus giving experimental validation for the existence of this isomer in group 5 tetramers. Gausa et al. found the lowest energy isomer of the Bi_4^- anion to be the C_{2v} structure,[27] begging the question of why the T_d isomer is not a minimum for the anion. Jia et al. determined the lowest energy isomer of neutral Bi_4 to be the T_d structure through PBE/DN+d with RECP computations. However, they computed the D_{2d} structure of anionic Bi_4^- to be the lowest in energy, again not finding an anionic T_d local minimum.[25] Considering the longstanding misassignment of spectra previously mentioned, no isomers of Bi_4 have been spectroscopically confirmed.

Theoretical treatment of bismuth clusters comes with its own set of challenges. The considerable number of electrons to be modeled, along with the presence of relativistic effects within the immense core has resulted in many low level theoretical treatments. One method of solving both of these problems has been the application of effective core potentials (ECPs).[42] This computational tool accounts for relativistic core effects while allowing for high-level correlation treatments, such as coupled-cluster (CC) theory, of the valence

electrons. In the case of bismuth, large core ECPs reduce the number of explicitly treated electrons to those occupying the valence 6s and 6p-orbitals. The Bi_4 molecule will thus be analyzed with the aid of ECPs in this study.

Optimized equilibrium geometries and harmonic vibrational frequencies for Bi_4 isomers of T_d and C_{2v} symmetry were computed in this study. These two isomers were found to be the only local minima of those mentioned by Lauher.[37] Additionally, the energy difference between these isomers and the dissociation energy of Bi_4 (T_d) into two Bi_2 molecules were obtained, and Natural Bond Orbital[43] (NBO) analysis was performed on the T_d and C_{2v} isomers.

2.3 Theoretical Methods

The equilibrium geometries were obtained by utilizing Peterson's[44] correlation consistent quadruple-ζ basis set designed for use with relativistic psuedopotentials[42] (cc-pVQZ-PP). The large core psuedopotentials used in this work were developed by Metz and coworkers[42] and encompass all electrons that are not present in the 6s or 6p orbitals of bismuth. This ECP78MDF encompasses 78 electrons per bismuth and allows for treatment of the remaining five electrons per bismuth with higher levels of theory. Coupled cluster theory with full single, double, and perturbative treatment of triple excitations[45,46] [CCSD(T)] was utilized in the geometry optimizations with the CFOUR 2.0[47] (henceforth CFOUR) suite of electronic structure codes. The T_d and C_{2v} isomer geometry optimizations had convergence criteria for the RMS energy gradient of 10^{-8}. MOLPRO 2010[48] was utilized to check for multireference character in the wavefunction space of each isomer through its T_1[49] and D_1[50] diagnostics. NBO[43] analysis was performed on both isomers utilizing the Q-Chem 5.0[51] quantum chemistry software package interfaced with NBO 6.0[10] augmented by Natural Resonance Theory (NRT).[52]

Harmonic vibrational frequencies were obtained using a 5-point finite difference method also utilizing CFOUR at the CCSD(T)/cc-pVQZ-PP level of theory as well, and with the same convergence criteria as the geometry optimizations. After the harmonic frequencies were obtained they were inspected to ensure that no imaginary vibrational modes were present and that each optimized geometry represented a genuine minimum on the potential energy surface (PES). Full cubic and semidiagonal quartic anharmonic corrections to the harmonic vibrational frequencies were computed using second order vibrational perturbation theory (VPT2)[53,54] through finite differences, as implemented within CFOUR and at the same level of theory as that for the harmonic vibrational frequencies.

Focal point analysis[5–8] was employed in determining the dissociation energy of $Bi_4 \rightarrow 2Bi_2$ and the relative energy between the T_d and C_{2v} isomers. The single point energies, computed in the range of cc-

pVnZ-PP ($n = D, T, Q, 5$), and with a reference geometry optimized at the CCSD(T)/cc-pVQZ-PP level of theory, were utilized to extrapolate to the complete basis set (CBS) limit. Correlation energy methods up to coupled cluster single, double, triple, and quadruple excitations (CCSDTQ) were utilized. Extrapolation to the CBS limit for the restricted Hartree–Fock energies and correlation energies were accomplished by three-point[55] and two-point[56] extrapolation schemes, respectively, with the following functions.

$$E_{\mathrm{HF}}(X) = E_{HF}^{\infty} + ae^{-bX} \tag{2.1}$$

$$E_{corr}(X) = E_{corr}^{\infty} + X^{-3} \tag{2.2}$$

The determination of the correlation energy due to full triples and perturbative quadruples excitation for basis set sizes up to the extrapolated CBS limit was accomplished by assuming additivity from the perturbative triples to the full triples and full triples correlation energy to the perturbative quadruples energy computed with the cc-pVTZ-PP basis set and utilizing this same energy difference for all larger basis set sizes.

The CCSD(T) and CCSDT(Q) computations were both run in CFOUR[47] utilizing the ECC[47] and NCC[57–59] modules, respectively. Diagonal Born–Oppenheimer corrections[60,61] (DBOCs) and relativistic corrections were carried out at the HF/cc-pVTZ-PP and CCSD(T)/cc-pVTZ-PP levels of theory, respectively. The scalar relativistic corrections were computed through second order perturbation theory with mass-velocity and Darwin terms (MVD2).[62,63]

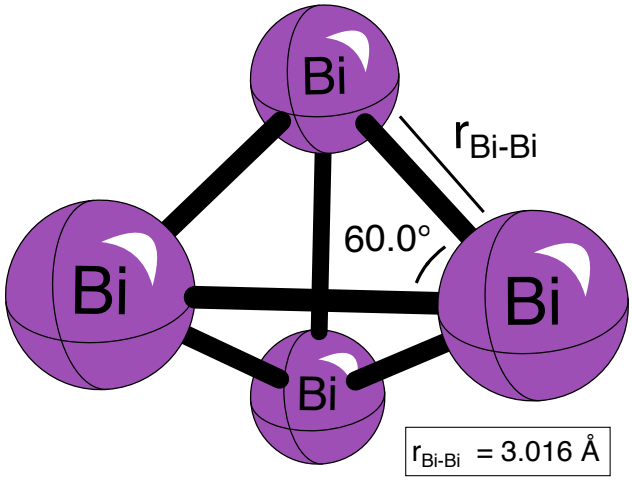

Figure 2.1: The equilibrium geometry of the T_d isomer of Bi_4 predicted at the CCSD(T)/cc-pVQZ-PP level of theory.

2.4 Results

2.4.1 Geometries

T_d Structure

The T_d is the more thoroughly studied of the two isomers of Bi_4 presented in this paper. The T_d isomer has a valence electron configuration of $1a_1^2 1b_1^2 2a_1^2 1b_2^2 3a_1^2 2b_1^2 4a_1^2 2b_2^2 5a_1^2 1a_2^2$. Numerous studies[24,25,29–31,64] report an equilibrium geometry for this isomer at low levels of theory, and these structures will be compared to the geometries predicted in this research. When examining the methods used among previous studies it may be seen that the geometries computed in this research were obtained at a more rigorous level than any of its predecessors. Many of the prior studies utilize plane-wave basis sets and DFT to recover the correlation energy and these methods are less reliable than the methods used in this work. Balasubramanian and Zhang[24] used multireference methods (CASSCF and MRCISD) to analyze excited states of the T_d isomer, and so the T_1 and D_1 diagnostics for this system were computed in the present research, and found to be 0.016 and 0.030, respectively. The value for the D_1 diagnostic is in an intermediary range[65] indicating that there may be some multireference character to the T_d isomer. Optimizing the geometry and computing the vibrational frequencies with a high level of dynamic correllation, however, should recover multireference character. This effect is supported by the focal point energies discussed in the Energetics section of this paper, as there is fairly good convergence of the electron correlation methods. So while Balasubramanian and Zhang used multireference methods, we are confident that our system geometry is well described by single reference CCSD(T). No previous studies have treated Bi_4 with coupled cluster methods and so this work represents the most rigorous treatment that Bi_4 has received thus far.

A serendipitous aspect of optimizing the T_d isomer is that due to the high amount of symmetry present, the only coordinate to be optimized is the Bi-Bi bond distance. This Bi-Bi bond distance is visualized in Figure 2.1 as $r_{Bi\text{-}Bi}$. The (most reliable) optimized $r_{Bi\text{-}Bi}$ bond length was computed to be 2.965 Å in this study. When this bond length is compared to the bond lengths computed in prior studies[24,25,29–31] it may be seen that the $r_{Bi\text{-}Bi}$ predicted in this research is the smallest. Gao et al.[31] compute a value of 3.02 Å for a difference from this work of 0.05 Å. It should be noted that Gao et al. utilized the PW91 functional with plane wave basis sets, so it is among the lower levels of theory discussed here. Zhang and Balasubramanian[24] computed the $r_{Bi\text{-}Bi}$ value with the highest deviation from our study, that deviation being 0.15 Å. They utilized MRCISD with a triple zeta equivalent basis set including d polarization functions and a relativistic ECP that spanned the same electrons as the ECP used in the present research. Bond lengths

can affect many properties of a molecule including the frequencies reported in this work and this effect will be discussed later.

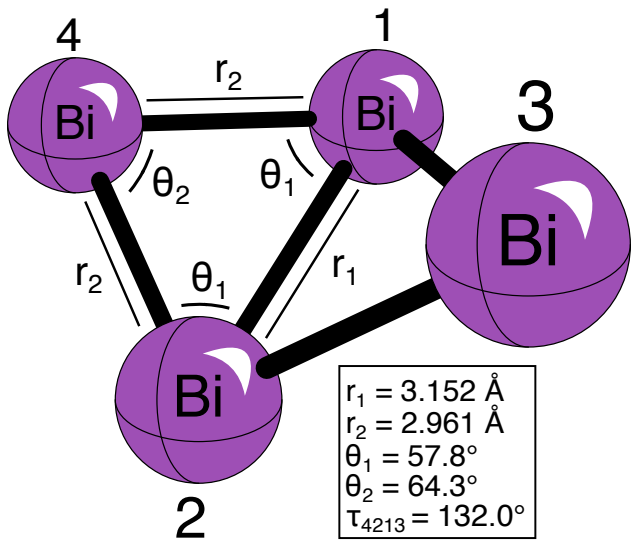

Figure 2.2: The equilibrium geometry of the C_{2v} isomer of Bi_4 predicted at the CCSD(T)/cc-pVQZ-PP level of theory.

C_{2v} Structure

When discussing the C_{2v} isomer, two terms will be used to describe pairs of symmetric atoms. These terms are the 'spine' and 'wing' atoms which will henceforth refer to atoms 1 and 2, and atoms 3 and 4, respectively, of Figure 2.2.

While performing optimizations on the C_{2v} isomer it was necessary to impose a specific electronic state to keep the geometry from relaxing to the T_d isomer, even though the C_{2v} is indeed a local minimum. It appears that the T_d and C_{2v} isomers lie on two different potential energy surfaces and while it was not rigorously studied in this work, the interaction between these surfaces (especially in geometries intermediate to the T_d and C_{2v} isomers) would be a fascinating avenue for future study. The valence electronic configuration of the C_{2v} structure is $1a_1^2 1b_1^2 1b_2^2 2a_1^2 3a_1^2 1a_2^2 2b_1^2 4a_1^2 2b_2^2 3b_1^2$.

The C_{2v} isomer has been studied far less in previous research than the T_d isomer. A straightforward explanation for this discrepancy is that the T_d isomer is the lowest energy isomer, and when Bi_4 is generated the T_d isomer is expected to be the most abundant of the two. Additionally, the C_{2v} isomer is on a separate electronic PES from the T_d isomer. The C_{2v} structure was found to exhibit strong multireference character with a T_1 diagnostic of 0.027 and a D_1 diagnostic of 0.087. In light of these obstacles, only one other study[30] has reported a geometry for the neutral C_{2v} isomer.

As with the T_d isomer the bond lengths reported by this work for the C_{2v} constiutional isomer are shorter

than those of the previous work.[30] Akola et al. (henceforth Akola) utilized the PBE functional with a plane wave basis. Akola report an r_1 of 3.19 Å and an r_2 of 2.98 Å, both deviating from this research by 0.11 Å. The geometric data show very little difference in the angles between Akola and this work, aside from the torsional angle of the Akola study being slightly closer to planarity, implying that the geometries are approximately similar, the geometry in this work being more compact.

Other Constitutional Isomers

It should be noted that the geometry of D_{2d} and D_{4h} structures were optimized but harmonic vibrational frequency computations found an imaginary vibrational mode for each of these structures, and they are not reported as valid local minima. Both isomers preferred to form a bond between two central bismuth atoms and descend along their PES to the C_{2v} isomer.

Bismuth Dimer

The geometry and vibrational frequency of Bi_2 were computed in this research to affirm the validity of the later energetics. The bond length was computed to be 2.627 Å and the harmonic vibrational frequency was computed to be 197.6 cm^{-1} utilizing CCSD(T)/cc-pVQZ-PP with the same large core ECP used in the T_d and C_{2v} Bi_4 optimizations. These predictions are in reasonable agreement with those computed by Peterson and Yousaf[66] utilizing CCSD(T)/CBS(45) with the cc-pwCVXZ-PP and a small core psuedopotential. Peterson and Yousaf predict the bond length to be 2.618 Å and the harmonic vibrational frequency to be 197.9 cm^{-1}. Gerber and Broida report the experimental bond length to be 2.6597 Å[67] and Effantin et al.[68] deduce the Bi_2 harmonic vibrational frequency to be 173 cm^{-1} from experiment.[68] A bond length of 2.637 Å, in closer agreement with experiment, was obtained with the higher level CCSDT(Q)/cc-pVQZ-PP method in this research.

2.4.2 Vibrational Frequencies

Table 2.1: Harmonic and anharmonic vibrational frequencies for the T_d Bi_4 (in cm^{-1}) structure at the CCSD(T)/cc-pVQZ-PP level of theory. The ν_3 harmonic IR intensity is reported in parentheses (in km mol^{-1})

Vibrational Mode	Harmonic Frequency	Fundamental Frequency
$\nu_1(a_1)$	176(0)	175
$\nu_2(e)$	101(0)	100
$\nu_3(t_2)$	131(0.20)	130

T_d Structure

While many studies have reported the geometry of the T_d isomer, only three others[25,30,64] have reported its vibrational frequencies. This should come as no surprise because Bi_4 is a system with massive nuclei and so its vibrational potential energy wells will be shallow, making the computation of vibrational frequencies challenging. VPT2 corrections were made to the computed harmonic frequencies in this study in order to obtain fundamental frequencies for the T_d structure. The previous three studies report only harmonic frequencies.

The harmonic vibrational frequencies reported by the other two studies are generally lower than those reported in this work. The three vibrational modes are computed to be 176, 101, and 131 cm^{-1} in this work (listed in Table 2.1) as compared to 165, 94, and 124 cm^{-1} (Jia et al.)[25] and 163, 93, and (120,122) cm^{-1} (Akola).[30] Akola reported a splitting of 2 cm^{-1} in ω_2, which is likely a slight geometric distortion due to numerical imprecision. Liang et al. report only one IR active vibrational frequency at 115 cm^{-1} which likely corresponds to ω_3.[64] This trend of lower harmonic frequencies in prior works could be due to the aforementioned disparity in geometries, as the earlier theoretical geometries have longer bond distances.

The only IR-active vibrational mode for T_d Bi_4 is ν_3. This vibrational feature could be used to confirm the presence of the T_d structure of the Bi_4 molecule. According to two mass spectrometry studies,[16,18] utilizing heat and laser vaporization respectively, Bi_2 and Bi_4 are produced in greatest abundance with very small amounts of Bi_3 and Bi_5. Many studies report vibrational frequencies for Bi_3.[30,33–35,64,69] However, only one fundamental, computed by Choi et al.,[69] is close enough to interfere with the detection of the T_d vibrational band (ν_3). This vibrational frequency has a value of approximately 124 cm^{-1}. According to Choi et al. this fundamental is not IR active (infrared intensity of 0). Additionally, Choi et al. report very low infrared intensities for the rest of the Bi_3 frequencies, the largest intensity being 0.01 km mol^{-1} for modes with frequencies of about 161 and 163 cm^{-1}. In conjuction with the low abundance of Bi_3 and Bi_5, it is unlikely that any other vibrational frequencies will overlap with ν_3 for T_d Bi_4 and its detection will confirm the presence of the T_d structure.

Anharmonic corrections are computed for the T_d isomer and found to very slightly lower each harmonic frequency. The corrections display a linear increase in absolute value as the harmonic frequency energies get larger. The harmonic frequencies computed in this work appear to be a good approximation for the frequencies of the T_d isomer as the largest anharmonic correction is -1 cm^{-1}.

Table 2.2: Harmonic and anharmonic vibrational frequencies for the C_{2v} Bi_4 (in cm^{-1}) structure at the CCSD(T)/cc-pVQZ-PP level of theory. Harmonic IR intensities are reported in parentheses (in km mol^{-1})

Vibrational Mode	Harmonic Frequency	Fundamental Frequency
$\nu_1(a_1)$	161(0.09)	160
$\nu_2(a_1)$	93(0.01)	93
$\nu_3(a_1)$	54(0)	54
$\nu_4(a_2)$	111(0)	110
$\nu_5(b_1)$	153(1.50)	152
$\nu_6(b_2)$	117(0.05)	117

C_{2v} structure

The C_{2v} isomer vibrational frequencies have been reported in only one other study.[30] Akola reported vibrational frequencies of 142, 76, 58, 89, 124, and 104 cm^{-1} for modes one through four, while this work predicts them to be 161, 93, 54, 111, 154, and 117 cm^{-1} (listed in Table 2.2). There is a broad range of deviation between this study and Akola, with most of Akola's frequencies being smaller aside from ω_3. This ω_3 vibrational mode corresponds to a 'flapping' motion of the C_{2v} structure. This disparity in the trend could stem from the difference in torsional angle between the two geometries, as the Akola geometry is slightly closer to planarity than the geometry of this work. Another possible contributing factor could be that the geometry of this work is wider set, as the 'wing' atoms are predicted to be 4.5 Å apart with a torsion angle (τ_{4213}) of 57.8°and Akola predict this distance to be 4.6 Å with a τ_{4213} of 57.7°. Similar to the T_d isomer, the anharmonic corrections for the C_{2v} isomer are small and negative. The largest anharmonic correction is -1 cm^{-1}.

2.4.3 Energetics

In addition to geometries and harmonic frequencies, the energy difference between the two isomers and the dissociation energy of T_d Bi_4 into two Bi_2 molecules have been computed. Both of these values were obtained by employing the Focal Point Analysis method discussed in the Theoretical Methods section.

From Table 2.3 it may be seen that after extrapolating out to the CCSDT(Q)/CBS level of theory the energy difference between the T_d and C_{2v} isomers is +43.59 kcal mol^{-1}. This energy can then be augmented by a DBOC of -0.08 kcal mol^{-1} and an anharmonic ZPVE correction of -0.12 kcal mol^{-1} (the relativistic correction is already accounted for in the ECP) yielding a final energy difference of +43.39 kcal mol^{-1}. The absolute DBOCs for the T_d and C_{2v} structures are 0.38 kcal mol^{-1} and 0.30 kcal mol^{-1}, respectively.

Table 2.3: Valence focal point analysis of the relative energy $T_d \longrightarrow C_{2v}$ in kcal mol^{-1}. Delta (δ) denotes the change in relative energy (ΔE_e) with respect to the preceding level of theory

	HF	$+\delta$MP2	$+\delta$CCSD	$+\delta$(T)	$+\delta$T	$+\delta$(Q)	$+\delta$Q	Net
cc-pVDZ-PP	+52.61	−5.74	+1.10	−3.17	−0.32	−1.22	+0.27	[+43.53]
cc-pVTZ-PP	+53.06	−3.19	−0.07	−2.91	−0.25	−1.40	[+0.27]	[+45.51]
cc-pVQZ-PP	+49.18	−1.76	+0.18	−2.91	[−0.25]	[−1.40]	[+0.27]	[+43.30]
cc-pV5Z-PP	+48.62	−1.45	+0.27	−2.86	[−0.25]	[−1.40]	[+0.27]	[+43.20]
CBS	[+48.53]	[−1.12]	[+0.36]	[−2.79]	[−0.25]	[−1.40]	[+0.27]	[+43.59]

ΔE_e(final) = ΔE_e[CCSDTQ/CBS] + Δ_{ZPVE}[CCSD(T)/cc-pVQZ-PP] + Δ_{DBOC}[HF/cc-pVTZ-PP] + Δ_{rel}[CCSD(T)/cc-pVTZ-PP]
ΔE_e(final) = $43.59 - 0.12 - 0.08 + 0.00 =$ **43.39** kcal mol^{-1}

Stability analysis was performed on the T_d structure and a nearby $^1A_1$ state (contained within a $^3T_1$ state) was identified that may be contributing to a Jahn-Teller distortion, leading to a large DBOC for both structures. This large energy difference suggests that the T_d isomer would exist in vast excess compared to the C_{2v} isomer.

Table 2.4: Valence focal point analysis of the relative energy $Bi_4(T_d) \longrightarrow 2\,Bi_2$ in kcal mol^{-1}. Delta (δ) denotes the change in relative energy (ΔE_e) with respect to the preceding level of theory

	HF	$+\delta$MP2	$+\delta$CCSD	$+\delta$(T)	$+\delta$T	$+\delta$(Q)	$+\delta$Q	Net
cc-pVDZ-PP	+73.54	−3.04	−4.85	−1.34	−0.55	−0.79	+0.01	[+62.96]
cc-pVTZ-PP	+80.93	+7.80	−7.38	−0.28	−0.91	−0.80	[+0.01]	[+79.37]
cc-pVQZ-PP	+75.86	+9.96	−6.51	+0.48	[−0.91]	[−0.80]	[+0.01]	[+78.10]
cc-pV5Z-PP	+73.82	+11.45	−6.40	+0.81	[−0.91]	[−0.80]	[+0.01]	[+77.97]
CBS	[+73.07]	[+13.01]	[−6.29]	[+1.15]	[−0.91]	[−0.80]	[+0.01]	[+79.24]

ΔE_e(final) = ΔE_e[CCSDTQ/CBS] + Δ_{ZPVE}[CCSD(T)/cc-pVQZ-PP] + Δ_{DBOC}[HF/cc-pVTZ-PP] + Δ_{rel}[CCSD(T)/cc-pVTZ-PP]
ΔE_e(final) = $79.24 - 0.53 - 0.36 + 0 =$ **78.35** kcal mol^{-1}

The dissociation energy of Bi_4 into two Bi_2 molecules is shown in Table 2.4. This dissociation energy is extrapolated out to the same level of theory as the conformational energy change and the result is an energy difference of +79.24 kcal mol^{-1}. A large DBOC of −0.36 kcal mol^{-1} (the relativistic correction again being negligible) can be applied alongside an anharmonic ZPVE correction of −0.53 kcal mol^{-1} to yield a corrected dissociation energy of 78.35 kcal mol^{-1}.

The vertical electronic excitation energies for both isomers were computed and found to be 170 kcal mol^{-1} for the electronic transition from the T_d electron configuration to the C_{2v} electron configuration at the T_d equilibrium geometry computed in the present research. An energy difference of 13 kcal mol^{-1} was found for the electronic transition from the C_{2v} electron configuration to the T_d electron configuration at the C_{2v} equilibrium geometry. Thus there must be a crossing of these potential energy surfaces somewhere

between these minima. While this phenomenon is not explored further in the present research, a future study could be done that examines the transition between the two isomers using multireference methods to compute both diabatic and adibatic potential energy surfaces between the isomers.

2.4.4 NBO analysis

Natural Bond Orbital (NBO) analyses were performed on both the T_d and C_{2v} isomers. The results obtained for the T_d isomer showed that the six bonds were almost doubly occupied (1.98) with four lone pairs being essentially doubly occupied (2.00). This bonding pattern matches exactly the conventional view of a group 5 T_d tetramer, such as P_4.

The C_{2v} structure, however, yields a fascinating result. The two bismuth atoms at the tips of the 'wings' (atoms 3 and 4 in Fig. 2.3 of the C_{2v} structure) have a "non-Lewis" bond connecting them with an occupancy of 0.54. We attribute this "non-Lewis"[43] interaction to long-bonding, a phenomenon recently explored by Landis and Weinhold.[70] This long-bonding orbital has primarily atomic p-orbital character. Landis and Weinhold stress the necessity of lowering the energy of the long bond through an intermediary electron density donating source. In the C_{2v} isomer of Bi_4, a Lewis bond between the 'spine' atoms, atoms 1 and 2 in Fig. 2.3, appears to be the primary donator of electron density. This deduction was made due to the aforementioned Lewis bond being geometrically in the correct position to donate electron density to the 'long-bond' and the occupancy of the orbital denoted in Figure 2.3(a) being 1.60. These 'wing' atoms are 4.488 Å apart, approximately 1.5 Å longer than the T_d bond distance of 2.965 Å. The NBO described by the in-phase p-orbitals on atoms 3 and 4 has an occupancy of 1.80, and it is reasonable to say that this NBO also donates a small amount of electron density to the long bond. This is due to its geometric and energetic proximity to the long-bond, as well as the other higher energy NBOs not having enough collective occupancy to fully explain the in-phase NBO's occupancy deficiency.

This C_{2v} structure 'long-bond' appears to be the energy lowering factor that distinguishes the C_{2v} structure as a local minimum where neither the D_{4h} nor D_{2d} structures are local minima. The extreme distance between the non-bonding bismuth atoms and the lack of an electron density donator for the D_{4h} and D_{2d} structures do not allow them to take advantage of this energy lowering effect. While no computations were performed on the Bi_4 anion in this work, it may be speculated that the C_{2v} isomer which is reported to be the global minimum of the Bi_4 anion by Gausa et al.,[27] is so because more electron density may then be donated into the long-bond, thus lowering the energy of this isomer. This does not explain, however, why the D_{2d} isomer was reported as a global maximum for this anion in the study by Jia et al.,[25] and more work should be done to assert the validity of the C_{2v} structure 'long-bond'. The T_d isomer is likely not the global

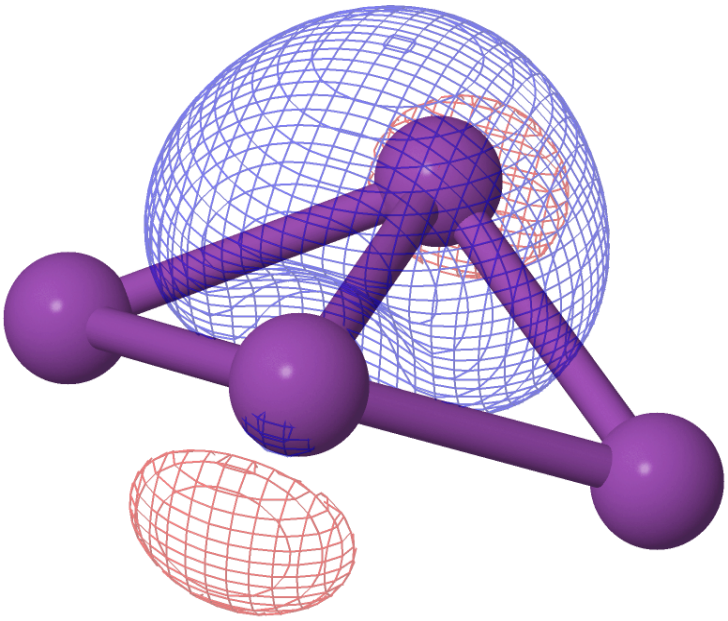

(a) The Lewis NBO of the C_{2v} isomer.

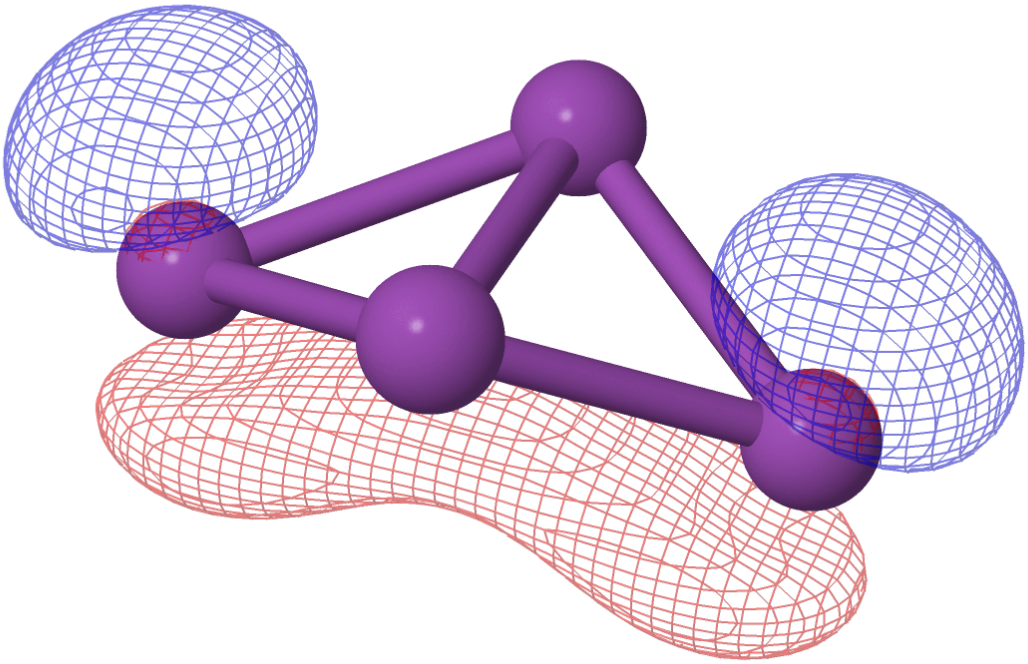

(b) The non-Lewis, long-bonding NBO of the C_{2v} isomer.

Figure 2.3: The Lewis NBO in (a) donates electron density into the non-Lewis NBO shown in (b). It is most likely that the electron density is donated by the overlap of the blue lobes of the two NBOs. Note that atoms 3 and 4 at the tips of the 'wings' of the C_{2v} isomer are separated by a distance of 4.488 Å.

minimum for the Bi_4 anion because its extra electron density will be donated into the antibonding orbital that pushes the T_d isomer into the C_{2v} isomer by splitting a Bi-Bi bond.

2.5 Conclusion

Two constitutional isomers of Bi_4 of T_d and C_{2v} symmetry were explored in this study. These two structures were found to be local minima while the D_{4h} and D_{2d} isomers were determined to be first-order saddle points. The optimized geometry of the T_d isomer can be fully described by the Bi-Bi interatomic radius, which is computed to be 2.965 Å and this leads to a more compact structure than reported in prior studies. The harmonic vibrational frequencies of the T_d isomer are computed to be, in general, larger than those of prior studies. The present research is the first to predict fundamental vibrational frequencies of Bi_4. The optimized geometry of the C_{2v} isomer computed in this research was found to be more compact than the geometry from a prior study,[30] while the two theoretical geometries have nearly identical conformational structures. The C_{2v} isomer is found to have higher harmonic vibrational frequencies in all modes but one, the ω_3 mode. The T_d and C_{2v} isomer energy difference was computed as +43 kcal mol^{-1}, with the T_d isomer being lower in energy. The dissociation of Bi_4 (T_d) into two Bi_2 molecules was computed to have an energy of +79 kcal mol^{-1}. Through NBO analysis, the C_{2v} isomer of Bi_4 was found to exhibit 'long-bonding' between the furthest apart 'wing' atoms. This 'long-bonding' is facilitated by the σ-bonding orbital between the 'spine' atoms of the C_{2v} isomer.

Finally, we point to the obvious way to spectroscopically observe the bismuth tetramer. The t_2 symmetry ν_3 fundamental predicted at 130 cm^{-1} has a moderate IR intensity, namely 0.20 km mol^{-1}. This Bi_4 fundamental is well separated from the previously observed Bi_2 (173 cm^{-1}) and Bi_3 (161, 163 cm^{-1}) vibrational frequencies.

CHAPTER 3

SUBSTITUTED ORTHO-BENZYNES: PROPERTIES OF THE TRIPLE BOND

3.1 Abstract

Ortho-benzyne has been well studied by both experiment and theory. Its substituted variants, however, have been less carefully examined. Benchmark data is computed for unsubstituted *ortho*-benzyne using several DFT functionals and basis sets, up to cc-pVQZ. Optimized geometries for the substituted *ortho*-benzyne as well as harmonic vibrational frequencies and singlet-triplet splittings are computed using the benchmarked functionals. A proximal (*syn*)OH substitution causes a mean θ_1 distortion of $+8.1 \pm 1.4^\circ$ from *ortho*-benzyne. Substituting in the proximal position with F shifts the singlet-triplet splitting by $+4.5 \pm 0.4$ kcal mol^{-1} from *ortho*-benzyne. Natural bond orbital (NBO) analysis, including Natural Coulomb Electrostatics (NCE), elucidates the presence of three influences from the selected substituents: hyperconjugative, resonance, and electrostatic effects.

3.2 Introduction

Ortho-benzyne, sketched in Figure 3.1, is of great interest to both experimental and theoretical chemists. Considerable research has been conducted on *ortho*-benzyne's properties such as its triple bond length,[71] triple bond stretching vibrational frequency,[72] dipole moment,[73] and electronic singlet-triplet splitting (Δ_{S-T}). The parent benzyne's singlet-triplet splitting has been well categorized by experiment[72] and is often used as a benchmark for multireference electronic structure theories.[74–76] Insufficient theoretical research, however, has been conducted to determine properties for substituted *ortho*-benzynes. It is well-known that substituents can have a variety of effects upon aromatic systems, electron density withdrawal and donation, being two. Therefore, the electronic properties of substituted *ortho*-benzyne should be better understood and will be the subject of the present research.

In the 1980s, a controversy arose regarding the spectroscopic assignment of the *ortho*-benzyne triple bond stretching frequency ($\nu_{C\equiv C}$). Four independent matrix isolation experiments[77–81] detected an IR band of approximately 2080 cm^{-1} and assigned this band to the $\nu_{C\equiv C}$ stretching mode. This assignment was bolstered by a normal mode analysis, which employed a mix of theoretical and experimental force constants (some coming from benzene) on top of a computationally determined geometry to predict the *ortho*-benzyne frequencies.[82,83] However, in 1986, Leopold, Miller, and Lineberger[72] (LML) detected a very different band at 1860 cm^{-1} using Negative Ion Photoelectron Spectroscopy (NIPES) and subsequently assigned this band to $\nu_{C\equiv C}$. In 1989, Scheiner and coworkers[84] computationally studied *ortho*-benzyne at the TCSCF/DZ+P and MP2/DZ+P levels of theory. They computed harmonic stretching frequencies for the triple bond ($\omega_{C\equiv C}$) of 1922 and 1931 cm^{-1} for each level of theory, respectively, lending very strong support to the controversial

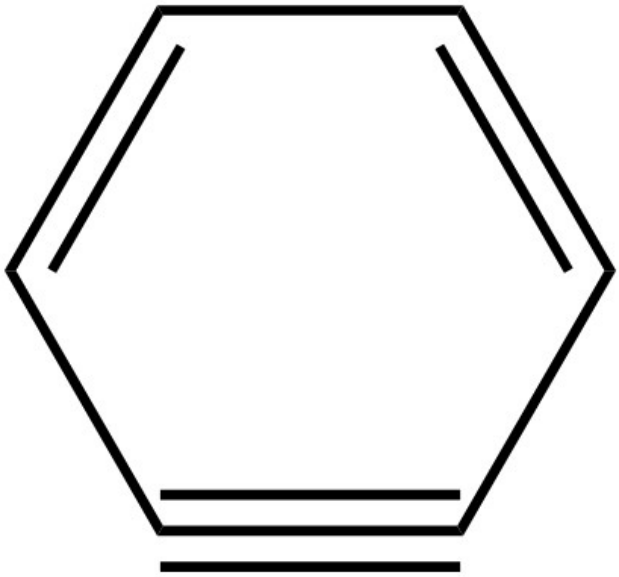

Figure 3.1: The *ortho*-benzyne molecule.

assignment made by LML. In 1991, Scheiner and Schaefer[85] solidified this assignment at the MP2/TZ+2P level of theory, yielding a stretching frequency of 1943 cm^{-1}. Kraka and Cremer[73] obtained the geometry of *ortho*-benzyne at the CCSD(T)/6-31G(d,p) level of theory. In a later paper by Ellison and coworkers,[86] the thermal dissocation of *ortho*-benzyne was studied experimentally and computationally. They found the dissociation energy of *ortho*-benzyne into acetylene and diacetylene to be 57 ± 3 kcal mol^{-1} using an experiment/theory hybrid method and 52.4 ± 0.5 kcal mol^{-1} at the CCSDT(Q)/CBS//CCSD(T)-AE/cc-pCVQZ level of theory via focal point extrapolation with additive corrections for non-correlation effects. In a recent joint experiment/theory study, Kleinpeter and Koch showed that *ortho*-benzyne has greater acetylenic than cumulenic character.[87]

Previous theoretical studies of the substituted variants of *ortho*-benzyne have mostly come from the groups of Cramer[88–92] and Garg.[93–103] Garg's group has performed many experimental/theoretical hybrid studies on these systems. Cramer primarily focuses on the quantities of the biradical stabilization energy and the singlet-triplet splitting. Johnson and Cramer[90] studied the impact on the aforementioned properties of a single hydroxyl substitution on the *ortho*-benzyne ring. They found that a hydroxyl substitution one carbon away from the triple bond yielded larger Δ_{S-T} values than substituting two carbons away. Additionally, they studied the different rotamers of the hydroxyl groups and found the rotamers that were *syn* to the triple bond tended to increase the splitting, in most cases by a small amount. In a paper published just one year later, Johnson and Cramer[89] studied the impact of a single substitution of cyano or aniline groups upon the same properties. They found that substitution at the distal position has little to no impact upon these properties; however, substitution at the proximal position to the triple bond increases the singlet-triplet splitting by

0–3 kcal mol^{-1} for both substituents. In a paper studying 2,3-didehydro-1,4-benzoquinone,[88] Cramer found a significant increase in Δ_{S-T} relative to unsubstituted *ortho*-benzyne of about +10 kcal mol^{-1}. Cramer additionally studied the bicyclic didehydronaphthalenes and didehydroindenes.[91,92] The former exhibited a ± 2 kcal mol^{-1} deviation of Δ_{S-T}, depending on the location of the triple bond, and the latter exhibited little to no deviation.

Table 3.1: Benchmark data for *ortho*-benzyne

$r_{C\equiv C}$ (Å)[71]	$\theta_{C-C\equiv C}$ (°)[71]	$\nu_{C\equiv C}$ (cm^{-1})[72]	Δ_{S-T}(kcal mol^{-1})[72]
1.264	126.1	1860	37.7(6)

Within synthetic organic chemistry there are four main subgroups of reactions in which *ortho*-benzyne is a vital intermediate. These are the nucleophilic addition, σ-bond insertion, [4 + 2]- and [2 + 2]-cycloaddition,[104] and metal-catalyzed aryne reactions. Tadross and Stoltz have written an extensive review on these classes of aryne reaction,[105] so they will not be discussed further here. In their 2018 paper, Hemberger and coworkers examined the products of high temperature *ortho*-benzyne self-reactions and detected various polycyclic aromatic hydrocarbons (PAHs) via Infrared and Photoelectron Spectroscopy.[106] *Ortho*-benzyne has also been identified as a PAH precursor in cold reaction regimes, an important factor for astronomical chemistry.[107,108]

Some experimental studies have been performed on substituted variants of *ortho*-benzyne. *Ortho*-benzyne may be experimentally synthesized by a plethora of schemes.[109,110] Therein, *o*-(trimethylsilyl)aryl triflate elimination has been a recent favorite,[111] with several containing a substituted *ortho*-benzyne variant as either a product or an intermediate. Garg has performed experimental/theoretical hybrid studies[93–103] exploring the reactivity of substituted *ortho*-benzynes, correlating nucleophilic attack with the bond angles on each of the triple bonded carbons. Hoye and coworkers showed that *ortho*-quinone methides may be synthesized via a thermally generated and fully substituted *ortho*-benzyne derivative.[112] In their 2020 paper, Li and coworkers elucidate the synthetic versatility of 1,2-benzdiyne, which relies heavily upon a singly substituted *ortho*-benzyne intermediate, to synthesize multifunctionalized aromatic systems.[113]

In the present research, six substituents have been selected to study the impact of substitution upon the *ortho*-benzyne triple bond. These are $-CN, -CF_3, -SF_5, -F, -OH$, and $-OCH_3$. Additionally, the $-OH$ and $-OCH_3$ species have two different rotamers that will be analyzed; *syn* and *anti*, where *syn* points towards the triple bond and *anti* away. These six substituents were chosen due to their simplicity, inductive strength, and relevance in the organic chemistry literature. Figure 3.2 shows the substitution positions, carbon indices, and angle labels that will be used throughout this work.

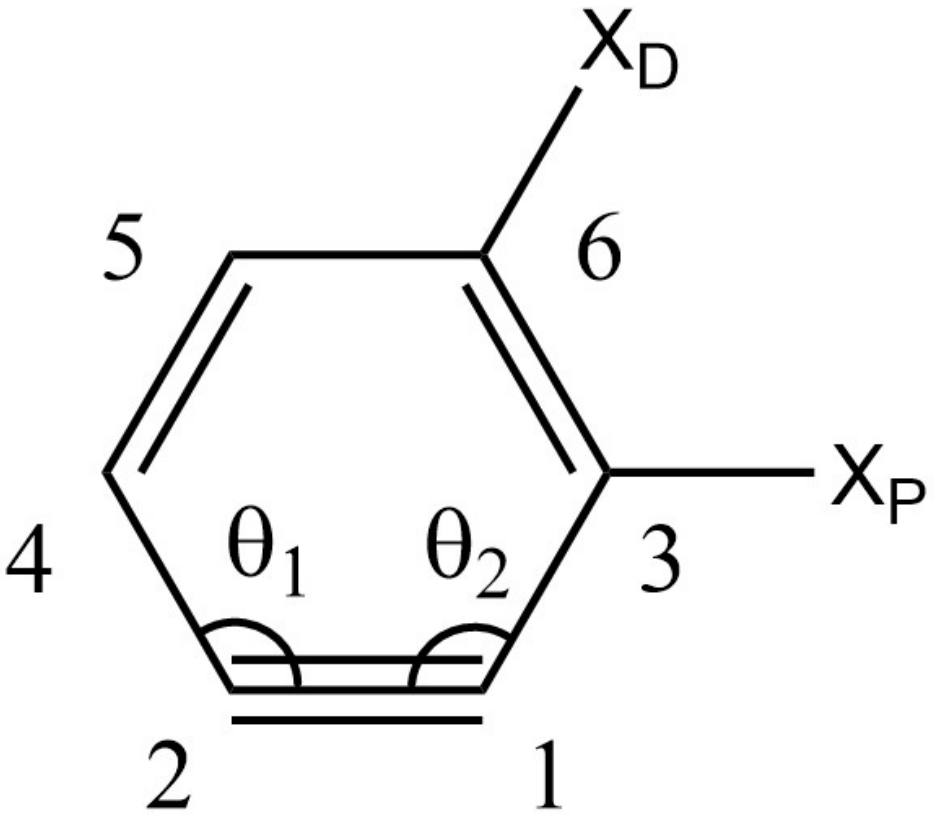

Figure 3.2: A general labeling scheme for substituted *ortho*-benzynes.

3.2.1 Computational Choices

The Psi4 quantum chemical software package[114] was utilized for most of the computations performed in this research. Correlation consistent double-ζ through quadruple-ζ [cc-pV(D-Q)Z][115] basis sets were used for the benchmarking of the functionals. The cc-pVDZ basis set was used for the computation of equilibrium geometries, harmonic vibrational frequencies, and properties of the substituted variants of *ortho*-benzyne.

In their important 2017 paper,[116] Grimme and coworkers, using their GMTKN55 benchmark database, ranked many of the popular functionals from various rungs of the famous DFT "Jacob's Ladder."[117] Among the highest rung of "Jacob's ladder", reserved for functionals with "exact exchange and exact partial correlation" according to the nomenclature specified in the 2001 Perdew and Schmidt paper, it was found that the DSD-BLYP,[118] DSD-PBEB95,[119] and DSD-PBEP86[120] functionals were particularly accurate. On the next rung down, the ωB97X-V[121] and M05-2X[122] functionals were found to be the the most accurate. These five functionals as well as B3LYP[123] and BP86,[124,125] due to their common use, were selected for this study. Coupled cluster singles, doubles and perturbative triples[45,46] [CCSD(T)] computations were performed for the benchmark properties using the Molpro 2010.1 quantum chemical software package.[48]

Gradients were computed for the geometric optimization of the structures. Psi4 has analytic gradients for the M06-2X, BP86, and B3LYP functionals, but not for the DSD-BLYP, DSD-PBEB95, DSD-PBEP86, or ωB97X-V functionals. Non-analytic gradients were computed by a 3-point finite differences of energy scheme with a 5×10^{-3} Å displacement size. In general, the geometries were converged to a max force of 3.0×10^{-4} atomic force units along all internal coordinates. Hessians were computed by a 3-point finite difference of energies formula with a 5×10^{-3} Å displacement size.

3.2.2 Benchmarking

Density functional theory (DFT) will be utilized to study the electronic structure of these systems. Several functionals have been benchmarked against the well established experimental data for unsubstituted *ortho*-benzyne. This allows for the selection of functionals that best describe the desired properties.

The *ortho*-benzyne reference data for the properties to be benchmarked is seen in Table 3.1. The reference bond length and angle were obtained by Kukolich et al.[71] via microwave spectroscopy. Any computed equilibrium bond distances ought to be shorter than the experimental value due to the vibrationally averaged nature of the bond resulting from the anharmonicity of the experimental molecular potential. The stretching frequency of the aforementioned bond, labeled in Table 3.1 as $\nu_{C\equiv C}$, was measured by Lineberger et al.[72] via NIPES (Negative Ion Photoelectron Spectroscopy). The Δ_{S-T} value was determined by Lineberger et al. in the same study as the stretching frequency utilizing the same spectroscopic method.

In Figure 3.3(a) the *ortho*-benzyne C≡C bond length has been computed and compared to the selected experimental bond length in Table 3.1. Of the three basis sets, cc-pVDZ appears to most closely approximate the benchmarked value across all seven functionals tested. There is a contraction of the bond length for all functionals as the size of the basis set increases. It may be that the larger basis sets are more accurate for some functionals as the computed bond lengths are equilibrium values whereas the experimental value is calculated from rotational constants which inherently hold anharmonic vibrational averaging in the structure. While a study on the anharmonics of this species would elucidate the basis set dependence of the bond length, such research is beyond the scope of this work. The MP2 influence on the DSD functionals is apparent, as each value is positively shifted compared to the other functionals. The MP2 and CCSD(T) levels of theory offer highly similar triple bond lengths. Four functionals show minor deviations from the benchmark value, these being DSD-BLYP, BP86, DSD-PBEB95, and DSD-PBEP86. Surprisingly, the lowest Jacob's ladder functional of the four, BP86, shows the closest agreement to the benchmark value across all three basis sets.

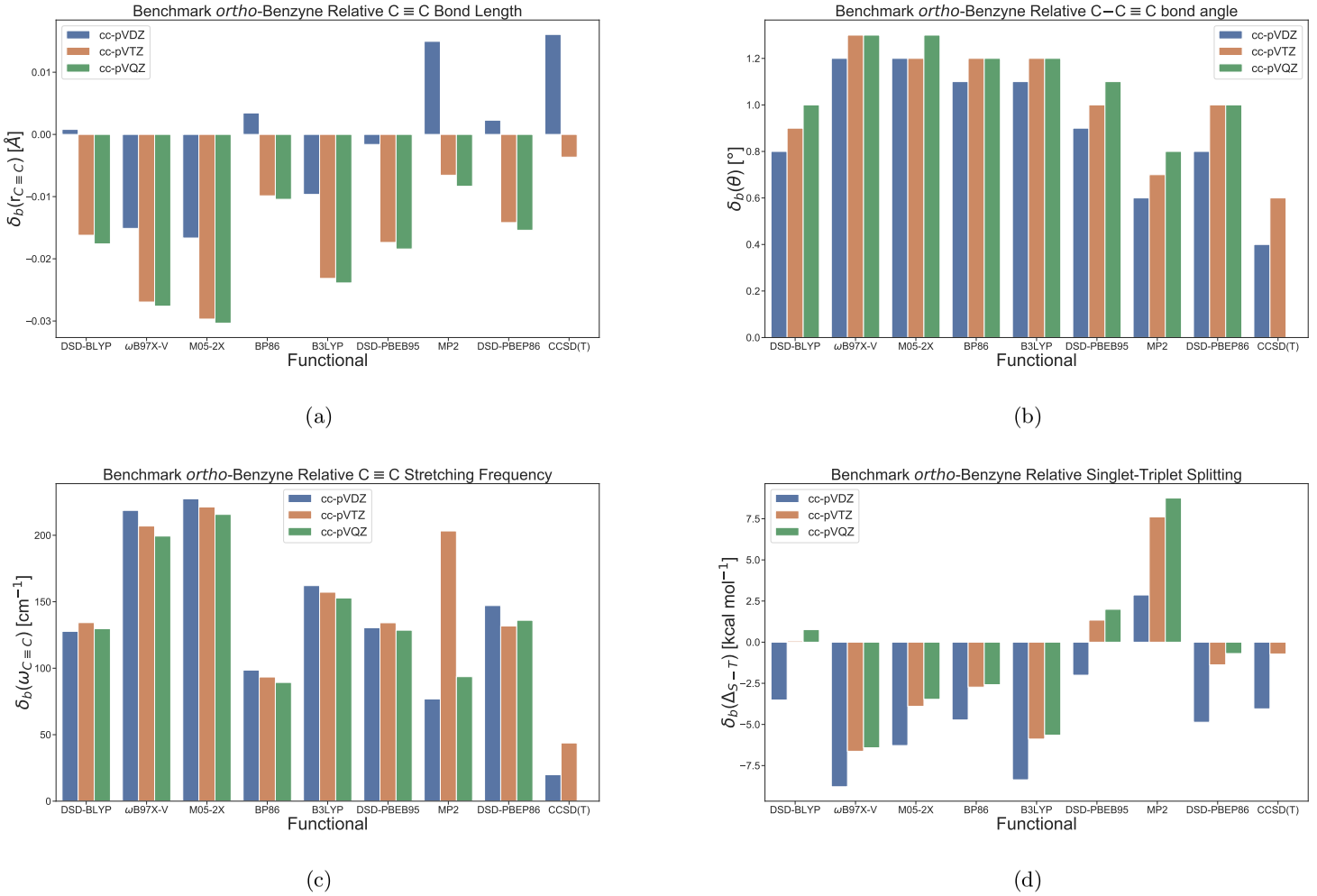

Figure 3.3: These four subfigures report our computed properties of *ortho*-benzyne relative to the corresponding propery reference data seen in Table 3.1 (denoted as δ_b). (a) The relative computed triple bond lengths. (b) The relative computed triple bond angles. (c) The relative computed triple bond harmonic stretching vibrational frequency. (d) The relative computed singlet-triplet splitting.

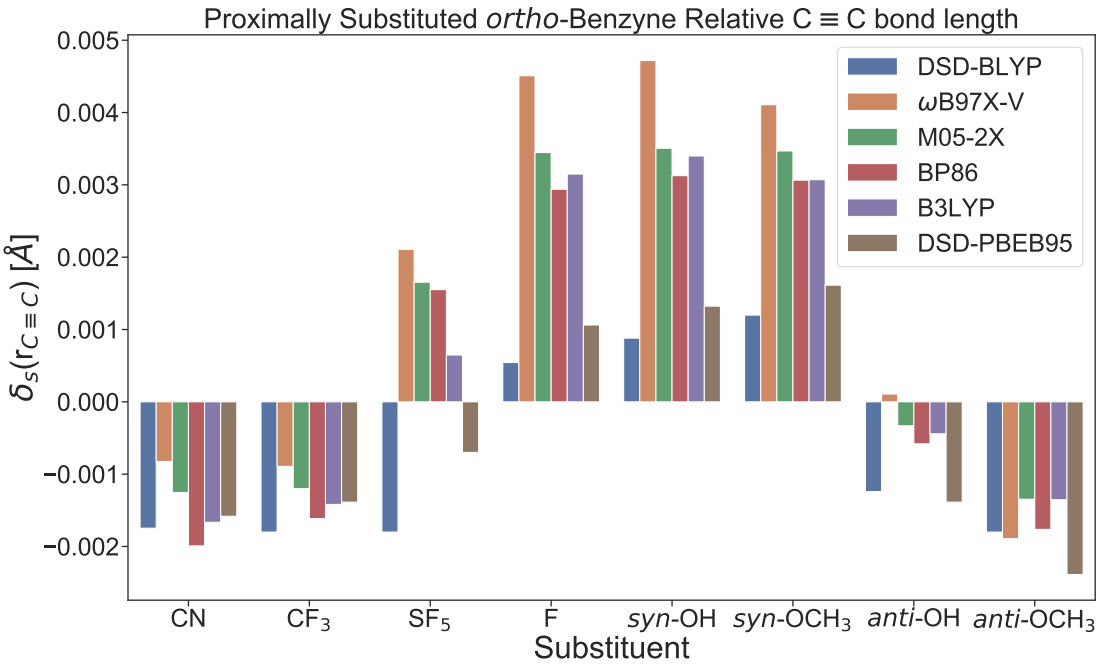

Figure 3.4: The computed triple bond lengths for each substituent and functional, using the cc-pVDZ basis set, relative to the unsubstituted *ortho*-benzyne results at the same level of theory for each entry (designated as δ_s).

In Figure 3.3(b) the *ortho*-benzyne C−C≡C bond angle has been computed and compared to the selected experimental bond angle in Table 3.1. Across the seven functionals there is a general trend of increasing positive deviation as the basis set increases in size, with cc-pVDZ again being in best agreement with the benchmark entry. The DSD-BLYP, DSD-PBEB95, and DSD-PBEP86 functionals provide a slightly better estimate of this bond angle than the other four functionals; however, the difference is marginal. The MP2 influence on these three functionals is apparent as their data sets are negatively shifted. The MP2 method yields the bond angles closest to the CCSD(T) results. In general, the computed bond angles predict a deviation towards linearity at carbons 1 and 2 of approximately 1°. Anharmonic effects were not taken into account for these computations, so the systematic positive deviation could be due to their absence.

In Figure 3.3(c) the harmonic C≡C stretching frequency has been computed and compared to the selected experimental frequency in Table 3.1. The frequency benchmarking results follow similar trends in the bond length, with four functionals showing the best performance and three showing larger deviations. However, it should be noted that anharmonic corrections would most likely not be sufficient to account for the large magnitude of positive deviation that these harmonic frequencies hold relative to the experimental value. The computed CCSD(T) harmonic frequencies are the closest to the experimental value of the methods used

in this benchmark. It is likely that a CCSD(T)/CBS triple bond frequency would closely approximate the experimental value with added anharmonic corrections. The frequencies reported in this work should not be used quantitatively; however, they may still be used to gain qualitative insight.

In Figure 3.3(d) the *ortho*-benzyne singlet-triplet splitting has been computed and compared to the selected experimental singlet-triplet splitting in Table 3.1. These results show that the cc-pVTZ basis set provides the most accurate estimates of the singlet-triplet splitting. The three DSD functionals most accurately capture the splitting, with the DSD-BLYP/cc-pVTZ method performing remarkably well. These three DSD functionals show good agreement with the CCSD(T) splittings, lending them greater credence. The MP2 within the DSD functionals appears to cause a positive shift in singlet-triplet splitting, following from the MP2 results. BP86 is the next best performing functional across the three basis sets and the other three functionals exhibit similar negative deviations.

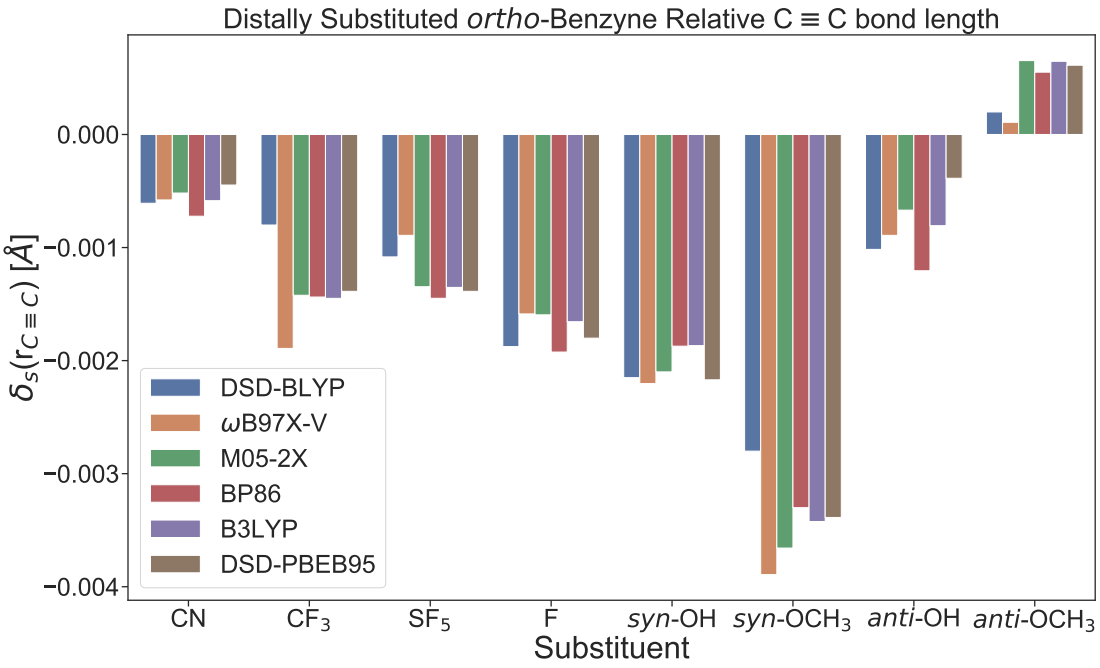

Figure 3.5: The computed triple bond lengths for each substituent and functional, using the cc-pVDZ basis set, relative to the unsubstituted *ortho*-benzyne results at the same level of theory for each entry (designated as δ_s).

The cc-pVDZ basis set will be used for the rest of this study as it is the computationally cheapest of the three and provides reasonably accurate results for the desired properties. When substituting with SF_5, a double ζ basis set with added tight d functions [cc-pVDZ(+d)] is assigned to the sulfur atom. The seven functionals have been trimmed down to six, as the DSD-PBEP86 functional was found to be redundant to

the two other DSD functionals. Additionally, zero-point vibrational energy (ZPVE) values were computed for all singlet-triplet splitting data in this work; however the splittings were never found to vary more than 1 kcal mol^{-1} on account of these corrections. When comparing the pre and post substituted *ortho*-benzyne variants, the ZPVEs will mostly cancel out, further reducing their impact.

3.3 Results

The following labeling scheme will be used to designate the position at which each *ortho*-benzyne variant has been substituted. Substituents located one carbon away from the carbon-carbon triple bond will be designated as proximal (P) and those that are two carbons away will be designated as distal (D). The two bond angles relevant to the triple bond are labeled as θ_1 (carbons 4, 2, and 1) and θ_2 (carbons 2, 1, and 3). A visualization of this labeling scheme is presented in Figure 3.2. Additionally, the hydroxyl substituents will have varying rotamers and these will be designated as either *syn* or *anti*, denoting whether the hydroxyl hydrogen is pointing towards the triple bond for the former and away from the triple bond for the latter. The same labels are used for the methoxy species. *Ortho*-benzyne has C_{2v} symmetry and so the substitution positions will be invariant under a C_2 rotation.

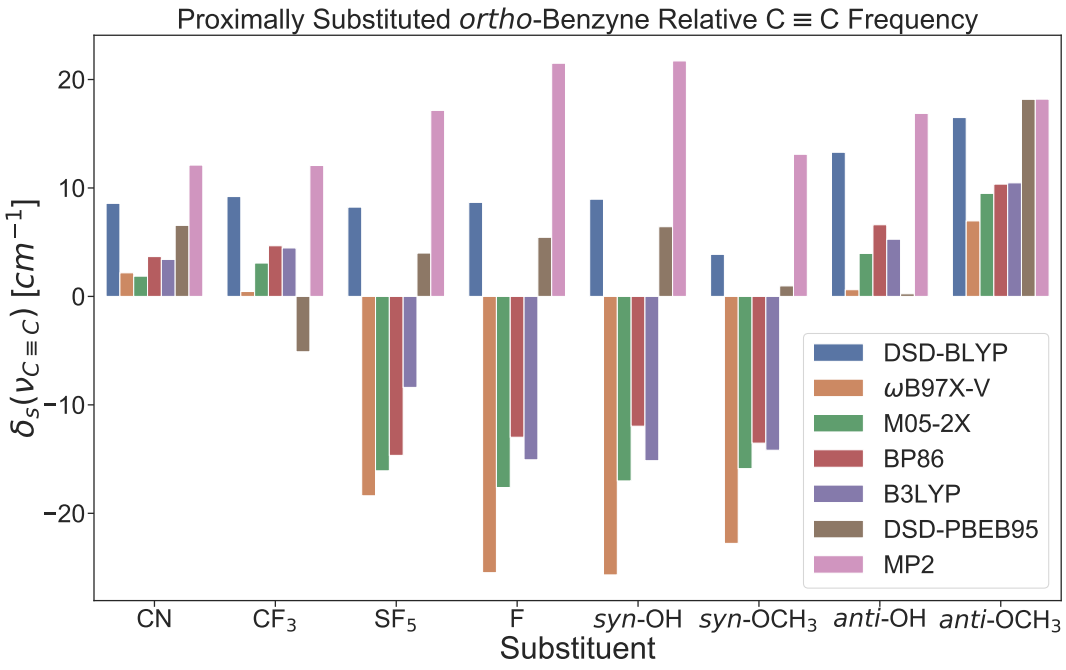

Figure 3.6: Computed triple bond stretching vibrational frequencies for each substituent and functional, using the cc-pVDZ basis set, relative to the unsubstituted *ortho*-benzyne results at the same level of theory for each entry (designated as δ_s).

3.3.1 Substituted Triple Bond Length

The carbon-carbon triple bond lengths, relative to the unsubstitued parent, shown in Figure 3.4, exhibit a trend of expansion moving from left to the middle. The CN and CF_3 proximal substitutions cause mean triple bond deviations from *ortho*-benzyne of $-1.5 \pm 0.4 \times 10^{-3}$ Å and $-1.4 \pm 0.3 \times 10^{-3}$ Å. The shape formed by the six different functionals is highly similar between these two substituents. The F, (*syn*)OH, and (*syn*)OCH_3 substituents exhibit mean triple bond deviations of $+2.6 \pm 1.5 \times 10^{-3}$ Å, $+2.8 \pm 1.4 \times 10^{-3}$ Å, and $+2.8 \pm 1.1 \times 10^{-3}$ Å, respectively. In the same fashion as with the prior two substituents, this trio of substituents has the same functional deviation structure. The SF_5 substituent has a bit more complicated deviation structure, as the DSD functionals exhibit a bond contraction, and the other four a bond expansion. Overall this substituent causes a mean bond length deviation of $+0.7 \pm 1.4 \times 10^{-3}$ Å. The (*anti*)OH and (*anti*)OCH_3 substituents exhibit mean deviations of the triple bond of $-0.6 \pm 0.6 \times 10^{-3}$ Å and $-1.8 \pm 0.4 \times 10^{-3}$ Å. The shape of the *anti* rotamers data resembles that of the CN and CF_3 substituents more than the *syn* rotamers.

The relative carbon-carbon triple bond lengths shown in Figure 3.5 exhibit a weak trend of contraction moving from the left to the middle. These distances are more noisy than those of the proximally substituted bond length deviations. The CN and CF_3 substituents exhibit mean bond length deviations of $-0.6 \pm 0.0 \times 10^{-3}$ Å and $-1.4 \pm 0.3 \times 10^{-3}$ Å. This pair of substituents has a marginal effect on the triple bond length in the distal position. The F, (*syn*)OH, and (*syn*)OCH_3 substituents exhibit mean bond length deviations of $-1.7 \pm 0.1 \times 10^{-3}$ Å, $-2.1 \pm 0.2 \times 10^{-3}$ Å, and $-3.4 \pm 0.4 \times 10^{-3}$ Å, respectively. The SF_5 substituent data have mean deviations of $-1.3 \pm 0.2 \times 10^{-3}$ Å. The distal SF_5 deviations resemble the mean of CN, CF_3, F, and (*syn*)OH quite closely. The (*anti*)OH and (*anti*)OCH_3 substituents exhibit mean deviations of $-0.8 \pm 0.3 \times 10^{-3}$ Å and $+0.5 \pm 0.2 \times 10^{-3}$ Å. Rotating the OH and OCH_3 groups appears to "turn off" their albeit modest effects on the triple bond length. There is generally a reduced impact upon the triple bond from distal substituents, due to their greater distance from the bond.

3.3.2 Substituted Triple Bond Frequency

An opposite trend to that of the proximally substituted triple bond lengths is observed for the triple bond stretching frequency relative deviations, displayed in Figure 3.6, with the frequency deviation becoming more negative moving from the left to the middle. The CN and CF_3 substituents exhibit mean frequency deviations of $+4.4 \pm 2.6$ cm^{-1} and $+2.8 \pm 4.8$ cm^{-1}. The F, (*syn*)OH, and (*syn*)OCH_3 substituents exhibit mean frequency deviations of -9.5 ± 13.5 cm^{-1}, -9.1 ± 13.8 cm^{-1}, and -10.3 ± 10.4 cm^{-1}, respectively. The SF_5 substituent has a mean frequency deviation of -7.5 ± 11.2 cm^{-1}. The (*anti*)OH and (*anti*)OCH_3

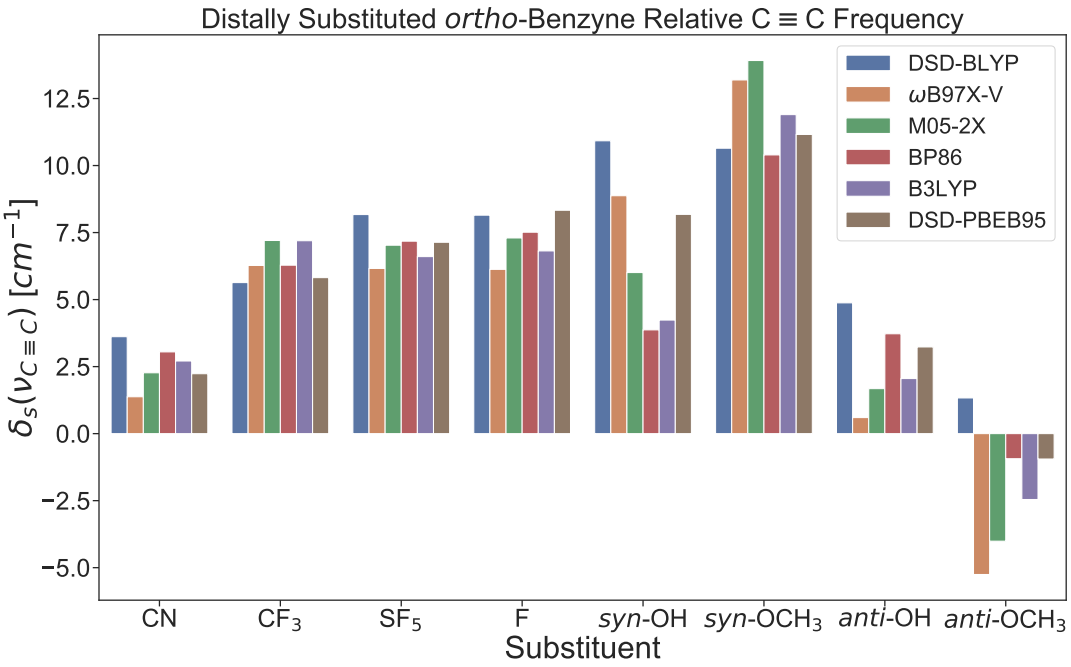

Figure 3.7: Computed triple bond stretching vibrational frequencies for each substituent and functional, using the cc-pVDZ basis set, relative to the unsubstituted *ortho*-benzyne results at the same level of theory for each entry (designated as δ_s).

substituents exhibit mean frequency deviations of +5.0 ± 4.8 cm^{-1} and +12.0 ± 4.4 cm^{-1}.

The distally substituted triple bond stretching frequencies, displayed in Figure 3.7, are affected in the expected manner. As the triple bond contracts, the frequency increases. The CN and CF_3 substituents exhibit mean frequency deviations of +2.5 ± 0.8 cm^{-1} and +6.4 ± 0.7 cm^{-1}. The F, (*syn*)OH, and (*syn*)OCH_3 substituents exhibit a mean frequency deviation of +7.4 ± 0.8 cm^{-1}, +7.0 ± 2.8 cm^{-1}, and +11.9 ± 1.4 cm^{-1}, respectively. The SF_5 substitution has a mean frequency deviation of +7.0 ± 0.7 cm^{-1}. The (*anti*)OH and (*anti*)OCH_3 substituents exhibit mean frequency deviations of +2.7 ± 1.5 cm^{-1} and −2.0 ± 2.4 cm^{-1}.

The proximal substituent frequency deviations are largely unsurprising when compared to their analogous bond length deviation results. These deviations follow Badger's rule, which states that as the strength of a bond increases, the stretching frequency of that bond will increase and vice versa. The triple bond length and strength correlate inversely to each other. What is strange is the counter trend exhibited by the DSD functionals. The cause of these countertrend deviations is appears to be the inclusion of MP2 in the double hybrid portion of the DSD functionals. MP2 has been known to struggle with the description of diradical systems such as *ortho*-benzyne and this is certainly true for the stretching frequency of the substituted

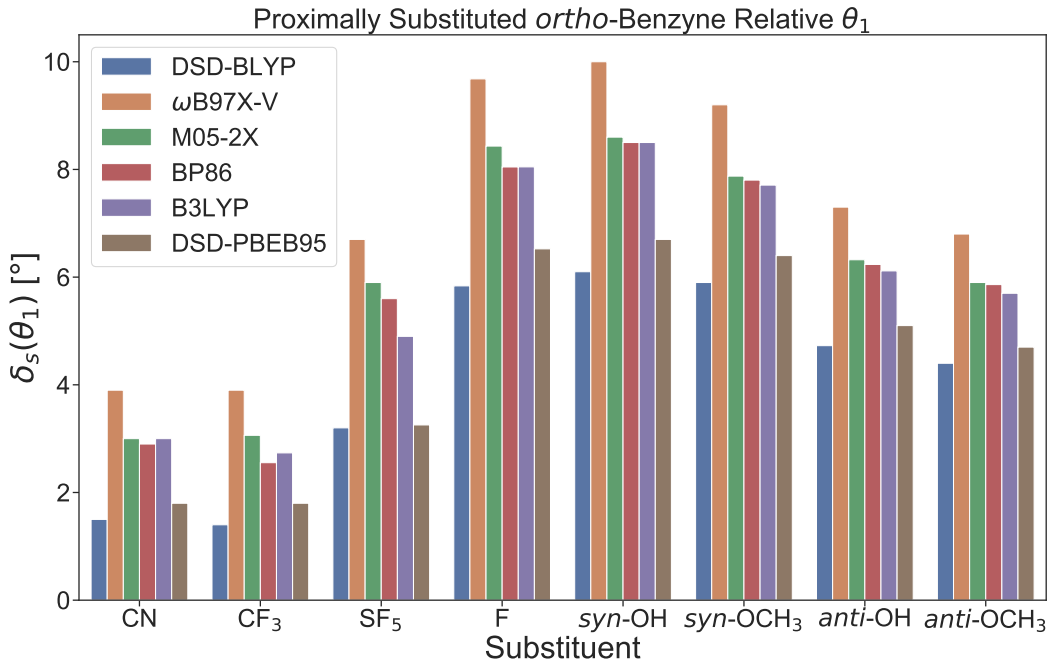

Figure 3.8: Computed $C_4{-}C_2 \equiv C_1$ bond angle for each substituent and functional, using the cc-pVDZ basis set, relative to the unsubstituted *ortho*-benzyne results at the same level of theory for each entry.

species. The DSD functionals exhibit varying trends, but in general, they are qualitatively similar to the MP2 results for these species. The distal substituent frequency deviations show no major differences from their analogous bond length deviation trends.

3.3.3 Substituted Bond Angles

The deviation in the θ_1 bond angle becomes more positive as the graph in Figure 3.8 runs to the right, following a similar trend to the previous properties. The CN and CF_3 substituents exhibit mean angle deviations of $+2.7 \pm 0.9°$ and $+2.6 \pm 0.9°$. The F, (*syn*)OH, and (*syn*)OCH_3 substituents exhibit larger mean angle deviations of $+7.8 \pm 1.4°$ $+8.1 \pm 1.4°$ and $+7.5 \pm 1.2°$, respectively. The SF_5 substituent has a mean angle deviation of $+4.9 \pm 1.4°$. The (*anti*)OH and (*anti*)OCH_3 substituents exhibit mean angle deviations of $+6.0 \pm 0.9°$ and $+5.6 \pm 0.9°$. Rotating these two substituents appears to dampen the angular distortion of the triple bond. The six different functionals show highly similar behavior relative to each other.

Houk and coworkers[101] have established that the change in bond angle correlates with a change in hybridization on carbon 2 as it gains more *s*-orbital character and loses *p*-orbital character. For the proximal substitutions, an equal but opposite bond angle deviation is exhibited by θ_2 (these results are available in

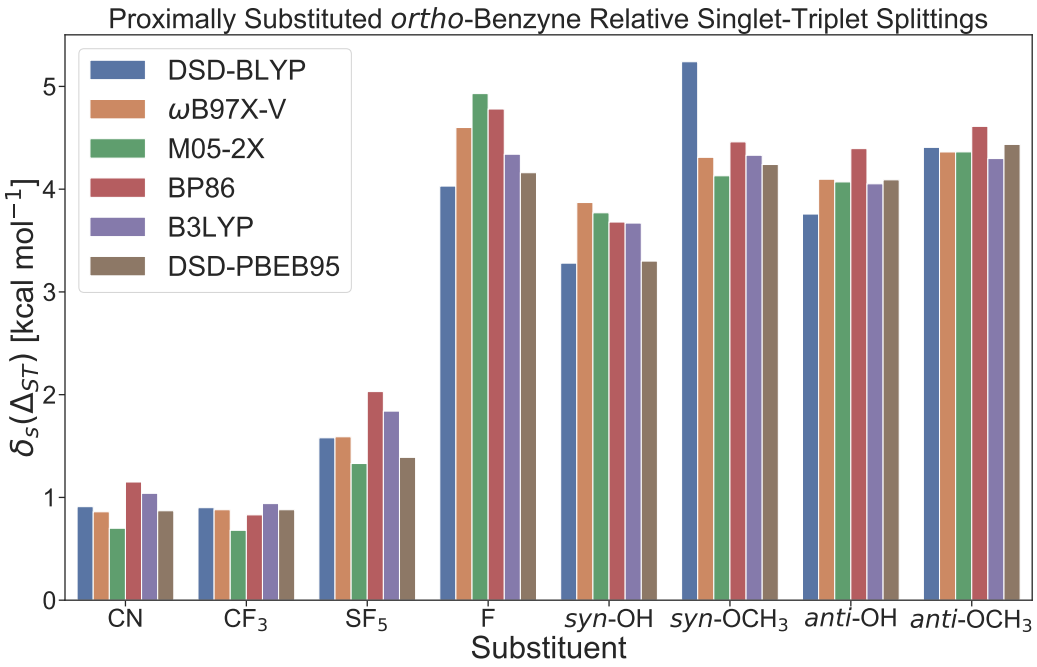

Figure 3.9: The computed singlet-triplet splittings for each substituent and functional, using the cc-pVDZ basis set, relative to the unsubstituted *ortho*-benzyne results at the same level of theory for each entry (designated as δ_s).

the supplemental information of this work). The negative deviations of θ_1 will correlate with a change in hybridization on carbon 1 as it gains more *p*-orbital character and loses *s*-orbital character. The *anti* species dampens the angle deviation, suggesting a connection to the polarizing electrostatic effect of the H and CH_3 groups. While this causes a bond polarization, not all of the negative charge exhibited by carbon 1 for the proximal F, OH, and OCH_3 species is contained within the in-plane π bond. Some electron density will be focused in the out-of-plane orbital on carbon 1 that contributes to the aromatic network. This is explained by the π-donating capability of these three substituents.

3.3.4 Substituted Singlet-Triplet Splitting

As is the case with the proximal triple bond length deviations, the proximal singlet-triplet splittings exhibit an increase in positive deviation moving from left to right of the graph shown in Figure 3.9. The CN and CF_3 substituents exhibit mean Δ_{S-T} deviations of $+0.9 \pm 0.2$ kcal mol^{-1} and $+0.9 \pm 0.1$ kcal mol^{-1}. The F, (*syn*)OH, and (*syn*)OCH_3 substituents exhibit mean Δ_{S-T} deviations of $+4.5 \pm 0.4$ kcal mol^{-1}, $+3.6 \pm 0.2$ kcal mol^{-1}, and $+4.4 \pm 0.4$ kcal mol^{-1}, respectively. The SF_5 substituent has a mean Δ_{S-T} deviation of $+1.6 \pm 0.3$ kcal mol^{-1}. The (*anti*)OH and (*anti*)OCH_3 substituents exhibit mean Δ_{S-T} deviations of +4.1

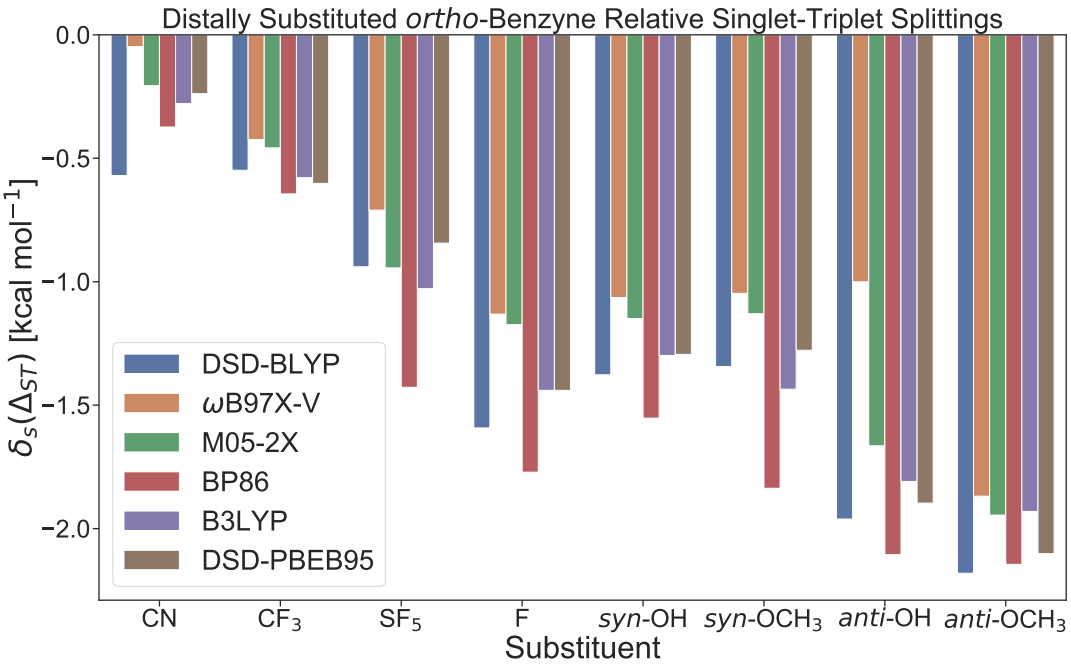

Figure 3.10: The computed singlet-triplet splittings for each substituent and functional, using the cc-pVDZ basis set, relative to the unsubstituted *ortho*-benzyne results at the same level of theory for each entry (designated as δ_s).

$\pm$ 0.2 kcal mol^{-1} and +4.4 $\pm$ 0.1 kcal mol^{-1}.

The singlet-triplet splitting does not seem to be significantly affected by the rotation of the OH or OCH_3 species. In fact, the element of the substituent attached at the proximal substitution site appears to have a greater significance. The increase in values from left to right in Figure 3.9 suggests that the proximal singlet-triplet splitting data roughly correlates with the electronegativity of the substituent atom connected to the ring.

The distal singlet-triplet splittings exhibit a slight increase in the negative deviation moving from left to right of the graph shown in Figure 3.10. The CN and CF_3 substituents exhibit mean Δ_{S-T} deviations of -0.3 $\pm$ 0.2 kcal mol^{-1} and -0.5 $\pm$ 0.1 kcal mol^{-1}. The F, (*syn*)OH, and (*syn*)OCH_3 substituents exhibit mean Δ_{S-T} deviations of -1.4 $\pm$ 0.2 kcal mol^{-1}, -1.3 $\pm$ 0.2 kcal mol^{-1}, and -1.3 $\pm$ 0.3 kcal mol^{-1}, respectively. The SF_5 substituent has a mean Δ_{S-T} deviation of -1.0 $\pm$ 0.2 kcal mol^{-1}. The (*anti*)OH and (*anti*)OCH_3 substituents exhibit mean Δ_{S-T} deviations of -1.8 $\pm$ 0.2 kcal mol^{-1} and -2.0 $\pm$ 0.1 kcal mol^{-1}.

The distal singlet-triplet splitting results exhibit an opposite but much more noisy trend compared to the proximal. Furthermore, distal substitution causes significantly smaller magnitude deviations than proximal. This again highlights the importance of proximity of substitution to the singlet-triplet splitting.

3.3.5 NBO Analysis

Many of the substitution effects may be rationalized by an analysis of the electron delocalization with respect to a lewis structure representation, as computed by the Natural Bond Orbital[126] (NBO) method. Electron delocalization will be discussed for each of the six substituents analyzed in this paper as well as their respective substitution positions and rotamers when pertinent. The magnitude of electron delocalization has been computed using the \$del[127] keyword within NBO 6.0. This keyword either fully fills a lewis orbital, or deletes all electron density from a non-lewis orbital that has been previously computed using NBO at a desired geometry and level of theory. After the electron density is modified, a single self-consistent field (SCF) cycle is computed and the resulting electron density is transformed back to natural bonding orbitals. This process causes a localization of electron density into NBOs. This density localization shows, in reverse, how the electron density flows from lewis orbitals towards non-lewis orbitals. So the localization and delocalization densities hold the same magnitudes with opposite signs, allowing the analysis of density localization to be sufficient to explain delocalization. The electron localization magnitudes have been computed using the NBO 7.0[126] software package in the GAMESS[128] package at the B3LYP/cc-pVDZ//B3LYP/cc-pVDZ level of theory. All electron density changes discussed will be in terms of atomic units of electronic charge.

CF_3 Substitution

For the CF_3 proximally substituted variant, the only significant localization energy deviation comes from the π^* C_1-C_2 bond. The π^* C_1-C_2 bond has a localization energy of -3.20 kcal mol^{-1}, relative to the unsubstituted parent, after an electron density deletion of -0.231 from this bond. The two out-of-plane $C-F$ σ^* bonds offer unique contributions to this delocalization and increase by $+0.005$ and $+0.004$. These contributions are quite small compared to the aromatic effects, however.

The CF_3 distally substituted variant doesn't have any relative localization energies above 2 kcal mol^{-1}. This is due to the increased distance of the CF_3 group from the triple bond.

SF_5 Substitution

The delocalization found by NBO for the SF_5 substitutions yields inconclusive results and furthermore did not exhibit any of the same delocalizations as the other substitutions.

CN Substitution

The CN proximal substition most strongly impacts the π^* C_1-C_2 bond, with an electron density change of -0.229 and localization energy of -4.84 kcal mol^{-1}, relative to the unsubstituted parent. The CN substituent

contributes to this change via the out-of-plane π^* C−N bond as it gains +0.026 electron density. This delocalization interaction between the C_1-C_2 and C−N π^*-bonds suggests that the CN distal substitution has the greatest impact on the π C_1-C_2 bond, yielding an electron density change of +0.343 and a relative localization energy of −3.72 kcal mol^{-1}. Two bonds from the CN group provide the greatest contributions, these being the out-of-plane π and π^* C−N bonds with electron density changes of −0.013 and −0.019, respectively. The CN substituent is a known π electron acceptor and this is exemplified in its effects on the *ortho*-benzyne triple bond.

F Substitution

The F proximally substituted variant has one component of the triple bond with significant deviation, relative to the unsubstituted parent, the localization of the $\sigma(2)$ C_1-C_2 bond. This bond has a localization energy of +9.28 kcal mol^{-1}, relative to the unsubstituted parent, and causes an electron density change of −0.041 in the σ^* C−F bond, accounting for approximately 40% of the electron delocalization of the $\sigma(2)$ bond. The out-of-plane F electron lone pair has a modest effect on the aromatic system, changing by −0.020 when the π C_1-C_2 bond localizes with an electron density change of +0.307.

The F distal substitution primarily impacts the triple bond through the out-of-plane F lone pair interaction with the aromatic π system. When the π C_1-C_2 bond is localized the F lone pair contributes −0.015, whereas deleting the π^* C_1-C_2 bond pushes +0.015 to the F lone pair.

It is clear that hyperconjugation of the C−F antibond with the triple bond has a large impact on the proximal variant due to the delocalization of $\sigma(2)$ into the C-F σ^* bond. The proximal variant has an atomic charge, relative to the unsubstituted parent, on carbon 2 of +0.10, supporting the hyperconjugation hypothesis. Both the proximally and distally substituted species experience π electron donation from the lone-pairs of the fluorines.

OH Substitution

Substituting at the proximal position with a *syn* OH group most significantly effects the localization of the $\sigma(2)$ and π C_1-C_2 bonds, with relative localization energies of +6.51 and −5.43 kcal mol^{-1}, respectively. The $\sigma(2)$ bond electron density increased by +0.093 upon localization, with a major contribution from the σ^* C−O bond of −0.029. This interaction suggests the presence of cationic hyperconjugation between these bonds. When the C_1-C_2 π bond is localized it increases in electron density by +0.286 with a moderate contribution of −0.039 from the out-of-plane oxygen lone pair.

When an *anti* OH group is substituted into the proximal position, the triple bond feels largely the same effects as the *syn* proximal substitution. A notable deviation is present between the relative localization

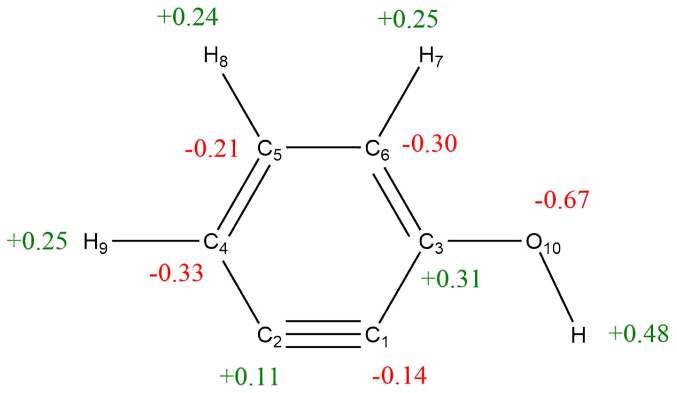

(a)

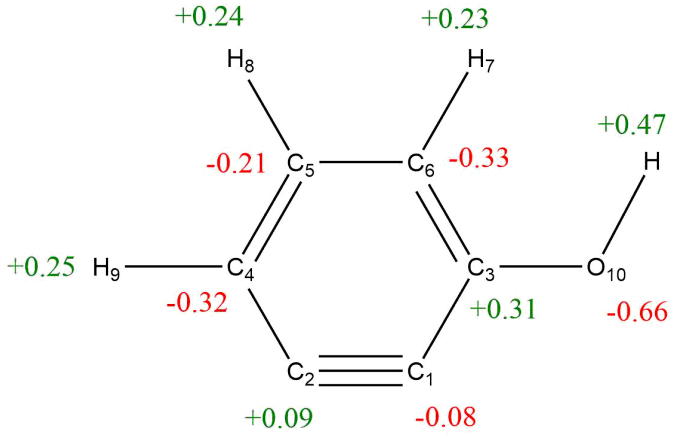

(b)

Figure 3.11: (a) The natural charges of the *syn* − OH proximally substituted *ortho*-benzyne molecule relative to the unsubstituted parent. (b) The natural charges of the *anti* − OH proximally substituted *ortho*-benzyne molecule relative to the unsubstituted parent.

energy of the C_1-C_2 $\sigma(2)$ bond for the *syn* and *anti* rotamers, +6.51 and +4.94 kcal mol^{-1}, respectively. The σ^* C−O bond contributes −0.028 electron density towards the C_1-C_2 $\sigma(2)$ bond, a slightly smaller contribution than the *syn* rotamer.

Natural Coulombic Electrostatics[129] (NCE) were computed for the *syn* and *anti* proximally substituted species. NCE allows for the change in atomic charges between the electronic Lewis structure and the delocalised electronic structure to be quantified. For the *syn* rotamer, carbons 1 and 2, and the hydroxyl hydrogen hold Lewis atomic charges of −0.15, +0.13, and +0.49, respectively. Upon delocalization these atomic charges change by +0.01, −0.01, and −0.01, respectively. The *anti* rotamer has analogous atomic lewis charges of −0.10, +0.09, and +0.48. When delocalized these charges vary by +0.02, +0.01, and −0.01. There is a small but significant difference in charges between these rotamers that cannot be explained by delocalization effects. This difference of charges is most likely due to an electrostatic interaction between the hydroxyl hydrogen and the carbons, increasing the polarization of the $\sigma(2)$ bond. The delocalized atomic

charges are displayed in Figure 3.11.

Both the distal *syn* and *anti* distal OH substitutions experience aromatic contributions from the oxygen lone pairs. An electron density change of -0.027 on the oxygen lone pair lightly contributes to the $+0.298$ density change of the π bond upon localization in the *syn* rotamer. The *anti* rotamer gets -0.024 from the oxygen lone pair upon localization of the π bond, which has a density change of $+0.311$.

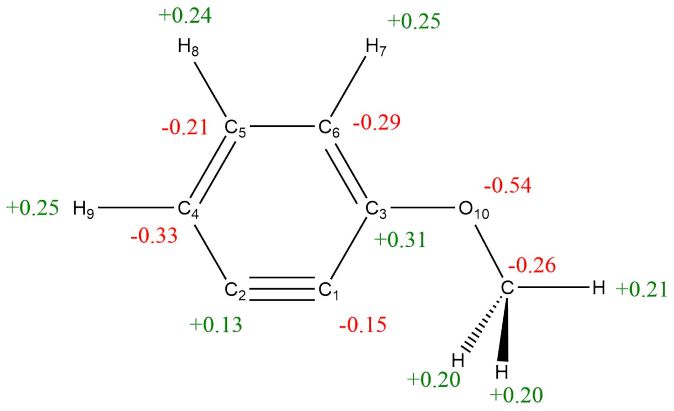

(a)

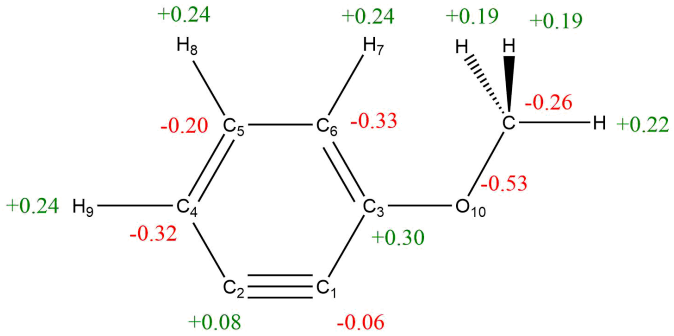

(b)

Figure 3.12: (a) The natural charges of the *syn* $-$ OCH_3 proximally substituted *ortho*-benzyne molecule relative to the unsubstituted parent. (b) The natural charges of the *anti* $-$ OCH_3 proximally substituted *ortho*-benzyne molecule relative to the unsubstituted parent.

OCH_3 Substitution

When the proximal *ortho*-benzyne position is substituted with a *syn* OCH_3 group the $\sigma(2)$ and $\pi(3)$ $C_1{-}C_2$ bonds have the largest relative delocalization energies of $+7.36$ and -4.19 kcal mol^{-1}. These two bonds have changes in electron density of $+0.093$ and $+0.291$ upon localization, respectively. The $\sigma(2)$ bond has a localization contribution of -0.028 from the C$-$O σ^* bond, suggesting a hyperconjugation interaction similar to OH. The $\pi(3)$ bond has a localization contribution of -0.039 from the out-of-plane oxygen lone pair.

A proximal substitution with *anti* OCH_3 has a highly similar effect to the *syn* substitution, with $\sigma(2)$ and $\pi(3)$ relative delocalization energies of +4.68 and −6.49 kcal mol^{-1}, respectively. They experience electron density changes of +0.089 and +0.284. Linked to the $\sigma(2)$ localization, the $C_3{-}O$ σ^* bond changes electron density by −0.026, a reduced hyperconjugative effect as compared to the *syn* rotamer. For the $\pi(3)$ localization, the electron density of the out-of-plane oxygen lone pair changes by −0.041.

NCE analysis was performed on the two OCH_3 proximal rotamers. The delocalized atomic charges are displayed in Figure 3.12. Carbons 1 and 2 hold lewis atomic charges of −0.16 and +0.13, respectively. The two OCH_3 hydrogens pointing towards the triple bond both have lewis atomic charges of +0.21. None of these atomic charges vary significantly upon delocalization. The *anti* rotamer has analogous lewis atomic charges of −0.09, +0.08, and +0.20, with no significant charge differences upon delocalization. The same coulombic interaction that occurs via the OH species appears to be occurring for the OCH_3 substitution, as shown by the greater polarization of the *syn* triple bond as compared to the *anti* triple bond.

In similar fashion to the OH distal substitution, the OCH_3 substitution and rotamers only experience significant substituent localization densities from the out-of-plane oxygen lone pair towards the $C_1{-}C_2$ $\pi(3)$ bond. The *syn* $\pi(3)$ bond changes in electron density by +0.029 with a contribution of −0.028 from the oxygen lone pair. The *anti* $\pi(3)$ bond shows a slight variance from the *syn*, with an electron density change of +0.320 and then −0.019 on the oxygen lone pair.

3.4 Conclusions

Seven density functionals were initially benchmarked with three basis sets against selected experimentally determined properties for *ortho*-benzyne. The triple bond length is best described by the DSD functionals and the BP86 functionals with a cc-pVDZ basis set. The triple bond angles showed no particularly accurate functionals among the seven and exhibited small expansions as the basis set size increased. The triple bond stretching vibrational frequency is best described by the BP86 functional and there were little to no basis set effects within this functional set. Computed stretching vibrational frequencies by these methods may yield qualitative, but not quantitative significance, due to the significant error from experiment and a lack of anharmonicity magnitude to cancel the error. The *ortho*-benzyne singlet-triplet splitting was best described by the DSD functionals, with the cc-pVTZ basis set being particularly accurate. The properties computed by the DSD functionals are strongly affected by their respective MP2 contributions. The cc-pVDZ basis set was chosen for the computation of properties and the DSD-PBEP86 functional was deemed superfluous, decreasing the functionals used in computing properties from seven to six.

Optimized geometries were computed for each substituted species using the benchmarked functionals,

and the triple bond length deviations of these geometries from *ortho*-benzyne at the same level of theory were analyzed. Substitution position offered the largest difference in substituent effects on the triple bond, with the distal substitutions having a smaller impact than the proximal.

Vibrational frequency deviations were computed using the previously computed equilibrium geometries at the same level of theory, and the triple bond stretching frequencies specifically were analyzed. These stretching frequencies generally exhibited expected trends with relation to the bond length, as the trends of these property deviations were inversely proportional. This trend does not hold for the DSD functionals, which is due to the MP2 effects included in the double hybrid portion.

The bond angle deviations of the optimized geometries were also analyzed. These data correlate with a change in orbital hybridization of the triply bonded carbons. Through-space electrostatic effects from the OH and OCH_3 groups have a significant impact on the carbon 1 and carbon 2 bond angle distortions.

The singlet-triplet splittings of the substituted species were analyzed. The deviations with respect to the parent *ortho*-benzyne hold a correlation with the electronegativity of the substituents' atom attached to the ring. The changes in the singlet-triplet splittings upon rotation of either the OH or OCH_3 species are insignificant.

NBO analysis was performed to elucidate the electronic delocalization of the different substituted species via the Lewis bond deletion method[127] and three major substituent effects were present. Significant negative hyperconjugation occurs for the F, OH, and OCH_3 proximal substitutions. The CN, F, OH, and OCH_3 substitution species, both proximal and distal, exhibit resonance interactions with the aromatic network. Resonance electron acceptance is exhibited by the CN species, while the other three exhibit resonance electron donation into the aromatic network. Natural Couloumbic Electrostatic[129] (NCE) computations are performed via NBO in order to elucidate the Lewis and delocalization dependence of the substitution species' atomic charges. Significant through space electrostatic effects manifest in the two rotamers of both the OH and OCH_3 substitution species, with the *syn* rotamers more strongly polarizing the triple bond than the *anti*. This electrostatic effect is present in the Lewis structure and does not qualitatively vary upon delocalization.

Syntheses involving substituted *ortho*-benzyne can be better informed by the properties studied in this work. Nucleophilic and electrophilic attacks to the *ortho*-benzyne triple bond will be directed by the carbon centric orbital hybridization and charges that result from angle distortion in the triple bond. Li and coworkers[113] study a reaction in which a proximal *ortho*-benzyne substituent behaves as a leaving group after nucleophilic attack to the triple bond. In such a case the degree of hyperconjugation between the substituent and triple bond may lead to a lower energy transition state barrier according to Hammond's postulate.[130] Furthermore, understanding which substituents are aromatic electron density donors and acceptors, as well

as the magnitude of this interaction via NBO, can help to guide the selection of substituents which may stabilize or destabilize the overall structure via steric or coulombic interactions with the aromatic network.

CHAPTER 4

THE *i*-PROPYL + O_2 REACTION MECHANISM: A MODEL OF SECONDARY ALKYL RADICAL OXIDATION

Lahm, M.E.; Bartlett, M.A.; Liang, T.; Pu, L.; Schaefer, H. F.; Allen, W.D To be submitted to the Journal of Physical Chemistry

4.1 Abstract

The *i*-propyl + O_2 reaction is an important model of chain branching reactions in larger combustion systems. In this work, focal point analyses (FPA) extrapolating to the *ab initio* limit were performed on the *i*-propyl + O_2 system based on explicit quantum chemical computations with electron correlation treatments through CCSDT(Q) and basis sets up to cc-pV5Z. All reaction species and transition states were fully optimized at the rigorous CCSD(T)/cc-pVTZ level of theory, revealing some substantial differences in comparison to the DFT geometries existing in the literature. Two key stationary points, *i*-propylperoxy radical (**MIN1**) and its concerted elimination transition state (**TS1**), were located 34.8 kcal mol^{-1} and 4.4 kcal mol^{-1} below the reactants, respectively. The β-hydrogen transfer transition state (**TS2**) exhibits an anomalously large diagonal Born-Oppenheimer correction (Δ_{DBOC} = 1.09 kcal mol^{-1}), which is indicative of a nearby surface crossing and possible nonadiabatic reaction dynamics. The α-proton abstraction transition state (**TS5**) is 5.72 kcal mol^{-1} above the reactants and can bifurcate into alphaperoxy radical (**MIN3**) hanging wells before its ultimate dissociation into acetone and the OH radical, located 64.4 kcal mol^{-1} below the reactants. Our definitive energetics for stationary points on the *i*-propyl + O_2 potential energy surface provide key benchmarks for future studies of hydrocarbon oxidation.

4.2 Introduction

Despite the extensive research that has been performed on hydrocarbon oxidation reactions,[131] a bounty of chemical insights remains undiscovered. Much of the research on these reactions has been driven by a desire for more efficient combustion processes and as such, new advances in engine technologies that are geared toward higher fuel efficiency and lower emissions are currently being developed.[131,132] Homogeneous charge compression ignition (HCCI) engines utilize high compression ratios and lean fuel mixtures, resulting in very high efficiency and low soot/NO_x formation. These types of engines perform at relatively low temperatures (500 – 1000 K) and execute rapid combustion, which results in a large portion of unburned hydrocarbons. Central to this process is the reactivity of alkyl radicals, and as a result of the lean fuel mixture, alkyl peroxy radicals. Thus, it is of great importance to achieve a detailed understanding of low temperature combustion processes of hydrocarbon species.

A generalized picture of low temperature hydrocarbon oxidation reactions is displayed in Figure 4.1. The reaction scheme is initiated by the association of an alkyl radical (R) with molecular oxygen (O_2). At low temperatures and moderate pressures the R + O_2 reaction produces alkyl peroxy radical (ROO) species in significant yield.[133] These ROO molecules can dissociate back to the R + O_2 reactants, produce the conjugate

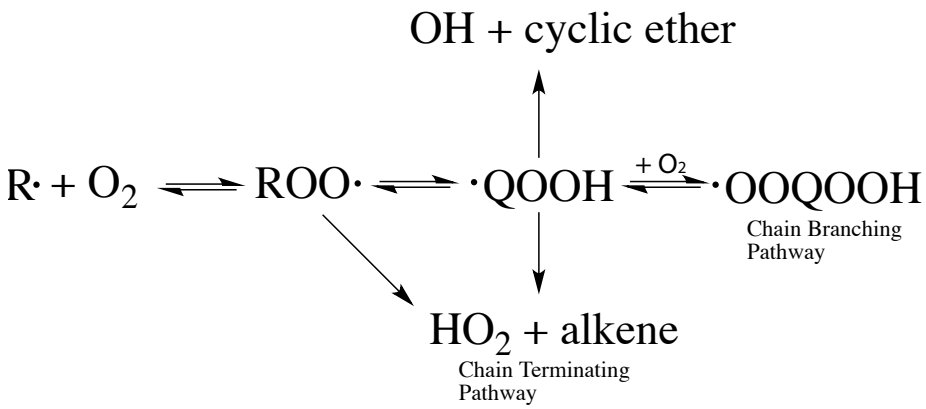

Figure 4.1: General mechanism for dominant alkyl + O_2 reactions.

alkene and HO_2 via a concerted elimination reaction, or isomerize via H-atom internal abstraction to form a hydroperoxyalkyl radical (QOOH). The latter avenue for the ROO radical to form QOOH has recently garnered a great deal of interest, because until 2015 the elusive QOOH species had escaped experimental detection.[134] These QOOH species rapidly decompose to form an OH radical and an oxygen heterocycle, or they fragment to HO_2 and an alkene. They can also dissociate to form low yields of an OH radical and an aldehyde. The formation of the OH radical is important for chain propagation because the OH radical can react with the hydrocarbon fuel source (RH) to create more alkyl radicals (R), thus creating a cycle of fuel consumption.

The ethyl + O_2 model reaction has been studied extensively, both theoretically and experimentally.[135–144] The lowest-energy ethyl + O_2 reaction channel involves the concerted elimination of HO_2 from the ethylperoxy intermediate (C_2H_5OO) to form ethylene + HO_2.[138–140] However, since HO_2 is relatively unreactive, the channel leading to alkene + HO_2 would be chain terminating at low temperatures. Master equation kinetic models12 fit to measured reaction rates agree with rigorous *ab initio* computations carried out through the CCSDT(Q) level[143] in placing the concerted elimination transition state below the ethyl + O_2 reactants by 3.0 kcal mol^{-1}.

The reactions of R + O_2 become increasingly complicated as the size of the alkyl radical chain grows due to an increase in the numbers of conformers and isomers. Knowledge obtained by studying larger alkyl + O_2 reactions contributes significant nuance to fuel combustion processes. A vast amount of research has been conducted on combustion reactions of propyl,[142,145–167] butyl,[154,168–173] neopentyl,[174–176] cyclopentyl,[177] and cyclohexyl[178,179] radicals. An experimental study by DeSain et al. found that as the length of the alkyl chain grows, intramolecular hydrogen abstraction reactions to produce QOOH radicals are able to better compete with the concerted elimination of HO_2.[175] Therefore propyl + O_2, and even more so butyl + O_2, may be a better paradigm of hydrocarbon combustion due to the ability to isomerize to QOOH species via

a 6-membered (*n*-propyl + O_2) or 7-membered (n-butyl + O_2) ring transition state. For a more detailed review of previous theoretical and experimental research surrounding the propyl + O_2 system, we direct the reader to a previous paper on the *n*-propyl + O_2 system.[167]

In a previous study[167] on *n*-propyl + O_2 the essential features of the potential energy surface were established utilizing highly accurate coupled cluster methods with large basis sets to obtain energies with errors of only tenths of a kcal mol^{-1}. In this work, we extend this protocol to firmly establish the features of the *i*-propyl + O_2 system. Utilizing focal point analyses (FPA) with correlation treatments up to CCSDT(Q) and basis sets up to cc-pV5Z has previously been shown to match Master Equation (ME) kinetic model results for the ethyl + O_2 system.[143] Employing zero-point vibrational energies (ZPVE) at high levels of theory is critical to the accuracy of our FPA relative energies. We employ a Concordant Modes methodology to compute ZPVE corrections of CCSD(T)/cc-pVTZ level quality, making these daunting computations feasible for larger combustion systems. In this work we perform FPA to the *ab initio* limit based on explicit computations through the CCSDT(Q) level of theory and basis sets up to cc-pV5Z, which is critically needed to establish the key features of the *i*-propyl + O_2 system.

4.2.1 Theoretical Methods

General Scheme

The following methods were utilized to study the electronic wavefunctions produced in this work. Restricted (RHF),[180] restricted open-shell (ROHF),[181] and unrestricted (UHF)[182] Hartree-Fock methods; second-order Mller-Plesset (MP2)[183] and second order Z-averaged (ZAPT2)[184] perturbation theory; and coupled cluster (CC)[185,186] theory incorporating up to single and double excitations (CCSD),[187] perturbative contributions from connected triple excitations [CCSD(T)],[188] full triple excitations (CCSDT),[189] as well as a perturbative treatment of quadruple excitations [CCSDT(Q)].[190] The correlation methods operate within a spin orbital formalism into which either ROHF or UHF orbitals are inserted, designated by an RO or U prefix. This study primarily used the correlation-consistent (cc) families of basis sets cc-pVXZ (X = D, T, Q, 5),[191,192] cc-pCVXZ (X = T),[193] and aug-cc-pVXZ (X = D, T).[194] CCSDT(Q) computations, however, were performed with the 6-31G* basis set.[195] The frozen core approximation was used for all computations aside from the all electron single point energy of the frozen core correction.

Precise relative energies for the lowest conformers of all stationary points were computed by extrapolation to full correlation and complete basis set limits, employing the focal point analysis (FPA)[4,196–198] scheme developed by Allen and co-workers. The quantum chemistry packages Molpro 2010.1,[48] CFOUR 1.0,[199] Psi 3.4,[200] Psi4,[201] GAMESS version 25 Mar 2010,[202,203] MPQC 2.3.0,[204]80 and Kállay's MRCC[205,206]

program were employed in this study.

Geometry Optimization

For all reactants, products, intermediates, conformations of the minima, and transition states, geometric structures were initially optimized at the ROMP2/aug-cc-pVDZ level of theory, and then single-point ROCCSD(T)/cc-pVTZ energies were computed to determine the lowest-energy conformers. These lower level structures were used as starting points for subsequent ROCCSD(T)/cc-pVTZ geometry optimizations. The preceding computations were performed with the CFOUR 1.0 package. A series of dihedral angles was chosen to uniquely identify each conformer: $\tau(C_1C_2O_4O_5)$, $\tau(C_3C_2O_4O_5)$, and $\tau(C_2O_4O_5H_{12})$. The **MIN2** structure required an additional dihedral angle for identification, $\tau(C_1C_2C_3H_{11})$. In every case, the $\tau(C_2C_3H_{10}H_{11})$ dihedral angle is close to 180° and these values are specified in Table S3 of the Supporting Information. The following Klyne-Prelog[207–210] labels were utilized for each dihedral angle: G^+ (gauche, $+30° < \tau < +90°$), G^- (gauche, $-90° < \tau < -30°$), A^+ (anticlinal, $+90° < \tau < +150°$), A^- (anticlinal, $-150° < \tau < -90°$), and T (trans, $|\tau| > 150°$). A systematic conformational analysis was performed for the reaction minima wherein a starting structure was varied about the aforementioned dihedral angles in increments of 15°. Single point energies atop the resulting scan structures were computed at the UB3LYP/6-31G* level of theory, with the Psi4 package, and conformational minima were subsequently identified. These structures were then optimized at the ROMP2/aug-cc-pVDZ level of theory and redundant structures were eliminated. ROCCSD(T)/cc-pVTZ single point energies were computed atop these structures. The geometry of the lowest-energy conformer of each species was then optimized at the ROCCSD(T)/cc-pVDZ level of theory.

The OPTKING module in the Psi 3.4 and Psi4 packages were utilized to perform all ROCCSD(T)/cc-pVTZ geometry optimizations with a 3-point numerical gradient furnished by single-point energies from the Molpro 2010.1 package. Fixed ROCCSD(T)/cc-pVDZ Hessians from the CFOUR 1.0 program were used to accelerate convergence.

Focal Point Analyses

In our FPA computations, E, ΔE, and δ refer to the absolute energies, relative energies between species, and relative energy increments with respect to preceding levels of electron correlation. The following equations

were utilized to extrapolate the Hartree-Fock[211] (E_{HF}) and correlation energies[212] (ε):

$$E_{HF}(X) = E_{HF}^{\infty} + A \exp(-bX) \tag{4.1}$$

$$\varepsilon = \varepsilon^{\infty} + \frac{B}{X^3} \tag{4.2}$$

where X is the cardinal number of a correlation consistent cc-pVXZ basis. The extrapolations in the Hartree-Fock case utilized $X = \{3, 4, 5\}$, while the extrapolations for ROCCSD, ROCCSD(T), and ZAPT2 correlation energies used $X = \{3, 4\}$. Additive approximations for the ROCCSDT and UCCSDT(Q) levels of theory were calculated using the following schemes:

$$\delta\,[\text{ROCCSDT}] = \Delta E\,(\text{ROCCSDT/cc-pVDZ}) - \Delta E\,(\text{ROCCSD(T)/cc-pVDZ}) \tag{4.3}$$

$$\delta\,[\text{ROCCSDT(Q)}] = \Delta E\,(\text{UCCSDT(Q)/6-31G*}) - \Delta E\,(\text{ROCCSDT/6-31g*}) \tag{4.4}$$

These computationally demanding ROCCSDT and UCCSDT(Q) correlation increments were computed with small basis sets (cc-pVDZ, 6-31G*) using CFOUR 1.0 and Kállay's MRCC program coupled with CFOUR 1.0, respectively. An additive approximation for the core electron correlation effects was calculated by subtracting all-electron (AE) and frozen-core (FC) ROCCSD(T) energies computed with the cc-pCVTZ basis set:

$$\Delta(\text{core}) = \Delta E_e\,(\text{AE-ROCCSD(T)/cc-pCVTZ}) - \Delta E_e\,(\text{FC-ROCCSD(T)/cc-pCVTZ}) \tag{4.5}$$

A first-order relativistic correction,[213] Δ(rel), was computed from the one-electron mass-velocity and Darwin terms at the ROCCSD(T)/cc-pVTZ level of theory. The diagonal correction to the Born-Oppenheimer approximation (DBOC),[214] which corrects for relaxation of the clamped nucleus assumption, was computed at the ROHF/aug-cc-pVTZ level of theory. Harmonic vibrational frequencies and zero-point vibrational energy (ZPVE) corrections, ΔZPVE(harm), were computed utilizing the concordant modes approach (CMA0), previously referred to as the mixed Hessian scheme in our work[167] on the n-propyl + O_2 system, to closely approximate vibrational frequencies obtained at the ROCCSD(T)/cc-pVTZ level of theory. Final ZPVE values employed in this study were explicit ROCCSD(T)/cc-pVTZ values for both reactant and product species and CMA0 approximations to ROCCSD(T)/cc-pVTZ for all transition states and intermediate species. The final focal point energy estimating ROCCSDT(Q) relative energies at the CBS limit was found by adding

the extrapolation results, additive corrections, and auxiliary terms to give:

$$\Delta E_{FP} = E_{HF}^{\infty} + \delta^{\infty}\,[\mathrm{ROCCSD(T)}] + \delta\,[\mathrm{ROCCSDT}] + \delta\,[\mathrm{CCSDT(Q)}] + \Delta(\mathrm{core}) + \Delta(\mathrm{rel}) + \Delta\mathrm{ZPVE(harm)} \tag{4.6}$$

ZPVE, relativistic, and DBOC computations were performed with the CFOUR 1.0 package, while core correlation corrections were computed with the Molpro 2010.1 package.

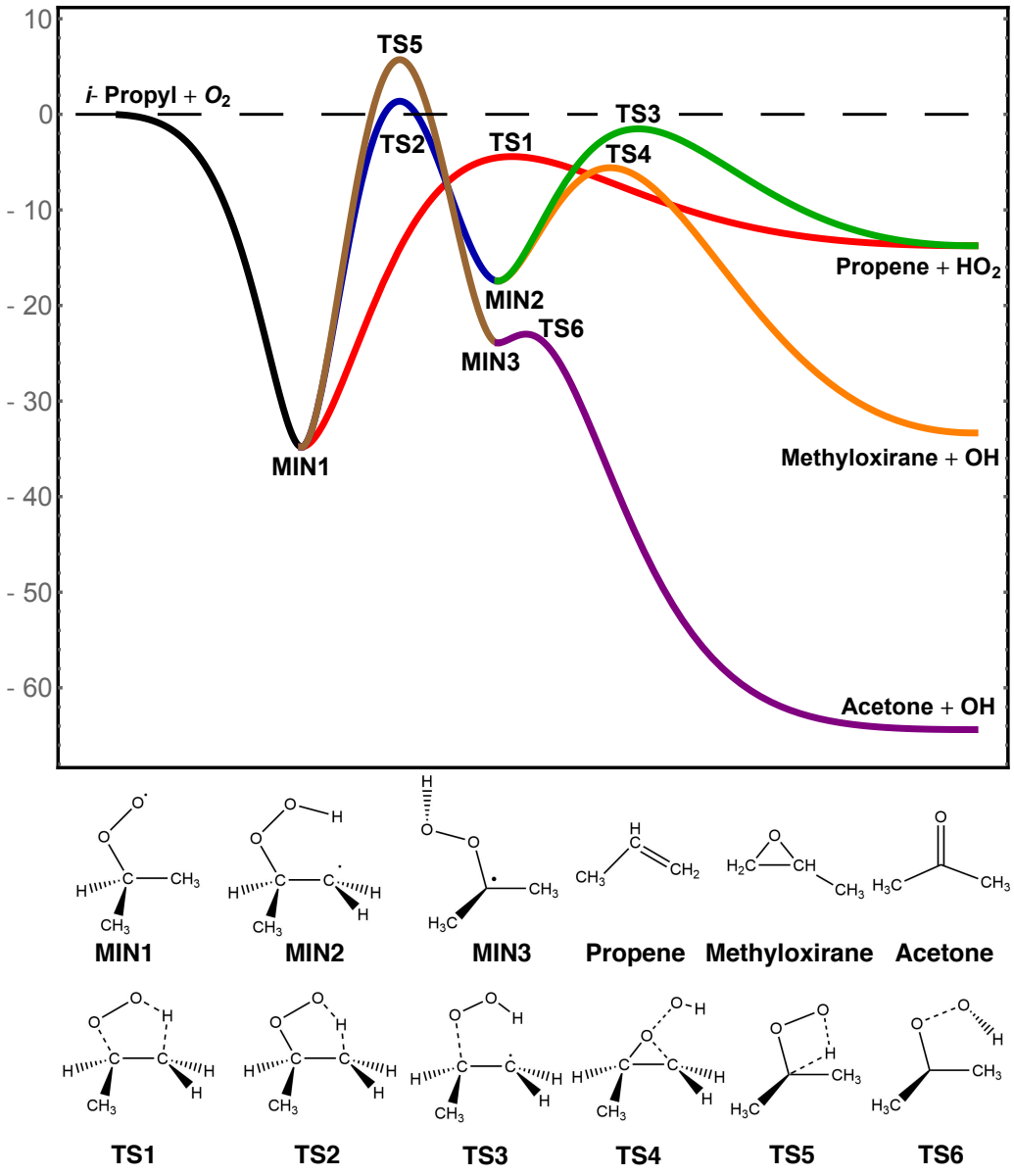

Figure 4.2: Schematic potential energy surface (PES) for i-propyl + O_2 reactions.

4.3 Results

The important features of the *i*-propyl + O_2 potential energy surface investigated in this work are depicted in Figure 4.2. In this study the stationary points previously used by Klippenstein and co-workers [142] in their master equation (ME) modeling were selected for more rigorous investigation. Table 4.1 includes relative enthalpies at 0 K (Δ_{rxn} H_0°) for all stationary points of the *i*-propyl + O_2 system, allowing comparison between our results and those obtained from previous studies. [142,154,159,161,162]

Table 4.1: Relative enthalpies at 0 K ($\Delta_{rxn}H_0$° kcal mol^{-1}) for stationary points of the *i*-propyl + O_2 system.

	$\Delta_{\text{rxn}} H_0^\circ$ (kcal mol^{-1})						
	QCISD(T) (2002)	ME[a] (2003)	ME[a] (2010)	ME[a] (2011)	CBS-Q[b] (2011)	QCISD(T)[c] (2012)	This Work
i-propyl+O_2	0.0	0.0	0.0	0.0	0.0	0.0	0.00
MIN1	–36.8	—	–34.8	–34.8	–36.2	–34.8	–34.79
MIN2	–20.2	—	—	—	—	–18.0	–17.44
MIN3	—	—	—	—	—	—	–23.91
TS1	–7.0	–4.7	–5.0	–5.0	–3.6	–4.2	–4.42
TS2	–1.4	–0.2	—	–1.7	+1.6	+1.2	+1.37
TS3	–1.9	—	—	—	—	–1.3	–1.52
TS4	–4.9	—	—	—	—	–5.6	–5.59
TS5	—	—	—	—	—	(+5.5)[d]	+5.72
TS6	—	—	—	—	—	—	–25.01
propene+HO_2	—	—	—	—	—	–13.4	–13.75
methyloxirane+OH	—	—	—	—	—	–35.5	–33.34
acetone + OH	—	—	—	—	—	–65.5	–64.38

[a]Fitted by master equation analysis to experimental kinetic data.

[b]Literature CBS-QB3 energies values.

[c]Restricted QCISD(T)/CBS energies including B3LYP/6-311++G(d,p) ZPVE corrections.

[d]Direct transition state from **MIN1** to acetone + OH.

Since cyclic transition states leading to QOOH species undergo distortion from ring planarity, we must investigate the presence of multireference electronic character. The presence of multireference character can be gauged using the open-shell T_1 diagnostic, [215,216] which measures the extent of orbital relaxation in the coupled cluster wave function. Values of T_1 greater than 0.02 are often taken as an indicator of multireference character [216] in closed-shell species, while open-shell species typically have a less defined threshold and exhibit larger T_1 values. [216] We also provide the largest doubles amplitudes ($T_{2,\max}$) in the CCSD(T)/cc-pVTZ wave function to add further certainty in our investigation of multireference character. The T_1 diagnostic, $T_{2,\max}$ amplitudes, and spin contamination $\left\langle S^2 - S_z^2 - S_z \right\rangle$ values are listed in Table 4.2 for the minima and transition states on the *i*-propyl + O_2 potential energy surface, as well as O_2 and OH.

We include the CN radical as a benchmark as it is reasonably well described at the single-reference CCSD(T) level of theory.[217–219] All reactions species in this study have T_1 and $T_{2,\max}$ values close to or smaller than CN and show no signs of significant multireference character. The spin contamination for these species is computed from the orbital distortion induced by UCCSD(T) from a ROHF reference, so spin contamination will have a minimal impact on the properties computed in this work.

Table 4.2: T_1 diagonistic values, $T_{2,\max}$, and spin contamination at the CCSD(T)/cc-pVTZ level of theory.

	T_1	$T_{2,\max}$	$< S^2 - S_z{}^2 - S_z >$		T_1	$T_{2,\max}$	$< S^2 - S_z{}^2 - S_z >$
MIN1	0.028	<0.05	0.002	**TS1**	0.032	0.080	0.003
MIN2	0.012	<0.05	0.001	**TS2**	0.025	<0.05	0.003
MIN3	0.016	<0.05	0.002	**TS3**	0.040	0.095	0.022
i-propyl	0.010	<0.05	0.001	**TS4**	0.027	0.053	0.040
HO_2 ($^2A''$)	0.037	0.056	0.003	**TS5**	0.019	<0.05	0.003
OH ($^2\Pi$)	0.006	<0.05	0.001	**TS6**	0.021	<0.05	0.007
				CN	0.053	0.093	0.009

4.3.1 Reactants and Products

Experimentally determined geometries are available for OH,[220] O_2,[220] HO_2,[221] propene,[222] and methyloxirane.[223] Our ROCCSD(T)/cc-pVTZ geometries are in excellent agreement with experiment with mean absolute deviations (MAD) of 0.004 Å for bond lengths and 0.6° for bond angles. A notable difference of 1.24° is seen for $\alpha(H_7{-}C_1{-}C_2)$ of propene. When comparing the B3LYP/6-311++G(d,p) *i*-propyl structure of Goldsmith et al.[162] to our result (Figure 4.3), we observe MADs of 0.002 Å for bond lengths and 0.73° for bond angles.

4.3.2 RO_2 Formation

Upon the initial abstraction reaction, the *i*-propyl + O_2 system undergoes a highly exothermic (−34.79 kcal mol^{-1}) barrierless combination reaction producing the *i*-propylperoxy (**MIN1** Figure 4.4) radical. The **MIN1** species has only 2 energetically distinct rotamers produced by internal rotations about the $C_2{-}O_4$ bond: T (0.00 kcal mol^{-1}) and G$^-$ (0.26 kcal mol^{-1}). The relative energies of these species were determined at the CCSD(T)/cc-pVTZ//MP2/aug-cc-pVDZ level of theory. The B3LYP/6-311++G(d,p) **MIN1** structure (T) of Goldsmith et al.[162] displays a MAD of 0.01 Å for bond lengths and 1.49° for bond angles when compared to our structure. Notable differences of 1.73°, 2.84°, and 1.87° are present for $\alpha(C_2{-}O_4{-}O_5)$, $\tau(C_1{-}C_2{-}O_4{-}O_5)$, and $\tau(C_3{-}C_2{-}O_4{-}O_5)$, respectively. We also find that our CCSD(T) bond lengths and angles display MADs of 0.008 Å and 0.4° when comparing cc-pVDZ and cc-pVTZ structures. Wilke et

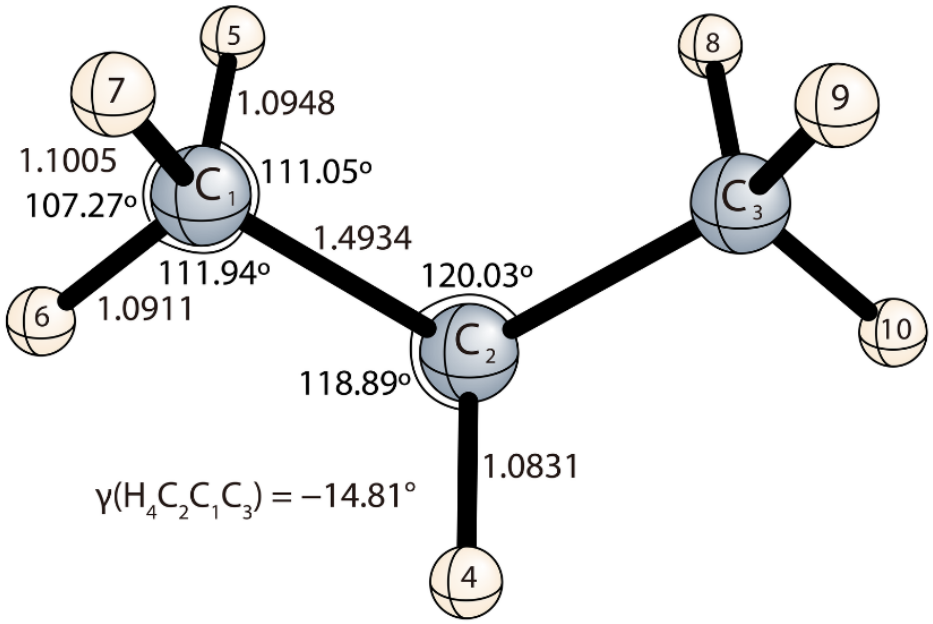

Figure 4.3: Optimum geometry of the *i*-propyl radical (C_s) at the ROCCSD(T)/cc-pVTZ level of theory. Bond lengths are in Å.

al.[143] observed changes in the ethylperoxy radical of only 0.003 Å and 0.3° for CCSD(T) bond lengths and angles, respectively, when comparing geometries computed via the cc-pVTZ and cc-pVQZ basis sets. Thus, we can assume that the **MIN1** geometry wouldn't change significantly from our results if optimized at the CCSD(T)/cc-pVQZ level of theory.

The focal point analysis for **MIN1** relative to the separated *i*-propyl + O_2 reactants is given in Table 4.3. We find that the relative energy Δ_{rxn} H_0° of **MIN1** is 34.8 kcal mol^{-1} with respect to the separated reactants, which amounts to a larger binding energy by 2.1 kcal mol^{-1} compared to the analogous species in the *n*-propyl + O_2 system.[167] This effect can be rationalized by the stabilizing 1,4-pair correlation effects[224] between C−H bonds in the methyl groups of **MIN1**, which is reduced in the *n*-propylperoxy radical due to the positioning of the O_2 moiety. The Hartree-Fock limit gives a R−O_2 binding energy that is 8.9 kcal mol^{-1} smaller than ROCCSDT(Q)/CBS and larger than ZAPT2/CBS by 4.5 kcal mol^{-1}. These observations are consistent with observations from previous CBS work performed on both the ethylperoxy radical[143] and the *n*-propylperoxy radical.[167] The majority of the electron correlation effect is accounted for once δ[ROCCSD(T)] = 1.31 kcal mol^{-1} is included, as the higher order correlation contributions δ[ROCCSDT] = 0.17 kcal mol^{-1} and δ[ROCCSDT(Q)] = +0.34 kcal mol^{-1} largely cancel. Interestingly, the magnitude of this cancelation differs by only 0.01 kcal mol^{-1} compared to the same correlation increment difference of the *n*-propylperoxy radical.[167] Similar to the *n*-propylperoxy radical, the FPA data suggests that the electron correlation contribution from δ[ROCCSDTQ] would be smaller than 0.3 kcal mol^{-1} and the difference

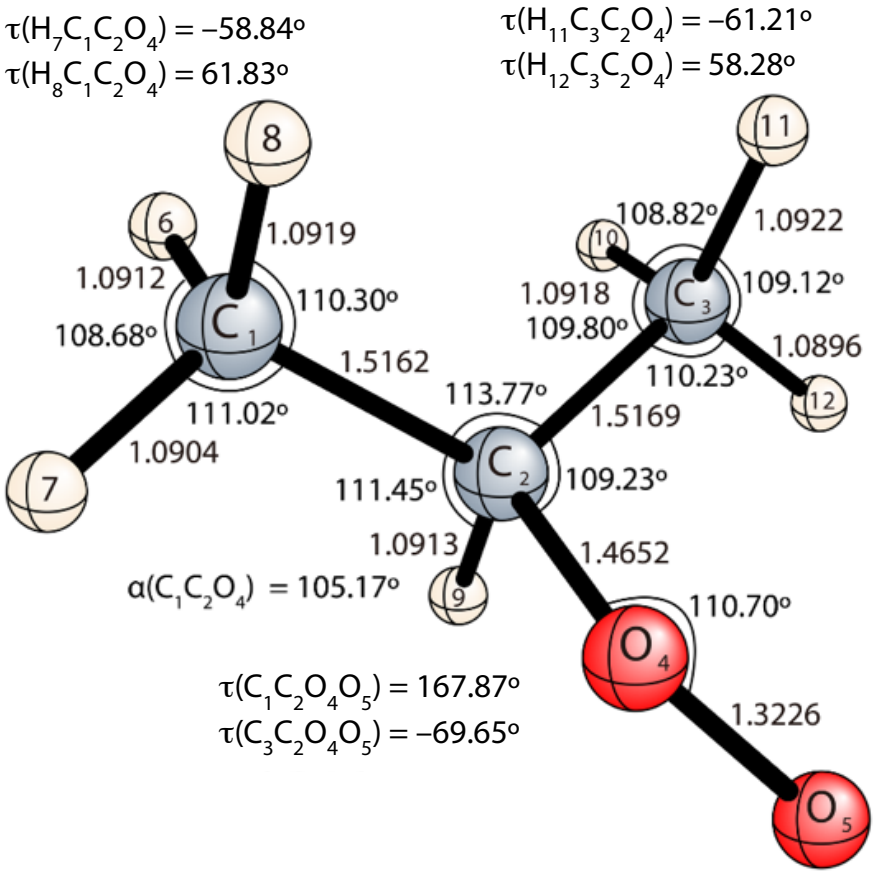

Figure 4.4: Optimum geometry of the *i*-propylperoxy radical (**MIN1**) at the ROCCSD(T)/cc-pVTZ level of theory. Bond lengths are in Å.

between cc-pV5Z and cc-pVQZ for δ[ROCCSD(T)] would be smaller than 0.1 kcal mol^{-1}.

Table 4.3: Focal point analysis (in kcal mol^{-1}) for **MIN1** relative to *i*-propyl + O_2.

	ΔE_e(ROHF)	$+\delta$ [ZAPT2]	$+\delta$ [ROCCSD]	$+\delta$ [ROCCSD(T)]	$+\delta$ [ROCCSDT]	$+\delta$ [UCCSDT(Q)]	NET
6-31G*	–32.11	+8.52	–12.38	–0.75	–0.18	+0.34	–36.55
cc-pVDZ	–30.47	+9.90	–11.89	–0.71	–0.17	[+0.34]	[–33.00]
cc-pVTZ	–31.24	+6.54	–12.12	–1.07	[–0.17]	[+0.34]	[–37.72]
cc-pVQZ	–30.96	+5.38	–12.20	–1.21	[–0.17]	[+0.34]	[–38.82]
cc-pV5Z	–30.90	[+4.96]	[–12.23]	[–1.26]	[–0.17]	[+0.34]	[–39.26]
CBS	[–30.89]	[+4.53]	[–12.26]	[–1.31]	[–0.17]	[+0.34]	[–39.77]
FC-ROCCSD(T)/cc-pVTZ reference geometries							
$\Delta E_{final} = \Delta E_e$(FPA) + ΔZPVE (harm) + Δ(rel) + Δ(core) = –39.77 + 4.91 + 0.13 –0.06 = **–34.79 kcal mol^{-1}**							

Our binding energy for **MIN1** is smaller than the original results of DeSain et al.[154] by 1.77 kcal mol^{-1} and larger than their subsequent modifications by 0.23 kcal mol^{-1}.[142,159] The CBS/QB3 binding energy of

Huynh et al.[161] is higher than our result by 1.2 kcal mol^{-1}, a discrepancy which is 0.9 kcal mol^{-1} smaller than that noted for the *n*-propylperoxy radical. The most recent binding energy (34.8 kcal mol^{-1}) reported by Goldsmith et al.,[162] at the QCISD(T)/CBS level of theory, is within 0.01 kcal mol^{-1} of our value for **MIN1**.

4.3.3 Pathways Leading From RO_2

Similar to the *n*-propyl + O_2 system, the concerted elimination reaction occurs through a 5-membered ring transition state (**TS1**, Figure 4.5) where the H_{12} atom transfers from C_3 to O_5. **TS1** is best viewed as a proton-transfer concerted elimination with the unpaired electron in an orbital perpendicular to the ring, as shown in Figure 4.6. The singly occupied molecular orbital (SOMO) is localized on the O_2 moiety and is perpendicular to the 5-membered ring. Again similar to the analogous concerted elimination species of the *n*-propyl + O_2 reaction, we observe via natural bond orbital analysis[225] (NBO) that 74% of the spin density of **TS1** is centered on O_4. This distribution of spin resembles that of free HO_2, which has 90% of its spin density on the terminal O atom. As the H_{12} species migrates from C_3 to O_5, the C_3H_{12} bond distance increases by 0.2776 Å. During this proton transfer, the C_2O_4 distance drastically increases by 0.6766 Å, while the $C_2{-}C_3$ distance decreases by 0.1244 Å. While the $\alpha(C_1{-}C_2{-}C_3)$ angle increases by 9.33° when going from **MIN1** to **TS1**, both the $\alpha(C_3{-}C_2{-}O_4)$ and $\alpha(C_2{-}O_4{-}O_5)$ angles decrease by 12.13° and 10.96°, respectively. The ring structure of **TS1** is nearly planar with $\tau(C_2{-}C_3{-}H_{12}{-}O_5) = 1.11°$ and $\tau(C_3{-}H_{12}{-}O_5{-}O_4) = 0.37°$. The B3LYP/6-311++G(d,p) **TS1** structure of Goldsmith et al.[162] displays a MAD of 0.03 Å for bond lengths and 1.1° for angles when compared to our structure. Notable discrepancies are observed for $r(C_2{-}O_4)$ and $\alpha(C_2{-}O_4{-}O_5)$ of 0.125 Å and 1.7°, respectively.

The direct elimination of HO_2 via transition state **TS1** was found to be the dominant fate of the RO_2 radical in previous work for both ethyl + O_2 and *n*-propyl + O_2.[143,167] Our concerted HO_2 elimination barrier (**TS1**) for *i*-propyl + O_2 is 4.42 kcal mol^{-1} below the reactants by FPA targeting the CCSDT(Q)/CBS level of theory, as compared to 3.0 kcal mol^{-1} in the ethyl + O_2 system and 2.4 kcal mol^{-1} in the *n*-propyl + O_2 system. While increasing the system size to larger alkyl radicals appears to slightly disfavor concerted elimination through **TS1** relative to other pathways, the trend of branched (*i*-propyl) vs. chained alkanes (*n*-propyl) shows that branching lowers **TS1** on the PES; however, this is more so a consequence of the stabilization of **MIN1** due to energy lowering 1,4-pair correlation effects.[224] Simply optimizing **TS1** at the ROCCSD(T)/cc-pVTZ level of theory places the barrier 1.93 kcal mol^{-1} below the reactants after correcting for zero-point energy. Extrapolating to the ROCCSD(T) basis set limit lowers the barrier of **TS1** by 2.0 kcal mol^{-1}. Both high-order correlation and basis set augmentation provide a continuing negative energy

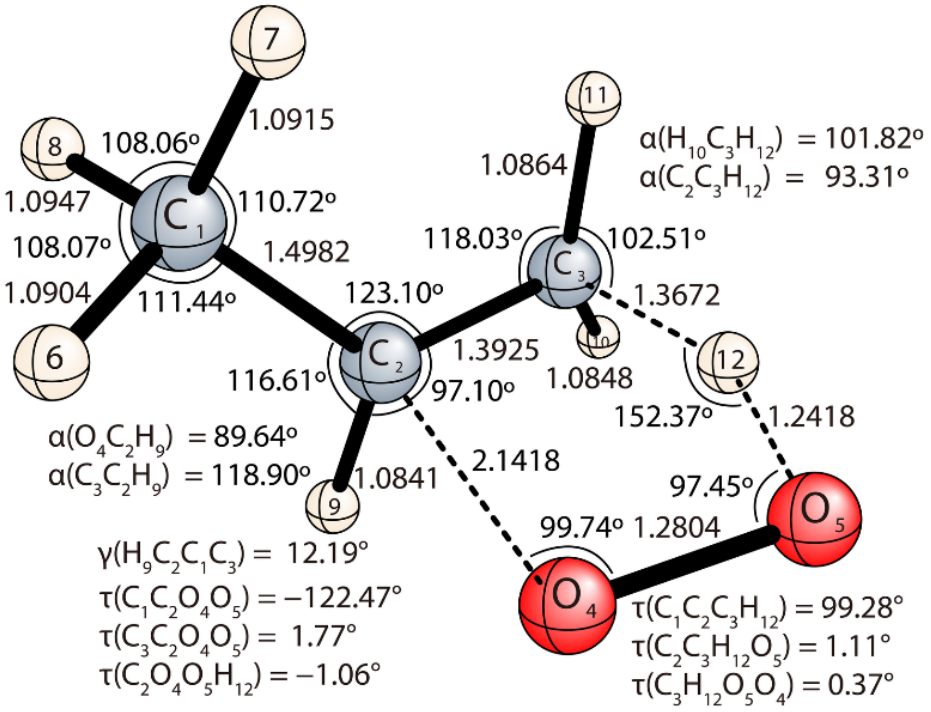

Figure 4.5: Optimum geometry of **TS1** at the ROCCSD(T)/cc-pVTZ level of theory. Bond lengths are in Å.

correction for **TS1**, as previously noted for both ethyl + O_2 and *n*-propyl + O_2,[143,167] which has been identified as the reason for systematic overestimation of the concerted elimination barrier. Our **TS1** barrier is higher in energy than that of DeSain et al.[154] and subsequent modifications[142,159] by 2.58 kcal mol^{-1} and (0.28, 0.58) kcal mol^{-1}, respectively. The work of Goldsmith et al.[162] places **TS1** 4.2 kcal mol^{-1} below the reactants, which is 0.22 kcal mol^{-1} higher in energy than our result. This discrepancy is 0.08 kcal mol^{-1} smaller than the analogous comparison in the *n*-propyl + O_2 system. The CBS-QB3 method value of Huynh et al.[161] produces a Δ_{rxn} H_0° value for **TS1** higher in energy than our result by 0.82 kcal mol^{-1}.

The focal point analysis for **TS1** relative to the separated *i*-propyl + O_2 reactants is given in Table 4.4. The energy correction that accounts for electron correlation beyond ROCCSD(T) (δ[ROCCSDT] + δ[UCCSDT(Q)]) for **TS1** is 0.49 kcal mol^{-1}, which is 0.09 kcal mol^{-1} and 0.4 kcal mol^{-1} smaller in magnitude than the corresponding correction for **TS1** in the *n*-propyl + O_2 ethyl + O_2 reactions, respectively.[143,167] We note that both the lengthening of alkyl chains and chain branching serves to diminish this energy increment. The associated increment for the concerted elimination reaction of the t-butyl + O_2 system is −0.40 kcal mol^{-1}, smaller in magnitude by 0.18 kcal mol^{-1} and only 0.09 kcal mol^{-1} than the corresponding **TS1** values of the *n*-propyl + O_2 and *i*-propyl + O_2 systems, respectively.[167]

TS1 exhibits a reaction mode frequency of 1312*i* cm^{-1} at the FC-ROCCSD(T)/CMA0(TZ,DZ) level of

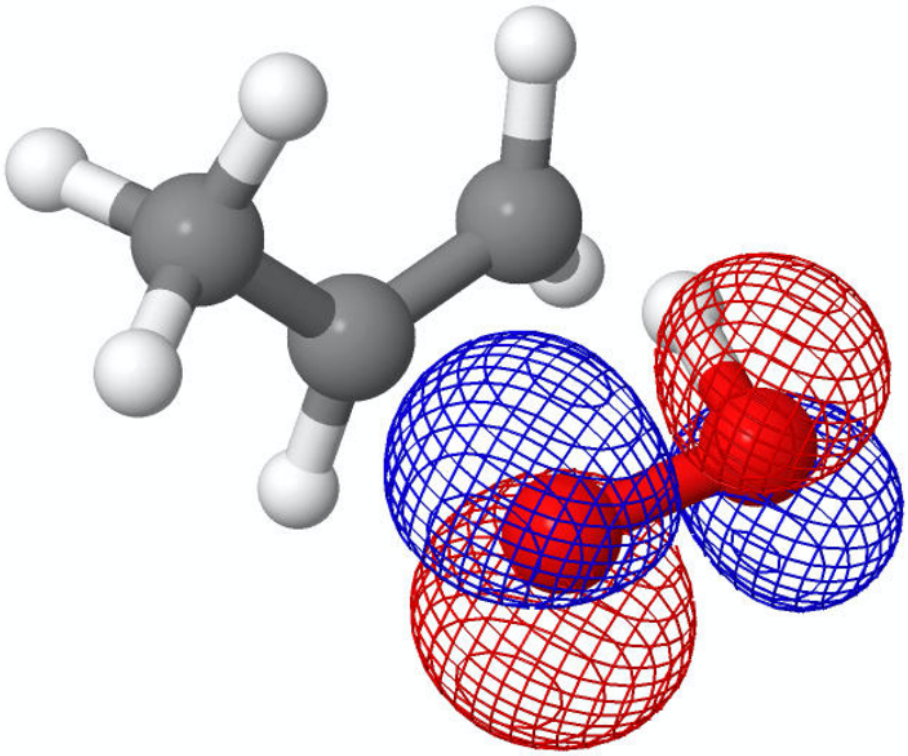

Figure 4.6: Depiction of the singly occupied molecular orbital (SOMO) of **TS1**.

Table 4.4: Focal point analysis (in kcal mol^{-1}) for **TS1** relative to *i*-propyl + O_2.

	ΔE_e(ROHF)	$+\delta$ [ZAPT2]	$+\delta$ [ROCCSD]	$+\delta$ [ROCCSD(T)]	$+\delta$ [ROCCSDT]	$+\delta$ [UCCSDT(Q)]	NET
6-31G*	30.79	–18.87	–3.83	–4.68	–0.22	–0.43	+2.77
cc-pVDZ	28.14	–17.89	–3.78	–5.32	–0.06	[–0.43]	[+0.66]
cc-pVTZ	28.55	–22.91	–2.17	–6.45	[–0.06]	[–0.43]	[–3.47]
cc-pVQZ	28.69	–24.31	–1.77	–6.69	[–0.06]	[–0.43]	[–4.57]
cc-pV5Z	28.71	[–24.81]	[–1.63]	[–6.78]	[–0.06]	[–0.43]	[–4.99]
CBS	[28.71]	[–25.34]	[–1.48]	[–6.87]	[–0.06]	[–0.43]	[–5.47]

FC-ROCCSD(T)/cc-pVTZ reference geometries

$\Delta E_{final} = \Delta E_e$(FPA) + ΔZPVE (harm) + Δ(rel) + Δ(core) = –5.47 + 0.98 + 0.07 + 0.00 = **–4.42 kcal mol^{-1}**

theory, in good agreement with the FC-ROCCSD(T)/CMA0(TZ,DZ) (1302i cm^{-1}) and FC-CCSD(T)/cc-pVTZ (1340i cm^{-1}) results for the *n*-propyl + O_2 and ethyl + O_2 systems, respectively.[143,167] Interestingly, our reaction mode frequency for **TS1** happens to be exactly the same as the FC-CCSD(T)/ANO0 result of Moore et al.[226] for the HO_2 elimination pathway of *t*-butyl + O_2. The CCSD(T) ΔZPVE(harm) correction to the **TS1** barrier changes by 0.46 kcal mol^{-1} when improving the basis set from cc-pVDZ to CMA0(TZ,DZ).

The next possible fate of **MIN1** is to traverse the β-hydrogen transfer transition state (**TS2**, Figure 4.7) leading to **MIN2**. **TS2** involves a hydrogen transfer and occurs through a non-planar 5-membered ring. The

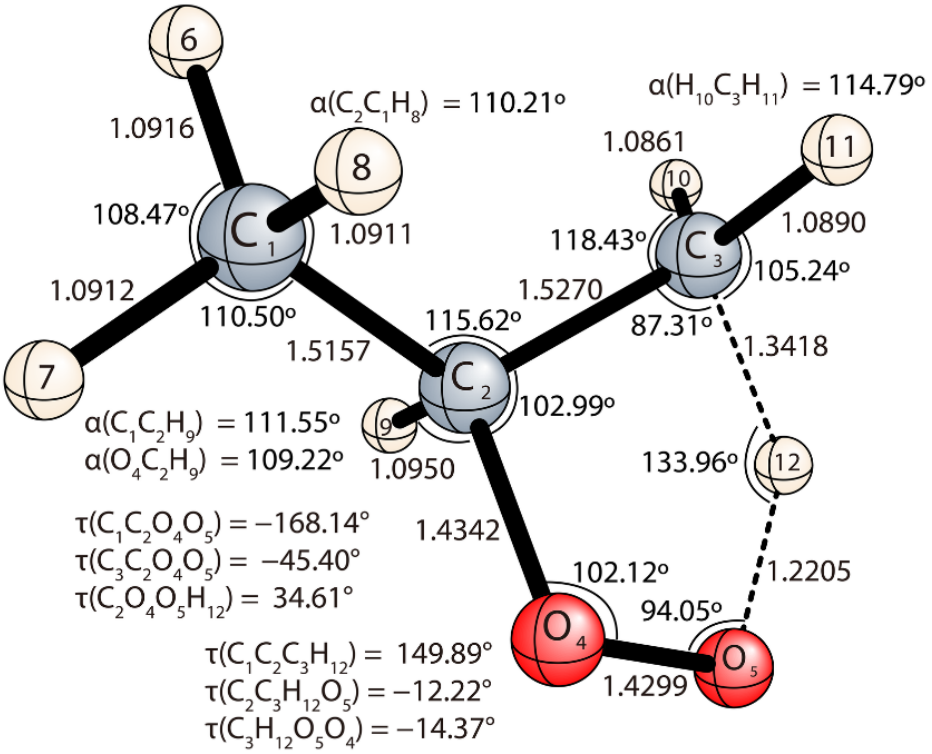

Figure 4.7: Optimum geometry of **TS2** at the ROCCSD(T)/cc-pVTZ level of theory. Bond lengths are in Å.

distortion from ring planarity occurs because the SOMO (Figure 4.8) must be directed into the $C_3{-}H_{12}{-}O_5$ plane in order to affect the hydrogen transfer. **TS2** exhibits an unphysically large Δ_{DBOC} correction (1.09 kcal mol^{-1}), which is nonetheless 0.62 kcal mol^{-1} smaller than the corresponding value in the *n*-propyl + O_2 system. This large Δ_{DBOC} correction is an indication of a nearby surface crossing on the Born-Oppenheimer potential energy surface. These indications of possible nonadiabatic reaction dynamics have previously been reported for the ethyl + O_2,[143] *n*-propyl + O_2,[167] and *t*-butyl + O_2 systems.[226] The β-hydrogen transfer transition state of *t*-butyl + O_2 system[226] exhibits a Δ_{DBOC} correction of 0.4 kcal mol^{-1}, smaller than our value for **TS2** by 0.69 kcal mol^{-1}. While Δ_{DBOC} is usually a small correction ($\pm$0.02 kcal mol^{-1}) to the Born-Oppenheimer potential energy surface, this is not the case in the vicinity of a conical intersection. Meek and Levine[227] show that E_{DBOC} is non-integrable over domains including a conical intersection because the second derivative of the $\hat{T}n$ operator blows up at such points. They recommend that DBOC not be used when employing mixed quantum-classical methods and approximate quantum dynamical methods.[227]

Similar to **TS1**, the **TS2** structure displays a relatively short H_{12}-O_5 bond distance of 1.221 Å. The $C_3{-}H_{12}$ bond increases by 0.25 Å when going from **MIN1** to **TS2**. The changes in r($C_2{-}C_3$) and r($C_2{-}O_4$) are less drastic than observed for **TS1**, increasing and decreasing by 0.01 Å and 0.03 Å, respectively. The $\alpha(C_1{-}C_2{-}C_3)$, $\alpha(C_3{-}C_2{-}O_4)$, and $\alpha(C_2{-}O_4{-}O_5)$ angles change by 1.85°, −6.24°, and −8.58°, respectively,

when going from **MIN1** to **TS2**. The ring structure of **TS2** is highly non-planar with $\tau(C_3{-}C_2O_4{-}O_5)$ $= -45.40°$ and $\tau(C_2{-}O_4{-}O_5{-}H_{12}) = 34.68°$. The B3LYP/6-311++G(d,p) **TS2** structure of Goldsmith et al.[162] displays a MAD of 0.01 Å for bond lengths and 0.7° for angles when compared to our structure. The n-propyl + O_2 system displayed two distinct conformers of the β-hydrogen transfer transition state which differ by the direction of puckering from ring planarity. The second distinct conformer is higher in energy than **TS2** and is thus dubbed **TS2′**(Figure 4.9).

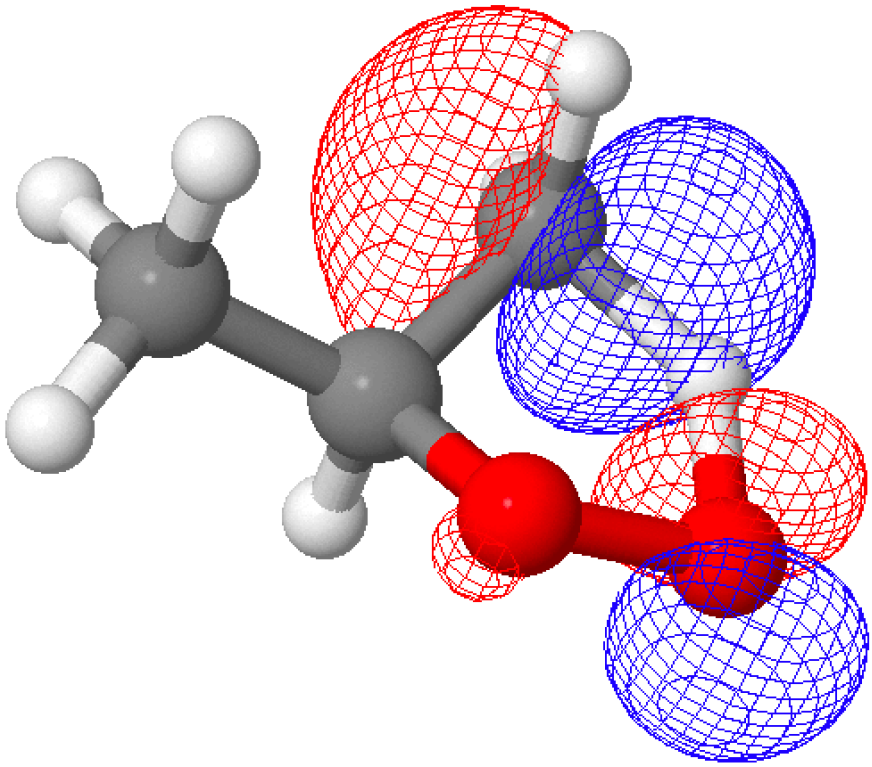

Figure 4.8: Depiction of the singly occupied molecular orbital (SOMO) of **TS1**.

Our **TS2** structure lies 1.37 kcal mol^{-1} above the separated reactants. The focal point layout of **TS2** (Table 4.5) indicates that the cc-pV5Z basis set yields Hartree-Fock results within 0.02 kcal mol^{-1} of the CBS limit. For the $+\delta$[ROCCSD(T)] correction, the difference between cc-pVTZ and cc-pVDZ basis sets is 1.0 kcal mol^{-1}, compared to a difference of only 0.25 kcal mol^{-1} between cc-pVQZ and cc-pVTZ. Much of the electron correlation is accounted for at the ROCCSD(T) level of theory (δ[ROCCSD(T)] = 4.59 kcal mol^{-1}), as the net δ[ROCCSDT] + δ[UCCSDT(Q)] correction for **TS2** is only 0.04 kcal mol^{-1}. This shift is smaller in magnitude by 0.45 kcal mol^{-1} when compared to the corresponding term for **TS1**. It is expected that the δ[ROCCSDTQ] contribution and the difference between cc-pVQZ and cc-pV5Z for δ[ROCCSD(T)] are both smaller than 0.1 kcal mol^{-1}. Our **TS2** barrier is higher in energy than that of DeSain et al.[154] and

subsequent modifications13, 31 by 2.77 kcal mol^{-1} and (1.57, 3.07) kcal mol^{-1}, respectively. The CBS-QB3 level of theory produces a value varying from our result by 0.12 kcal mol^{-1}.[161] The work of Goldsmith et al.[162] places **TS2** 1.2 kcal mol^{-1} above the reactants, which is 0.17 kcal mol^{-1} lower in energy than our result. **TS2** exhibits a hydrogen-transfer reaction-mode frequency of $2445i$ cm^{-1}, which is larger than the analogous value for the β-hydrogen transfer transition state of the n-propyl + O_2 system by 246 cm^{-1}. There is a change of +0.19 kcal mol^{-1} for ΔZPVE(harm) when using our CMA0(TZ,DZ) basis set over cc-pVDZ; this change is smaller by 0.53 kcal mol^{-1} when compared to the same change in the n-propyl + O_2 system.

Table 4.5: Focal point analysis (in kcal mol^{-1}) for **TS2** relative to i-propyl + O_2.

	ΔE_e(ROHF)	$+\delta$ [ZAPT2]	$+\delta$ [ROCCSD]	$+\delta$ [ROCCSD(T)]	$+\delta$ [ROCCSDT]	$+\delta$ [UCCSDT(Q)]	NET
6-31G*	33.386	–19.263	–2.228	–2.765	–0.060	–0.032	9.037
cc-pVDZ	32.175	–17.850	–2.371	–3.159	–0.007	[–0.032]	[8.756]
cc-pVTZ	31.049	–23.686	–0.706	–4.157	[–0.007]	[–0.032]	[2.460]
cc-pVQZ	31.325	–25.434	–0.203	–4.406	[–0.007]	[–0.032]	[1.243]
cc-pV5Z	31.347	[–26.057]	[–0.024]	[–4.494]	[–0.007]	[–0.032]	[0.733]
CBS LIMIT	[31.331]	[–26.710]	[0.164]	[–4.587]	[–0.007]	[–0.032]	[0.159]

FC-ROCCSD(T)/cc-pVTZ reference geometries

$\Delta E_{final} = \Delta E_e$(FPA) + ΔZPVE (harm) + Δ(rel) + Δ(core) = 0.16 +1.00 + 0.13 + 0.08 = **1.37 kcal mol^{-1}**

The energy of the focal pointed **TS2′** structure lies 2.45 kcal mol^{-1} above the separated reactants and a substantial 1.08 kcal mol^{-1} above **TS2**. The corresponding structures in the n-propyl + O_2 system have an energy difference of 0.16 kcal mol^{-1} which is likely due to the greater torsional freedom for the O_4O_5 group on C_3. For the i-propyl + O_2 system the O_4-O_5 group is attached to C_2 and so a rotation about the C_2-C_3 bond offers a lesser degree of conformational relaxation to the n-propyl + O_2 system.[167] While **TS2** executes its β-abstraction further away from the C_1 methyl group [$\tau(C_1-C_2-O_4-O_5) = -168.14°$], **TS2′** executes its β-abstraction in an area of greater proximity and thus greater steric repulsion from the C_1 methyl group [$\tau(C_1-C_2-O_4-O_5) = 75.88°$]. **TS2′** exhibits a Δ_{DBOC} value of 1.07 kcal mol^{-1} which is smaller than **TS2** by a scant 0.02 kcal mol^{-1} and so this correction is quite large for both conformers.

Our **TS2′** structure has an $H_{12}-O_5$ bond distance of 1.221 Å, matching **TS2** to the third decimal. The r(C_3-H_{12}) bond of **TS2′** nearly matches **TS2**, showing a deviation of +0.001 Å. The r(C_2-C_3) and r(C_2-O_4) bonds are nearly identical, with changes from **TS2TS2′** of +0.002 and +0.006 Å, respectively. The $\alpha(C_3-C_2-O_4)$ and $\alpha(C_2-O_4-O_5)$ angles show minimal changes from **TS2** to **TS2′** of $-0.31°$ and $+0.18°$ respectively, but the $\alpha(C_1-C_2-C_3)$ angle exhibits a sizeable change of $-3.02°$. The ring structure of **TS2′** has torsion angles of $\tau(C_3-C_2-O_4-O_5) = 45.44°$ and $\tau(C_2-O_4-O_5-H_{12}) = 34.29°$ which again shows the non-planarity of the 5-membered hydrogen abstraction ring. The **TS2** and **TS2′** 5-membered

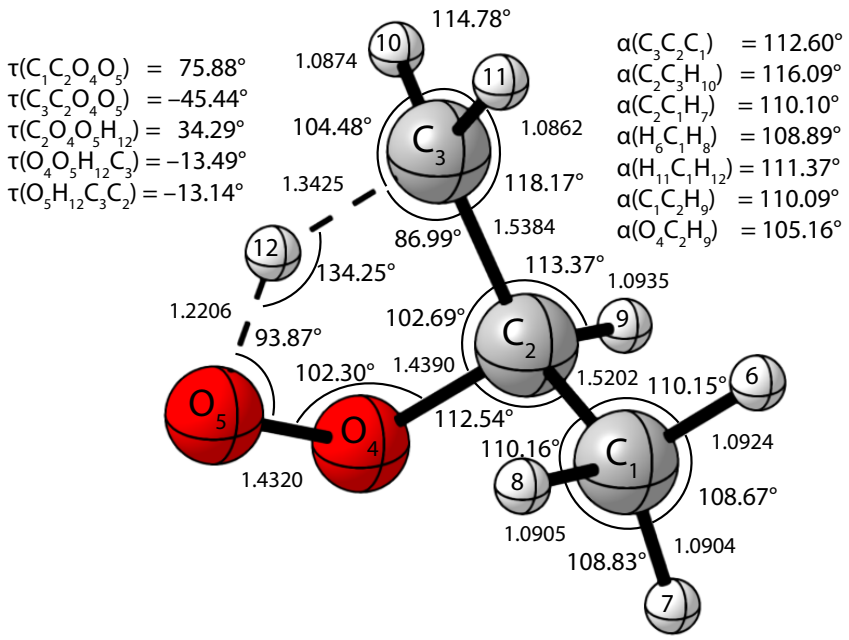

Figure 4.9: Optimum geometry of **TS2′** at the ROCCSD(T)/cc-pVTZ level of theory. Bond lengths are in Å.

hydrogen abstraction rings have nearly equal torsion values, with deviations of $\Delta\tau(C_3{-}C_2{-}O_4{-}O_5) = 0.04°$ and $\Delta\tau(C_2{-}O_4{-}O_5{-}H_{12} = 0.39°$.

The final "low-energy" pathway leading from **MIN1** runs through the α-hydrogen transfer transition state (**TS5**, Figure 4.10) and this transition state runs straight down to the acetone + OH products through a bifurcated pathway, which connects to **MIN3**. This bifurcated pathway is discussed in greater detail further below. **TS5** involves a hydrogen transfer via a 4-membered ring.

In contrast to the **TS1** and **TS2**/**TS2′** structures, **TS5** has a lengthened $H_{12}{-}O_5$ bond distance of 1.286 Å. An increase in the $C_3{-}H_{12}$ bond length of 0.21 Å is observed going from **MIN1** to **TS5**. The $r(C_2{-}C_3)$ and $r(C_2{-}O_4)$ bonds both contract, showing deviations of -0.01 and -0.06 Å, respectively. The $\alpha(C_1{-}C_2{-}C_3)$, $\alpha(C_3{-}C_2{-}O_4)$, and $\alpha(C_2{-}O_4{-}O_5)$ angles change by 4.96°, 4.73°, and 22.21°, respectively, when going from **MIN1** to **TS5**, exhibiting the necessary contraction of the $\alpha(C_2{-}O_4{-}O_5)$ angle to perform the α-hydrogen abstraction. The pertinent torsion angles of **TS5** are $\tau(C_3{-}C_2{-}O_4{-}O_5) = 112.08°$ and $\tau(C_2{-}O_4{-}O_5{-}H_{12}) = -1.61°$ making the 4-membered hydrogen abstraction ring very nearly planar.

The **TS5** focal pointed energy lies 5.72 kcal mol^{-1} above the separated reactants. The ROHF/CBS value is tightly converged for this species as it differs from the ROHF/cc-pV5Z result by a mere 0.003 kcal mol^{-1}. The $+\delta$[ROCCSD(T)] correction for this **TS5** converges similarly to **TS2**, with differences of 0.87 kcal

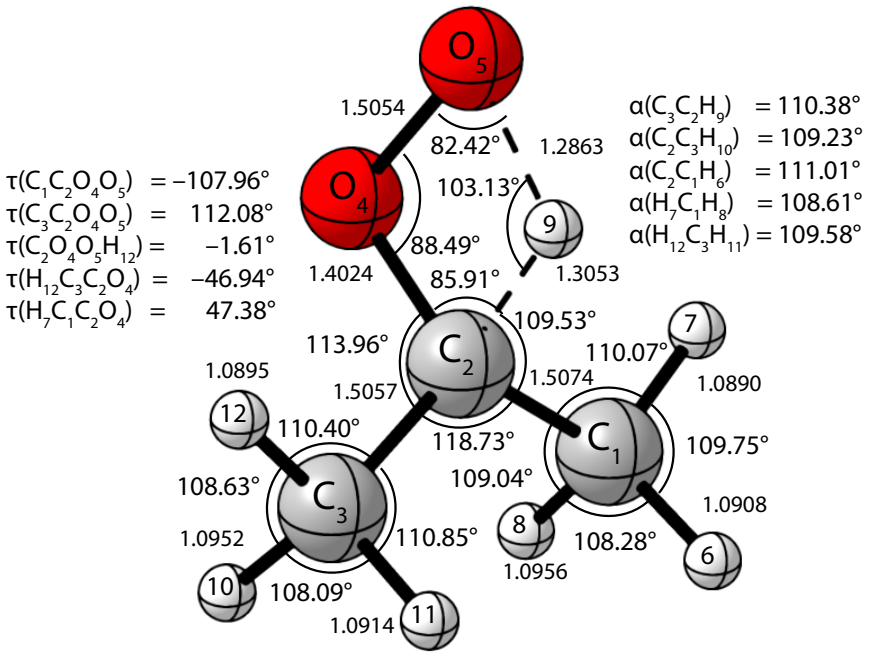

Figure 4.10: Optimum geometry of **TS5** at the ROCCSD(T)/cc-pVTZ level of theory. Bond lengths are in Å.

mol^{-1} and 0.28 kcal mol^{-1} between the cc-pVDZ and cc-pVTZ, and the cc-pVTZ and cc-pVQZ basis sets, respectively. The electron correlation of this system is well described by the $+\delta$[ROCCSD(T)] correction as the net δ[ROCCSDT] + δ[UCCSDT(Q)] correction is only 0.11 kcal mol^{-1}. Our **TS5** barrier is higher than that of Goldsmith et al.[162] by +0.22 kcal mol^{-1}. As seen in Table 4.1, this is the only possible literature comparison for this species. **TS5** has a hydrogen-transfer reaction-mode frequency of 1836i cm^{-1}. This mode's frequency differs from the analogous mode frequency of the n-propyl + O_2 α-hydrogen abstraction transition state by 74i cm^{-1}. The ΔZPVE (harm) changes by +0.23 kcal mol^{-1} using the CMA0(TZ,DZ) basis set over cc-pVDZ.

4.3.4 QOOH Species

The next transition state (**TS2**) leading from **MIN1** produces a QOOH species. These QOOH species are distinguished by the location of the carbon radical center. There is only one possible QOOH species (**MIN2**, Figure 4.11) in the i-propyl + O_2 system produced via β-hydrogen transfer, because abstraction from either methyl group in **MIN1** produces the same product. However, seven **MIN2** rotamers were identified at the FCROCCSD(T)/ccpVTZ//MP2/aug-cc-pVDZ level of theory, all lying within the (0, 0.91) kcal mol^{-1} window. These rotamers are TA$^+$G$^+$ (0.00 kcal mol^{-1}), TA$^-$G$^+$ (0.46 kcal mol^{-1}), TA$^-$A$^+$ (0.41 kcal

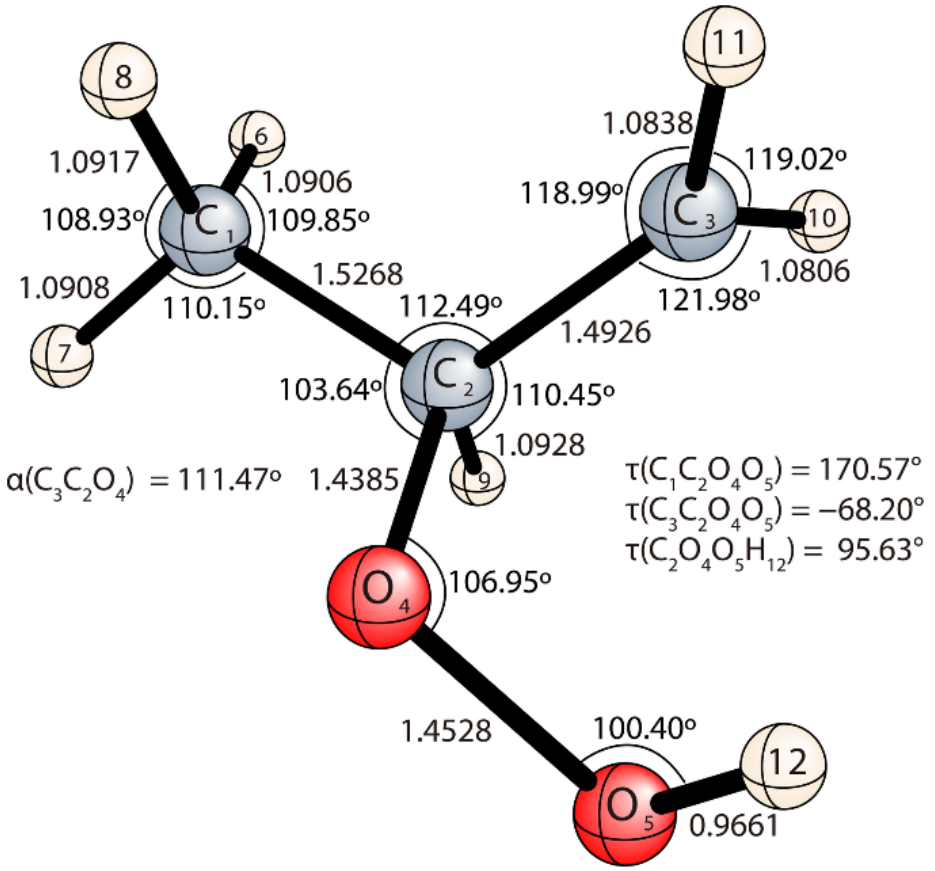

Figure 4.11: Optimum geometry of **MIN2** at the ROCCSD(T)/cc-pVTZ level of theory. Bond lengths are in Å.

mol^{-1}), G$^-$A$^+$C (0.91 kcal mol^{-1}), G$^-$A$^-$C (0.54 kcal mol^{-1}), G$^+$A$^+$C (0.46 kcal mol^{-1}), and G$^+$A$^-$C (0.38 kcal mol^{-1}). The **MIN2** structure of Goldsmith et al.34 is the only other available geometry in the literature and exhibits a rotamer label of TA$^+$G$^+$. Our FPA computations (Table 4.1) place the lowest-energy rotamer of **MIN2** below the reactants by 17.44 kcal mol^{-1}. The QCISD(T)/CBS work of Goldsmith et al.[162] places **MIN2** below our converged FPA result by 0.56 kcal mol^{-1}.

Another possible QOOH species (**MIN3**, Figure 4.12) in the *i*-propyl + O_2 system is produced via a-hydrogen transfer (**TS5**) and there is only one α-hydrogen to abstract in **MIN1**. Two **MIN3** rotamers were identified at the FCROCCSD(T)/ccpVTZ//MP2/aug-cc-pVDZ level of theory. These rotamers are TA$^-$ (0.00 kcal mol^{-1}) and TA$^+$ (0.30 kcal mol^{-1}). We compute the lowest energy rotamer of **MIN3** to be 23.91 kcal mol^{-1} below the separated reactants via FPA (Table 4.1). **MIN3** is not characterized in any of the cited studies.

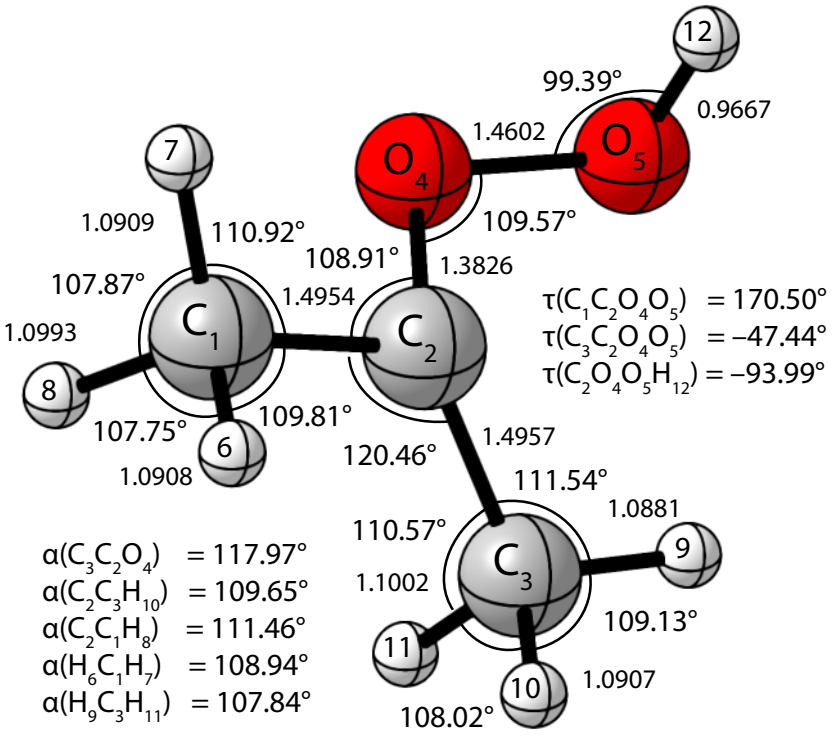

Figure 4.12: Optimum geometry of **MIN3** at the ROCCSD(T)/cc-pVTZ level of theory. Bond lengths are in Å.

4.3.5 TS5 Bifurcated Dissociation Pathway

An intrinsic reaction coordinate (IRC) computation was performed for the **TS5** stationary point in the forward direction at the CCSD(T)/cc-pVDZ level of theory, with **TS5** optimized and a starting Hessian computed at the same level. Single point energies were computed atop these IRC geometries at the CCSD(T)/cc-pVTZ//CCSD(T)/cc-pVDZ level of theory. **TS5** dissociates without barrier down to products of acetone + OH. The dissociation from **TS5** into these products is strongly exothermic as separated acetone + OH lie 64.38 kcal mol^{-1} below the separated reactants and 70.10 kcal mol^{-1} below **TS5**, according to our focal pointed values.

A projected Hessian analysis, using the INTDER program,[228,229] was performed atop the IRC geometries along the arc length range of 0-2.6 a.u.. The lowest energy vibrational mode crosses from real to imaginary at an arc length between 0.2-0.4 a.u., signaling a bifurcation point. The lowest energy vibrational mode for these species is a highly coupled mixture of the $C_2-O_4-O_5-H_{12}$ and $C_3-C_2-O_4-O_5$ torsions. These normal modes lead to a hanging-well QOOH species (**MIN3**) and this minimum is discussed below. The CCSD(T)/cc-pVTZ electronic energies of the IRC species and the **MIN3** cross at an arc length of approximately 2.6 a.u., justifying the constraints of our projected Hessian analysis. This information is qualitatively

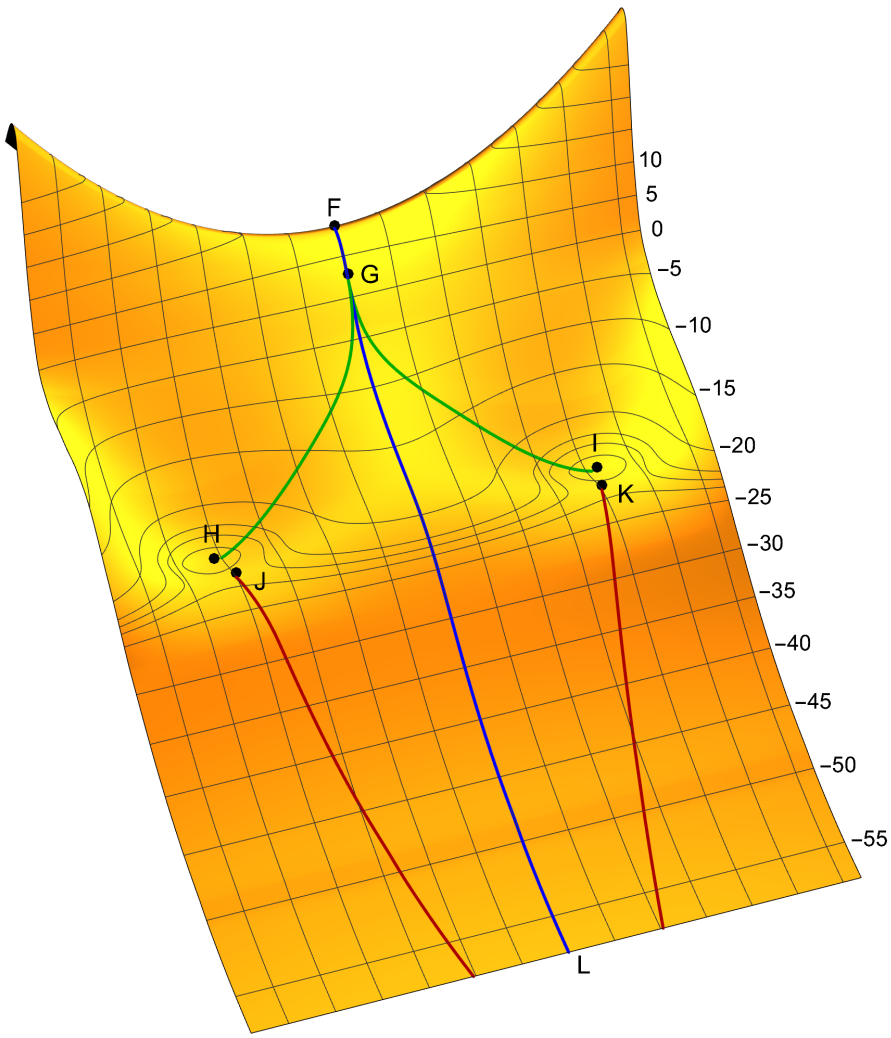

Figure 4.13: A qualitative representation of the **TS5** bifurcated disocciation pathway. Point **F** is the **TS5** equilibrium geometry. Point **G** is the valley-ridge inflection point. Points **H** and **I** are symmetric **MIN3** equilibrium geometries. Points **J** and **K** are symmetric **TS6** equilibrium geometries. All paths lead towards the Acetone + OH dissociated products.

summarized in Figure 4.13, including **TS6** which is discussed below.

4.3.6 Pathways Leading From QOOH

Two possible fragmentation pathways (Figure 4.2) were investigated that originate from **MIN2**: C_2-O_4 bond cleavage and HO_2 elimination (**TS3**, Figure 4.14) and C_3-O_4 bond formation and OH elimination (**TS4**, Figure 4.15). There is a limited amount of previous information on these two transition states in the literature with only two studies[154,162] supplying energies and one study supplying geometries.[162] Similar to the *n*-propyl + O_2 system,[167] major discrepancies are observed, mainly involving dihedral angles,

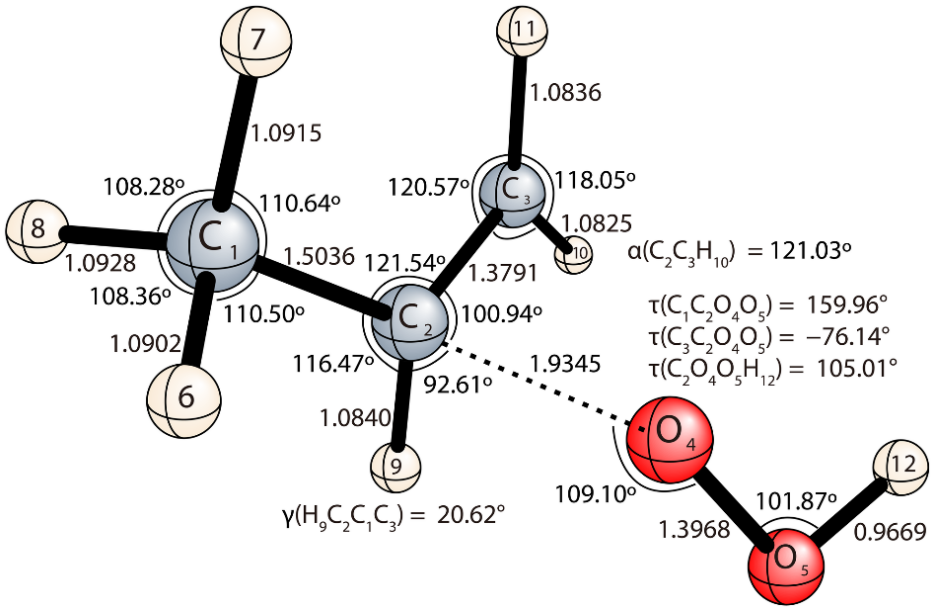

Figure 4.14: Optimum geometry of **TS3** at the ROCCSD(T)/cc-pVTZ level of theory. Bond lengths are in Å.

between our fragmentation structures (**TS3**−**TS4**) and those found in the literature. While the B3LYP/6-311++G(d,p) **TS3** structure of Goldsmith et al.[162] displays a MAD of only 0.005 Å for bond lengths, it exhibits large MADs of 1.6° and 66.5° for bond and torsion angles, respectively, when compared to our structure. The largest discrepancy of 189.3° is observed for $\tau(C_2{-}O_4{-}O_5{-}H_{12})$ because the H_{12} atom is pointed in an opposite direction. Similarly, the **TS4** structure of Goldsmith et al.[162] displays a MAD of 0.009 Å for bond lengths and (1.8°, 9.1°) for (bond, torsion) angles. Again, the largest discrepancy (21.3°) is noted for $\tau(C_2{-}O_4{-}O_5{-}H_{12})$. Once **TS2** is passed, both **TS3** and **TS4**, lying well below the reactants, provide no further hindrance to direct product formation from *i*-propyl + O_2. As shown in Figure 4.2, the chain propagating pathway through **TS4** is the most favorable (Δ_{rxn} H_0°= −5.59 kcal mol^{-1}) leading out of **MIN2**, lying 4.07 kcal mol^{-1} below the chain terminating pathway through **TS3**.

There is one discovered pathway leading to acetone + OH from a QOOH (**MIN3**) species produced by falling off the side of the **TS5** bifurcated pathway. By simply rotating about the $C_2{-}O_4$ bond of the **MIN3** alphaperoxy radical to place the $O_4{-}O_5$ closer in line with the radical orbital, one can find **TS6** (Figure 6.5 in the appendix), the transition state to the acetone + OH dissociated products from **MIN3**. Our FPA computations find that **TS6** lies 25.01 kcal mol^{-1} below the separated reactants, meaning **TS6** provides a meager 1.10 kcal mol^{-1} barrier to dissociation for **MIN3**. With the significant amount of energy present in the system as the reaction progresses from **TS5** to **MIN3** of 29.63 kcal mol^{-1}, it is unlikely that **TS6** would provide much more than a bump in the road towards full dissociation into acetone + OH.

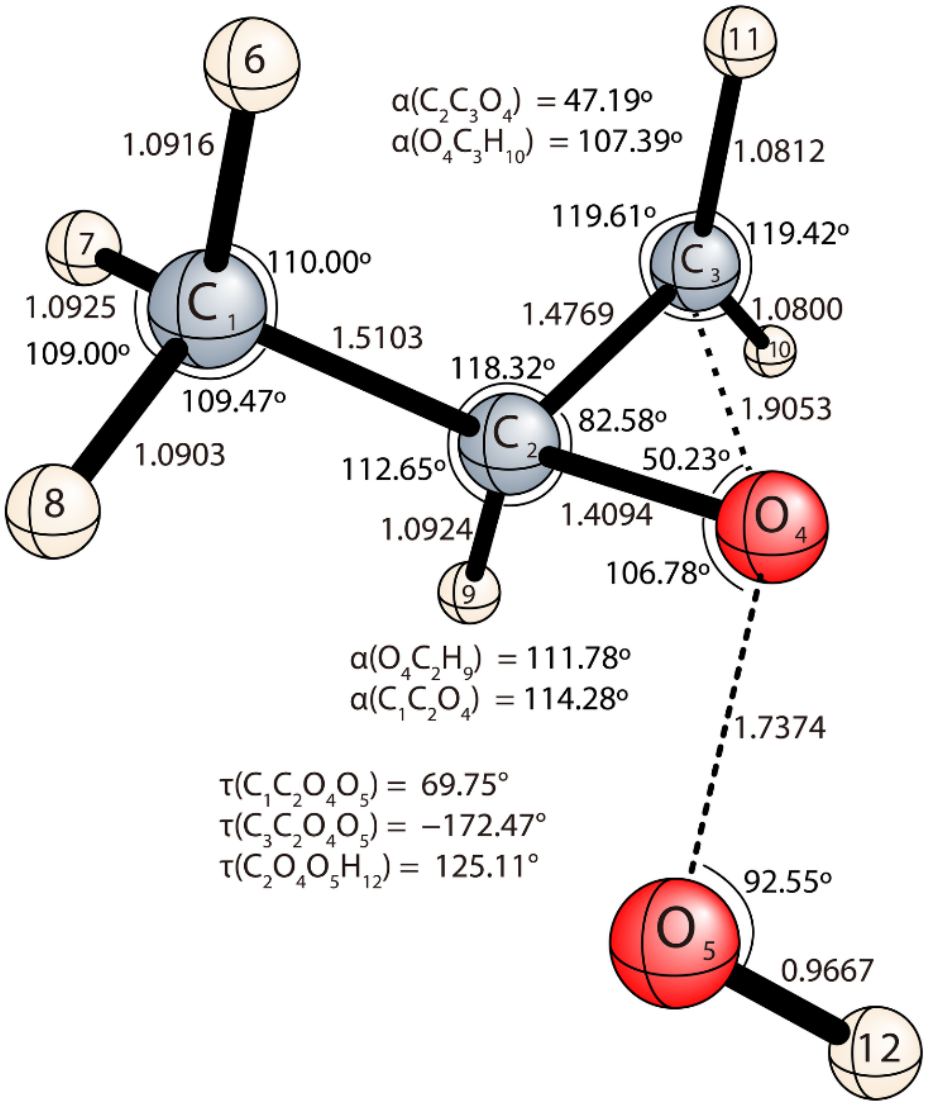

Figure 4.15: Optimum geometry of **TS4** at the ROCCSD(T)/cc-pVTZ level of theory. Bond lengths are in Å.

The experimental model of Huang et al.,[159] assuming that methyloxirane + OH was the dominant source of OH, overpredicted the measured methyloxirane yield. At 670 K, Welz and co-workers[165] observed that methyloxirane was the major C_3H_6O isomer product; however, at temperatures ranging between 530 to 600 K propanal was produced in comparable amounts. Their experiment produced a substantially lower yield of methyloxirane than given by the earlier study,[159] and they suggest the existence of another significant OH channel. Welz et al.[165] find that the sum concentration of acetone, propanal, and oxetane is comparable to that of methyloxirane. Large barriers must be surmounted in order to produce these species as evidenced in this work as well as the earlier work on *n*-propyl + O_2.[167]

While the propanal found by Welz et al.[165] can be attributed to the *n*-propyl + O_2 reaction, the observed acetone is due to the constitutional isomer *i*-propyl reacting with O_2. A transition state from **MIN1** leading directly to acetone + OH that is 5.5 kcal mol^{-1} above the separated reactants has been reported;[162] however, no molecular geometry was supplied. This transition state corresponds to our **TS5** stationary point at 5.72 kcal mol^{-1}. Such saddle points have been reported elsewhere,[161] but they were found to be prohibitively high. In an attempt to rationalize their experimental yields of acetone, Welz et al.[165] suggest that the previously reported[162] barrier height of 5.5 kcal mol^{-1} would need to be lowered by 3.8 kcal mol^{-1}. The **TS5** energy in this work, computed at a high level of theory, does not fulfill the aforementioned energy lowering criterion, however the 2021 work by Klippenstein and coworkers[230] introduces a new wrinkle into these PESs, heavy-atom tunneling. Kinetic studies will have to be re-evaluated with the possibility of heavy-atom tunneling in mind as the acetone + OH products are the clear thermodynamic product of this reaction. Rigorous, high-level of theory PESs such as this work and the prior *n*-propyl study[167] will be vital to the kinetics as reference data.

4.4 Conclusion

The essential features of the *i*-propyl + O_2 reaction system were explored utilizing focal point analyses (FPA) to obtain *ab initio* energetics that push the boundaries of accuracy for combustion systems. FPA energetics were obtained with electron correlation treatments through CCSDT(Q) and with basis sets up to cc-pV5Z. The primary minimum (**MIN1**) and the most favorable pathway transition state (**TS1**) were found to lie 34.8 kcal mol^{-1} and 4.4 kcal mol^{-1}, respectively, below the reactants. Fully optimized CCSD(T)/cc-pVTZ geometries were compared to the large number of DFT structures in the literature for stationary points on the *i*-propyl + O_2 potential energy surface. Substantial mean absolute deviations were observed for both bond lengths and angles in some cases, demonstrating the necessity of highly correlated methods for geometry optimizations of combustion chemistry species. Accurate ZPVE corrections, which are crucial for definitive energetics, were determined utilizing our newly developed Concordant Modes approach. The effect of TZ quality basis sets for ZPVE corrections is nonetheless smaller for the *i*-propyl + O_2 system than was observed for *n*-propyl + O_2, with cc-pVDZ ΔZPVE(harm) values displaying a MAD of only 0.31 kcal mol^{-1} when compared to utilizing CMA0(TZ,DZ) values. **TS2** exhibits an anomalously large DBOC correction, which is indicative of a nearby conical intersection. This is further demonstration that the DBOC correction can be utilized as a diagnostic for the presence of nearby conical intersections and possible nonadiabatic reaction dynamics on potential energy surfaces.

While the chain-terminating, concerted elimination of HO_2 pathway predominates in the *n*-propyl +

O_2 system with **TS1** lying at -2.4 kcal mol^{-1}, this pathway is less favorable when compared to ethyl + O_2, whose corresponding barrier is 0.6 kcal mol^{-1} lower.[143] However, chain branching stabilizes **TS1** in the *i*-propyl + O_2 system, thus making it more favorable compared to ethyl + O_2. The most energetically favorable OH producing pathway begins with a **MIN1** $\rightleftharpoons$ **MIN2** isomerization over **TS2** followed by O$-$O bond scission and ring closure over **TS4** to yield methyloxirane + OH. A bifurcated PES was discovered for the dissociation from the α-proton abstraction, **TS5**, to acetone + OH. The PES bifurcates into symmetric alphaperoxy radicals, **MIN3**, which can dissociate to the same products via a low lying transition state, **TS6**.

It is important to extend high-level computational studies to the *n*-butyl + O_2 system to understand the prototypical behavior of autoignition chemistry. We hypothesize that the pathway through the 7-membered ring hydrogen-transfer transition state to the δ-QOOH species followed by a 6-membered ring transition to oxacyclopentane + OH is more favorable in the *n*-butyl + O_2 system than the associated concerted elimination of HO_2.

CHAPTER 5

THE CONCORDANT MODE APPROACH: A NOVEL BASIS FOR COMPUTING VIBRATIONAL FREQUENCIES

Lahm, M.E.; Kitzmiller, N.; Mull, H.; Allen, W. D.; Schaefer, H. F. To be published as a communication in the Journal of Chemical Physics Letters

5.1 Abstract

The Concordant Mode Approach (CMA) is an umbrella of methods for computing harmonic vibrational frequencies using lower level of theory normal modes as a basis for higher level of theory force constant computation. CMA0 approximates harmonic frequencies at a high level of theory using lower level of theory normal modes to compute the diagonal force constants at a higher level, utilizing stationary points for each Hessian computed. Utilizing CCSD(T)/cc-pVDZ and B3LYP/6-31g(*2df,p*) starting Hessians for CMA0 on the G2 test set yields a mean deviation of harmonic frequencies from CCSD(T)/cc-pVTZ of -0.03 cm^{-1} and -0.08 cm^{-1}, respectively. Both approaches agree with the CCSD(T)/cc-pVTZ zero point vibrational energies (ZPVEs) to 2 decimal places, with a mean deviation of 0.00 kcal mol^{-1}.

5.2 Introduction

The determination and assignment of the vibrational frequencies of molecular systems has been a mainstay of quantum chemistry since its inception. The energy of fundamental vibrational excitations falls into the energy range utilized by infrared and Raman Spectroscopy. Spectra generated by these techniques can provide insights into molecular motifs due to the unique character of certain chemical bonds and their respective force constants. Furthermore, the zero-point vibrational energy (ZPVE) of molecular systems is vital for calculating accurate thermodynamic and kinetic properties of chemical reactions. *Ab initio* computation of vibrational frequencies and subsequent prediction of vibrational spectra would not come into vogue until the 1960s when more powerful computers were constructed. This is due to the inherent necessity of computing second and higher order derivatives of the electronic energy to calculate vibrational frequencies of a molecular system.

In spite of the existence of efficient algorithms for the computation of harmonic frequencies, the computation of harmonic vibrational frequencies with high level *ab initio* theories such as the coupled cluster singles, doubles, and perturbative triples[45,46] [CCSD(T)] theory remains elusive for systems with more than 10 heavy atoms. Harmonic vibrational frequency computations are limited for even large systems when using faster but less accurate methods such as density functional theory (DFT) or any approximate high level theories without analytic gradients. Computing the necessary second derivatives of the nuclear coordinate potential energy, which is parametrically dependant upon electronic structure, can be accomplished via a finite differences of single point energies procedure.

This procedure is embarassingly parallelizable for the rate determining step of computing the electronic energy at a particular structure of the target system, however the quadratic scaling of this procedure greatly

hinders its computational efficiency. For some electronic structure theories analytic gradients are available, in which case a finite difference of gradients procedure may be employed. Nonetheless, many high level electronic structure methods do not have analytic gradients formulated, let alone implemented. If a finite differences of energies procedure is employed, a non-linear system with N atoms requires $9N^2 - 33N + 31$ single-point computations. Strategies that reduce this scaling could allow for larger molecules to be described.

We propose here a Concordant Mode Approach (CMA) for computing harmonic vibrational frequencies. This approach utilizes the normal modes of a particular molecular system at a lower level of theory, atop a geometry optimized at the same level of theory, as the coordinate basis for the computation of force constants via finite differences. If one makes the approximation that the supplied normal modes are identical to the normal modes of a desired level of theory, the coupling force constants of the normal modes reduce to zero, necessitating only the computation of the diagonal force constants so that the scaling of necessary single-point energies reduces from the aforementioned, quadratic $9N^2 - 33N + 31$ to a linear $6N - 11$. The more accurate this diagonal approximation is, the greater the "concordance" is between the normal modes of the different levels of theory. Such an approximation to the CMA will be dubbed CMA zero (CMA0).

5.2.1 Theory

The theoretical grounding of the CMA begins with the GF-matrix method of Wilson and Decius.[231] The GF-matrix method describes the harmonic vibrational freqencies of molecules in terms of translationally and rotationally invariant internal coordinates. The **G** matrix of this method contains the kinetic enery information of the molecular system in internal coordinates. **G** matrix elements are calculated as follows,

$$\mathbf{G}_{tt'} = \sum_{i=1}^{3N} \frac{1}{m_i} \mathbf{B}_{ti} \mathbf{B}_{t'i} \quad t, t' = 1, 2, \ldots, 3N - 6. \tag{5.1}$$

Where **B** is a tensor that transforms a cartesian differential ($\mathrm{d}x_i$) into an internal coordinate differential ($\mathrm{d}s_t$) and is mathematically defined as follows,

$$\mathbf{B}_{ti} = \left(\frac{\mathrm{d}s_t}{\mathrm{d}x_i} \right)_0 . \tag{5.2}$$

The zero subscript of the derivative signifies that the **B**-tensor is calculated at the reference structure. The **F** matrix of this method contains the potential energy information of the system in internal coordinates. The **F** matrix elements are defined as follows,

$$\mathbf{F}_{tt'} = \left(\frac{\partial^2 \mathrm{V}}{\partial t \partial t'} \right)_0 . \tag{5.3}$$

Where each element is a force constant calculated as the second derivative of the vibrational potential energy function with respect to internal coordinates t and t'. These two matrices when multiplied form a nonsymetric eigensystem that when diagonalized yields the force constant of each harmonic vibrational frequency. This nonsymetric eigensystem is as follows,

$$\mu\mathbf{\Lambda} = \mathbf{L}^{-1}(\mathbf{GF})\mathbf{L} \tag{5.4}$$

where $\mathbf{L}$ contains the non-orthonormal eigenvectors of the GF system and μ and $\mathbf{\Lambda}$ are the diagonalized counterparts of $\mathbf{G}$ and $\mathbf{F}$, respectively. The harmonic vibrational frequencies obey the following relation,

$$c\sqrt{\mu_i\Lambda_i} = \omega_i \tag{5.5}$$

where c is a unit conversion constant. In order to use a traditional eigensolver on this system the GF matrix product must be symmetrized. Thus the following equations are used,

$$\mathbf{L}' = \mathbf{G}^{-\frac{1}{2}}\mathbf{L} \tag{5.6}$$

$$\mu\mathbf{\Lambda} = \mathbf{L}'^{-1}(\mathbf{G}^{\frac{1}{2}}\mathbf{F}\mathbf{G}^{\frac{1}{2}})\mathbf{L}' \tag{5.7}$$

and L may be easily retrieved by left multiplying L$'$ by G$^{\frac{1}{2}}$.

The GF product may be solved to acquire a set of force constants at two particular levels of theory, A and B, as follows,

$$\mu_A\mathbf{\Lambda}_\mathrm{A} = \mathbf{L}_\mathrm{A}^{-1}(\mathbf{G}_\mathrm{A}\mathbf{F}_\mathrm{A})\mathbf{L}_\mathrm{A} \tag{5.8}$$

$$\mu_B\mathbf{\Lambda}_\mathrm{B} = \mathbf{L}_\mathrm{B}^{-1}(\mathbf{G}_\mathrm{B}\mathbf{F}_\mathrm{B})\mathbf{L}_\mathrm{B} \tag{5.9}$$

The $\mathbf{G}$ and $\mathbf{F}$ matrices of theory B may then be transformed by the eigenvector matrix $\mathbf{L}_\mathrm{A}$,

$$\mu_\mathrm{A,B} = \mathbf{L}_\mathrm{A}^{-1}\mathbf{G}_\mathrm{B}(\mathbf{L}_\mathrm{A}^{-1})^\mathrm{T} \tag{5.10}$$

$$\mathbf{\Lambda}_\mathrm{A,B} = \mathbf{L}_\mathrm{A}^\mathrm{T}\mathbf{F}_\mathrm{B}\mathbf{L}_\mathrm{A} \tag{5.11}$$

If the $\mathbf{L}_\mathrm{A}$ and $\mathbf{L}_\mathrm{B}$ eigenvectors are sufficiently similar then it will be the case that $\mathbf{\Lambda}_\mathrm{A,B}$ will have a strong diagonal with some sparse off-diagonal elements, and that $\mathbf{\Lambda}_\mathrm{A,B} \approx \mathbf{\Lambda}_\mathrm{B}$.

The CMA0 approximation only necessitates that one compute the diagonal force constants of $\mathbf{\Lambda}_\mathrm{A,B}$ as it assumes that $\mathbf{\Lambda}_\mathrm{A,B} = \mathbf{\Lambda}_\mathrm{B}$. $\mu_\mathrm{A,B}$ will also have to be computed; however, this task is trivial as the geometric

structure of the target system at the B level of theory contains all the necessary information to fully compute the $\mathbf{G}_{\mathrm{B}}$ matrix. To compute $\mathbf{\Lambda}_{\mathrm{A,B}}$, finite differences of single point electronic energies will be utilized to numerically compute the second derivatives. For uncoupled differentiations, the finite difference formula is as follows,

$$\frac{\partial^2 \mathrm{E}_{elec}(Q_i)}{\partial Q_i^2} \approx \frac{\mathrm{E}_{elec}(Q_i + h) - 2\mathrm{E}_{elec}(Q_i) + \mathrm{E}_{elec}(Q_i - h)}{h^2} \tag{5.12}$$

where Q_i refers to the value of the ith normal coordinate and h is a small displacement that adds onto Q_i to displace the reference structure. While the generation of geometric structures atop a cartesian geometry is easily performed using a Cartesian h, this process is complicated by using normal coordinate displacements as a linear combination of curvilinear, internal coordinates. This is due to the fact that the transformation between curvilinear internal coordinates and rectilinear Cartesian coordinates is non-linear.

One can approximately transform a cartesian displacement to an internal coordinate displacement using our previously defined B-tensor as follows,

$$\mathbf{B}\Delta\vec{x} \approx \Delta\vec{s}. \tag{5.13}$$

The **B**-tensor has an inverse operation, referred to as the **A**-tensor, and it has the following properties,

$$\mathbf{A}_{it} = \left(\frac{\mathrm{d}x_i}{\mathrm{d}s_t}\right)_0 \tag{5.14}$$

$$\mathbf{A}\Delta\vec{s} \approx \Delta\vec{x}. \tag{5.15}$$

The **A**- and **B**-tensors are not square matrices, and their inversion requires care. One must then generate the **A**-tensor using the following formula,

$$\mathbf{A} = \mathbf{u}\mathbf{B}^{\mathrm{T}}(\mathbf{B}\mathbf{u}\mathbf{B}^{\mathrm{T}})^{-1} \tag{5.16}$$

Where **u** is a diagonal matrix of the appropriate dimensions for the matrix multiplication. **u** must be mass weighted with triads of reciprical atomic masses to obtain properties such as dipole derivatives, however for the finite differences displacements of scalar properties such as the potential energy surface **u** may simply be the identity matrix.

The GF eigenvector matrix, **L**, may be utilized to linearly convert normal coordinates into internal

coordinates and so the following transformation may occur,

$$\vec{s} = \mathbf{L}\vec{Q} \tag{5.17}$$

$$\mathbf{A}\Delta(\mathbf{L}\vec{Q}) \approx \Delta\vec{x}. \tag{5.18}$$

$$\mathbf{AL}\Delta\vec{Q} \approx \Delta\vec{x}. \tag{5.19}$$

Thus, a rectilinear, Cartesian displacement may be generated to first order (exact in the limit of infinitesimal displacements) of a curvilinear, normal mode displacement. One can utilize an iterative procedure to converge the cartesian displacments to the normal coordinate displacement within a particular tolerance using the following algorithm,

- Generate the reference $\vec{Q}$ values from the reference cartesian structure, $\vec{x}$.
- Add $\Delta\vec{Q}$ onto the reference $\vec{Q}$ values.
- Generate the cartesian displacement, $\Delta\vec{x}$, from $\Delta\vec{Q}$ using the A-tensor.
- Add $\Delta\vec{x}$ onto the reference cartesian geometry to generate the displaced cartesian structure, $\vec{x'}$.
- Compute the updated basis internal coordinate values from $\vec{x'}$ and transform them using $\mathbf{L}^{-1}$ to obtain the actual displaced normal coordinate values $\vec{Q}'$.
- Set $\Delta\vec{Q}'$ equal to $\vec{Q} - \vec{Q}'$, $\vec{Q}$ equal to $\vec{Q}'$, and $\vec{x}$ equal to $\vec{x'}$.
- Check if the norm of $\Delta\vec{Q}$ is less than a predetermined tolerance. If not, return to step one. If the norm of $\Delta\vec{Q}$ is lower than the tolerance, break from the loop.

Using this algorithm, the requisite displaced geometries for the finite difference formula may be generated and single point electronic energies may be computed at the desired level of theory atop these structures. The normal coordinate force constant matrix, $\mathbf{\Lambda}_{\mathrm{A,B}}$, is then generated via numerical differentiation and run back through the GF method with the updated $\mu_{\mathrm{A,B}}$ matrix to yield the final frequencies.

5.2.2 Theoretical Methods

CMA0 will be benchmarked atop the G2 test set,[232,233] of the G2 method, with two sets of theories. The first set utilizes a CCSD(T)/cc-pVDZ//CCSD(T)/cc-pVDZ[45,46,191,192] starting Hessian and geometry with diagonal force constants calculated with the CCSD(T)/cc-pVTZ//CCSD(T)/cc-pVTZ[45,46,191,192] level of theory (henceforth CMA0[(T)/DZ,(T)/TZ]). The second set is again targeting CCSD(T)/cc-pVTZ//CCSD(T)/cc-pVTZ,[45,46,191,192] but the starting Hessian is calculated at the B3LYP/6-31g(*2df,p*)//B3LYP/6-31g(*2df,p*)[123,195,234]

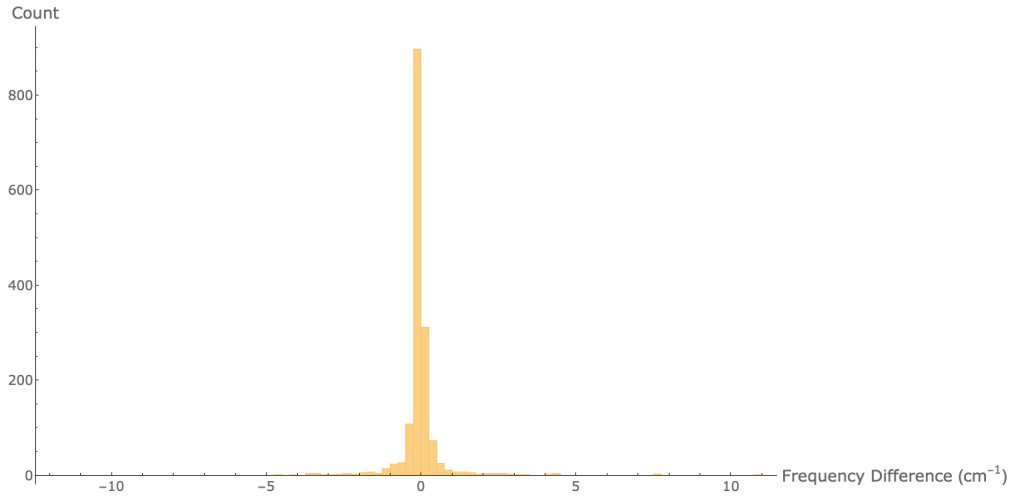

(a)

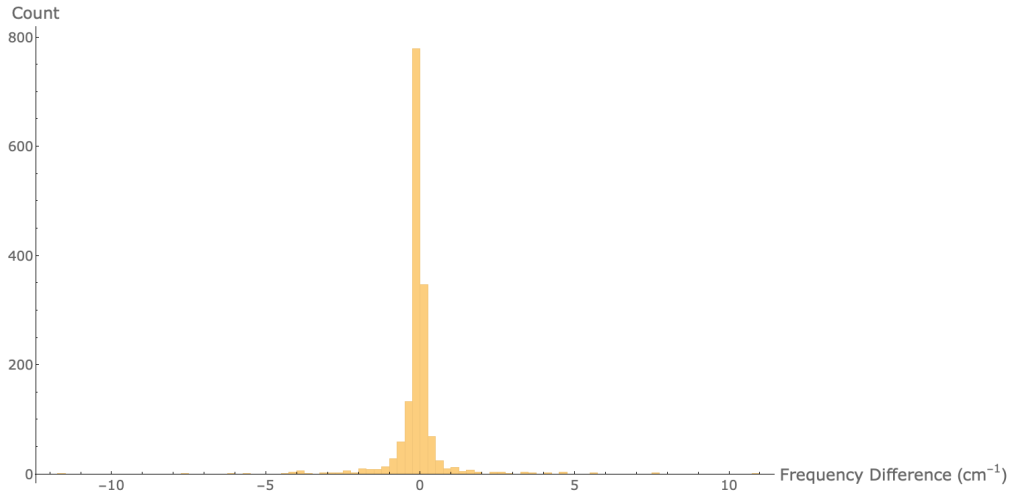

(b)

Figure 5.1: (a) The binned counts of differences for all vibrational modes within the selected G2 test set between the CMA0[(T)/DZ,(T)/TZ] and the reference CCSD(T)/cc-pVTZ data. (b) The binned counts of differences for all vibrational modes within the selected G2 test set between the CMA0[B3LYP/6-31g(*2df,p*),(T)/TZ] and the reference CCSD(T)/cc-pVTZ data.

level of theory (henceforth CMA0[B3LYP/6-31g(*2df,p*),(T)/TZ]). A combination of finite differences of single point energies and finite differences of gradients was employed to calculate the Hessians via a 3-point formula. Analytic and finite difference gradients were utilized for the optimizations. The CFOUR quantum chemical software package[47] was used for all thereference geometry and frequency computations, PSI4[114] was utilized for the DFT computations, and Molpro 2010[48] was used for all CMA0 CCSD(T)/cc-pVTZ single point energies.

5.3 Results

All diatomic species in the G2 test set were neglected as their CMA0 and reference computation will be identical due to the existence of only one vibrational mode. Furthermore, the methoxy, methylthio, and ethoxy radicals were thrown out as they each experience a Jahn-Teller[235] distortion making them inherently problematic cases for the computation of harmonic vibrational frequencies. Finally, the acetamide molecule was thrown out due to an excessive geometric shift between level A and B theories that causes problems for CMA0.

The first set of CMA0 data utilizes the cc-pVDZ/cc-pVTZ initial/final Hessian combination, all computed with CCSD(T). A histogram containing the signed differences between all harmonic vibrational modes in the G2 test set is shown in Figure 5.1(a). These data have a mean of -0.03 cm^{-1}, a standard deviation of 0.71 cm^{-1}, skewness of 4.05, and kurtosis of 67.70. The mean and standard deviation are highly promising, however the kurtosis is quite large, a consequence of the few outliers in the -10 to 10 cm^{-1} range. This is most likely due to the large concentration of small, well behaved vibrational systems in the G2 test set. Overall the agreement of CMA0[(T)/DZ,(T)/TZ] with the CCSD(T)/cc-pVTZ frequencies is quite exceptional. Somewhere between 90 and 95% of the differences will lie within a 2 cm^{-1} range, by merit of the standard deviation of these data.

The second set of CMA0 data utilizes the B3LYP/6-31G(*d,p*) initial Hessian with CCSD(T)/cc-pVTZ final Hessian. The histogram of these data is shown in Figure 5.1(b). These data have a mean of -0.08 cm^{-1}, a standard deviation of 0.90 cm^{-1}, skewness of 0.19, and kurtosis of 52.81. Similar trends to the DZ/TZ CMA0 data are seen here, with a relative, slight decrease in accuracy from the CCSD(T)/cc-pVDZ initial Hessian. These DFT CMA0 data show a remarkable agreement with the CCSD(T)/cc-pVTZ harmonic frequencies. Similar to above, somewhere between 90 and 95% of the frequency differences will lie within a 2 cm^{-1} range, though the prior method will be more accurate.

Figure 5.2(a) contains a histogram of the root mean square deviations (RMSDs) for each molecular set of vibrational frequencies between the CMA0[(T)/DZ,(T)/TZ] and the reference CCSD(T)/cc-pVTZ data. These data strongly support the above assertion of strong confidence for data matching frequencies to 2 cm^{-1}. There are two outliers, the ethynyl radical and the *tert*-butyl radical. For the ethyl radical it should be noted that there is a 136 cm^{-1} deviation between the CCSD(T)/cc-pVDZ and CCSD(T)/cc-pVTZ degenerate bending modes, whereas CMA0[(T)/DZ,(T)/TZ] deviates by only 4.6 cm^{-1}. CMA0 shows a powerful ability to describe high level of theory frequencies even when the starting and final Hessians are profoundly different.

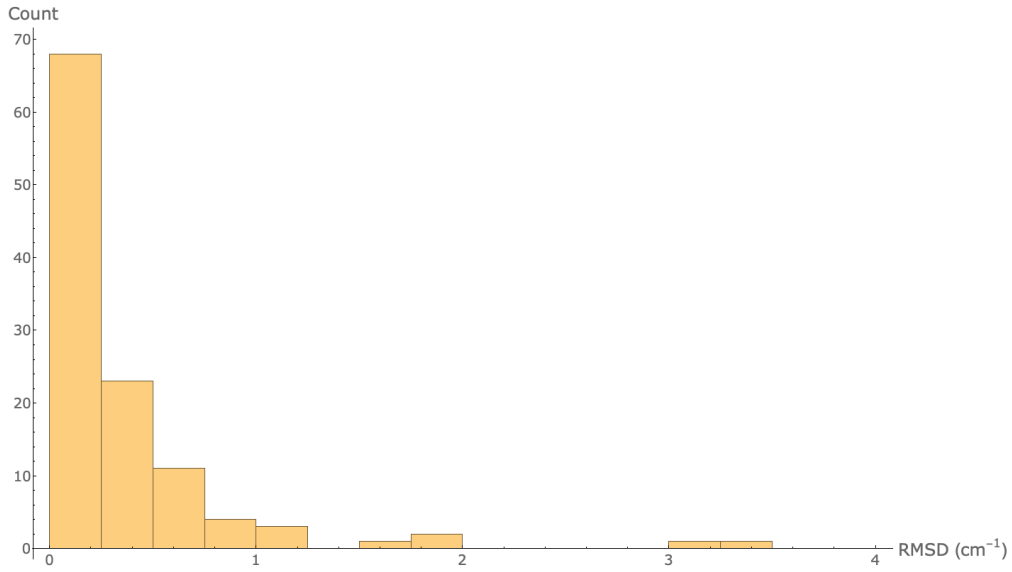

(a)

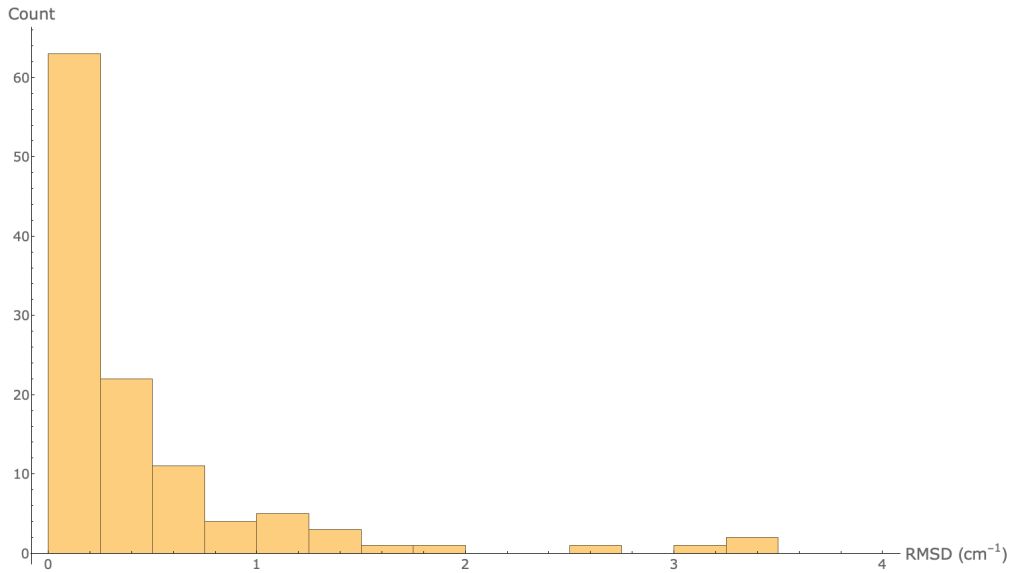

(b)

Figure 5.2: (a) The binned counts of RMSDs for all vibrational modes within the selected G2 test set between the CMA0[(T)/DZ,(T)/TZ] and the reference CCSD(T)/cc-pVTZ data. (b) The binned counts of RMSDs for all vibrational modes within the selected G2 test set between the CMA0[B3LYP/6-31g(*2df,p*),(T)/TZ] and the reference CCSD(T)/cc-pVTZ data.

Figure 5.2(b) contains the RMSDs for each set of vibrational frequencies between the CMA0[B3LYP/6-31g(*2df,p*),(T)/TZ] and the reference CCSD(T)/cc-pVTZ data. The vast bulk of the molecules have RMSDs of 2 cm^{-1} or lower, however there are four outliers for this approach. The outliers are the ethynyl radical, aziridine, bicyclo[1.1.0]butane, and the *tert*-butyl radical. While CMA0 with starting DFT Hessians and geometries results in more outliers, it maintains the general shape of the RMSD histogram and supports the

fidelity of using a cheaper starting Hessian.

While the absolute frequencies hold a 90-95% confidence to 2 cm^{-1}, the zero point vibrational energies (ZPVEs) exhibit even stronger agreement for both approaches as compared to the CCSD(T)/cc-pVTZ ZPVEs. Indeed both of the CMA0[(T)/DZ,(T)/TZ] and CMA0[B3LYP/6-31g(*2df,p*),(T)/TZ] ZPVEs exhibit a mean deviation of 0.00 kcal mol^{-1} from the CCSD(T)/cc-pVTZ ZPVEs. This incredible agreement is likely a result of cancellation of error, as any mixing of the normal mode basis will generally affect equal and opposite positive and negative frequency deviations.

5.4 Conclusion

The Concordant Mode Approach has been formulated as a novel basis for the computation of harmonic vibrational frequencies using lower level of theory normal modes as a basis for the higher level of theory. CMA0 exhibits a linearly scaling number of necessary single point energy computations for an approximate Hessian computation, where a full Hessian computation scales quadratically with respect to necessary single point displacements. This approximation has the potential to open up an entirely new regime of molecular sizes to harmonic vibrational description by CC and DFT. Two approaches were tested with CMA0, one using an initial CCSD(T)/cc-pVDZ Hessian and geometry and the other using an initial B3LYP/6-31G(*d,p*) Hessian and geometry, both calculating diagonal CCSD(T)/cc-pVTZ force constants in the lower level of theory basis. Both of these approaches showed remarkable agreement with the reference CCSD(T)/cc-pVTZ harmonic vibrational frequencies. CMA0 shows excellent promise as an approximate method for calculating accurate frequencies and highly accurate ZPVEs.

CHAPTER 6

CONCLUSION

Bi_4 was studied and characterized using high level *ab initio* methods. Two constitutional Bi_4 isomers of T_d and C_{2v} symmetry were found to be local energetic minima. The optimized geometries and fundamental vibrational frequencies of these two isomers were obtained at the CCSD(T)/cc-pVQZ-PP level of theory, utilizing a 78-electron effective core potential. Focal Point analysis was performed for the dissociation energy of Bi_4 (T_d) into two Bi_2 and the adiabatic energy difference between the C_{2v} and T_d isomers of Bi_4, from a maximum basis set of cc-pV5Z-PP, and proceeding to a maximum correlation method of CCSDTQ yielding +78 kcal mol^{-1} and +43 kcal mol^{-1}, respectively. The most probable approach to laboratory spectroscopic identification of Bi_4 is via an infrared spectrum. The predicted fundamentals (cm^{-1}) with IR intensities in parentheses (km mol^{-1}) were found to be 100(0), 130(0.20), and 175(0) for the T_d isomer. Natural bond orbital analysis predicts that the C_{2v} isomer of Bi_4 was exhibits "long-bonding" between the furthest apart 'wing' atoms.

Several DFT Functionals and basis sets were benchmarked for unsubstituted *ortho*-benzyne. Optimized geometries for the substituted *ortho*-benzyne as well as harmonic vibrational frequencies and singlet-triplet splittings were computed using the benchmarked functionals. A proximal (*syn*)OH substitution was found to cause a mean θ_1 distortion of $+8.1 \pm 1.4^\circ$. Substituting in the proximal position with F was found to shift the singlet-triplet splitting by $+4.5 \pm 0.4$ kcal mol^{-1}. Natural bond orbital (NBO) analysis, including Natural Coulomb Electrostatics (NCE), elucidated the presence of three influences from the selected substituents: hyperconjugative, resonance, and electrostatic effects.

The *i*-propyl + O_2 potential energy surface was studied using high-level *ab initio* methods. Focal Point analyses extrapolating to the *ab initio* limit were performed on the *i*-propyl + O_2 system based on explicit quantum chemical computations with electron correlation treatments through CCSDT(Q) and basis sets up to cc-pV5Z. All reaction species and transition states were fully optimized at the rigorous CCSD(T)/cc-pVTZ level of theory, revealing some substantial differences in comparison to the DFT geometries existing in the literature. Two key stationary points, *i*-propylperoxy radical (**MIN1**) and its concerted elimination

transition state (**TS1**), were found to be 34.8 kcal mol^{-1} and 4.4 kcal mol^{-1} below the reactants, respectively. The β-hydrogen transfer transition state (**TS2**) was found to exhibit an anomalously large diagonal Born-Oppenheimer correction (Δ_{DBOC} = 1.09 kcal mol^{-1}), which is indicative of a nearby surface crossing and possible nonadiabatic reaction dynamics. The α-proton abstraction transition state (**TS5**) is 5.72 kcal mol^{-1} above the reactants and can bifurcate into alphaperoxy radical (**MIN3**) hanging wells before its ultimate dissociation into acetone and the OH radical, located 64.4 kcal mol^{-1} below the reactants. Normally **TS5** lies prohibitively high to be a major pathway, however the quantum effect of heavy-atom tunneling paired with the extreme exothermicity of the **TS5** pathway could explain open questions in the literature. Our definitive energetics for stationary points on the *i*-propyl + O_2 potential energy surface provide key benchmarks for future studies of hydrocarbon oxidation.

The Concordant Mode Approach (CMA) was defined and and benchmarked. CMA is an umbrella of methods for computing harmonic vibrational frequencies using lower level of theory normal modes as a basis for higher level of theory force constant computation. Harmonic frequencies were approximated via CMA0 using a lower level of theory Hessian atop a geometry at the same level to compute the diagonal force constants at the higher level atop the higher level geometry. Utilizing CCSD(T)/cc-pVDZ and B3LYP/6-31g(*d,p*) starting Hessians for CMA0 on the G2 test set yielded a mean deviation of harmonic frequencies from CCSD(T)/cc-pVTZ of -0.03 cm^{-1} and -0.08 cm^{-1}, respectively. Both approaches held mean ZPVE deviations with the CCSD(T)/cc-pVTZ of 0.00 kcal mol^{-1}.

Bibliography

[1] God,; coworkers, *The Holy Bible*; Psalm 23.

[2] Levine, I. N. *Quantum CHemistry*, 5th ed.; Prentice Hall, 2000.

[3] Szabo, A.; Ostlund, N. S. *Modern Quantum Chemistry: Introduction to Advanced Electronic Structure Theory*; MacMillan Publishing Co., Inc., 1982.

[4] East, A. L.; Allen, W. D. *J. Chem. Phys.* **1993**, *99*, 4638–4650.

[5] Allinger, N. L.; Fermann, J. T.; Allen, W. D.; Schaefer, H. F. *J. Chem. Phys.* **1997**, *106*, 5143–5150.

[6] Császár, A. G.; Allen, W. D.; Schaefer, H. F. *J. Chem. Phys.* **1998**, *108*, 9751–9764.

[7] Gonzales, J. M.; Pak, C.; Sidney Cox, R.; Allen, W. D.; Schaefer, H. F.; Császár, A. G.; Tarczay, G. *Chem. Eur. J.* **2003**, *9*, 2173–2192.

[8] A. G. Császár, G. Tarczay, M. L. Leininger, O. L. Polyansky, J. Tennyson and W. D. Allen, Dream or reality: complete basis set full configuration interaction potential energy hypersurfaces, in *Spectroscopy from Space*, ed. J. Demaison and K. Sarka, Kluwer Academic Publishers, Dordrecht, The Netherlands, 2001, ch. 19, pp. 317-340.

[9] Weinhold, F.; Landis, C. *Valency and Bonding: A Natural Bond Orbital Donor-Acceptor Perspective*; Cambridge, 2005.

[10] *NBO 6.0* E. D. Glendening, J. K. Badenhoop, A. E. Reed, J. E. Carpenter, J. A. Bohmann, C. M. Morales, C. R. Landis, and F. Weinhold, Theoretical Chemistry Institute, Universtiy of Wisconsin, Madison (2013).

[11] Lahm, M. E.; Hoobler, P. R.; Turney, J. M.; Peterson, K. A.; Schaefer, H. F. *Phys. Chem. Chem. Phys.* **2018**, *20*, 21881–21889.

[12] Bernhardt, T.; Kaiser, B.; Rademann, K. *Z. Phys. D: At., Mol. Clusters* **1997**, *40*, 327.

[13] Kohl, F. J.; Uy, O. M.; Carlson, K. D. *J. Chem. Phys.* **1967**, *47*, 2667–2676.

[14] Yoo, R. K.; Ruscic, B.; Berkowitz, J. *J. Electron. Spectrosc. Relat. Phenom.* **1993**, *66*, 39–54.

[15] Ross, M. M.; McElvany, S. W. *J. Chem. Phys.* **1988**, *89*, 4821–4828.

[16] Rovner, L.; Drowart, A.; Drowart, J. *Trans. Far. Soc.* **1967**, *63*, 2906–2912.

[17] Geusic, M. E.; Freeman, R. R.; Duncan, M. A. *J. Chem. Phys.* **1988**, *89*, 223–229.

[18] Geusic, M. E.; Freeman, R. R.; Duncan, M. A. *J. Chem. Phys.* **1988**, *88*, 163–166.

[19] Bondybey, V.; Schwartz, G.; Griffiths, J.; H. English, J. *Chem. Phys. Lett.* **1980**, *76*, 30–34.

[20] Bondybey, V. E.; English, J. H. *J. Chem. Phys.* **1980**, *73*, 42.

[21] Manzel, K.; Engelhardt, U.; Abe, H.; Schulze, W.; Froben, F. *Chem. Phys. Lett.* **1981**, *77*, 514–516.

[22] Eberle, B.; Sontag, H.; Weber, R. *Chem. Phys.* **1985**, *92*, 417–422.

[23] Ahmed, F.; Nixon, E. R. *J. Chem. Phys.* **1981**, *75*, 110–113.

[24] Zhang, H.; Balasubramanian, K. *J. Chem. Phys.* **1992**, *97*, 3437–3444.

[25] Jia, J. M.; Chen, G. B.; Shi, D. N.; Wang, B. L. *Eur. Phys. J. D* **2008**, *47*, 359–365.

[26] Lohr, L. L.; Pyykkö, P. *Chem. Phys. Lett.* **1979**, *62*, 333–338.

[27] Gausa, M.; Kaschner, R.; Seifert, G.; Faehrmann, J.; Lutz, H.; Meiwes-Broer, K.-H. *J. Chem. Phys.* **1996**, *104*, 9719–9728.

[28] Polak, M. L.; Ho, J.; Gerber, G.; Lineberger, W. C. *J. Chem. Phys.* **1991**, *95*, 3053.

[29] Yuan, H. K.; Chen, H.; Kuang, A. L.; Miao, Y.; Xiong, Z. H. *J. Chem. Phys.* **2008**, *128*, 094305.

[30] Akola, J.; Atodiresei, N.; Kalikka, J.; Larrucea, J.; Jones, R. O. *J. Chem. Phys.* **2014**, *141*, 194503.

[31] Gao, L.; Li, P.; Lu, H.; Li, S. F.; Guo, Z. X. *J. Chem. Phys.* **2008**, *128*, 194304.

[32] Kelting, R.; Baldes, A.; Schwarz, U.; Rapps, T.; Schooss, D.; Weis, P.; Neiss, C.; Weigend, F.; Kappes, M. M. *J. Chem. Phys.* **2012**, *136*, 154309.

[33] Arrington, C. A.; Morse, M. D. *J. Phys. Chem. B* **2008**, *112*, 16182–16192.

[34] Wakabayashi, T.; Tomioka, M.; Wada, Y.; Miyamoto, Y.; Tang, J.; Kawaguchi, K.; Kuma, S.; Sasao, N.; Nanjo, H.; Uetake, S.; Yoshimura, M.; Nakano, I. *Eur. Phys. J. D* **2013**, *67*, 36.

[35] Wakabayashi, T.; Wada, Y.; Nakajima, K.; Morisawa, Y.; Kuma, S.; Miyamoto, Y.; Sasao, N.; Yoshimura, M.; Sato, T.; Kawaguchi, K. *J. Phys. Chem. A* **2015**, *119*, 2644–2650.

[36] Lewis, G. N. *J. Am. Chem. Soc.* **1916**, *38*, 762–785.

[37] Lauher, J. W. *J. Am. Chem. Soc.* **1978**, *100*, 5305–5315.

[38] Köchner, T.; Riedel, S.; Lehner, A. J.; Scherer, H.; Raabe, I.; Engesser, T. A.; Scholz, F. W.; Gellrich, U.; Eiden, P.; Paz Schmidt, R. A.; Plattner, D. A.; Krossing, I. *Angew. Chem. Int. Ed.* **2010**, *49*, 8139–8143.

[39] Martin, C. D.; Weinstein, C. M.; Moore, C. E.; Rheingold, A. L.; Bertrand, G. *Chem. Commun.* **2013**, *49*, 4486.

[40] Damrauer, R.; Pusede, S. E.; Staton, G. M. *Organometallics* **2008**, *27*, 3399–3402.

[41] Scheer, M.; Balazs, G.; Seitz, A. *Chem. Rev.* **2010**, *110*, 4236–4256.

[42] Stoll, H.; Metz, B.; Dolg, M. *J. Comp. Chem.* **2002**, *23*, 767–78.

[43] NBO 6.0. E. D. Glendening, J. K. Badenhoop, A. E. Reed, J. E. Carpenter, J. A. Bohmann, C. M. Morales, C.R. Landis, and F. Weinhold, Theoretical Chemistry Institute, University of Wisconsin, Madison, (2013).

[44] Peterson, K. A. *J. Chem. Phys.* **2003**, *119*, 11099–11112.

[45] Raghavachari, K.; Trucks, G. W.; Pople, J. A.; Head-Gordon, M. *Chem. Phys. Lett.* **1989**, *157*, 479–483.

[46] Bartlett, R. J.; Musiał, M. *Rev. Mod. Phys.* **2007**, *79*, 291–352.

[47] CFOUR, a quantum chemical program package written by J.F. Stanton, J. Gauss, L. Cheng, M.E. Harding, D.A. Matthews, P.G. Szalay with contributions from A.A. Auer, R.J. Bartlett, U. Benedikt, C. Berger, D.E. Bernholdt, Y.J. Bomble, O. Christiansen, F. Engel, R. Faber, M. Heckert, O. Heun, C. Huber, T.-C. Jagau, D. Jonsson, J. Juslius, K. Klein, W.J. Lauderdale, F. Lipparini, T. Metzroth, L.A. Mck, D.P. O'Neill, D.R. Price, E. Prochnow, C. Puzzarini, K. Ruud, F. Schiffmann, W. Schwalbach, C. Simmons, S. Stopkowicz, A. Tajti, J. Vzquez, F. Wang, J.D. Watts and the integral packages MOLECULE (J. Almlf and P.R. Taylor), PROPS (P.R. Taylor), ABACUS (T. Helgaker, H.J. Aa. Jensen, P. Jrgensen, and J. Olsen), and ECP routines by A. V. Mitin and C. van Wllen. For the current version, see http://www.cfour.de.

[48] Werner, H.-J.; Knowles, P. J. MOLPRO, version 2010.1, a package of ab initio programs. 2010.

[49] Lee, T. J.; Taylor, P. R. *Int. J. Quant. Chem.* **1989**, *36*, 199–207.

[50] Nielsen, I. M.; Janssen, C. L. *Chem. Phys. Lett.* **1999**, *310*, 568–576.

[51] Y. Shao, Z. Gan, E. Epifanovsky, A. T. B. Gilbert, M. Wormit, J. Kussmann, A. W. Lange, A. Behn, J. Deng, X. Feng, D. Ghosh, M. Goldey P. R. Horn, L. D. Jacobson, I. Kaliman, R. Z. Khaliullin, T. Ks, A. Landau, J. Liu, E. I. Proynov, Y. M. Rhee, R. M. Richard, M. A. Rohrdanz, R. P. Steele, E. J. Sundstrom, H. L. Woodcock, P. M. Zimmerman, D. Zuev, B. Albrecht, E. Alguire, B. Austin, G. J. O. Beran, Y. A. Bernard, E. Berquist, K. Brandhorst, K. B. Bravaya, S. T. Brown, D. Casanova, C.-M. Chang, Y. Chen, S. H. Chien, K. D. Closser, D. L. Crittenden, M. Diedenhofen, R. A. DiStasio Jr., H. Dop, A. D. Dutoi, R. G. Edgar, S. Fatehi, L. Fusti-Molnar, A. Ghysels, A. Golubeva-Zadorozhnaya, J. Gomes, M. W. D. Hanson-Heine, P. H. P. Harbach, A. W. Hauser, E. G. Hohenstein, Z. C. Holden, T.-C. Jagau, H. Ji, B. Kaduk, K. Khistyaev, J. Kim, J. Kim, R. A. King, P. Klunzinger, D. Kosenkov, T. Kowalczyk, C. M. Krauter, K. U. Lao, A. Laurent, K. V. Lawler, S. V. Levchenko, C. Y. Lin, F. Liu, E. Livshits, R. C. Lochan, A. Luenser, P. Manohar, S. F. Manzer, S.-P. Mao, N. Mardirossian, A. V. Marenich, S. A. Maurer, N. J. Mayhall, C. M. Oana, R. Olivares-Amaya, D. P. ONeill, J. A. Parkhill, T. M. Perrine, R. Peverati, P. A. Pieniazek, A. Prociuk, D. R. Rehn, E. Rosta, N. J. Russ, N. Sergueev, S. M. Sharada, S. Sharmaa, D. W. Small, A. Sodt, T. Stein, D. Stck, Y.-C. Su, A. J. W. Thom, T. Tsuchimochi, L. Vogt, O. Vydrov, T. Wang, M. A. Watson, J. Wenzel, A. White, C. F. Williams, V. Vanovschi, S. Yeganeh, S. R. Yost, Z.-Q. You, I. Y. Zhang, X. Zhang, Y. Zhou, B. R. Brooks, G. K. L. Chan, D. M. Chipman, C. J. Cramer, W. A. Goddard, M. S. Gordon, W. J. Hehre, A. Klamt, H. F. Schaefer, M. W. Schmidt, C. D. Sherrill, D. G. Truhlar, A. Warshel, X. Xua, A. Aspuru-Guzik, R. Baer, A. T. Bell, N. A. Besley, J.-D. Chai, A. Dreuw, B. D. Dunietz, T. R. Furlani, S. R. Gwaltney, C.-P. Hsu, Y. Jung, J. Kong, D. S. Lambrecht, W. Liang, C. Ochsenfeld, V. A. Rassolov, L. V. Slipchenko, J. E. Subotnik, T. Van Voorhis, J. M. Herbert, A. I. Krylov, P. M. W. Gill, and M. Head-Gordon. *Advances in molecular quantum chemistry contained in the Q-Chem 4 program package.* [*Mol. Phys.* **113**, 184-215 (2015)].

[52] Glendeling, E. D.; Weinhold, F. *J. Comp. Chem.* **1998**, *19*, 593–609.

[53] Nielsen, H. H. *Rev. Mod. Phys.* **1951**, *23*, 90–136.

[54] Clabo, D. A.; Allen, W. D.; Remington, R. B.; Yamaguchi, Y.; Schaefer, H. F. *Chem. Phys.* **1988**, *123*, 187–239.

[55] Feller, D. *J. Chem. Phys.* **1993**, *98*, 7059–7071.

[56] Helgaker, T.; Klopper, W.; Koch, H.; Noga, J. *J. Chem. Phys.* **1997**, *106*, 9639–9646.

[57] Matthews, D. A.; Gauss, J.; Stanton, J. F. *J. Chem. Theory Comput.* **2013**, *9*, 2567–2572.

[58] Matthews, D. A.; Stanton, J. F. *J. Chem. Phys.* **2015**, *142*, 064108.

[59] Matthews, D. A.; Stanton, J. F. *J. Chem. Phys.* **2015**, *143*, 204103.

[60] Handy, N.; Yamaguchi, Y.; Schaefer, H. F. *J. Chem. Phys.* **1986**, *84*, 4481–4484.

[61] Sellers, H.; Pulay, P. *Chem. Phys. Lett.* **1984**, *103*, 463–465.

[62] Cowan, R. D.; Griffin, D. C. *J. Opt. Soc. Am.* **1976**, *66*, 1010.

[63] Ottschofski, E.; Kutzelnigg, W. *J. Chem. Phys.* **1995**, *102*, 1752–1757.

[64] Liang, D.; Shen, W.; Zhang, C.; Lu, P.; Wang, S. *Mod. Phys. Lett. B* **2017**, *31*, 1750260.

[65] Nielsen, I. M.; Janssen, C. L. *Chem. Phys. Lett.* **1999**, *310*, 568–576.

[66] Peterson, K. A.; Yousaf, K. E. *J. Chem. Phys.* **2010**, *133*.

[67] Gerber, G. *J. Chem. Phys.* **1976**, *64*, 3423.

[68] Effantin, C.; Topouzkhanian, A.; Figuet, J.; D'Incan, J.; Barrow, R. F.; Verges, J. *Journal of Physics B: Atomic and Molecular Physics* **1982**, *15*, 3829–3840.

[69] Choi, H.-C.; Park, C.-M.; Baeck, K. K. *J. Chem. Phys. A* **2002**, *106*, 5177–5187.

[70] Landis, C. R.; Weinhold, F. *Inorg. Chem.* **2013**, *52*, 5154–5166.

[71] Kukolich, S. G.; McCarthy, M. C.; Thaddeus, P. *J. Phys. Chem. A* **2004**, *108*, 2645–2651.

[72] Leopold, D. G.; Lineberger, W. C.; Miller, A. E. *J. Am. Chem. Soc.* **1986**, *108*, 1379–1384.

[73] Kraka, E.; Cremer, D. *Chem. Phys. Lett.* **1993**, *216*, 333–340.

[74] Evangelista, F. A.; Allen, W. D.; Schaefer, H. F. *J. Chem. Phys.* **2007**, *127*, 024102.

[75] Li, X.; Paldus, J. *J. Chem. Phys.* **2008**, *129*, 174101.

[76] Hanauer, M.; Köhn, A. *J. Chem. Phys.* **2011**, *134*, 204111.

[77] Chapman, O. L.; Mattes, K.; McIntosh, C. L.; Pacansky, J.; Calder, G. V.; Orr, G. *J. Am. Chem. Soc.* **1973**, *95*, 6134–6135.

[78] Chapman, O. L.; Chang, C. C.; Hole, J.; Rosenquist, N. R.; Tomioka, H. *J. Am. Chem. Soc.* **1975**, *97*, 6586–6588.

[79] Dunkin, I. R.; MacDonald, J. G. *J. Chem. Soc. Chem. Commun.* **1979**, *17*, 772–773.

[80] Nam, H. H.; Leroi, G. E. *J. Mol. Struct.* **1987**, *157*, 301–304.

[81] Wentrup, C.; Blanch, R.; Briehl, H.; Grosslb, G. *J. Am. Chem. Soc.* **1988**, *110*, 1874–1880.

[82] Laing, J. W.; Berry, R. S. *J. Am. Chem. Soc.* **1976**, *98*, 660–664.

[83] Nam, H.-H.; Leroi, G. E. *Spectrochim. Acta A* **1985**, *41*, 67–73.

[84] Scheiner, A. C.; Schaefer, H. F.; Liu, B. *J. Am. Chem. Soc.* **1989**, *111*, 3118–3124.

[85] Scheiner, A. C.; Schaefer, H. F. *Chem. Phys. Lett.* **1991**, *177*, 471–476.

[86] Zhang, X.; MacCarone, A. T.; Nimlos, M. R.; Kato, S.; Bierbaum, V. M.; Ellison, G. B.; Ruscic, B.; Simmonett, A. C.; Allen, W. D.; Schaefer, H. F. *J. Chem. Phys.* **2007**, *126*, 044312.

[87] Kleinpeter, E.; Koch, A. *Tetrahedron* **2019**, *75*, 4663–4668.

[88] Cramer, C. *J. Chem. Soc., Perkin Trans.* **1999**, *2*, 2273–2283.

[89] Johnson, W. T.; Cramer, C. J. *J. Phys. Org. Chem.* **2001**, *14*, 597–603.

[90] Johnson, W. T.; Cramer, C. J. *J. Am. Chem. Soc.* **2001**, *123*, 923–928.

[91] Squires, R. R.; Cramer, C. J. *J. Phys. Chem. A* **1998**, *102*, 9072–9081.

[92] Cramer, C. J.; Thompson, J. *J. Phys. Chem. A* **2001**, *105*, 2091–2098.

[93] Medina, J. M.; Jackl, M. K.; Susick, R. B.; Garg, N. K. *Tetrahedron* **2016**, *72*, 3629–3634.

[94] Corsello, M. A.; Kim, J.; Garg, N. K. *Nat. Chem.* **2017**, *9*, 944–949.

[95] Bronner, S. M.; MacKey, J. L.; Houk, K. N.; Garg, N. K. *J. Am. Chem. Soc.* **2012**, *134*, 13966–13969.

[96] Goetz, A. E.; Shah, T. K.; Garg, N. K. *Chem. Comm.* **2015**, *51*, 34–45.

[97] McMahon, T. C.; Medina, J. M.; Yang, Y. F.; Simmons, B. J.; Houk, K. N.; Garg, N. K. *J. Am. Chem. Soc.* **2015**, *137*, 4082–4085.

[98] Picazo, E.; Anthony, S. M.; Giroud, M.; Simon, A.; Miller, M. A.; Houk, K. N.; Garg, N. K. *J. Am. Chem. Soc.* **2018**, *140*, 7605–7610.

[99] Medina, J. M.; Ko, J. H.; Maynard, H. D.; Garg, N. K. *Macromolecules* **2017**, *50*, 580–586.

[100] Shah, T. K.; Medina, J. M.; Garg, N. K. *J. Am. Chem. Soc.* **2016**, *138*, 4948–4954.

[101] Medina, J. M.; MacKey, J. L.; Garg, N. K.; Houk, K. N. *J. Am. Chem. Soc.* **2014**, *136*, 15798–15805.

[102] Picazo, E.; Houk, K. N.; Garg, N. K. *Tetrahedron Lett.* **2015**, *56*, 3511–3514.

[103] Bronner, S. M.; Garg, N. K. *J. Org. Chem.* **2009**, *74*, 8842–8843.

[104] Suzuki, S.; Itami, K.; Yamaguchi, J. *Angew. Chem. Int. Ed.* **2017**, *129*, 15206–15209.

[105] Tadross, P. M.; Stoltz, B. M. *Chem. Rev.* **2012**, *112*, 3550–3577.

[106] Hirsch, F.; Reusch, E.; Constantinidis, P.; Fischer, I.; Bakels, S.; Rijs, A.; Hemberger, P. *J. Phys. Chem. A* **2018**, *122*, 9563–9571.

[107] Zhang, F.; Parker, D.; Kim, Y. S.; Kaiser, R. I.; Mebel, A. M. *Astrophys. J.* **2011**, *728*, 141.

[108] McCabe, M. N.; Hemberger, P.; Reusch, E.; Bodi, A.; Bouwman, J. *J. Phys. Chem. Lett.* **2020**, *11*, 2859–2863.

[109] Idiris, F. I.; Jones, C. R. *Org. Biomol. Chem.* **2017**, *15*, 9044–9056.

[110] Holden, C.; Greaney, M. F. *Angew. Chem. Int. Ed.* **2014**, *53*, 5746–5749.

[111] Himeshima, Y.; Sonoda, T.; Kobayashi, H. *Chem. Lett.* **1983**, *12*, 1211–1214.

[112] Shen, H.; Xiao, X.; Hoye, T. R. *Org. Lett.* **2019**, *21*, 1672–1675.

[113] He, J.; Qiu, D.; Li, Y. *Acc. Chem. Res.* **2020**, *53*, 508–519.

[114] "Psi4 1.1: An Open-Source Electronic Structure Program Emphasizing Automation, Advanced Libraries, and Interoperability", R. M. Parrish, L. A. Burns, D. G. A. Smith, A. C. Simmonett, A. E. DePrince III, E. G. Hohenstein, U. Bozkaya, A. Yu. Sokolov, R. Di Remigio, R. M. Richard, J. F. Gonthier, A. M. James, H. R. McAlexander, A. Kumar, M. Saitow, X. Wang, B. P. Pritchard, P. Verma, H. F. Schaefer, K. Patkowski, R. A. King, E. F. Valeev, F. A. Evangelista, J. M. Turney, T. D. Crawford, and C. D. Sherrill, *J. Chem. Theory Comput.*, **13** 3185–3197 (2017).

[115] Kendall, R. A.; Dunning, T. H.; Harrison, R. J. *J. Chem. Phys.* **1992**, *96*, 6796–6806.

[116] Goerigk, L.; Hansen, A.; Bauer, C.; Ehrlich, S.; Najibi, A.; Grimme, S. *Phys. Chem. Chem. Phys.* **2017**, *19*, 32184–32215.

[117] Perdew, J. P.; Schmidt, K. *AIP Conf. Proc.* **2001**, *577*, 1–20.

[118] Kozuch, S.; Gruzman, D.; Martin, J. M. *J. Phys. Chem. C* **2010**, *114*, 20801–20808.

[119] Kozuch, S.; Martin, J. M. *J. Comp. Chem.* **2013**, *34*, 2327–2344.

[120] Kozuch, S.; Martin, J. M. *Phys. Chem. Chem. Phys.* **2011**, *13*, 20104–20107.

[121] Mardirossian, N.; Head-Gordon, M. *Phys. Chem. Chem. Phys.* **2014**, *16*, 9904–9924.

[122] Zhao, Y.; Schultz, N. E.; Truhlar, D. G. *J. Chem. Theory Comput.* **2006**, *2*, 364–382.

[123] Stephens, P. J.; Devlin, F. J.; Chabalowski, C. F.; Frisch, M. J. *J. Phys. Chem.* **1994**, *98*, 11623–11627.

[124] Becke, A. D. *Phys. Rev. A* **1988**, *38*, 3098–3100.

[125] Perdew, J. P. *Phys. Rev. B* **2011**, *33*, 8822–8824.

[126] NBO 7.0. E. D. Glendening, J, K. Badenhoop, A. E. Reed, J. E. Carpenter, J. A. Bohmann, C. M. Morales, P. Karafiloglou, C. R. Landis, and F. Weinhold, Theoretical Chemistry Institute, University of Wisconsin, Madison (2018).

[127] Salzner, U.; Schleyer, P. v. R. *J. Am. Chem. Soc.* **1993**, *115*, 10231–10236.

[128] "General Atomic and Molecular Electronic Structure System" M.W.Schmidt, K.K.Baldridge, J.A.Boatz, S.T.Elbert, M.S.Gordon, J.H.Jensen, S.Koseki, N.Matsunaga, K.A.Nguyen, S.Su, T.L.Windus, M.Dupuis, J.A.Montgomery *J. Comput. Chem.*, 14, 1347-1363(1993).

[129] F. Weinhold and C. R. Landis, *Discovering Chemistry with Natural Bond Orbitals* (Wiley-VCH, Hoboken NJ, 2012), p. 145ff.

[130] Hammond, G. S. *J. Am. Chem. Soc.* **1955**, *77*, 334–338.

[131] Dec, J. E. *Proc. Combust. Inst.* **2009**, *32*, 2727–2742.

[132] Taatjes, C. A. *J. Phys. Chem. A* **2006**, *110*, 4299–4312.

[133] Zádor, J.; Taatjes, C. A.; Fernandes, R. X. *Prog. Energy Combust. Sci.* **2011**, *37*, 371–421.

[134] Savee, J. D.; Papajak, E.; Rotavera, B.; Huang, H.; Eskola, A. J.; Welz, O.; Sheps, L.; Taatjes, C. A.; Zádor, J.; Osborn, D. L. *Science* **2015**, *347*, 643–646.

[135] Baldwin, R. R.; Dean, C. E.; Walker, R. W. *J. Chem. Soc. Faraday Trans. 2* **1986**, *82*, 1445–1455.

[136] Gulati, S. K.; Walker, R. W. *J. Chem. Soc. Faraday Trans. 2* **1988**, *84*, 401–407.

[137] Quelch, G. E.; Gallo, M. M.; Schaefer, H. F. *J. Am. Chem. Soc.* **1992**, *114*, 8239–8247.

[138] Quelch, G. E.; Gallo, M. M.; Shen, M.; Xie, Y.; Schaefer, H. F.; Moncrieff, D. *J. Am. Chem. Soc.* **1994**, *116*, 4953–4962.

[139] Ignatyev, I. S.; Xie, Y.; Allen, W. D.; Schaefer, H. F. *J. Chem. Phys.* **1997**, *107*, 141–155.

[140] Rienstra-Kiracofe, J. C.; Allen, W. D.; Schaefer, H. F. *J. Phys. Chem. A* **2000**, *104*, 9823–9840.

[141] Miller, J. A.; Klippenstein, S. J. *Int. J. Chem. Kinet.* **2001**, *33*, 654–668.

[142] DeSain, J. D.; Klippenstein, S. J.; Miller, J. A.; Taatjes, C. A. *J. Phys. Chem. A* **2003**, *107*, 4415–4427.

[143] Wilke, J. J.; Allen, W. D.; Schaefer, H. F. *J. Chem. Phys.* **2008**, *128*, 074308.

[144] Franke, P. R.; Brice, J. T.; Moradi, C. P.; Schaefer, H. F.; Douberly, G. E. *J. Phys. Chem. A* **2019**, *123*, 3558–3568.

[145] Knox, J. H. *T. Faraday Soc.* **1959**, *55*, 1362–1374.

[146] Knox, J. H. *Transactions of the Faraday Society* **1960**, *56*, 1225–1234.

[147] Knox, J. H. *Chemical Communications (London)* **1965**, 108–109.

[148] Baker, R.; Baldwin, R.; Walker, R. *Transactions of the Faraday Society* **1970**, *66*, 3016–3031.

[149] Slagle, I. R.; Park, J.-Y.; Gutman, D. Experimental Investigation of the Kinetics and Mechanism of the Reaction of n-Propyl Radicals with Molecular Oxygen from 297 to 635 K. Symposium (International) on Combustion. 1985; pp 733–741.

[150] Slagle, I. R.; Ratajczak, E.; Heaven, M. C.; Gutman, D.; Wagner, A. F. *J. Am. Chem. Soc.* **1985**, *107*, 1838–1845.

[151] Kaiser, E.; Wallington, T. *J. Phys. Chem.* **1996**, *100*, 18770–18774.

[152] Kaiser, E. *J. Phys. Chem. A* **1998**, *102*, 5903–5906.

[153] DeSain, J. D.; Clifford, E. P.; Taatjes, C. A. *J. Phys. Chem. A* **2001**, *105*, 3205–3213.

[154] DeSain, J. D.; Taatjes, C. A.; Miller, J. A.; Klippenstein, S. J.; Hahn, D. K. *Faraday Discuss.* **2002**, *119*, 101–120.

[155] Wijaya, C. D.; Sumathi, R.; Green, W. H. *J. Phys. Chem. A* **2003**, *107*, 4908–4920.

[156] Green, W. H.; Wijaya, C. D.; Yelvington, P. E.; Sumathi, R. *Mol. Phys.* **2004**, *102*, 371–380.

[157] Merle, J. K.; Hayes, C. J.; Zalyubovsky, S. J.; Glover, B. G.; Miller, T. A.; Hadad, C. M. *J. Phys. Chem. A* **2005**, *109*, 3637–3646.

[158] Estupiñán, E. G.; Klippenstein, S. J.; Taatjes, C. A. *J. Phys. Chem. B* **2005**, *109*, 8374–8387.

[159] Huang, H.; Merthe, D. J.; Zádor, J.; Jusinski, L. E.; Taatjes, C. A. *Proc. Combust. Inst.* **2011**, *33*, 293–299.

[160] Miyoshi, A. *J. Phys. Chem. A* **2011**, *115*, 3301–3325.

[161] Huynh, L. K.; Carstensen, H.-H.; Dean, A. M. *J. Phys. Chem. A* **2010**, *114*, 6594–6607.

[162] Goldsmith, C. F.; Green, W. H.; Klippenstein, S. J. *J. Phys. Chem. A* **2012**, *116*, 3325–3346.

[163] Cord, M.; Husson, B.; Lizardo Huerta, J. C.; Herbinet, O.; Glaude, P.-A.; Fournet, R.; Sirjean, B.; Battin-Leclerc, F.; Ruiz-Lopez, M.; Wang, Z. *J. Phys. Chem. A* **2012**, *116*, 12214–12228.

[164] Goldsmith, C. F.; Tomlin, A. S.; Klippenstein, S. J. *Proc. Combust. Inst.* **2013**, *34*, 177–185.

[165] Welz, O.; Burke, M. P.; Antonov, I. O.; Goldsmith, C. F.; Savee, J. D.; Osborn, D. L.; Taatjes, C. A.; Klippenstein, S. J.; Sheps, L. *J. Phys. Chem. A* **2015**, *119*, 7116–7129.

[166] Burke, M. P.; Goldsmith, C. F.; Klippenstein, S. J.; Welz, O.; Huang, H.; Antonov, I. O.; Savee, J. D.; Osborn, D. L.; Zádor, J.; Taatjes, C. A. *J. Phys. Chem. A* **2015**, *119*, 7095–7115.

[167] Bartlett, M. A.; Liang, T.; Pu, L.; Schaefer, H. F.; Allen, W. D. *J. Chem. Phys.* **2018**, *148*, 094303.

[168] Wilk, R. D.; Cohen, R. S.; Cernansky, N. P. *Ind. Eng. Chem. Res.* **1995**, *34*, 2285–2297.

[169] Chen, C.-J.; Bozzelli, J. W. *J. Phys. Chem. A* **1999**, *103*, 9731–9769.

[170] Strelkova, M.; Safonov, A.; Sukhanov, L.; Umanskiy, S. Y.; Kirillov, I.; Potapkin, B.; Pasman, H.; Tentner, A. *Combust. Flame* **2010**, *157*, 641–652.

[171] Zhang, F.; Dibble, T. S. *Phys. Chem. Chem. Phys.* **2011**, *13*, 17969–17977.

[172] Cord, M.; Sirjean, B.; Fournet, R.; Tomlin, A.; Ruiz-Lopez, M.; Battin-Leclerc, F. *J. Phys. Chem. A* **2012**, *116*, 6142–6158.

[173] Eskola, A. J.; Welz, O.; Savee, J. D.; Osborn, D. L.; Taatjes, C. A. *J. Phys. Chem. A* **2013**, *117*, 12216–12235.

[174] Wang, S.; Miller, D. L.; Cernansky, N. P.; Curran, H. J.; Pitz, W. J.; Westbrook, C. K. *Combust. Flame* **1999**, *118*, 415–430.

[175] DeSain, J. D.; Klippenstein, S. J.; Taatjes, C. A. *Phys. Chem. Chem. Phys.* **2003**, *5*, 1584–1592.

[176] Petway, S. V.; Ismail, H.; Green, W. H.; Estupiñán, E. G.; Jusinski, L. E.; Taatjes, C. A. *J. Phys. Chem. A* **2007**, *111*, 3891–3900.

[177] DeSain, J. D.; Taatjes, C. A. *J. Phys. Chem. A* **2001**, *105*, 6646–6654.

[178] Fernandes, R. X.; Zádor, J.; Jusinski, L. E.; Miller, J. A.; Taatjes, C. A. *Phys. Chem. Chem. Phys.* **2009**, *11*, 1320–1327.

[179] Knepp, A. M.; Meloni, G.; Jusinski, L. E.; Taatjes, C. A.; Cavallotti, C.; Klippenstein, S. J. *Phys. Chem. Chem. Phys.* **2007**, *9*, 4315–4331.

[180] Roothaan, C. C. J. *Rev. Mod. Phys.* **1951**, *23*, 69–89.

[181] Roothaan, C. C. J. *Rev. Mod. Phys.* **1960**, *32*, 179–185.

[182] Pople, J. A.; Nesbet, R. K. *J. Chem. Phys.* **1954**, *22*, 571–572.

[183] Møller, C.; Plesset, M. S. *Phys. Rev.* **1934**, *46*, 618.

[184] Lee, T. J.; Jayatilaka, D. *Chem. Phys. Lett.* **1993**, *201*, 1–10.

[185] Čížek, J. *J. Chem. Phys.* **1966**, *45*, 4256–4266.

[186] Crawford, T. HF Schaefer in Reviews in Computational Chemistry, Vol. 14. 2000.

[187] Purvis III, G. D.; Bartlett, R. J. *J. Chem. Phys.* **1982**, *76*, 1910–1918.

[188] Raghavachari, K.; Trucks, G. W.; Pople, J. A.; Head-Gordon, M. *Chem. Phys. Lett.* **1989**, *157*, 479–483.

[189] Noga, J.; Bartlett, R. J. *J. Chem. Phys.* **1987**, *86*, 7041–7050.

[190] Bomble, Y. J.; Stanton, J. F.; Kállay, M.; Gauss, J. *J. Chem. Phys.* **2005**, *123*, 054101.

[191] Dunning Jr, T. H. *J. Chem. Phys.* **1989**, *90*, 1007–1023.

[192] Peterson, K. A.; Woon, D. E.; Dunning Jr, T. H. *J. Chem. Phys.* **1994**, *100*, 7410–7415.

[193] Woon, D. E.; Dunning Jr, T. H. *J. Chem. Phys.* **1995**, *103*, 4572–4585.

[194] Kendall, R. A.; Dunning Jr, T. H.; Harrison, R. J. *J. Chem. Phys.* **1992**, *96*, 6796–6806.

[195] Hariharan, P. C.; Pople, J. A. *Theor. Chem. Acc.* **1973**, *28*, 213–222.

[196] Császár, A. G.; Allen, W. D.; Schaefer, H. F. *J. Chem. Phys.* **1998**, *108*, 9751–9764.

[197] Tarczay, G. *J. Chem. Phys* **2001**, *115*, 1229.

[198] Gonzales, J. M.; Allen, W. D.; Schaefer, H. F. *J. Phys. Chem. A* **2005**, *109*, 10613–10628.

[199] Matthews, D. A.; Cheng, L.; Harding, M. E.; Lipparini, F.; Stopkowicz, S.; Jagau, T.-C.; Szalay, P. G.; Gauss, J.; Stanton, J. F. *J. Chem. Phys.* **2020**, *152*, 214108.

[200] Crawford, T. D.; Sherrill, C. D.; Valeev, E. F.; Fermann, J. T.; King, R. A.; Leininger, M. L.; Brown, S. T.; Janssen, C. L.; Seidl, E. T.; Kenny, J. P. *J. Comp. Chem.* **2007**, *28*, 1610–1616.

[201] Smith, D. G.; Burns, L. A.; Simmonett, A. C.; Parrish, R. M.; Schieber, M. C.; Galvelis, R.; Kraus, P.; Kruse, H.; Di Remigio, R.; Alenaizan, A. *J. Chem. Phys.* **2020**, *152*, 184108.

[202] Schmidt, M. W.; Baldridge, K. K.; Boatz, J. A.; Elbert, S. T.; Gordon, M. S.; Jensen, J. H.; Koseki, S.; Matsunaga, N.; Nguyen, K. A.; Su, S. *J. Comp. Chem.* **1993**, *14*, 1347–1363.

[203] Gordon, M. S.; Schmidt, M. W. *Theory and applications of computational chemistry*; Elsevier, 2005; pp 1167–1189.

[204] Janssen, C.; Nielsen, I.; Leininger, M.; Valeev, E.; Seidl, E. *Sandia National Laboratories, Livermore, CA, USA*

[205] MRCC, a quantum chemical program suite written by M. Kállay, P. R. Nagy, D. Mester, Z. Rolik, G. Samu, J. Csontos, J. Csóka, P. B. Szabó, L. Gyevi-Nagy, B. Hégely, I. Ladjánszki, L. Szegedy, B. Ladóczki, K. Petrov, M. Farkas, P. D. Mezei, and Á. Ganyecz. See WWW.MRCC.HU.

[206] Kállay, M.; Nagy, P. R.; Mester, D.; Rolik, Z.; Samu, G.; Csontos, J.; Csóka, J.; Szabó, P. B.; Gyevi-Nagy, L.; Hégely, B. *J. Chem. Phys.* **2020**, *152*, 074107.

[207] Eliel, E. L.; Wilen, S. H. *Stereochemistry of organic compounds*; John Wiley & Sons, 1994.

[208] Dobrowolski, J. C.; Rode, J. E.; Sadlej, J. *J. Mol. Struct.* **2007**, *810*, 129–134.

[209] Wilke, J. J.; Lind, M. C.; Schaefer, H. F.; Császár, A. G.; Allen, W. D. *J. Chem. Theory Comput.* **2009**, *5*, 1511–1523.

[210] He, K.; Allen, W. D. *J. Chem. Theory Comput.* **2016**, *12*, 3571–3582.

[211] Feller, D. *J. Chem. Phys.* **1992**, *96*, 6104–6114.

[212] Helgaker, T.; Klopper, W.; Koch, H.; Noga, J. *J. Chem. Phys.* **1997**, *106*, 9639–9646.

[213] Perera, S. A.; Bartlett, R. J. *Chem. Phys. Lett.* **1993**, *216*, 606–612.

[214] Handy, N. C.; Yamaguchi, Y.; Schaefer, H. F. *J. Chem. Phys.* **1986**, *84*, 4481–4484.

[215] Jayatilaka, D.; Lee, T. J. *J. Chem. Phys.* **1993**, *98*, 9734–9747.

[216] Lee, T. J.; Taylor, P. R. *Int. J. Quant. Chem.* **1989**, *36*, 199–207.

[217] Lauderdale, W.; Stanton, J. *Chem. Phys. Lett* **1991**, *187*, 21–28.

[218] Lauderdale, W. J.; Stanton, J. F.; Gauss, J.; Watts, J. D.; Bartlett, R. J. *J. Chem. Phys.* **1992**, *97*, 6606–6620.

[219] Urban, M.; Watts, J. D.; Bartlett, R. J. *Int. J. Quant. Chem.* **1994**, *52*, 211–225.

[220] Kerr, J. KP Huber and G. Herzberg, molecular spectra and molecular structure: IV constants of diatomic molecules: Von NostrandReinhold, New York, 1979, pp. 498-508, price£ 20.65. 1982.

[221] Lubic, K. G.; Amano, T.; Uehara, H.; Kawaguchi, K.; Hirota, E. *J. Chem. Phys.* **1984**, *81*, 4826–4831.

[222] Lide Jr, D. R.; Christensen, D. *J. Chem. Phys.* **1961**, *35*, 1374–1378.

[223] Creswell, R. A.; Schwendeman, R. *J. Mol. Spec.* **1977**, *64*, 295–301.

[224] McKee, W. C.; Schleyer, P. v. R. *J. Am. Chem. Soc.* **2013**, *135*, 13008–13014.

[225] Weinhold, F. *J. Comp. Chem.* **2012**, *33*, 2363–2379.

[226] Moore III, K. B.; Turney, J. M.; Schaefer, H. F. *J. Chem. Phys.* **2017**, *146*, 194304.

[227] Meek, G. A.; Levine, B. G. *J. Chem. Phys.* **2016**, *144*, 184109.

[228] Allen, W. D.; Császár, A. G. *J. Chem. Phys.* **1993**, *98*, 2983–3015.

[229] INTDER2005 is a general program developed by Wesley D. Allen and co-workers which performs various vibrational analyses and higher-order nonlinear transformations among force field representations.

[230] Hansen, A. S.; Bhagde, T.; Moore III, K. B.; Moberg, D. R.; Jasper, A. W.; Georgievskii, Y.; Vansco, M. F.; Klippenstein, S. J.; Lester, M. I. *Science* **2021**, *373*, 679–682.

[231] Wilson, E. B.; Decius, J. C.; Cross, P. C. *Molecular vibrations: the theory of infrared and Raman vibrational spectra*; Courier Corporation, 1980.

[232] Curtiss, L. A.; Raghavachari, K.; Redfern, P. C.; Pople, J. A. *J. Chem. Phys.* **1997**, *106*, 1063–1079.

[233] Curtiss, L. A.; Redfern, P. C.; Raghavachari, K.; Pople, J. A. *J. Chem. Phys.* **1998**, *109*, 42–55.

[234] Hehre, W. J.; Ditchfield, R.; Pople, J. A. *J. Chem. Phys.* **1972**, *56*, 2257–2261.

[235] Jahn, H. A.; Teller, E. *Proc. R. Soc. Lond. A Math. Phys. Sci.* **1937**, *161*, 220–235.

APPENDIX

6.1 Chapter 2

6.1.1 Cartesian coordinates of geometries

Table 6.1: Tetrahedral (T_d) Bi_4 cartesian coordinates of the CCSD(T)/cc-pVQZ-PP geometry in Å.

Atom	x	y	z
Bi	0.0000000000	-1.5302363927	1.0820405299
Bi	0.0000000000	1.5302363927	1.0820405299
Bi	1.5302363927	0.0000000000	-1.0820405299
Bi	-1.5302363927	0.0000000000	-1.0820405299

Table 6.2: Tetrahedral (C_{2v}) Bi_4 cartesian coordinates of the CCSD(T)/cc-pVQZ-PP geometry in Å.

Atom	x	y	z
Bi	0.0000000000	-1.5758532126	-0.5093775319
Bi	0.0000000000	1.5758532126	-0.5093775319
Bi	2.2900687222	0.0000000000	0.5093775319
Bi	-2.2900687222	0.0000000000	0.5093775319

6.1.2 Absolute electronic energy focal point tables and corrections

Table 6.3: Valence focal point analysis of the absolute electronic energy of T_d Bi_4 in Hartrees. Delta (δ) denotes the change in relative energy (ΔE_e) with respect to the preceding level of theory.

	HF	+δMP2	+δCCSD	+δ(T)	+δT	+δ(Q)	+δQ
cc-pVDZ-PP	−854.2976737	−854.6516485	−854.6546264	−854.6834010	−854.6837169	−854.6898406	−854.6885150
cc-pVTZ-PP	−854.3244542	−854.7618166	−854.7618023	−854.8008450	−854.8003193	−854.8077054	[−854.8063798]
cc-pVQZ-PP	−854.3294516	−854.8071780	−854.7993980	−854.8429570	[−854.8424313]	[−854.8498174]	[−854.8484918]
cc-pV5Z-PP	−854.3302002	−854.8252684	−854.8116404	−854.8569174	[−854.8563917]	[−854.8637778]	[−854.8624522]
CBS	[−854.3303321]	[−854.8435949]	[−854.8238313]	[−854.8709109]	[−854.8703852]	[−854.8777713]	[−854.8764457]

$\Delta_{Bi_4\ (T_d),\mathrm{ZPVE,Harmonic}}$[CCSD(T)/cc-pVQZ-PP] = 1.0397 kcal mol^{-1}

$\Delta_{Bi_4\ (T_d),\mathrm{ZPVE,Anharmonic}}$[CCSD(T)/cc-pVQZ-PP] = 1.0377 kcal mol^{-1}

$\Delta_{Bi_4\ (T_d),\mathrm{DBOC}}$[HF/cc-pVTZ-PP] = 0.507344872 kcal mol^{-1}

$\Delta_{Bi_4\ (T_d),\mathrm{rel}}$[CCSD(T)/cc-pVTZ-PP] = 35.764346293629 kcal mol^{-1}

$\Delta_{Bi_4\ (C_{2v}),\mathrm{ZPVE,Harmonic}}$[CCSD(T)/cc-pVQZ-PP] = 0.8871 kcal mol^{-1}

$\Delta_{Bi_4\ (C_{2v}),\mathrm{DBOC}}$[HF/cc-pVTZ-PP] = 0.517046279 kcal mol^{-1}

$\Delta_{Bi_4\ (C_{2v}),\mathrm{rel}}$[CCSD(T)/cc-pVTZ-PP] = 35.762332985260 kcal mol^{-1}

Table 6.4: Valence focal point analysis of the absolute electronic energy of C_{2v} Bi_4 in Hartrees. Delta (δ) denotes the change in relative energy (ΔE_e) with respect to the preceding level of theory.

	HF	+δMP2	+δCCSD	+δ(T)	+δT	+δ(Q)	+δQ
cc-pVDZ-PP	−854.3716361	−854.7145861	−854.7207238	−854.7428023	−854.7424185	−854.7455414	−854.7450601
cc-pVTZ-PP	−854.3983828	−854.8286873	−854.8301955	−854.8633170	−854.8622740	−854.8665538	[−854.8660724]
cc-pVQZ-PP	−854.4020911	−854.8746103	−854.8683428	−854.9063030	[−854.9052600]	[−854.9095398]	[−854.9090584]
cc-pV5Z-PP	−854.4026046	−854.8930851	−854.8810427	−854.9208364	[−854.9197934]	[−854.9240732]	[−854.9235918]
CBS	[−854.4026871]	[−854.9120124]	[−854.8939110]	[−854.9356284]	[−854.9345853]	[−854.9388651]	[−854.9383838]

Table 6.5: Valence focal point analysis of the absolute electronic energy of Bi_2 in Hartrees. Delta (δ) denotes the change in relative energy (ΔE_e) with respect to the preceding level of theory.

	HF	+δMP2	+δCCSD	+δ(T)	+δT	+δ(Q)	+δQ
cc-pVDZ-PP	−427.1375648	−427.3182280	−427.3219849	−427.3342986	−427.3346699	−427.3372520	−427.3368614
cc-pVTZ-PP	−427.1489818	−427.3650444	−427.3679834	−427.3848895	−427.3850675	−427.3881902	[−427.3877996]
cc-pVQZ-PP	−427.1510933	−427.3848200	−427.3841785	−427.4029479	[−427.4031259]	[−427.4062486]	[−427.4058580]
cc-pV5Z-PP	−427.1513961	−427.3929656	−427.3893783	−427.4088121	[−427.4089901]	[−427.4121128]	[−427.4117222]
CBS	[−427.1514468]	[−427.4012448]	[−427.3945668]	[−427.4146977]	[−427.4148757]	[−427.4179984]	[−427.4176078]

$\Delta_{Bi_2,ZPVE,Harmonic}$[CCSD(T)/cc-pVQZ-PP] = 0.2641kcal mol^{-1}

$\Delta_{Bi_2,ZPVE,Anharmonic}$[CCSD(T)/cc-pVQZ-PP] = 0.2636kcal mol^{-1}

$\Delta_{Bi_2,DBOC}$[HF/cc-pVTZ-PP] = 0.147018442 kcal mol^{-1}

$\Delta_{Bi_2,rel}$[CCSD(T)/cc-pVTZ-PP] = 17.88241774 kcal mol^{-1}

Table 6.6: Valence focal point analysis of the absolute electronic energy of 2Bi in Hartrees. Delta (δ) denotes the change in relative energy (ΔE_e) with respect to the preceding level of theory.

	HF	+δMP2	+δCCSD	+δ(T)	+δT	+δ(Q)	+δQ
cc-pVDZ-PP	−427.1819483	−427.2575190	−427.2774270	−427.2781610	−427.2783520	−427.2784115	−427.2784304
cc-pVTZ-PP	−427.1885840	−427.2884351	−427.3089095	−427.3121565	−427.3129013	−427.3129604	[−427.3129793]
cc-pVQZ-PP	−427.1890378	−427.3002333	−427.3186177	−427.3227303	[−427.3234751]	[−427.3235342]	[−427.3235531]
cc-pV5Z-PP	−427.1891071	−427.3043778	−427.3211040	−427.3255074	[−427.3262522]	[−427.3263113]	[−427.3263302]
CBS	[−427.1891196]	[−427.3086659]	[−427.3236524]	[−427.3283609]	[−427.3291057]	[−427.3291648]	[−427.3291837]

$\Delta_{2Bi,rel}$[CCSD(T)/cc-pVTZ-PP] = 17.87665078 kcal mol^{-1}

6.1.3 NBO analysis

NBO analysis transforms the computed wavefunction orbitals into natural bonding orbitals through the following process: input basis AOs → NAOs → NHOs → NBOs → NLMOs. For further information on these transformations, reference the the NBO 6.0 manual at http://nbo.chem.wisc.edu/nbo6ab_man.pdf.

SECOND ORDER PERTURBATION THEORY ANALYSIS OF FOCK MATRIX IN NBO BASIS

Threshold for printing: 0.50 kcal/mol

==========

within unit 1

Donor (L) NBO | Acceptor (NL) NBO | E(2) kcal/mol | E(NL)-E(L)a.u. | F(L,NL)a.u.

1. LP (1)Bi 1 | 16. BD*(1)Bi 3-Bi 4 | 2.30 | 0.35 | 0.026
2. LP (1)Bi 2 | 16. BD*(1)Bi 3-Bi 4 | 2.30 | 0.35 | 0.026
3. LP (1)Bi 3 | 13. BD*(1)Bi 1-Bi 4 | 0.85 | 0.50 | 0.018
3. LP (1)Bi 3 | 15. BD*(1)Bi 2-Bi 4 | 0.85 | 0.50 | 0.018
4. LP (1)Bi 4 | 12. BD*(1)Bi 1-Bi 3 | 0.85 | 0.50 | 0.018
4. LP (1)Bi 4 | 14. BD*(1)Bi 2-Bi 3 | 0.85 | 0.50 | 0.018
5. BD (1)Bi 1-Bi 2 | 12. BD*(1)Bi 1-Bi 3 | 6.85 | 0.28 | 0.039
5. BD (1)Bi 1-Bi 2 | 13. BD*(1)Bi 1-Bi 4 | 6.85 | 0.28 | 0.039
5. BD (1)Bi 1-Bi 2 | 14. BD*(1)Bi 2-Bi 3 | 6.85 | 0.28 | 0.039
5. BD (1)Bi 1-Bi 2 | 15. BD*(1)Bi 2-Bi 4 | 6.85 | 0.28 | 0.039
5. BD (1)Bi 1-Bi 2 | 16. BD*(1)Bi 3-Bi 4 | 33.37 | 0.13 | 0.058
5. BD (1)Bi 1-Bi 2 | 21. RY (5)Bi 1 | 2.89 | 4.60 | 0.103
5. BD (1)Bi 1-Bi 2 | 23. RY (7)Bi 1 | 2.67 | 6.22 | 0.115
5. BD (1)Bi 1-Bi 2 | 30. RY (5)Bi 2 | 2.89 | 4.60 | 0.103
5. BD (1)Bi 1-Bi 2 | 32. RY (7)Bi 2 | 2.71 | 6.28 | 0.116
5. BD (1)Bi 1-Bi 2 | 35. RY (1)Bi 3 | 1.08 | 1.44 | 0.035
5. BD (1)Bi 1-Bi 2 | 36. RY (2)Bi 3 | 2.08 | 1.00 | 0.041
5. BD (1)Bi 1-Bi 2 | 38. RY (4)Bi 3 | 2.92 | 5.26 | 0.111
5. BD (1)Bi 1-Bi 2 | 40. RY (6)Bi 3 | 1.87 | 1.32 | 0.044
5. BD (1)Bi 1-Bi 2 | 43. RY (9)Bi 3 | 2.77 | 3.30 | 0.085
5. BD (1)Bi 1-Bi 2 | 44. RY (1)Bi 4 | 1.08 | 1.44 | 0.035
5. BD (1)Bi 1-Bi 2 | 45. RY (2)Bi 4 | 2.08 | 1.00 | 0.041
5. BD (1)Bi 1-Bi 2 | 47. RY (4)Bi 4 | 2.92 | 5.26 | 0.111
5. BD (1)Bi 1-Bi 2 | 49. RY (6)Bi 4 | 1.87 | 1.32 | 0.044
5. BD (1)Bi 1-Bi 2 | 52. RY (9)Bi 4 | 2.73 | 3.10 | 0.082
6. BD (1)Bi 1-Bi 3 | 14. BD*(1)Bi 2-Bi 3 | 0.51 | 0.30 | 0.011
6. BD (1)Bi 1-Bi 3 | 16. BD*(1)Bi 3-Bi 4 | 1.64 | 0.15 | 0.014
6. BD (1)Bi 1-Bi 3 | 30. RY (5)Bi 2 | 0.55 | 4.62 | 0.045
6. BD (1)Bi 1-Bi 3 | 32. RY (7)Bi 2 | 0.52 | 6.30 | 0.051

7. BD (1)Bi 1-Bi 4 | 15. BD*(1)Bi 2-Bi 4 | 0.51 | 0.30 | 0.011

7. BD (1)Bi 1-Bi 4 | 16. BD*(1)Bi 3-Bi 4 | 1.64 | 0.15 | 0.014

7. BD (1)Bi 1-Bi 4 | 30. RY (5)Bi 2 | 0.55 | 4.62 | 0.045

7. BD (1)Bi 1-Bi 4 | 32. RY (7)Bi 2 | 0.52 | 6.30 | 0.051

8. BD (1)Bi 2-Bi 3 | 12. BD*(1)Bi 1-Bi 3 | 0.51 | 0.30 | 0.011

8. BD (1)Bi 2-Bi 3 | 16. BD*(1)Bi 3-Bi 4 | 1.64 | 0.15 | 0.014

8. BD (1)Bi 2-Bi 3 | 21. RY (5)Bi 1 | 0.55 | 4.62 | 0.045

8. BD (1)Bi 2-Bi 3 | 23. RY (7)Bi 1 | 0.52 | 6.23 | 0.051

9. BD (1)Bi 2-Bi 4 | 13. BD*(1)Bi 1-Bi 4 | 0.51 | 0.30 | 0.011

9. BD (1)Bi 2-Bi 4 | 16. BD*(1)Bi 3-Bi 4 | 1.64 | 0.15 | 0.014

9. BD (1)Bi 2-Bi 4 | 21. RY (5)Bi 1 | 0.55 | 4.62 | 0.045

9. BD (1)Bi 2-Bi 4 | 23. RY (7)Bi 1 | 0.52 | 6.23 | 0.051

10. BD (1)Bi 3-Bi 4 | 12. BD*(1)Bi 1-Bi 3 | 9.59 | 0.15 | 0.034

10. BD (1)Bi 3-Bi 4 | 13. BD*(1)Bi 1-Bi 4 | 9.59 | 0.15 | 0.034

10. BD (1)Bi 3-Bi 4 | 14. BD*(1)Bi 2-Bi 3 | 9.59 | 0.15 | 0.034

10. BD (1)Bi 3-Bi 4 | 15. BD*(1)Bi 2-Bi 4 | 9.59 | 0.15 | 0.034

10. BD (1)Bi 3-Bi 4 | 17. RY (1)Bi 1 | 0.68 | 0.65 | 0.019

10. BD (1)Bi 3-Bi 4 | 26. RY (1)Bi 2 | 0.68 | 0.65 | 0.019

10. BD (1)Bi 3-Bi 4 | 35. RY (1)Bi 3 | 5.31 | 1.32 | 0.075

10. BD (1)Bi 3-Bi 4 | 36. RY (2)Bi 3 | 3.53 | 0.88 | 0.050

10. BD (1)Bi 3-Bi 4 | 38. RY (4)Bi 3 | 6.09 | 5.14 | 0.158

10. BD (1)Bi 3-Bi 4 | 40. RY (6)Bi 3 | 2.21 | 1.20 | 0.046

10. BD (1)Bi 3-Bi 4 | 41. RY (7)Bi 3 | 1.67 | 0.75 | 0.032

10. BD (1)Bi 3-Bi 4 | 43. RY (9)Bi 3 | 4.89 | 3.17 | 0.111

10. BD (1)Bi 3-Bi 4 | 44. RY (1)Bi 4 | 5.31 | 1.32 | 0.075

10. BD (1)Bi 3-Bi 4 | 45. RY (2)Bi 4 | 3.53 | 0.88 | 0.050

10. BD (1)Bi 3-Bi 4 | 47. RY (4)Bi 4 | 6.09 | 5.14 | 0.158

10. BD (1)Bi 3-Bi 4 | 49. RY (6)Bi 4 | 2.21 | 1.20 | 0.046

10. BD (1)Bi 3-Bi 4 | 50. RY (7)Bi 4 | 2.05 | 0.88 | 0.038

10. BD (1)Bi 3-Bi 4 | 51. RY (8)Bi 4 | 1.43 | 0.96 | 0.033

10. BD (1)Bi 3-Bi 4 | 52. RY (9)Bi 4 | 4.63 | 2.97 | 0.105

NATURAL BOND ORBITALS (Summary):

Principal Delocalizations

NBO Occupancy Energy (geminal,vicinal,remote)

==========

Molecular unit 1 (Bi4)

—— Lewis ——————————

NBO | Occupancy | Energy | (geminal,vicinal,remote)

1. LP (1)Bi 1 | 1.98574 | -0.50270 | 16(v)

2. LP (1)Bi 2 | 1.98574 | -0.50270 | 16(v)

3. LP (1)Bi 3 | 1.98574 | -0.49342 | 13(v),15(v)

4. LP (1)Bi 4 | 1.98574 | -0.49342 | 12(v),14(v)

5. BD (1)Bi 1-Bi 2 | 1.60131 | -0.27584 | 16(v),12(g),13(g),14(g)

15(g),38(v),47(v),21(g)

30(g),43(v),52(v),32(g)

23(g),36(v),45(v),40(v)

49(v),35(v),44(v)

6. BD (1)Bi 1-Bi 3 | 1.92844 | -0.29491 | 16(g),30(v),32(v),14(g)

7. BD (1)Bi 1-Bi 4 | 1.92844 | -0.29491 | 16(g),30(v),32(v),15(g)

8. BD (1)Bi 2-Bi 3 | 1.92844 | -0.29491 | 16(g),21(v),23(v),12(g)

9. BD (1)Bi 2-Bi 4 | 1.92844 | -0.29491 | 16(g),21(v),23(v),13(g)

10. BD (1)Bi 3-Bi 4 | 1.80488 | -0.15072 | 12(g),13(g),14(g),15(g)

38(g),47(g),35(g),44(g)

43(g),52(g),36(g),45(g)

40(g),49(g),50(g),41(g)

51(g),17(v),26(v)

—— non-Lewis ——————————-

NBO | Occupancy | Energy

11. BD*(1)Bi 1-Bi 2 | 0.01125 | -0.04348

12. BD*(1)Bi 1-Bi 3 | 0.09138 | 0.00398

13. BD*(1)Bi 1-Bi 4 | 0.09138 | 0.00398

14. BD*(1)Bi 2-Bi 3 | 0.09138 | 0.00398

15. BD*(1)Bi 2-Bi 4 | 0.09138 | 0.00398

16. BD*(1)Bi 3-Bi 4 | 0.53998 | -0.14802

17. RY (1)Bi 1 | 0.00220 | 0.50324
18. RY (2)Bi 1 | 0.00153 | 0.52046
19. RY (3)Bi 1 | 0.00104 | 0.51990
20. RY (4)Bi 1 | 0.00025 | 0.66575
21. RY (5)Bi 1 | 0.00003 | 4.32517
22. RY (6)Bi 1 | 0.00000 | 0.62008
23. RY (7)Bi 1 | 0.00000 | 5.93928
24. RY (8)Bi 1 | 0.00000 | 0.77505
25. RY (9)Bi 1 | 0.00000 | 0.49016
26. RY (1)Bi 2 | 0.00220 | 0.50324
27. RY (2)Bi 2 | 0.00153 | 0.52046
28. RY (3)Bi 2 | 0.00104 | 0.51990
29. RY (4)Bi 2 | 0.00025 | 0.66575
30. RY (5)Bi 2 | 0.00003 | 4.32517
31. RY (6)Bi 2 | 0.00000 | 0.59523
32. RY (7)Bi 2 | 0.00000 | 6.00251
33. RY (8)Bi 2 | 0.00000 | 0.77505
34. RY (9)Bi 2 | 0.00000 | 0.45177
35. RY (1)Bi 3 | 0.00370 | 1.16869
36. RY (2)Bi 3 | 0.00072 | 0.72609
37. RY (3)Bi 3 | 0.00056 | 0.46244
38. RY (4)Bi 3 | 0.00012 | 4.98753
39. RY (5)Bi 3 | 0.00002 | 0.52181
40. RY (6)Bi 3 | 0.00000 | 1.04704
41. RY (7)Bi 3 | 0.00000 | 0.60360
42. RY (8)Bi 3 | 0.00000 | 0.73165
43. RY (9)Bi 3 | 0.00000 | 3.02157
44. RY (1)Bi 4 | 0.00370 | 1.16869
45. RY (2)Bi 4 | 0.00072 | 0.72609
46. RY (3)Bi 4 | 0.00056 | 0.46244
47. RY (4)Bi 4 | 0.00012 | 4.98753
48. RY (5)Bi 4 | 0.00002 | 0.52181
49. RY (6)Bi 4 | 0.00000 | 1.04704

50. RY (7)Bi 4 | 0.00000 | 0.72738

51. RY (8)Bi 4 | 0.00000 | 0.80916

52. RY (9)Bi 4 | 0.00000 | 2.82028

Total Lewis 331.06290 (99.7177%)

Valence non-Lewis 0.91677 (0.2761%)

Rydberg non-Lewis 0.02034 (0.0061%)

Total unit 1 332.00000 (100.0000%)

Charge unit 1 0.00000

NBO input file

Below is the input file used to run the NBO computations for the C2v structure utilizing Qchem 5.0.

```
$comment
 Bi4 C2V NBO Analysis
$end

$molecule
0 1
BI 0.0000000000 -1.5758532126 -0.5093775319
BI 0.0000000000 1.5758532126 -0.5093775319
BI 2.2900687222 0.0000000000 0.5093775319
BI -2.2900687222 0.0000000000 0.5093775319
$end

$rem
 jobtype sp
 exchange b3lyp
 basis srlc
 MAX_SCF_CYCLES 200
 ecp srlc
 NBO 1
 RUN_NBO6 1
```

MEM_TOTAL 2000

$end

$nbo

nrt

$end

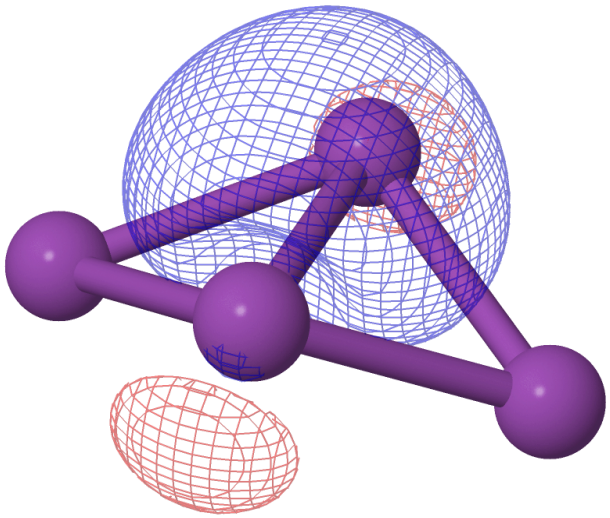

(a) The Lewis NBO of the C_{2v} isomer.

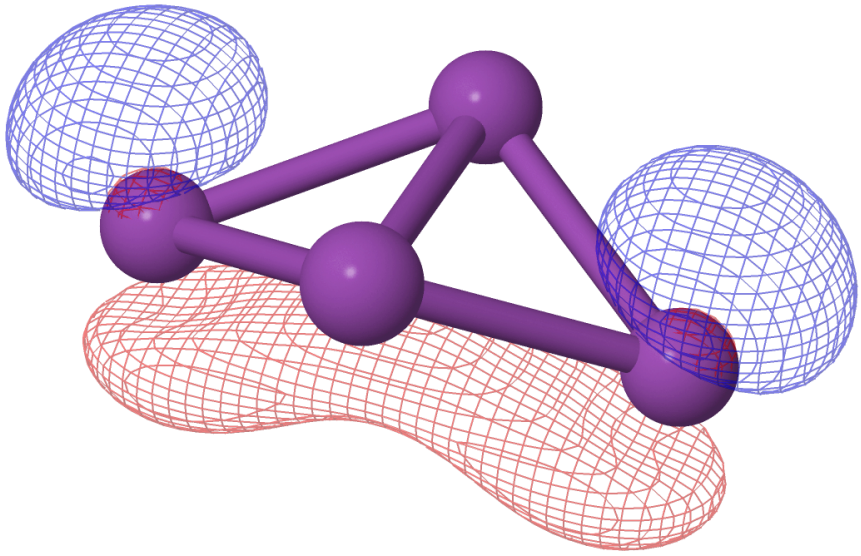

(b) The non-Lewis, long-bonding NBO of the C_{2v} isomer.

6.2 Chapter 4

6.2.1 Extra *i*-propyl + O_2 figures of stationary point structures

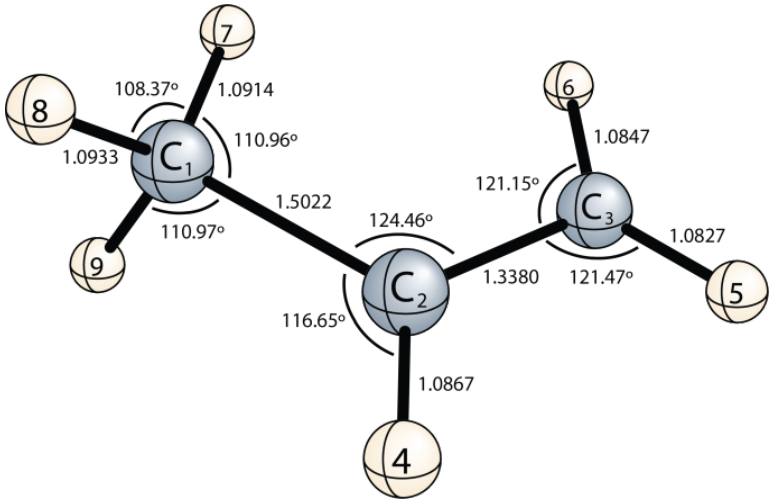

Figure 6.2: Depiction of the Propene FC-ROCCSD(T)/cc-pVTZ structure.

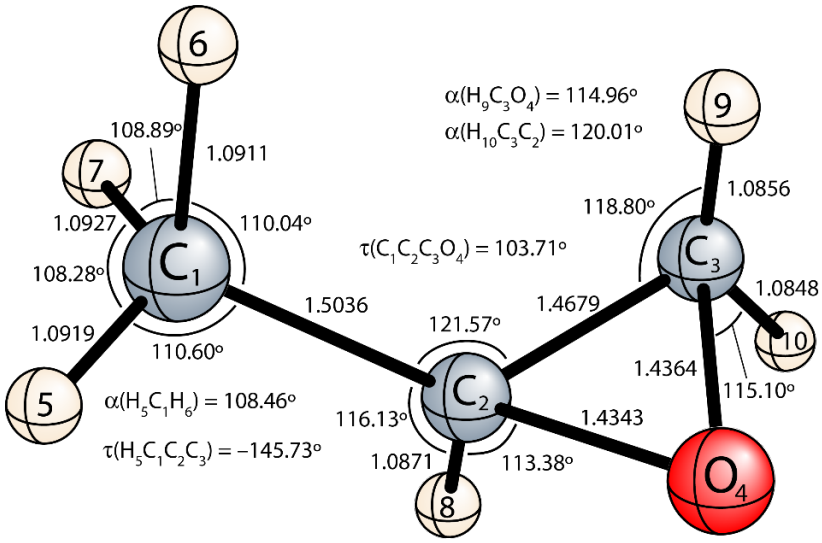

Figure 6.3: Depiction of the Methyloxirane FC-ROCCSD(T)/cc-pVTZ structure.

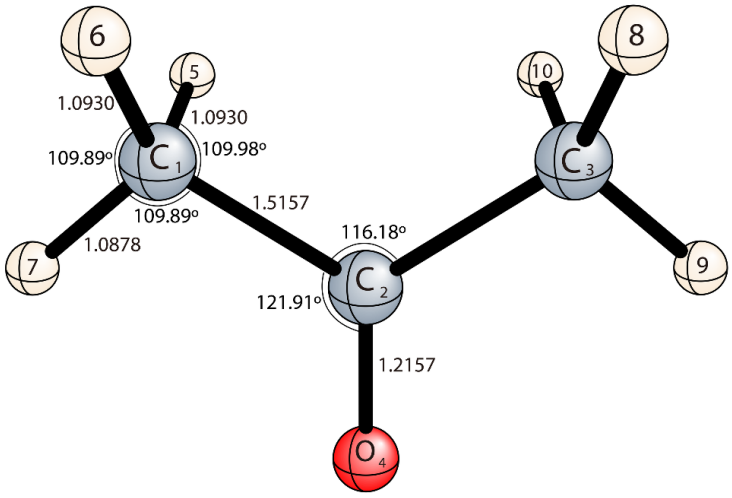

Figure 6.4: Depiction of the Acetone FC-ROCCSD(T)/cc-pVTZ structure.

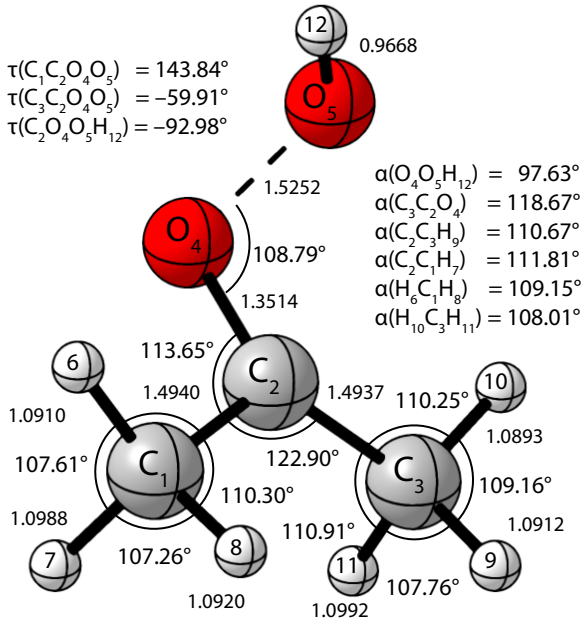

Figure 6.5: Depiction of the **TS6** FC-ROCCSD(T)/cc-pVTZ structure.

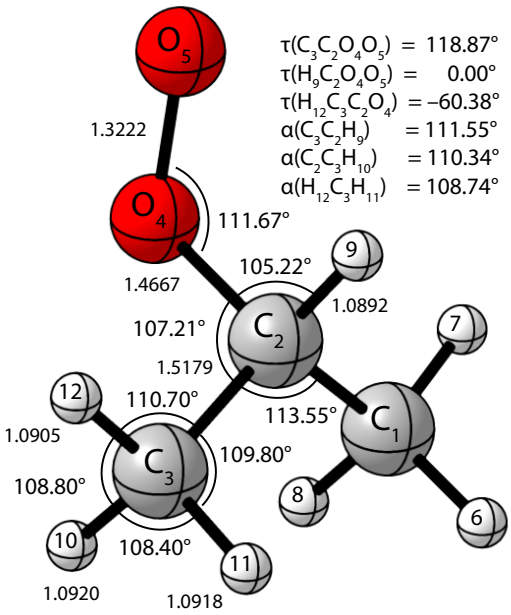

Figure 6.6: Depiction of the **TS7** FC-ROCCSD(T)/cc-pVTZ structure.

6.3 Chapter 5

	TZ/TZ	B3LYP/6-31G(2df,p) Freq	TZ/DFT CMA	Shift	Abs Shift	Diff	Abs Diff	DZ/DZ Freq	TZ/DZ MH	Shift	Abs Shift	Diff	Abs Diff
Cyclopropane (1.1)	740.8535	736.4695	740.86	4.3840	4.3840	-0.01	0.01	730.2796	740.94	10.5739	10.5739	-0.09	0.09
CH2CH2CH2 (Cyclic)	740.8535	736.4779	740.88	4.3756	4.3756	-0.03	0.03	730.2796	740.94	10.5739	10.5739	-0.09	0.09
	857.6839	853.8819	857.70	3.8020	3.8020	-0.02	0.02	848.6873	857.71	8.9966	8.9966	-0.03	0.03
	891.9603	893.7667	892.08	-1.8064	1.8064	-0.12	0.12	894.4242	892.73	-2.4639	2.4639	-0.77	0.77
	891.9603	893.7699	892.28	-1.8096	1.8096	-0.32	0.32	894.4242	892.74	-2.4639	2.4639	-0.78	0.78
	1060.5218	1063.3939	1060.25	-2.8721	2.8721	0.27	0.27	1059.1559	1059.90	1.3659	1.3659	0.62	0.62
	1060.5218	1063.3982	1060.34	-2.8764	2.8764	0.18	0.18	1059.1559	1059.90	1.3659	1.3659	0.62	0.62
	1088.5691	1090.7955	1088.58	-2.2264	2.2264	-0.01	0.01	1071.7615	1088.58	16.8076	16.8076	-0.01	0.01
	1160.8706	1159.0990	1160.85	1.7716	1.7716	0.02	0.02	1149.1364	1160.87	11.7342	11.7342	0.00	0.00
	1214.3894	1212.9328	1214.34	1.4566	1.4566	0.05	0.05	1203.5200	1215.03	10.8694	10.8694	-0.64	0.64
	1217.3474	1212.9353	1217.37	4.4121	4.4121	-0.02	0.02	1203.5200	1217.30	13.8274	13.8274	0.05	0.05
	1217.3474	1221.8111	1217.38	-4.4637	4.4637	-0.03	0.03	1216.8303	1217.30	0.5171	0.5171	0.05	0.05
	1478.3201	1474.9049	1478.36	3.4152	3.4152	-0.04	0.04	1457.3533	1478.29	20.9668	20.9668	0.03	0.03
	1478.3201	1474.9078	1478.77	3.4123	3.4123	-0.45	0.45	1457.3533	1478.29	20.9668	20.9668	0.03	0.03
	1528.6132	1516.9890	1528.91	11.6242	11.6242	-0.30	0.30	1519.5368	1528.01	9.0764	9.0764	0.60	0.60
	3146.2939	3136.3773	3146.31	9.9166	9.9166	-0.02	0.02	3143.8047	3146.30	2.4892	2.4892	-0.01	0.01
	3146.2939	3136.3803	3146.32	9.9136	9.9136	-0.03	0.03	3143.8047	3146.31	2.4892	2.4892	-0.02	0.02
	3156.9476	3145.1678	3156.94	11.7798	11.7798	0.01	0.01	3156.3703	3156.93	0.5773	0.5773	0.02	0.02
	3228.7270	3210.8202	3228.74	17.9068	17.9068	-0.01	0.01	3232.9201	3228.75	-4.1931	4.1931	-0.02	0.02
	3228.7270	3210.8208	3228.74	17.9062	17.9062	-0.01	0.01	3232.9201	3228.75	-4.1931	4.1931	-0.02	0.02
	3248.6232	3233.9745	3248.63	14.6487	14.6487	-0.01	0.01	3252.4578	3248.64	-3.8346	3.8346	-0.02	0.02
Methane (1.2)	1343.9921	1348.4257	1343.99	-4.4336	4.4336	0.00	0.00	1333.8129	1344.02	10.1792	10.1792	-0.03	0.03
CH4	1343.9921	1348.4274	1344.00	-4.4353	4.4353	-0.01	0.01	1333.8129	1344.02	10.1792	10.1792	-0.03	0.03
	1343.9921	1348.4298	1344.00	-4.4377	4.4377	-0.01	0.01	1333.8129	1344.03	10.1792	10.1792	-0.04	0.04
	1570.8040	1566.3426	1570.81	4.4614	4.4614	-0.01	0.01	1550.4945	1570.80	20.3095	20.3095	0.00	0.00
	1570.8040	1566.3484	1570.81	4.4556	4.4556	-0.01	0.01	1550.4945	1570.80	20.3095	20.3095	0.00	0.00
	3034.6584	3045.7853	3034.68	-11.1269	11.1269	-0.02	0.02	3040.3713	3034.68	-5.7129	5.7129	-0.02	0.02
	3153.7849	3157.2481	3153.82	-3.4632	3.4632	-0.04	0.04	3174.9626	3153.81	-21.1777	21.1777	-0.03	0.03
	3153.7849	3157.2525	3153.85	-3.4676	3.4676	-0.07	0.07	3174.9626	3153.84	-21.1777	21.1777	-0.06	0.06
	3153.7849	3157.2644	3153.85	-3.4795	3.4795	-0.07	0.07	3174.9626	3153.84	-21.1777	21.1777	-0.06	0.06
Ammonia (1.3)	1109.2148	1095.0648	1109.24	14.1500	14.1500	-0.03	0.03	1182.0330	1109.41	-72.8182	72.8182	-0.20	0.20
NH3	1687.9253	1677.8080	1687.93	10.1173	10.1173	0.00	0.00	1685.9797	1687.92	1.9456	1.9456	0.01	0.01
	1687.9284	1677.8142	1687.93	10.1142	10.1142	0.00	0.00	1685.9801	1687.92	1.9483	1.9483	0.01	0.01
	3471.9107	3462.6508	3471.96	9.2599	9.2599	-0.05	0.05	3434.0370	3472.13	37.8737	37.8737	-0.22	0.22
	3597.5357	3580.5745	3597.61	16.9612	16.9612	-0.07	0.07	3561.3806	3597.62	36.1551	36.1551	-0.08	0.08
	3597.5378	3580.5836	3597.61	16.9542	16.9542	-0.07	0.07	3561.3811	3597.62	36.1567	36.1567	-0.08	0.08

	TZ/TZ	B3LYP/6-31G(2df,p) Freq	TZ/DFT CMA	Shift	Abs Shift	Diff	Abs Diff	DZ/DZ Freq	TZ/DZ MH	Shift	Abs Shift	Diff	Abs Diff
Silane (1.6)	930.8032	918.2125	930.81	12.5907	12.5907	-0.01	0.01	925.8531	930.81	4.9501	4.9501	-0.01	0.01
SiH4	930.8032	918.2144	930.81	12.5888	12.5888	-0.01	0.01	925.8531	930.81	4.9501	4.9501	-0.01	0.01
	930.8032	918.2154	930.81	12.5878	12.5878	-0.01	0.01	925.8531	930.81	4.9501	4.9501	-0.01	0.01
	983.6942	975.5292	983.70	8.1650	8.1650	-0.01	0.01	978.3707	983.69	5.3235	5.3235	0.00	0.00
	983.6942	975.5295	983.70	8.1647	8.1647	-0.01	0.01	978.3707	983.69	5.3235	5.3235	0.00	0.00
	2250.5076	2241.2771	2250.52	9.2305	9.2305	-0.01	0.01	2242.3558	2250.52	8.1518	8.1518	-0.01	0.01
	2258.4730	2251.1990	2258.49	7.2740	7.2740	-0.02	0.02	2253.5162	2258.48	4.9568	4.9568	-0.01	0.01
	2258.4730	2251.2021	2258.49	7.2709	7.2709	-0.02	0.02	2253.5162	2258.49	4.9568	4.9568	-0.02	0.02
	2258.4730	2251.2079	2258.50	7.2651	7.2651	-0.03	0.03	2253.5162	2258.49	4.9568	4.9568	-0.02	0.02
Benzene (1.7)	401.3400	411.3236	401.41	-9.9836	9.9836	-0.07	0.07	394.5720	401.41	6.7680	6.7680	-0.07	0.07
(CH)6 (Cyclic, duh)	401.3400	411.3248	401.41	-9.9848	9.9848	-0.07	0.07	394.5721	401.41	6.7679	6.7679	-0.07	0.07
	607.1342	617.0813	607.16	-9.9471	9.9471	-0.03	0.03	602.7858	607.16	4.3484	4.3484	-0.03	0.03
	607.1342	617.0821	607.16	-9.9479	9.9479	-0.03	0.03	602.7859	607.16	4.3483	4.3483	-0.03	0.03
	674.6719	696.8515	678.54	-22.1796	22.1796	-3.87	3.87	624.8677	676.23	49.8042	49.8042	-1.56	1.56
	685.2934	720.3683	685.29	-35.0749	35.0749	0.00	0.00	676.6515	685.29	8.6419	8.6419	0.00	0.00
	856.4425	870.3284	856.44	-13.8859	13.8859	0.00	0.00	847.2355	856.44	9.2070	9.2070	0.00	0.00
	856.4425	870.3309	856.44	-13.8884	13.8884	0.00	0.00	847.2356	856.44	9.2069	9.2069	0.00	0.00
	959.0773	983.6899	959.03	-24.6126	24.6126	0.05	0.05	943.6981	959.07	15.3792	15.3792	0.01	0.01
	959.0773	983.6912	959.03	-24.6139	24.6139	0.05	0.05	943.6983	959.07	15.3790	15.3790	0.01	0.01
	966.6623	1010.7578	963.82	-44.0955	44.0955	2.84	2.84	947.4927	965.62	19.1696	19.1696	1.04	1.04
	1004.5387	1017.3763	1004.54	-12.8376	12.8376	0.00	0.00	994.5608	1004.56	9.9779	9.9779	-0.02	0.02
	1010.3319	1019.0863	1010.35	-8.7544	8.7544	-0.02	0.02	1003.8592	1010.36	6.4727	6.4727	-0.03	0.03
	1054.3619	1061.0868	1054.39	-6.7249	6.7249	-0.03	0.03	1050.0207	1054.39	4.3412	4.3412	-0.03	0.03
	1054.3619	1061.1164	1054.39	-6.7545	6.7545	-0.03	0.03	1050.0208	1054.39	4.3411	4.3411	-0.03	0.03
	1158.8810	1176.7522	1160.79	-17.8712	17.8712	-1.91	1.91	1151.5457	1159.02	7.3353	7.3353	-0.14	0.14
	1190.5718	1199.9370	1190.64	-9.3652	9.3652	-0.07	0.07	1181.0010	1190.55	9.5708	9.5708	0.02	0.02
	1190.5718	1199.9378	1190.64	-9.3660	9.3660	-0.07	0.07	1181.0017	1190.55	9.5701	9.5701	0.02	0.02
	1328.1741	1346.9839	1326.59	-18.8098	18.8098	1.58	1.58	1340.4431	1328.13	-12.2690	12.2690	0.04	0.04
	1370.1810	1375.1526	1370.18	-4.9716	4.9716	0.00	0.00	1353.6407	1370.18	16.5403	16.5403	0.00	0.00
	1506.9415	1514.4398	1506.94	-7.4983	7.4983	0.00	0.00	1499.9456	1506.93	6.9959	6.9959	0.01	0.01
	1506.9415	1514.4528	1506.94	-7.5113	7.5113	0.00	0.00	1499.9457	1506.93	6.9958	6.9958	0.01	0.01
	1637.2319	1641.3005	1637.23	-4.0686	4.0686	0.00	0.00	1640.4595	1637.29	-3.2276	3.2276	-0.06	0.06
	1637.2319	1641.3068	1637.23	-4.0749	4.0749	0.00	0.00	1640.4596	1637.29	-3.2277	3.2277	-0.06	0.06
	3169.3913	3163.0959	3169.41	6.2954	6.2954	-0.02	0.02	3172.9434	3169.39	-3.5521	3.5521	0.00	0.00
	3180.7379	3173.7890	3180.75	6.9489	6.9489	-0.01	0.01	3183.7486	3180.75	-3.0107	3.0107	-0.01	0.01
	3180.7379	3173.8169	3180.75	6.9210	6.9210	-0.01	0.01	3183.7487	3180.75	-3.0108	3.0108	-0.01	0.01
	3198.3347	3191.0330	3198.36	7.3017	7.3017	-0.03	0.03	3201.1979	3198.36	-2.8632	2.8632	-0.03	0.03

	TZ/TZ	B3LYP/6-31G(2df,p) Freq	TZ/DFT CMA	Shift	Abs Shift	Diff	Abs Diff	DZ/DZ Freq	TZ/DZ MH	Shift	Abs Shift	Diff	Abs Diff
Benzene (1.7)	401.3400	411.3236	401.41	-9.9836	9.9836	-0.07	0.07	394.5720	401.41	6.7680	6.7680	-0.07	0.07
(CH)6 (Cyclic, duh)	401.3400	411.3248	401.41	-9.9848	9.9848	-0.07	0.07	394.5721	401.41	6.7679	6.7679	-0.07	0.07
	607.1342	617.0813	607.16	-9.9471	9.9471	-0.03	0.03	602.7858	607.16	4.3484	4.3484	-0.03	0.03
	607.1342	617.0821	607.16	-9.9479	9.9479	-0.03	0.03	602.7859	607.16	4.3483	4.3483	-0.03	0.03
	674.6719	696.8515	678.54	-22.1796	22.1796	-3.87	3.87	624.8677	676.23	49.8042	49.8042	-1.56	1.56
	685.2934	720.3683	685.29	-35.0749	35.0749	0.00	0.00	676.6515	685.29	8.6419	8.6419	0.00	0.00
	856.4425	870.3284	856.44	-13.8859	13.8859	0.00	0.00	847.2355	856.44	9.2070	9.2070	0.00	0.00
	856.4425	870.3309	856.44	-13.8884	13.8884	0.00	0.00	847.2356	856.44	9.2069	9.2069	0.00	0.00
	959.0773	983.6899	959.03	-24.6126	24.6126	0.05	0.05	943.6981	959.07	15.3792	15.3792	0.01	0.01
	959.0773	983.6912	959.03	-24.6139	24.6139	0.05	0.05	943.6983	959.07	15.3790	15.3790	0.01	0.01
	966.6623	1010.7578	963.82	-44.0955	44.0955	2.84	2.84	947.4927	965.62	19.1696	19.1696	1.04	1.04
	1004.5387	1017.3763	1004.54	-12.8376	12.8376	0.00	0.00	994.5608	1004.56	9.9779	9.9779	-0.02	0.02
	1010.3319	1019.0863	1010.35	-8.7544	8.7544	-0.02	0.02	1003.8592	1010.36	6.4727	6.4727	-0.03	0.03
	1054.3619	1061.0868	1054.39	-6.7249	6.7249	-0.03	0.03	1050.0207	1054.39	4.3412	4.3412	-0.03	0.03
	1054.3619	1061.1164	1054.39	-6.7545	6.7545	-0.03	0.03	1050.0208	1054.39	4.3411	4.3411	-0.03	0.03
	1158.8810	1176.7522	1160.79	-17.8712	17.8712	-1.91	1.91	1151.5457	1159.02	7.3353	7.3353	-0.14	0.14
	1190.5718	1199.9370	1190.64	-9.3652	9.3652	-0.07	0.07	1181.0010	1190.55	9.5708	9.5708	0.02	0.02
	1190.5718	1199.9378	1190.64	-9.3660	9.3660	-0.07	0.07	1181.0017	1190.55	9.5701	9.5701	0.02	0.02
	1328.1741	1346.9839	1326.59	-18.8098	18.8098	1.58	1.58	1340.4431	1328.13	-12.2690	12.2690	0.04	0.04
	1370.1810	1375.1526	1370.18	-4.9716	4.9716	0.00	0.00	1353.6407	1370.18	16.5403	16.5403	0.00	0.00
	1506.9415	1514.4398	1506.94	-7.4983	7.4983	0.00	0.00	1499.9456	1506.93	6.9959	6.9959	0.01	0.01
	1506.9415	1514.4528	1506.94	-7.5113	7.5113	0.00	0.00	1499.9457	1506.93	6.9958	6.9958	0.01	0.01
	1637.2319	1641.3005	1637.23	-4.0686	4.0686	0.00	0.00	1640.4595	1637.29	-3.2276	3.2276	-0.06	0.06
	1637.2319	1641.3068	1637.23	-4.0749	4.0749	0.00	0.00	1640.4596	1637.29	-3.2277	3.2277	-0.06	0.06
	3169.3913	3163.0959	3169.41	6.2954	6.2954	-0.02	0.02	3172.9434	3169.39	-3.5521	3.5521	0.00	0.00
	3180.7379	3173.7890	3180.75	6.9489	6.9489	-0.01	0.01	3183.7486	3180.75	-3.0107	3.0107	-0.01	0.01
	3180.7379	3173.8169	3180.75	6.9210	6.9210	-0.01	0.01	3183.7487	3180.75	-3.0108	3.0108	-0.01	0.01
	3198.3347	3191.0330	3198.36	7.3017	7.3017	-0.03	0.03	3201.1979	3198.36	-2.8632	2.8632	-0.03	0.03
	3198.3347	3191.0613	3198.36	7.2734	7.2734	-0.03	0.03	3201.1980	3198.36	-2.8633	2.8633	-0.03	0.03
	3209.1476	3202.3150	3209.17	6.8326	6.8326	-0.02	0.02	3212.0814	3209.16	-2.9338	2.9338	-0.01	0.01

	TZ/TZ	B3LYP/6-31G(2df,p) Freq	TZ/DFT CMA	Shift	Abs Shift	Diff	Abs Diff	DZ/DZ Freq	TZ/DZ MH	Shift	Abs Shift	Diff	Abs Diff
Cyclopropene (1.8)	575.6804	630.2629	576.21	-54.5825	54.5825	-0.53	0.53	562.7721	575.72	12.9083	12.9083	-0.04	0.04
CH2CCH2 (Cyclic)	791.6864	799.7567	791.86	-8.0703	8.0703	-0.17	0.17	782.6374	791.81	9.0490	9.0490	-0.12	0.12
	824.7389	880.6538	824.84	-55.9149	55.9149	-0.10	0.10	797.1673	824.85	27.5716	27.5716	-0.11	0.11
	927.4568	942.5080	927.60	-15.0512	15.0512	-0.14	0.14	916.3161	927.37	11.1407	11.1407	0.09	0.09
	1020.5860	1021.0992	1020.76	-0.5132	0.5132	-0.17	0.17	1006.6319	1021.01	13.9541	13.9541	-0.42	0.42
	1042.0832	1046.5371	1039.37	-4.4539	4.4539	2.71	2.71	1028.0219	1043.79	14.0613	14.0613	-1.71	1.71
	1074.2337	1078.3035	1078.61	-4.0698	4.0698	-4.38	4.38	1063.4166	1072.31	10.8171	10.8171	1.92	1.92
	1108.9634	1115.3088	1109.15	-6.3454	6.3454	-0.19	0.19	1090.3730	1109.36	18.5904	18.5904	-0.40	0.40
	1158.1601	1168.5324	1158.12	-10.3723	10.3723	0.04	0.04	1167.4157	1158.49	-9.2556	9.2556	-0.33	0.33
	1524.7720	1525.1484	1524.02	-0.3764	0.3764	0.75	0.75	1505.5183	1523.88	19.2537	19.2537	0.89	0.89
	1682.9552	1742.3291	1684.18	-59.3739	59.3739	-1.22	1.22	1676.8192	1684.64	6.1360	6.1360	-1.68	1.68
	3071.8576	3043.1531	3071.68	28.7045	28.7045	0.18	0.18	3069.1315	3071.89	2.7261	2.7261	-0.03	0.03
	3143.0250	3105.0813	3143.07	37.9437	37.9437	-0.05	0.05	3144.9479	3143.09	-1.9229	1.9229	-0.07	0.07
	3264.5702	3266.2503	3265.41	-1.6801	1.6801	-0.84	0.84	3258.9435	3264.63	5.6267	5.6267	-0.06	0.06
	3310.7461	3314.7796	3311.20	-4.0335	4.0335	-0.45	0.45	3302.0430	3310.81	8.7031	8.7031	-0.06	0.06
Allene (1.9)	347.9743	377.4062	348.41	-29.4319	29.4319	-0.44	0.44	339.6736	348.12	8.3007	8.3007	-0.15	0.15
CH2CCH2	347.9743	377.4067	348.42	-29.4324	29.4324	-0.45	0.45	339.6736	348.13	8.3007	8.3007	-0.16	0.16
	856.7230	868.2183	856.85	-11.4953	11.4953	-0.13	0.13	832.0007	856.76	24.7223	24.7223	-0.04	0.04
	856.7230	868.2184	857.33	-11.4954	11.4954	-0.61	0.61	832.0007	856.76	24.7223	24.7223	-0.04	0.04
	870.3062	888.0072	869.93	-17.7010	17.7010	0.38	0.38	853.0346	870.30	17.2716	17.2716	0.01	0.01
	1017.7534	1019.4607	1017.42	-1.7073	1.7073	0.33	0.33	1012.5895	1017.75	5.1639	5.1639	0.00	0.00
	1017.7534	1019.4610	1017.52	-1.7076	1.7076	0.23	0.23	1012.5895	1017.75	5.1639	5.1639	0.00	0.00
	1080.7595	1117.8350	1080.86	-37.0755	37.0755	-0.10	0.10	1076.1445	1080.74	4.6150	4.6150	0.02	0.02
	1438.4093	1425.3963	1438.54	13.0130	13.0130	-0.13	0.13	1425.2003	1438.41	13.2090	13.2090	0.00	0.00
	1488.5611	1483.2622	1488.50	5.2989	5.2989	0.06	0.06	1477.7493	1488.63	10.8118	10.8118	-0.07	0.07
	2012.1479	2077.9578	2012.23	-65.8099	65.8099	-0.08	0.08	2011.9564	2012.21	0.1915	0.1915	-0.06	0.06
	3142.7558	3131.6687	3142.64	11.0871	11.0871	0.12	0.12	3146.2310	3142.77	-3.4752	3.4752	-0.01	0.01
	3144.2767	3135.7161	3144.32	8.5606	8.5606	-0.04	0.04	3147.2389	3144.29	-2.9622	2.9622	-0.01	0.01
	3226.4140	3209.0325	3226.43	17.3815	17.3815	-0.02	0.02	3240.4699	3226.48	-14.0559	14.0559	-0.07	0.07
	3226.4140	3209.0325	3226.47	17.3815	17.3815	-0.06	0.06	3240.4699	3226.48	-14.0559	14.0559	-0.07	0.07

	TZ/TZ	B3LYP/6-31G(2df,p) Freq	TZ/DFT CMA	Shift	Abs Shift	Diff	Abs Diff	DZ/DZ Freq	TZ/DZ MH	Shift	Abs Shift	Diff	Abs Diff
Spiropentane (1.10)	293.0627	291.8039	293.07	1.2588	1.2588	-0.01	0.01	289.3579	293.07	3.7048	3.7048	-0.01	0.01
CH2CH2CCH2CH2 (Bicyclic)	297.1516	309.2709	297.18	-12.1193	12.1193	-0.03	0.03	296.4929	297.18	0.6587	0.6587	-0.03	0.03
	297.1516	309.3166	297.18	-12.1650	12.1650	-0.03	0.03	296.4934	297.18	0.6582	0.6582	-0.03	0.03
	598.4339	607.0946	598.67	-8.6607	8.6607	-0.24	0.24	598.5536	598.56	-0.1197	0.1197	-0.13	0.13
	786.2672	784.5741	786.22	1.6931	1.6931	0.05	0.05	779.1036	786.30	7.1636	7.1636	-0.03	0.03
	786.2673	784.5744	786.22	1.6929	1.6929	0.05	0.05	779.1038	786.30	7.1635	7.1635	-0.03	0.03
	840.1286	839.6329	840.13	0.4957	0.4957	0.00	0.00	825.6461	840.24	14.4825	14.4825	-0.11	0.11
	897.4239	891.8833	897.42	5.5406	5.5406	0.00	0.00	896.0528	897.60	1.3711	1.3711	-0.18	0.18
	897.4239	891.8913	897.43	5.5326	5.5326	-0.01	0.01	896.0528	897.60	1.3711	1.3711	-0.18	0.18
	900.8273	912.4735	901.48	-11.6462	11.6462	-0.65	0.65	906.2429	901.69	-5.4156	5.4156	-0.86	0.86
	1019.2489	1023.6926	1018.93	-4.4437	4.4437	0.32	0.32	1013.8472	1018.82	5.4017	5.4017	0.43	0.43
	1027.3204	1027.1863	1027.24	0.1341	0.1341	0.08	0.08	1014.3394	1027.37	12.9810	12.9810	-0.05	0.05
	1054.4067	1057.9678	1054.46	-3.5611	3.5611	-0.05	0.05	1050.6517	1054.14	3.7550	3.7550	0.27	0.27
	1076.0225	1080.4444	1075.86	-4.4219	4.4219	0.16	0.16	1065.0287	1076.67	10.9938	10.9938	-0.65	0.65
	1077.3354	1080.4538	1077.50	-3.1184	3.1184	-0.16	0.16	1065.0287	1077.58	12.3067	12.3067	-0.24	0.24
	1077.3354	1090.1930	1077.51	-12.8576	12.8576	-0.17	0.17	1082.8266	1077.58	-5.4912	5.4912	-0.24	0.24
	1173.4660	1173.1156	1173.54	0.3504	0.3504	-0.07	0.07	1161.5266	1173.41	11.9394	11.9394	0.06	0.06
	1183.5048	1182.1620	1183.67	1.3428	1.3428	-0.17	0.17	1170.9493	1183.46	12.5555	12.5555	0.04	0.04
	1189.8807	1183.1433	1189.95	6.7374	6.7374	-0.07	0.07	1181.8384	1189.55	8.0423	8.0423	0.33	0.33
	1189.8807	1183.1472	1189.95	6.7335	6.7335	-0.07	0.07	1181.8384	1189.56	8.0423	8.0423	0.32	0.32
	1439.2574	1435.3704	1439.24	3.8870	3.8870	0.02	0.02	1423.2794	1439.06	15.9780	15.9780	0.20	0.20
DFT RMSE	1468.8148	1464.9620	1469.00	3.8528	3.8528	-0.19	0.19	1448.5838	1468.79	20.2310	20.2310	0.02	0.02
DZ RMSE	1468.8150	1464.9660	1469.00	3.8490	3.8490	-0.18	0.18	1448.5843	1468.79	20.2307	20.2307	0.03	0.03
	1501.4253	1493.8419	1501.54	7.5834	7.5834	-0.11	0.11	1486.7313	1501.13	14.6940	14.6940	0.30	0.30
	1596.2089	1580.6110	1596.19	15.5979	15.5979	0.02	0.02	1605.2095	1596.31	-9.0006	9.0006	-0.10	0.10
	3130.0411	3119.3078	3130.10	10.7333	10.7333	-0.06	0.06	3127.3857	3130.06	2.6554	2.6554	-0.02	0.02
	3130.0411	3119.3236	3130.10	10.7175	10.7175	-0.06	0.06	3127.3858	3130.06	2.6553	2.6553	-0.02	0.02
	3134.8528	3122.8117	3134.91	12.0411	12.0411	-0.06	0.06	3133.4556	3134.88	1.3972	1.3972	-0.03	0.03
	3135.9317	3123.9666	3135.95	11.9651	11.9651	-0.02	0.02	3134.1548	3135.95	1.7769	1.7769	-0.02	0.02
12.98	3212.3172	3194.1690	3212.23	18.1482	18.1482	0.09	0.09	3217.1060	3212.35	-4.7888	4.7888	-0.03	0.03
0.12	3213.2222	3195.5405	3213.36	17.6817	17.6817	-0.14	0.14	3217.9859	3213.26	-4.7637	4.7637	-0.04	0.04
	3225.3203	3209.4438	3225.37	15.8765	15.8765	-0.05	0.05	3230.2702	3225.36	-4.9499	4.9499	-0.04	0.04
	3225.3204	3209.4450	3225.37	15.8754	15.8754	-0.05	0.05	3230.2703	3225.36	-4.9499	4.9499	-0.04	0.04

	TZ/TZ	B3LYP/6-31G(2df,p) Freq	TZ/DFT CMA	Shift	Abs Shift	Diff	Abs Diff	DZ/DZ Freq	TZ/DZ MH	Shift	Abs Shift	Diff	Abs Diff
Aluminum trichloride (1.11)	146.3233	146.8445	146.34	-0.5212	0.5212	-0.02	0.02	146.6964	146.33	-0.3731	0.3731	-0.01	0.01
AlCl3	146.3234	146.8508	146.34	-0.5274	0.5274	-0.02	0.02	146.6965	146.33	-0.3731	0.3731	-0.01	0.01
	207.3565	203.7298	207.36	3.6267	3.6267	0.00	0.00	209.7219	207.36	-2.3654	2.3654	0.00	0.00
	388.1561	379.4653	388.16	8.6908	8.6908	0.00	0.00	380.5012	388.16	7.6549	7.6549	0.00	0.00
	628.1448	615.1656	628.15	12.9792	12.9792	-0.01	0.01	621.6413	628.15	6.5035	6.5035	-0.01	0.01
	628.1449	615.1916	628.15	12.9533	12.9533	-0.01	0.01	621.6414	628.15	6.5035	6.5035	-0.01	0.01
Aluminum trifluoride (1.12)	240.9405	241.9426	240.95	-1.0021	1.0021	-0.01	0.01	235.1264	241.01	5.8141	5.8141	-0.07	0.07
AlF3	240.9406	242.5837	240.95	-1.6431	1.6431	-0.01	0.01	235.1267	241.01	5.8139	5.8139	-0.07	0.07
	302.1239	297.6371	302.12	4.4868	4.4868	0.00	0.00	294.0036	302.13	8.1203	8.1203	-0.01	0.01
	691.9681	702.4015	691.98	-10.4334	10.4334	-0.01	0.01	672.1842	691.98	19.7839	19.7839	-0.01	0.01
	960.0461	981.0778	960.06	-21.0317	21.0317	-0.01	0.01	945.8817	960.13	14.1644	14.1644	-0.08	0.08
	960.0461	981.0956	960.06	-21.0495	21.0495	-0.01	0.01	945.8818	960.13	14.1643	14.1643	-0.08	0.08
Boron trichloride (1.13)	257.1138	251.5600	257.12	5.5538	5.5538	-0.01	0.01	258.1244	257.12	-1.0106	1.0106	-0.01	0.01
BCl3	257.1140	251.5801	257.12	5.5339	5.5339	-0.01	0.01	258.1244	257.13	-1.0104	1.0104	-0.02	0.02
	461.5947	453.6766	461.60	7.9181	7.9181	-0.01	0.01	461.8516	461.60	-0.2569	0.2569	-0.01	0.01
	476.3372	468.6205	476.34	7.7167	7.7167	0.00	0.00	479.9079	476.34	-3.5707	3.5707	0.00	0.00
	972.5564	943.2622	972.57	29.2942	29.2942	-0.01	0.01	993.6819	972.58	-21.1255	21.1255	-0.02	0.02
	972.5566	943.2706	972.57	29.2860	29.2860	-0.01	0.01	993.6820	972.58	-21.1254	21.1254	-0.02	0.02
Boron trifluoride (1.14)	483.7049	467.9584	483.89	15.7465	15.7465	-0.19	0.19	482.2942	483.75	1.4107	1.4107	-0.05	0.05
BF3	483.7049	468.0058	483.89	15.6991	15.6991	-0.19	0.19	482.2943	483.76	1.4106	1.4106	-0.06	0.06
	700.1044	695.8482	700.11	4.2562	4.2562	-0.01	0.01	711.2494	700.11	-11.1450	11.1450	-0.01	0.01
	899.3017	897.1945	899.31	2.1072	2.1072	-0.01	0.01	867.1192	899.31	32.1825	32.1825	-0.01	0.01
	1493.1388	1482.2956	1493.11	10.8432	10.8432	0.03	0.03	1469.2406	1493.26	23.8982	23.8982	-0.12	0.12
	1493.1388	1482.2968	1493.11	10.8420	10.8420	0.03	0.03	1469.2408	1493.26	23.8980	23.8980	-0.12	0.12
Tetrachloromethane (1.15)	217.9365	214.6020	217.94	3.3345	3.3345	0.00	0.00	221.4778	217.94	-3.5413	3.5413	0.00	0.00
CCl4	217.9365	214.6052	217.94	3.3313	3.3313	0.00	0.00	221.4778	217.94	-3.5413	3.5413	0.00	0.00
	315.9226	311.9431	316.26	3.9795	3.9795	-0.34	0.34	318.1759	315.98	-2.2533	2.2533	-0.06	0.06
	315.9226	311.9524	316.26	3.9702	3.9702	-0.34	0.34	318.1759	315.98	-2.2533	2.2533	-0.06	0.06
	315.9226	311.9530	316.26	3.9696	3.9696	-0.34	0.34	318.1759	315.98	-2.2533	2.2533	-0.06	0.06
	461.7965	453.7281	461.80	8.0684	8.0684	0.00	0.00	457.0351	461.80	4.7614	4.7614	0.00	0.00
	801.6847	755.9787	801.64	45.7060	45.7060	0.04	0.04	796.1251	801.77	5.5596	5.5596	-0.09	0.09
	801.6847	755.9828	801.64	45.7019	45.7019	0.04	0.04	796.1251	801.77	5.5596	5.5596	-0.09	0.09
	801.6847	755.9848	801.65	45.6999	45.6999	0.03	0.03	796.1251	801.77	5.5596	5.5596	-0.09	0.09

	TZ/TZ	B3LYP/6-31G(2df,p) Freq	TZ/DFT CMA	Shift	Abs Shift	Diff	Abs Diff	DZ/DZ Freq	TZ/DZ MH	Shift	Abs Shift	Diff	Abs Diff
Tetrafluoromethane (1.16)	440.0383	429.4068	440.04	10.6315	10.6315	0.00	0.00	437.3692	440.05	2.6691	2.6691	-0.01	0.01
CF4	440.0383	429.6888	440.04	10.3495	10.3495	0.00	0.00	437.3693	440.05	2.6690	2.6690	-0.01	0.01
	638.9925	627.0018	639.00	11.9907	11.9907	-0.01	0.01	633.4125	639.00	5.5800	5.5800	-0.01	0.01
	638.9925	627.0462	639.00	11.9463	11.9463	-0.01	0.01	633.4126	639.00	5.5799	5.5799	-0.01	0.01
	638.9925	627.1611	639.00	11.8314	11.8314	-0.01	0.01	633.4127	639.01	5.5798	5.5798	-0.02	0.02
	923.2062	917.4619	923.22	5.7443	5.7443	-0.01	0.01	909.0414	923.22	14.1648	14.1648	-0.01	0.01
	1323.0047	1301.5076	1323.05	21.4971	21.4971	-0.05	0.05	1333.6434	1323.04	-10.6387	10.6387	-0.04	0.04
	1323.0047	1301.5182	1323.05	21.4865	21.4865	-0.05	0.05	1333.6442	1323.05	-10.6395	10.6395	-0.05	0.05
	1323.0047	1301.5268	1323.05	21.4779	21.4779	-0.05	0.05	1333.6442	1323.05	-10.6395	10.6395	-0.05	0.05
Dichloromethane (1.17)	283.6602	279.3611	283.72	4.2991	4.2991	-0.06	0.06	285.3335	283.69	-1.6733	1.6733	-0.03	0.03
CH2Cl2	722.0012	707.0324	722.03	14.9688	14.9688	-0.03	0.03	716.7542	722.07	5.2470	5.2470	-0.07	0.07
	775.1935	733.0538	775.47	42.1397	42.1397	-0.28	0.28	774.0206	775.24	1.1729	1.1729	-0.05	0.05
	906.4562	897.3565	906.50	9.0997	9.0997	-0.04	0.04	899.8931	906.49	6.5631	6.5631	-0.03	0.03
	1179.3516	1164.7799	1179.36	14.5717	14.5717	-0.01	0.01	1173.3445	1179.36	6.0071	6.0071	-0.01	0.01
	1291.9215	1282.2217	1291.76	9.6998	9.6998	0.16	0.16	1289.6873	1291.90	2.2342	2.2342	0.02	0.02
	1473.8993	1457.4171	1473.93	16.4822	16.4822	-0.03	0.03	1459.2183	1473.88	14.6810	14.6810	0.02	0.02
	3129.9028	3128.6153	3129.93	1.2875	1.2875	-0.03	0.03	3127.2026	3129.95	2.7002	2.7002	-0.05	0.05
	3206.0915	3210.5934	3206.14	-4.5019	4.5019	-0.05	0.05	3209.1955	3206.16	-3.1040	3.1040	-0.07	0.07
Difluoromethane (1.18)	536.9881	533.4557	537.02	3.5324	3.5324	-0.03	0.03	533.0788	537.03	3.9093	3.9093	-0.04	0.04
CH2F2	1141.5926	1140.9575	1141.74	0.6351	0.6351	-0.15	0.15	1131.6039	1141.70	9.9887	9.9887	-0.11	0.11
	1142.1669	1141.4451	1142.19	0.7218	0.7218	-0.02	0.02	1149.3615	1142.87	-7.1946	7.1946	-0.70	0.70
	1202.5673	1184.2399	1202.58	18.3274	18.3274	-0.01	0.01	1186.7691	1202.56	15.7982	15.7982	0.01	0.01
	1292.3323	1264.4592	1292.33	27.8731	27.8731	0.00	0.00	1280.0361	1292.35	12.2962	12.2962	-0.02	0.02
	1482.3132	1462.8123	1482.31	19.5009	19.5009	0.00	0.00	1481.6776	1481.68	0.6356	0.6356	0.63	0.63
	1556.4626	1540.7386	1556.52	15.7240	15.7240	-0.06	0.06	1538.4318	1556.40	18.0308	18.0308	0.06	0.06
	3075.7560	3026.5442	3075.76	49.2118	49.2118	0.00	0.00	3073.7303	3075.79	2.0257	2.0257	-0.03	0.03
	3148.0052	3083.8104	3148.06	64.1948	64.1948	-0.05	0.05	3145.1159	3148.07	2.8893	2.8893	-0.06	0.06
Formic acid (1.19)	629.4054	626.6213	629.52	2.7841	2.7841	-0.11	0.11	629.5248	629.54	-0.1194	0.1194	-0.13	0.13
CH2O2 (Formic Acid)	675.6400	690.0096	675.63	-14.3696	14.3696	0.01	0.01	691.7545	675.75	-16.1145	16.1145	-0.11	0.11
	1061.2051	1058.4844	1061.25	2.7207	2.7207	-0.04	0.04	1053.6083	1061.24	7.5968	7.5968	-0.03	0.03
	1137.1219	1134.9358	1137.58	2.1861	2.1861	-0.46	0.46	1147.5137	1137.62	-10.3918	10.3918	-0.50	0.50
	1326.1930	1313.2294	1325.96	12.9636	12.9636	0.23	0.23	1334.8252	1326.61	-8.6322	8.6322	-0.42	0.42
	1415.8021	1403.5165	1416.04	12.2856	12.2856	-0.24	0.24	1414.4857	1415.40	1.3164	1.3164	0.40	0.40
	1824.5481	1849.1724	1824.36	-24.6243	24.6243	0.19	0.19	1843.9046	1824.46	-19.3565	19.3565	0.09	0.09
	3089.2108	3052.9746	3089.26	36.2362	36.2362	-0.05	0.05	3082.9098	3089.32	6.3010	6.3010	-0.11	0.11
	3763.9994	3735.4756	3764.19	28.5238	28.5238	-0.19	0.19	3745.1246	3764.19	18.8748	18.8748	-0.19	0.19

	TZ/TZ	B3LYP/6-31G(2df,p) Freq	TZ/DFT CMA	Shift	Abs Shift	Diff	Abs Diff	DZ/DZ Freq	TZ/DZ MH	Shift	Abs Shift	Diff	Abs Diff
Formaldehyde (1.20)	1192.1927	1203.0041	1192.20	-10.8114	10.8114	-0.01	0.01	1175.6785	1192.21	16.5142	16.5142	-0.02	0.02
CH2O	1274.8761	1263.6333	1274.92	11.2428	11.2428	-0.04	0.04	1265.9047	1274.89	8.9714	8.9714	-0.01	0.01
	1543.2070	1539.1283	1544.46	4.0787	4.0787	-1.25	1.25	1534.8751	1542.85	8.3319	8.3319	0.36	0.36
	1780.7645	1844.9049	1779.62	-64.1404	64.1404	1.14	1.14	1786.6125	1781.35	-5.8480	5.8480	-0.59	0.59
	2929.2254	2888.1632	2929.28	41.0622	41.0622	-0.05	0.05	2924.4851	2929.28	4.7403	4.7403	-0.05	0.05
	2995.8489	2935.8758	2995.90	59.9731	59.9731	-0.05	0.05	2986.4419	2995.91	9.4070	9.4070	-0.06	0.06
Singlet carbene (1.21)	1406.5853	1431.5635	1406.61	-24.9782	24.9782	-0.02	0.02	1405.9001	1406.57	0.6852	0.6852	0.02	0.02
CH2 (Singlet)	2912.0519	2894.2883	2912.09	17.7636	17.7636	-0.04	0.04	2897.4069	2912.09	14.6450	14.6450	-0.04	0.04
	2983.1169	2955.9853	2983.17	27.1316	27.1316	-0.05	0.05	2975.1129	2983.17	8.0040	8.0040	-0.05	0.05
Chloromethane (1.22)	743.9562	722.4286	744.15	21.5276	21.5276	-0.19	0.19	744.1650	744.03	-0.2088	0.2088	-0.07	0.07
CH3Cl	1030.8822	1024.6958	1030.98	6.1864	6.1864	-0.10	0.10	1025.0327	1030.93	5.8495	5.8495	-0.05	0.05
	1030.8832	1024.7669	1030.98	6.1163	6.1163	-0.10	0.10	1025.0334	1030.93	5.8498	5.8498	-0.05	0.05
	1384.1480	1377.0175	1384.13	7.1305	7.1305	0.02	0.02	1377.9341	1384.15	6.2139	6.2139	0.00	0.00
	1493.0478	1482.8821	1493.04	10.1657	10.1657	0.01	0.01	1475.8047	1493.07	17.2431	17.2431	-0.02	0.02
	1493.0491	1482.8876	1493.04	10.1615	10.1615	0.01	0.01	1475.8049	1493.07	17.2442	17.2442	-0.02	0.02
	3079.8814	3083.8904	3079.91	-4.0090	4.0090	-0.03	0.03	3081.1020	3079.93	-1.2206	1.2206	-0.05	0.05
	3181.3137	3185.8206	3181.39	-4.5069	4.5069	-0.08	0.08	3192.5289	3181.39	-11.2152	11.2152	-0.08	0.08
	3181.3138	3185.8209	3181.39	-4.5071	4.5071	-0.08	0.08	3192.5292	3181.39	-11.2154	11.2154	-0.08	0.08
Thiomethanol (1.23)	237.5736	236.3890	237.61	1.1846	1.1846	-0.04	0.04	256.7761	237.56	-19.2025	19.2025	0.01	0.01
CH3SH	720.8977	702.9542	721.28	17.9435	17.9435	-0.38	0.38	721.4702	720.95	-0.5725	0.5725	-0.05	0.05
	799.8936	795.5906	799.79	4.3030	4.3030	0.10	0.10	799.9486	800.07	-0.0550	0.0550	-0.18	0.18
	976.2822	971.8232	976.35	4.4590	4.4590	-0.07	0.07	973.1502	976.31	3.1320	3.1320	-0.03	0.03
	1099.8198	1097.2334	1099.87	2.5864	2.5864	-0.05	0.05	1101.4724	1099.70	-1.6526	1.6526	0.12	0.12
	1362.1464	1359.0799	1362.12	3.0665	3.0665	0.03	0.03	1356.9525	1362.10	5.1939	5.1939	0.05	0.05
	1482.9342	1478.0664	1482.92	4.8678	4.8678	0.01	0.01	1467.3831	1482.95	15.5511	15.5511	-0.02	0.02
	1497.0262	1490.7821	1496.96	6.2441	6.2441	0.07	0.07	1481.4057	1497.00	15.6205	15.6205	0.03	0.03
	2712.6329	2686.4468	2712.71	26.1861	26.1861	-0.08	0.08	2728.7153	2712.71	-16.0824	16.0824	-0.08	0.08
	3059.9147	3065.5095	3060.03	-5.5948	5.5948	-0.12	0.12	3059.9018	3060.02	0.0129	0.0129	-0.11	0.11
	3150.0134	3153.8845	3149.97	-3.8711	3.8711	0.04	0.04	3157.0030	3150.00	-6.9896	6.9896	0.01	0.01
	3151.2686	3155.4793	3151.37	-4.2107	4.2107	-0.10	0.10	3161.4130	3151.37	-10.1444	10.1444	-0.10	0.10

	TZ/TZ	B3LYP/6-31G(2df,p) Freq	TZ/DFT CMA	Shift	Abs Shift	Diff	Abs Diff	DZ/DZ Freq	TZ/DZ MH	Shift	Abs Shift	Diff	Abs Diff
Trichloromethane (1.24)	260.9941	256.4367	261.13	4.5574	4.5574	-0.14	0.14	263.4943	261.01	-2.5002	2.5002	-0.02	0.02
CHCl3	260.9943	256.4730	261.13	4.5213	4.5213	-0.14	0.14	263.4943	261.02	-2.5000	2.5000	-0.03	0.03
	367.4486	363.2633	367.51	4.1853	4.1853	-0.06	0.06	367.4982	367.50	-0.0496	0.0496	-0.05	0.05
	677.3695	666.5902	677.32	10.7793	10.7793	0.05	0.05	671.8759	677.43	5.4936	5.4936	-0.06	0.06
	788.7875	744.0754	789.01	44.7121	44.7121	-0.22	0.22	783.4016	788.86	5.3859	5.3859	-0.07	0.07
	788.7877	744.0796	789.01	44.7081	44.7081	-0.22	0.22	783.4016	788.86	5.3861	5.3861	-0.07	0.07
	1243.4274	1227.6762	1243.37	15.7512	15.7512	0.06	0.06	1239.4415	1243.48	3.9859	3.9859	-0.05	0.05
	1243.4274	1227.6768	1243.37	15.7506	15.7506	0.06	0.06	1239.4415	1243.48	3.9859	3.9859	-0.05	0.05
	3185.5566	3183.6147	3185.58	1.9419	1.9419	-0.02	0.02	3179.7226	3185.59	5.8340	5.8340	-0.03	0.03
Trifluoromethane (1.25)	514.8020	505.5109	514.84	9.2911	9.2911	-0.04	0.04	511.6147	514.81	3.1873	3.1873	-0.01	0.01
CHF3	514.8021	505.5301	514.84	9.2720	9.2720	-0.04	0.04	511.6147	514.82	3.1874	3.1874	-0.02	0.02
	710.2290	701.7829	710.27	8.4461	8.4461	-0.04	0.04	702.2279	710.25	8.0011	8.0011	-0.02	0.02
	1161.9031	1154.2204	1162.02	7.6827	7.6827	-0.12	0.12	1148.6467	1161.95	13.2564	13.2564	-0.05	0.05
	1203.1687	1189.3931	1203.22	13.7756	13.7756	-0.05	0.05	1207.1425	1204.13	-3.9738	3.9738	-0.96	0.96
	1203.1693	1189.3950	1203.22	13.7743	13.7743	-0.05	0.05	1207.1426	1204.13	-3.9733	3.9733	-0.96	0.96
	1424.3422	1395.2439	1424.27	29.0983	29.0983	0.07	0.07	1422.4586	1423.36	1.8836	1.8836	0.98	0.98
	1424.3424	1395.2464	1424.27	29.0960	29.0960	0.07	0.07	1422.4586	1423.36	1.8838	1.8838	0.98	0.98
	3160.8655	3100.2103	3160.93	60.6552	60.6552	-0.06	0.06	3163.8470	3160.98	-2.9815	2.9815	-0.11	0.11
Methyl nitrite (1.26)	79.6667	125.5245	81.34	-45.8578	45.8578	-1.67	1.67	88.7028	80.53	-9.0361	9.0361	-0.86	0.86
H3CONO	220.9292	231.7388	220.60	-10.8096	10.8096	0.33	0.33	218.5063	220.81	2.4229	2.4229	0.12	0.12
	380.3242	373.5204	380.59	6.8038	6.8038	-0.27	0.27	377.7359	380.55	2.5883	2.5883	-0.23	0.23
	595.0151	599.7523	595.14	-4.7372	4.7372	-0.12	0.12	570.2215	596.04	24.7936	24.7936	-1.02	1.02
	847.8031	855.4886	848.35	-7.6855	7.6855	-0.55	0.55	832.3774	847.53	15.4257	15.4257	0.27	0.27
	1086.7822	1080.1626	1086.84	6.6196	6.6196	-0.06	0.06	1088.3050	1086.93	-1.5228	1.5228	-0.15	0.15
	1176.7930	1165.8663	1176.80	10.9267	10.9267	-0.01	0.01	1165.1950	1176.83	11.5980	11.5980	-0.04	0.04
	1209.1378	1199.8874	1208.92	9.2504	9.2504	0.22	0.22	1194.5386	1209.10	14.5992	14.5992	0.04	0.04
	1462.9797	1450.1250	1462.91	12.8547	12.8547	0.07	0.07	1448.4731	1463.00	14.5066	14.5066	-0.02	0.02
	1494.3487	1486.5684	1494.27	7.7803	7.7803	0.08	0.08	1475.5307	1494.32	18.8180	18.8180	0.03	0.03
	1518.6275	1507.5213	1518.61	11.1062	11.1062	0.02	0.02	1499.8705	1518.55	18.7570	18.7570	0.08	0.08
	1710.2999	1775.8535	1710.38	-65.5536	65.5536	-0.08	0.08	1734.8992	1710.35	-24.5993	24.5993	-0.05	0.05
	3048.9760	3043.4869	3049.08	5.4891	5.4891	-0.10	0.10	3048.0832	3049.02	0.8928	0.8928	-0.04	0.04
	3137.2608	3122.8165	3137.34	14.4443	14.4443	-0.08	0.08	3143.2145	3137.35	-5.9537	5.9537	-0.09	0.09
	3138.4635	3130.5563	3138.45	7.9072	7.9072	0.01	0.01	3146.6846	3138.52	-8.2211	8.2211	-0.06	0.06

	TZ/TZ	B3LYP/6-31G(2df,p) Freq	TZ/DFT CMA	Shift	Abs Shift	Diff	Abs Diff	DZ/DZ Freq	TZ/DZ MH	Shift	Abs Shift	Diff	Abs Diff
Methylamine (1.28)	306.3389	308.3685	306.43	-2.0296	2.0296	-0.09	0.09	341.6669	306.37	-35.3280	35.3280	-0.03	0.03
H3CNH2	878.3540	848.9239	879.35	29.4301	29.4301	-1.00	1.00	913.9112	882.01	-35.5572	35.5572	-3.66	3.66
	976.3130	975.5301	976.32	0.7829	0.7829	-0.01	0.01	979.1679	976.45	-2.8549	2.8549	-0.14	0.14
	1065.5727	1066.9230	1065.67	-1.3503	1.3503	-0.10	0.10	1072.0577	1066.54	-6.4850	6.4850	-0.97	0.97
	1188.0230	1178.1797	1188.03	9.8433	9.8433	-0.01	0.01	1198.7760	1187.68	-10.7530	10.7530	0.34	0.34
	1359.3923	1357.0185	1359.42	2.3738	2.3738	-0.03	0.03	1365.7060	1359.30	-6.3137	6.3137	0.09	0.09
	1458.0638	1459.2019	1457.98	-1.1381	1.1381	0.08	0.08	1452.7520	1457.97	5.3118	5.3118	0.09	0.09
	1508.1619	1500.3592	1508.22	7.8027	7.8027	-0.06	0.06	1491.1505	1508.22	17.0114	17.0114	-0.06	0.06
	1527.6514	1520.1049	1527.66	7.5465	7.5465	-0.01	0.01	1510.0387	1527.64	17.6127	17.6127	0.01	0.01
	1667.4638	1663.1956	1667.39	4.2682	4.2682	0.07	0.07	1660.9766	1667.15	6.4872	6.4872	0.31	0.31
	2996.9778	2969.8922	2998.51	27.0856	27.0856	-1.53	1.53	2989.6497	2997.01	7.3281	7.3281	-0.03	0.03
	3079.9421	3067.8808	3078.51	12.0613	12.0613	1.43	1.43	3084.7274	3079.99	-4.7853	4.7853	-0.05	0.05
	3115.3633	3106.3710	3115.42	8.9923	8.9923	-0.06	0.06	3126.4737	3115.44	-11.1104	11.1104	-0.08	0.08
	3498.2731	3497.5614	3498.35	0.7117	0.7117	-0.08	0.08	3463.6300	3498.40	34.6431	34.6431	-0.13	0.13
	3579.1240	3573.5034	3579.18	5.6206	5.6206	-0.06	0.06	3544.6008	3579.19	34.5232	34.5232	-0.07	0.07
Ethylene (1.29)	823.0434	824.3109	823.08	-1.2675	1.2675	-0.04	0.04	819.7136	823.07	3.3298	3.3298	-0.03	0.03
H2CCH2	941.8281	973.8388	941.85	-32.0107	32.0107	-0.02	0.02	908.6537	941.86	33.1744	33.1744	-0.03	0.03
	966.6661	984.7029	966.69	-18.0368	18.0368	-0.02	0.02	949.2078	966.70	17.4583	17.4583	-0.03	0.03
	1046.9557	1070.0950	1046.97	-23.1393	23.1393	-0.01	0.01	1030.4783	1046.98	16.4774	16.4774	-0.02	0.02
	1242.1574	1239.7500	1242.19	2.4074	2.4074	-0.03	0.03	1228.7442	1242.19	13.4132	13.4132	-0.03	0.03
	1368.9816	1389.1720	1372.12	-20.1904	20.1904	-3.14	3.14	1358.0309	1368.80	10.9507	10.9507	0.18	0.18
	1479.0559	1474.8121	1479.06	4.2438	4.2438	0.00	0.00	1460.5430	1479.07	18.5129	18.5129	-0.01	0.01
	1671.7330	1700.8749	1669.09	-29.1419	29.1419	2.64	2.64	1670.8216	1672.02	0.9114	0.9114	-0.29	0.29
	3139.1093	3137.3323	3139.14	1.7770	1.7770	-0.03	0.03	3144.1674	3139.13	-5.0581	5.0581	-0.02	0.02
	3157.0900	3154.3968	3157.09	2.6932	2.6932	0.00	0.00	3163.1139	3157.10	-6.0239	6.0239	-0.01	0.01
	3219.2589	3209.4401	3219.30	9.8188	9.8188	-0.04	0.04	3233.3126	3219.28	-14.0537	14.0537	-0.02	0.02
	3246.1361	3238.6542	3246.17	7.4819	7.4819	-0.03	0.03	3259.0373	3246.17	-12.9012	12.9012	-0.03	0.03

	TZ/TZ	B3LYP/6-31G(2df,p) Freq	TZ/DFT CMA	Shift	Abs Shift	Diff	Abs Diff	DZ/DZ Freq	TZ/DZ MH	Shift	Abs Shift	Diff	Abs Diff
Tetrafluoroethylene (1.30)	201.3744	205.7675	201.38	-4.3931	4.3931	-0.01	0.01	199.3392	201.38	2.0352	2.0352	-0.01	0.01
F2C=CF2	210.8786	209.8518	210.92	1.0268	1.0268	-0.04	0.04	204.3647	210.90	6.5139	6.5139	-0.02	0.02
	401.0441	401.2587	401.09	-0.2146	0.2146	-0.05	0.05	395.5974	401.09	5.4467	5.4467	-0.05	0.05
	418.4408	439.2318	418.44	-20.7910	20.7910	0.00	0.00	424.3766	418.44	-5.9358	5.9358	0.00	0.00
	511.8204	553.5489	511.82	-41.7285	41.7285	0.00	0.00	498.0887	511.85	13.7317	13.7317	-0.03	0.03
	556.4050	556.1057	556.52	0.2993	0.2993	-0.12	0.12	548.6723	556.40	7.7327	7.7327	0.00	0.00
	559.7931	557.9292	559.80	1.8639	1.8639	-0.01	0.01	553.3621	559.81	6.4310	6.4310	-0.02	0.02
	797.3223	805.5158	797.33	-8.1935	8.1935	-0.01	0.01	786.9121	797.37	10.4102	10.4102	-0.05	0.05
	1208.5464	1214.6359	1208.55	-6.0895	6.0895	0.00	0.00	1192.5595	1208.58	15.9869	15.9869	-0.03	0.03
	1376.5388	1362.7828	1376.56	13.7560	13.7560	-0.02	0.02	1369.2883	1376.56	7.2505	7.2505	-0.02	0.02
	1385.8144	1368.9723	1385.81	16.8421	16.8421	0.00	0.00	1384.7376	1385.90	1.0768	1.0768	-0.09	0.09
	1921.1527	1924.2825	1921.18	-3.1298	3.1298	-0.03	0.03	1923.1014	1921.11	-1.9487	1.9487	0.04	0.04
Tetrachloroethylene (1.31)	98.9218	98.8295	98.92	0.0923	0.0923	0.00	0.00	96.8966	98.92	2.0252	2.0252	0.00	0.00
Cl2C=CCl2	176.0058	176.4937	176.03	-0.4879	0.4879	-0.02	0.02	176.8645	176.04	-0.8587	0.8587	-0.03	0.03
	235.7683	237.1664	235.78	-1.3981	1.3981	-0.01	0.01	237.1399	235.79	-1.3716	1.3716	-0.02	0.02
	287.0940	294.9169	287.10	-7.8229	7.8229	-0.01	0.01	286.4239	287.10	0.6701	0.6701	-0.01	0.01
	311.1206	312.9202	311.14	-1.7996	1.7996	-0.02	0.02	312.5843	311.13	-1.4637	1.4637	-0.01	0.01
	347.1213	346.9176	347.41	0.2037	0.2037	-0.29	0.29	345.2675	347.12	1.8538	1.8538	0.00	0.00
	450.6786	449.5299	450.86	1.1487	1.1487	-0.18	0.18	447.9175	450.68	2.7611	2.7611	0.00	0.00
	514.5431	543.1910	514.55	-28.6479	28.6479	-0.01	0.01	489.4032	514.57	25.1399	25.1399	-0.03	0.03
	782.8885	777.6744	782.91	5.2141	5.2141	-0.02	0.02	774.8803	782.92	8.0082	8.0082	-0.03	0.03
	926.8378	894.3384	926.85	32.4994	32.4994	-0.01	0.01	925.4082	926.85	1.4296	1.4296	-0.01	0.01
	1006.5262	973.4179	1006.32	33.1083	33.1083	0.21	0.21	1008.0733	1006.64	-1.5471	1.5471	-0.11	0.11
	1619.0737	1628.0762	1619.14	-9.0025	9.0025	-0.07	0.07	1620.7241	1619.12	-1.6504	1.6504	-0.05	0.05
Acetylene (1.32)	577.5918	586.7841	577.61	-9.1923	9.1923	-0.02	0.02	526.8988	577.60	50.6930	50.6930	-0.01	0.01
HCCH	577.5918	586.7842	577.61	-9.1924	9.1924	-0.02	0.02	526.8988	577.64	50.6930	50.6930	-0.05	0.05
	746.2838	787.9450	746.32	-41.6612	41.6612	-0.04	0.04	733.8835	746.30	12.4003	12.4003	-0.02	0.02
	746.2838	787.9452	746.32	-41.6614	41.6614	-0.04	0.04	733.8835	746.31	12.4003	12.4003	-0.03	0.03
	2000.8642	2079.1183	2001.47	-78.2541	78.2541	-0.61	0.61	1985.5336	2001.19	15.3306	15.3306	-0.33	0.33
	3409.9461	3439.6610	3410.02	-29.7149	29.7149	-0.07	0.07	3409.7820	3410.02	0.1641	0.1641	-0.07	0.07
	3510.9374	3544.7034	3510.71	-33.7660	33.7660	0.23	0.23	3500.4185	3511.06	10.5189	10.5189	-0.12	0.12

	TZ/TZ	B3LYP/6-31G(2df,p) Freq	TZ/DFT CMA	Shift	Abs Shift	Diff	Abs Diff	DZ/DZ Freq	TZ/DZ MH	Shift	Abs Shift	Diff	Abs Diff
Glyoxal (1.33)	136.2627	140.3991	136.54	-4.1364	4.1364	-0.28	0.28	152.4980	136.31	-16.2353	16.2353	-0.05	0.05
HCOHCO	330.9779	330.2961	331.00	0.6818	0.6818	-0.02	0.02	324.7451	331.01	6.2328	6.2328	-0.03	0.03
	560.0604	554.4521	560.78	5.6083	5.6083	-0.72	0.72	559.9929	560.13	0.0675	0.0675	-0.07	0.07
	823.8640	820.0312	824.01	3.8328	3.8328	-0.15	0.15	818.5845	823.93	5.2795	5.2795	-0.07	0.07
	1068.7950	1070.9822	1068.81	-2.1872	2.1872	-0.01	0.01	1060.0892	1068.81	8.7058	8.7058	-0.01	0.01
	1095.3970	1086.3285	1096.08	9.0685	9.0685	-0.68	0.68	1090.0744	1095.41	5.3226	5.3226	-0.01	0.01
	1342.0031	1338.5678	1342.08	3.4353	3.4353	-0.08	0.08	1326.7382	1342.00	15.2649	15.2649	0.00	0.00
	1384.8428	1384.6886	1384.96	0.1542	0.1542	-0.12	0.12	1373.4106	1384.77	11.4322	11.4322	0.07	0.07
	1757.8902	1820.5694	1757.93	-62.6792	62.6792	-0.04	0.04	1761.7488	1757.96	-3.8586	3.8586	-0.07	0.07
	1779.7666	1825.9288	1779.32	-46.1622	46.1622	0.45	0.45	1786.9038	1779.89	-7.1372	7.1372	-0.12	0.12
	2982.1299	2935.1341	2982.15	46.9958	46.9958	-0.02	0.02	2971.6356	2982.19	10.4943	10.4943	-0.06	0.06
	2987.0974	2940.7126	2987.09	46.3848	46.3848	0.01	0.01	2979.8923	2987.15	7.2051	7.2051	-0.05	0.05
Ketene (1.34)	434.1805	446.6456	434.67	-12.4651	12.4651	-0.49	0.49	433.0581	434.25	1.1224	1.1224	-0.07	0.07
H2CCO (Ketene)	514.8602	548.5491	515.24	-33.6889	33.6889	-0.38	0.38	477.3687	517.58	37.4915	37.4915	-2.72	2.72
	590.7919	593.5034	590.50	-2.7115	2.7115	0.29	0.29	576.7248	588.39	14.0671	14.0671	2.40	2.40
	993.5483	987.2730	993.37	6.2753	6.2753	0.18	0.18	988.3894	993.58	5.1589	5.1589	-0.03	0.03
	1151.9978	1176.2878	1152.32	-24.2900	24.2900	-0.32	0.32	1147.1921	1152.05	4.8057	4.8057	-0.05	0.05
	1419.9553	1410.8718	1419.92	9.0835	9.0835	0.04	0.04	1408.1585	1419.98	11.7968	11.7968	-0.02	0.02
	2196.6967	2247.8132	2196.67	-51.1165	51.1165	0.03	0.03	2195.0359	2196.74	1.6608	1.6608	-0.04	0.04
	3201.1515	3194.1330	3201.17	7.0185	7.0185	-0.02	0.02	3207.9472	3201.19	-6.7957	6.7957	-0.04	0.04
	3305.8076	3290.6906	3305.86	15.1170	15.1170	-0.05	0.05	3324.0012	3305.87	-18.1936	18.1936	-0.06	0.06
Vinyl fluoride (1.35)	481.3745	480.7679	481.48	0.6066	0.6066	-0.11	0.11	473.3604	481.46	8.0141	8.0141	-0.09	0.09
H2CCHF	725.0133	738.0093	725.69	-12.9960	12.9960	-0.68	0.68	718.0172	725.02	6.9961	6.9961	-0.01	0.01
	871.0320	887.6196	871.08	-16.5876	16.5876	-0.05	0.05	843.4401	871.08	27.5919	27.5919	-0.05	0.05
	945.5499	947.4849	946.19	-1.9350	1.9350	-0.64	0.64	940.3883	945.55	5.1616	5.1616	0.00	0.00
	956.1659	979.8910	955.66	-23.7251	23.7251	0.51	0.51	948.6498	956.16	7.5161	7.5161	0.01	0.01
	1186.1628	1190.2701	1185.98	-4.1073	4.1073	0.18	0.18	1177.4638	1186.50	8.6990	8.6990	-0.34	0.34
	1335.3776	1341.5171	1336.25	-6.1395	6.1395	-0.87	0.87	1322.7284	1335.23	12.6492	12.6492	0.15	0.15
	1424.8681	1416.5761	1425.15	8.2920	8.2920	-0.28	0.28	1411.8433	1424.92	13.0248	13.0248	-0.05	0.05
	1703.2167	1727.9361	1702.24	-24.7194	24.7194	0.98	0.98	1709.6309	1703.26	-6.4142	6.4142	-0.04	0.04
	3178.2750	3173.7950	3178.98	4.4800	4.4800	-0.70	0.70	3183.8762	3178.31	-5.6012	5.6012	-0.03	0.03
	3216.7285	3198.2384	3216.21	18.4901	18.4901	0.52	0.52	3221.4544	3216.85	-4.7259	4.7259	-0.12	0.12
	3280.4554	3273.1436	3280.42	7.3118	7.3118	0.04	0.04	3294.8462	3280.48	-14.3908	14.3908	-0.02	0.02

	TZ/TZ	B3LYP/6-31G(2df,p) Freq	TZ/DFT CMA	Shift	Abs Shift	Diff	Abs Diff	DZ/DZ Freq	TZ/DZ MH	Shift	Abs Shift	Diff	Abs Diff
Vinyl chloride (1.36)	392.3633	396.1754	392.42	-3.8121	3.8121	-0.06	0.06	391.4530	392.39	0.9103	0.9103	-0.03	0.03
H2CCHCl	624.2829	637.7227	624.51	-13.4398	13.4398	-0.23	0.23	612.4969	624.44	11.7860	11.7860	-0.16	0.16
	726.6607	708.7859	727.37	17.8748	17.8748	-0.71	0.71	728.3845	726.75	-1.7238	1.7238	-0.09	0.09
	906.7643	929.9525	906.53	-23.1882	23.1882	0.23	0.23	879.0795	906.79	27.6848	27.6848	-0.03	0.03
	966.9459	982.1403	966.92	-15.1944	15.1944	0.03	0.03	951.4671	966.81	15.4788	15.4788	0.14	0.14
	1042.7268	1037.0538	1042.72	5.6730	5.6730	0.01	0.01	1036.2197	1042.79	6.5071	6.5071	-0.06	0.06
	1302.8910	1299.8673	1304.57	3.0237	3.0237	-1.68	1.68	1291.4172	1302.82	11.4738	11.4738	0.07	0.07
	1408.7592	1407.7329	1409.26	1.0263	1.0263	-0.50	0.50	1395.2627	1408.79	13.4965	13.4965	-0.03	0.03
	1649.5434	1675.6205	1647.70	-26.0771	26.0771	1.84	1.84	1651.1272	1649.69	-1.5838	1.5838	-0.15	0.15
	3163.2040	3164.6168	3163.42	-1.4128	1.4128	-0.22	0.22	3168.9914	3163.28	-5.7874	5.7874	-0.08	0.08
	3221.5087	3222.9355	3221.54	-1.4268	1.4268	-0.03	0.03	3222.8453	3221.69	-1.3366	1.3366	-0.18	0.18
	3261.7437	3259.8473	3261.64	1.8964	1.8964	0.10	0.10	3275.5822	3261.71	-13.8385	13.8385	0.03	0.03
Acetyl chloride (1.37)	143.5140	138.8467	143.79	4.6673	4.6673	-0.28	0.28	158.5177	143.60	-15.0037	15.0037	-0.09	0.09
H3CCClO	342.3849	340.8074	342.49	1.5775	1.5775	-0.11	0.11	343.7532	342.44	-1.3683	1.3683	-0.06	0.06
	447.2255	430.7845	448.66	16.4410	16.4410	-1.43	1.43	442.8085	447.28	4.4170	4.4170	-0.05	0.05
	517.2533	521.1545	517.26	-3.9012	3.9012	-0.01	0.01	515.4780	517.28	1.7753	1.7753	-0.03	0.03
	612.2958	598.7623	611.94	13.5335	13.5335	0.36	0.36	608.7233	612.34	3.5725	3.5725	-0.04	0.04
	969.9073	958.4158	971.12	11.4915	11.4915	-1.21	1.21	971.8412	970.15	-1.9339	1.9339	-0.24	0.24
	1047.5825	1043.1468	1047.56	4.4357	4.4357	0.02	0.02	1038.0371	1047.73	9.5454	9.5454	-0.15	0.15
	1126.4429	1115.0112	1125.68	11.4317	11.4317	0.76	0.76	1123.3054	1126.43	3.1375	3.1375	0.01	0.01
	1394.1644	1388.5083	1394.17	5.6561	5.6561	-0.01	0.01	1383.0069	1394.05	11.1575	11.1575	0.11	0.11
	1472.2244	1463.9129	1472.11	8.3115	8.3115	0.11	0.11	1456.0577	1472.23	16.1667	16.1667	-0.01	0.01
	1478.0780	1465.8268	1478.04	12.2512	12.2512	0.04	0.04	1463.0750	1478.05	15.0030	15.0030	0.03	0.03
	1862.1864	1915.4647	1862.17	-53.2783	53.2783	0.02	0.02	1874.3424	1862.24	-12.1560	12.1560	-0.05	0.05
	3062.4526	3063.7514	3062.56	-1.2988	1.2988	-0.11	0.11	3070.3766	3062.54	-7.9240	7.9240	-0.09	0.09
	3143.2982	3138.4184	3143.38	4.8798	4.8798	-0.08	0.08	3165.3088	3143.38	-22.0106	22.0106	-0.08	0.08
	3169.2303	3164.1468	3169.22	5.0835	5.0835	0.01	0.01	3187.2246	3169.24	-17.9943	17.9943	-0.01	0.01

	TZ/TZ	B3LYP/6-31G(2df,p) Freq	TZ/DFT CMA	Shift	Abs Shift	Diff	Abs Diff	DZ/DZ Freq	TZ/DZ MH	Shift	Abs Shift	Diff	Abs Diff
Acetyl fluoride (1.38)	135.3946	129.8007	135.70	5.5939	5.5939	-0.31	0.31	139.7881	135.49	-4.3935	4.3935	-0.10	0.10
H3CCFO	412.9481	409.3125	413.01	3.6356	3.6356	-0.06	0.06	406.0879	413.01	6.8602	6.8602	-0.06	0.06
	572.4500	574.5019	572.61	-2.0519	2.0519	-0.16	0.16	567.9809	572.48	4.4691	4.4691	-0.03	0.03
	605.0702	602.9671	605.14	2.1031	2.1031	-0.07	0.07	599.9877	605.18	5.0825	5.0825	-0.11	0.11
	854.8063	859.7166	855.51	-4.9103	4.9103	-0.70	0.70	849.6444	854.89	5.1619	5.1619	-0.08	0.08
	1017.1357	1010.3639	1017.23	6.7718	6.7718	-0.09	0.09	1010.2902	1017.35	6.8455	6.8455	-0.21	0.21
	1073.0582	1069.3143	1073.07	3.7439	3.7439	-0.01	0.01	1062.6818	1073.17	10.3764	10.3764	-0.11	0.11
	1229.9576	1227.2124	1230.15	2.7452	2.7452	-0.19	0.19	1232.3110	1230.23	-2.3534	2.3534	-0.27	0.27
	1409.0660	1400.9374	1409.13	8.1286	8.1286	-0.06	0.06	1399.7940	1408.75	9.2720	9.2720	0.32	0.32
	1478.0509	1470.6653	1478.02	7.3856	7.3856	0.03	0.03	1461.1987	1478.06	16.8522	16.8522	-0.01	0.01
	1486.5827	1476.3330	1486.49	10.2497	10.2497	0.09	0.09	1469.4280	1486.53	17.1547	17.1547	0.05	0.05
	1905.6359	1926.2942	1905.41	-20.6583	20.6583	0.23	0.23	1917.7209	1905.63	-12.0850	12.0850	0.01	0.01
	3067.8877	3064.2292	3067.86	3.6585	3.6585	0.03	0.03	3075.0405	3067.87	-7.1528	7.1528	0.02	0.02
	3141.3729	3128.4124	3141.37	12.9605	12.9605	0.00	0.00	3160.3924	3141.37	-19.0195	19.0195	0.00	0.00
	3183.9447	3178.1795	3183.89	5.7652	5.7652	0.05	0.05	3200.8877	3183.88	-16.9430	16.9430	0.06	0.06
Acetic acid (1.39)	77.6710	83.5840	78.69	-5.9130	5.9130	-1.02	1.02	88.8970	78.51	-11.2260	11.2260	-0.84	0.84
CH3COOH	418.7814	417.9922	418.81	0.7892	0.7892	-0.03	0.03	415.6330	418.83	3.1484	3.1484	-0.05	0.05
	545.7222	546.6827	545.75	-0.9605	0.9605	-0.03	0.03	543.3260	546.02	2.3962	2.3962	-0.30	0.30
	584.1260	581.8982	584.21	2.2278	2.2278	-0.08	0.08	584.1560	584.19	-0.0300	0.0300	-0.06	0.06
	664.4689	675.6083	664.46	-11.1394	11.1394	0.01	0.01	671.9390	664.31	-7.4701	7.4701	0.16	0.16
	869.6824	863.6833	870.53	5.9991	5.9991	-0.85	0.85	872.9210	869.78	-3.2386	3.2386	-0.10	0.10
	1005.0143	998.8889	1005.06	6.1254	6.1254	-0.05	0.05	998.2690	1005.51	6.7453	6.7453	-0.50	0.50
	1071.3409	1066.1272	1071.40	5.2137	5.2137	-0.06	0.06	1061.4800	1071.45	9.8609	9.8609	-0.11	0.11
	1220.3411	1209.1254	1220.29	11.2157	11.2157	0.05	0.05	1232.8470	1220.21	-12.5059	12.5059	0.13	0.13
	1355.1789	1347.9862	1355.49	7.1927	7.1927	-0.31	0.31	1352.4940	1356.39	2.6849	2.6849	-1.21	1.21
	1422.2648	1410.6759	1422.55	11.5889	11.5889	-0.29	0.29	1423.5140	1421.16	-1.2492	1.2492	1.10	1.10
	1481.2309	1473.7469	1481.08	7.4840	7.4840	0.15	0.15	1464.4360	1481.12	16.7949	16.7949	0.11	0.11
	1487.6212	1478.6937	1487.58	8.9275	8.9275	0.04	0.04	1469.8480	1487.60	17.7732	17.7732	0.02	0.02
	1837.1104	1851.5511	1836.77	-14.4407	14.4407	0.34	0.34	1854.4830	1836.96	-17.3726	17.3726	0.15	0.15
	3064.9570	3063.8804	3065.00	1.0766	1.0766	-0.04	0.04	3071.4410	3065.01	-6.4840	6.4840	-0.05	0.05
	3137.3917	3126.7482	3137.44	10.6435	10.6435	-0.05	0.05	3155.3270	3137.44	-17.9353	17.9353	-0.05	0.05
	3180.5641	3177.5929	3180.56	2.9712	2.9712	0.00	0.00	3196.1340	3180.55	-15.5699	15.5699	0.01	0.01
	3776.2934	3755.4233	3776.50	20.8701	20.8701	-0.21	0.21	3759.3260	3776.51	16.9674	16.9674	-0.22	0.22

	TZ/TZ	B3LYP/6-31G(2df,p) Freq	TZ/DFT CMA	Shift	Abs Shift	Diff	Abs Diff	DZ/DZ Freq	TZ/DZ MH	Shift	Abs Shift	Diff	Abs Diff
Methyl formate (1.40)	144.9217	128.0300	145.06	16.8917	16.8917	-0.14	0.14	155.1827	145.01	-10.2610	10.2610	-0.09	0.09
CH3OCH=O	310.9853	301.8186	311.05	9.1667	9.1667	-0.06	0.06	314.7970	311.12	-3.8117	3.8117	-0.13	0.13
	339.9755	344.8609	339.98	-4.8854	4.8854	0.00	0.00	339.1622	340.00	0.8133	0.8133	-0.02	0.02
	776.7888	776.7737	776.88	0.0151	0.0151	-0.09	0.09	773.5376	776.91	3.2512	3.2512	-0.12	0.12
	957.5958	946.6385	957.84	10.9573	10.9573	-0.24	0.24	958.1099	957.72	-0.5141	0.5141	-0.12	0.12
	1049.4644	1044.3366	1049.50	5.1278	5.1278	-0.04	0.04	1038.1207	1049.49	11.3437	11.3437	-0.03	0.03
	1185.1204	1175.5736	1185.15	9.5468	9.5468	-0.03	0.03	1173.7664	1185.14	11.3540	11.3540	-0.02	0.02
	1195.9059	1186.1884	1195.89	9.7175	9.7175	0.02	0.02	1188.8017	1195.76	7.1042	7.1042	0.15	0.15
	1243.8389	1235.8750	1244.15	7.9639	7.9639	-0.31	0.31	1234.8880	1244.09	8.9509	8.9509	-0.25	0.25
	1404.5515	1394.7217	1404.67	9.8298	9.8298	-0.12	0.12	1396.2317	1404.55	8.3198	8.3198	0.00	0.00
	1472.5037	1466.8378	1472.57	5.6659	5.6659	-0.07	0.07	1461.1468	1472.90	11.3569	11.3569	-0.40	0.40
	1495.3222	1484.8996	1495.34	10.4226	10.4226	-0.02	0.02	1477.5668	1495.33	17.7554	17.7554	-0.01	0.01
	1509.7868	1498.3656	1509.78	11.4212	11.4212	0.01	0.01	1490.8028	1509.42	18.9840	18.9840	0.37	0.37
	1799.6042	1824.4111	1799.48	-24.8069	24.8069	0.12	0.12	1818.3309	1799.70	-18.7267	18.7267	-0.10	0.10
	3063.3009	3044.3837	3064.11	18.9172	18.9172	-0.81	0.81	3065.3761	3063.53	-2.0752	2.0752	-0.23	0.23
	3078.2642	3061.8446	3077.51	16.4196	16.4196	0.75	0.75	3074.7184	3078.12	3.5458	3.5458	0.14	0.14
	3143.8822	3135.4542	3143.94	8.4280	8.4280	-0.06	0.06	3153.8389	3143.94	-9.9567	9.9567	-0.06	0.06
	3176.9495	3171.3378	3177.01	5.6117	5.6117	-0.06	0.06	3189.9405	3177.01	-12.9910	12.9910	-0.06	0.06
Acetaldehyde (1.41)	156.1174	167.4931	156.47	-11.3757	11.3757	-0.35	0.35	166.3442	156.14	-10.2268	10.2268	-0.02	0.02
CH3CH=O	503.5555	505.4538	503.60	-1.8983	1.8983	-0.04	0.04	499.2587	503.58	4.2968	4.2968	-0.02	0.02
	777.4092	774.8476	777.90	2.5616	2.5616	-0.49	0.49	771.3311	777.48	6.0781	6.0781	-0.07	0.07
	895.5434	887.3471	896.40	8.1963	8.1963	-0.86	0.86	896.1367	895.69	-0.5933	0.5933	-0.15	0.15
	1132.4098	1130.8117	1132.28	1.5981	1.5981	0.13	0.13	1120.6559	1132.53	11.7539	11.7539	-0.12	0.12
	1134.4418	1135.5911	1134.55	-1.1493	1.1493	-0.11	0.11	1125.5274	1134.48	8.9144	8.9144	-0.04	0.04
	1383.1646	1377.8902	1383.46	5.2744	5.2744	-0.30	0.30	1370.9833	1383.16	12.1813	12.1813	0.00	0.00
	1431.3214	1427.8327	1431.73	3.4887	3.4887	-0.41	0.41	1422.0516	1431.25	9.2698	9.2698	0.07	0.07
	1469.9303	1463.7087	1469.53	6.2216	6.2216	0.40	0.40	1453.3386	1469.94	16.5917	16.5917	-0.01	0.01
	1481.1920	1473.2853	1481.11	7.9067	7.9067	0.08	0.08	1465.6369	1481.16	15.5551	15.5551	0.03	0.03
	1793.1441	1841.7036	1792.85	-48.5595	48.5595	0.29	0.29	1802.8543	1793.29	-9.7102	9.7102	-0.15	0.15
	2918.8766	2868.6551	2918.96	50.2215	50.2215	-0.08	0.08	2907.9153	2919.00	10.9613	10.9613	-0.12	0.12
	3037.7159	3034.9565	3037.75	2.7594	2.7594	-0.03	0.03	3045.5332	3037.81	-7.8173	7.8173	-0.09	0.09
	3105.9659	3092.5650	3106.05	13.4009	13.4009	-0.08	0.08	3126.2421	3106.05	-20.2762	20.2762	-0.08	0.08
	3156.2157	3153.1191	3156.25	3.0966	3.0966	-0.03	0.03	3172.4572	3156.19	-16.2415	16.2415	0.03	0.03

	TZ/TZ	B3LYP/6-31G(2df,p) Freq	TZ/DFT CMA	Shift	Abs Shift	Diff	Abs Diff	DZ/DZ Freq	TZ/DZ MH	Shift	Abs Shift	Diff	Abs Diff
Ethyl chloride (1.42)	261.8763	254.7525	261.94	7.1238	7.1238	-0.06	0.06	273.8580	261.96	-11.9817	11.9817	-0.08	0.08
H3CCH2Cl	330.9751	328.6736	331.12	2.3015	2.3015	-0.14	0.14	333.0546	331.01	-2.0795	2.0795	-0.03	0.03
	686.5688	660.3236	687.27	26.2452	26.2452	-0.70	0.70	685.5435	686.63	1.0253	1.0253	-0.06	0.06
	787.7562	787.1946	787.90	0.5616	0.5616	-0.14	0.14	783.6761	787.82	4.0801	4.0801	-0.06	0.06
	992.9208	983.0749	993.34	9.8459	9.8459	-0.42	0.42	995.4304	993.16	-2.5096	2.5096	-0.24	0.24
	1080.0866	1073.3789	1080.24	6.7077	6.7077	-0.15	0.15	1075.1434	1080.12	4.9432	4.9432	-0.03	0.03
	1094.4559	1088.2743	1094.21	6.1816	6.1816	0.25	0.25	1094.3619	1094.55	0.0940	0.0940	-0.09	0.09
	1280.0099	1274.4712	1279.90	5.5387	5.5387	0.11	0.11	1269.7990	1280.03	10.2109	10.2109	-0.02	0.02
	1320.9096	1312.8970	1320.87	8.0126	8.0126	0.04	0.04	1315.8706	1321.06	5.0390	5.0390	-0.15	0.15
	1414.4126	1415.9833	1414.22	-1.5707	1.5707	0.19	0.19	1405.8702	1414.15	8.5424	8.5424	0.26	0.26
	1492.7779	1486.9135	1492.77	5.8644	5.8644	0.01	0.01	1475.8951	1492.78	16.8828	16.8828	0.00	0.00
	1498.4663	1491.0041	1498.82	7.4622	7.4622	-0.35	0.35	1484.4230	1498.26	14.0433	14.0433	0.21	0.21
	1507.4662	1504.9415	1507.42	2.5247	2.5247	0.05	0.05	1491.1621	1507.57	16.3041	16.3041	-0.10	0.10
	3042.9498	3045.0237	3043.48	-2.0739	2.0739	-0.53	0.53	3050.7449	3043.11	-7.7951	7.7951	-0.16	0.16
	3092.7565	3092.3049	3092.85	0.4516	0.4516	-0.09	0.09	3093.4262	3093.10	-0.6697	0.6697	-0.34	0.34
	3119.7572	3116.7061	3119.29	3.0511	3.0511	0.47	0.47	3137.8314	3119.42	-18.0742	18.0742	0.34	0.34
	3128.4152	3128.8022	3128.50	-0.3870	0.3870	-0.08	0.08	3144.0348	3130.06	-15.6196	15.6196	-1.64	1.64
	3156.0100	3157.0690	3156.02	-1.0590	1.0590	-0.01	0.01	3165.3891	3154.46	-9.3791	9.3791	1.55	1.55
Ethane (1.43)	310.0062	306.1513	310.05	3.8549	3.8549	-0.04	0.04	326.4571	310.04	-16.4509	16.4509	-0.03	0.03
H3CCH3	820.8542	823.7925	820.89	-2.9383	2.9383	-0.04	0.04	816.0484	820.88	4.8058	4.8058	-0.03	0.03
	820.8550	823.7946	820.89	-2.9396	2.9396	-0.03	0.03	816.0484	820.88	4.8066	4.8066	-0.02	0.02
	1013.9286	1005.5202	1014.18	8.4084	8.4084	-0.25	0.25	1024.8263	1014.24	-10.8977	10.8977	-0.31	0.31
	1224.7919	1225.7761	1224.82	-0.9842	0.9842	-0.03	0.03	1216.8718	1224.80	7.9201	7.9201	-0.01	0.01
	1224.7931	1225.7773	1224.82	-0.9842	0.9842	-0.03	0.03	1216.8738	1224.81	7.9193	7.9193	-0.02	0.02
	1406.5336	1413.7007	1406.53	-7.1671	7.1671	0.00	0.00	1393.8078	1406.53	12.7258	12.7258	0.00	0.00
	1427.4632	1426.6747	1427.43	0.7885	0.7885	0.03	0.03	1425.6787	1427.24	1.7845	1.7845	0.22	0.22
	1510.8253	1505.9461	1510.83	4.8792	4.8792	0.00	0.00	1492.0859	1510.85	18.7394	18.7394	-0.02	0.02
	1510.8273	1505.9495	1510.83	4.8778	4.8778	0.00	0.00	1492.0882	1510.86	18.7391	18.7391	-0.03	0.03
	1512.5184	1511.4799	1512.51	1.0385	1.0385	0.01	0.01	1495.1332	1512.54	17.3852	17.3852	-0.02	0.02
	1512.5194	1511.4840	1512.51	1.0354	1.0354	0.01	0.01	1495.1338	1512.54	17.3856	17.3856	-0.02	0.02
	3038.0017	3040.5987	3038.03	-2.5970	2.5970	-0.03	0.03	3041.4254	3038.06	-3.4237	3.4237	-0.06	0.06
	3039.5289	3041.0836	3039.59	-1.5547	1.5547	-0.06	0.06	3046.8939	3039.54	-7.3650	7.3650	-0.01	0.01
	3096.8844	3090.3906	3096.93	6.4938	6.4938	-0.05	0.05	3114.0106	3096.92	-17.1262	17.1262	-0.04	0.04
	3096.8852	3090.3964	3096.93	6.4888	6.4888	-0.04	0.04	3114.0108	3096.92	-17.1256	17.1256	-0.03	0.03
	3120.0622	3115.8242	3120.11	4.2380	4.2380	-0.05	0.05	3135.6080	3120.11	-15.5458	15.5458	-0.05	0.05
	3120.0627	3115.8318	3120.11	4.2309	4.2309	-0.05	0.05	3135.6081	3120.11	-15.5454	15.5454	-0.05	0.05

	TZ/TZ	B3LYP/6-31G(2df,p) Freq	TZ/DFT CMA	Shift	Abs Shift	Diff	Abs Diff	DZ/DZ Freq	TZ/DZ MH	Shift	Abs Shift	Diff	Abs Diff
View site information													
Dimethyl ether (1.44)	203.0997	213.8989	203.36	-10.7992	10.7992	-0.26	0.26	211.3165	203.17	-8.2168	8.2168	-0.07	0.07
H3COCH3	255.0741	243.4040	255.12	11.6701	11.6701	-0.05	0.05	262.5229	255.10	-7.4488	7.4488	-0.03	0.03
	418.8350	411.7893	418.90	7.0457	7.0457	-0.06	0.06	423.5804	418.98	-4.7454	4.7454	-0.15	0.15
	964.0643	956.4418	964.20	7.6225	7.6225	-0.14	0.14	969.6177	964.28	-5.5534	5.5534	-0.22	0.22
	1128.7880	1129.1301	1128.70	-0.3421	0.3421	0.09	0.09	1125.9695	1128.87	2.8185	2.8185	-0.08	0.08
	1169.3623	1163.9597	1169.50	5.4026	5.4026	-0.14	0.14	1159.5705	1169.42	9.7918	9.7918	-0.06	0.06
	1202.3948	1195.5019	1202.56	6.8929	6.8929	-0.17	0.17	1193.7598	1202.42	8.6350	8.6350	-0.03	0.03
	1212.1088	1208.8986	1212.52	3.2102	3.2102	-0.41	0.41	1213.8258	1212.19	-1.7170	1.7170	-0.08	0.08
	1277.4077	1270.1837	1277.40	7.2240	7.2240	0.01	0.01	1270.8759	1277.45	6.5318	6.5318	-0.04	0.04
	1460.1079	1458.0864	1460.10	2.0215	2.0215	0.01	0.01	1451.6671	1460.13	8.4408	8.4408	-0.02	0.02
	1490.4548	1485.1831	1490.41	5.2717	5.2717	0.04	0.04	1472.0461	1490.47	18.4087	18.4087	-0.02	0.02
	1494.9763	1491.5564	1494.41	3.4199	3.4199	0.57	0.57	1480.4366	1496.56	14.5397	14.5397	-1.58	1.58
	1500.0730	1493.7228	1500.05	6.3502	6.3502	0.02	0.02	1483.7696	1500.09	16.3034	16.3034	-0.02	0.02
	1508.7002	1502.4879	1508.74	6.2123	6.2123	-0.04	0.04	1491.7032	1508.73	16.9970	16.9970	-0.03	0.03
	1526.8171	1520.8710	1527.55	5.9461	5.9461	-0.73	0.73	1513.6866	1525.21	13.1305	13.1305	1.61	1.61
	2978.1927	2965.7512	2978.29	12.4415	12.4415	-0.10	0.10	2975.3942	2978.23	2.7985	2.7985	-0.04	0.04
	2987.4342	2979.4526	2987.58	7.9816	7.9816	-0.15	0.15	2988.2474	2987.44	-0.8132	0.8132	-0.01	0.01
	3030.8448	3011.3368	3030.90	19.5080	19.5080	-0.06	0.06	3035.1729	3030.90	-4.3281	4.3281	-0.06	0.06
	3036.2516	3015.6307	3036.29	20.6209	20.6209	-0.04	0.04	3039.7545	3036.30	-3.5029	3.5029	-0.05	0.05
	3129.1477	3120.5626	3129.03	8.5851	8.5851	0.12	0.12	3141.1319	3129.14	-11.9842	11.9842	0.01	0.01
	3130.9407	3122.5071	3130.83	8.4336	8.4336	0.11	0.11	3142.9586	3130.91	-12.0179	12.0179	0.03	0.03

	TZ/TZ	B3LYP/6-31G(2df,p) Freq	TZ/DFT CMA	Shift	Abs Shift	Diff	Abs Diff	DZ/DZ Freq	TZ/DZ MH	Shift	Abs Shift	Diff	Abs Diff
Ethanol (1.45)	235.4305	240.5985	235.65	-5.1680	5.1680	-0.22	0.22	253.0386	236.67	-17.6081	17.6081	-1.24	1.24
H3CCH2OH	280.6303	274.2351	280.53	6.3952	6.3952	0.10	0.10	298.2824	280.03	-17.6521	17.6521	0.60	0.60
	413.7451	413.2889	413.80	0.4562	0.4562	-0.05	0.05	412.2682	413.80	1.4769	1.4769	-0.05	0.05
	818.6927	819.4144	818.80	-0.7217	0.7217	-0.11	0.11	816.2131	818.65	2.4796	2.4796	0.04	0.04
	909.1383	906.0479	909.37	3.0904	3.0904	-0.23	0.23	912.0778	909.25	-2.9395	2.9395	-0.11	0.11
	1050.7826	1035.3019	1051.40	15.4807	15.4807	-0.62	0.62	1054.4994	1051.81	-3.7168	3.7168	-1.03	1.03
	1121.4749	1121.9791	1121.24	-0.5042	0.5042	0.23	0.23	1128.0997	1121.40	-6.6248	6.6248	0.07	0.07
	1187.0327	1182.6113	1187.38	4.4214	4.4214	-0.35	0.35	1182.2096	1187.07	4.8231	4.8231	-0.04	0.04
	1285.1284	1275.0888	1284.86	10.0396	10.0396	0.27	0.27	1291.3340	1285.01	-6.2056	6.2056	0.12	0.12
	1306.0874	1299.2569	1305.74	6.8305	6.8305	0.35	0.35	1295.5191	1306.08	10.5683	10.5683	0.01	0.01
	1403.2154	1405.8566	1403.26	-2.6412	2.6412	-0.04	0.04	1392.2243	1403.18	10.9911	10.9911	0.04	0.04
	1468.0399	1459.1976	1468.22	8.8423	8.8423	-0.18	0.18	1472.1820	1468.30	-4.1421	4.1421	-0.26	0.26
	1489.6679	1486.9802	1489.66	2.6877	2.6877	0.01	0.01	1472.9122	1489.64	16.7557	16.7557	0.03	0.03
	1508.4069	1504.9036	1508.59	3.5033	3.5033	-0.18	0.18	1493.7672	1507.72	14.6397	14.6397	0.69	0.69
	1538.4012	1531.6056	1538.30	6.7956	6.7956	0.10	0.10	1524.6116	1538.20	13.7896	13.7896	0.20	0.20
	3000.3215	2971.7227	3000.34	28.5988	28.5988	-0.02	0.02	2985.9377	3000.40	14.3838	14.3838	-0.08	0.08
	3032.3304	2993.0128	3032.45	39.3176	39.3176	-0.12	0.12	3020.0197	3032.52	12.3107	12.3107	-0.19	0.19
	3045.1139	3047.8467	3045.12	-2.7328	2.7328	-0.01	0.01	3051.7197	3045.12	-6.6058	6.6058	-0.01	0.01
	3123.3288	3119.8398	3123.35	3.4890	3.4890	-0.02	0.02	3141.0161	3123.34	-17.6873	17.6873	-0.01	0.01
	3128.3528	3123.1680	3128.34	5.1848	5.1848	0.01	0.01	3145.0285	3128.27	-16.6757	16.6757	0.08	0.08
	3857.2969	3834.8252	3857.52	22.4717	22.4717	-0.22	0.22	3833.1279	3857.53	24.1690	24.1690	-0.23	0.23
Acetonitrile (1.46)	361.1423	382.9716	361.23	-21.8293	21.8293	-0.09	0.09	357.1252	361.15	4.0171	4.0171	-0.01	0.01
H3CCN	361.1423	382.9719	361.26	-21.8296	21.8296	-0.12	0.12	357.1252	361.15	4.0171	4.0171	-0.01	0.01
	921.2760	933.2446	921.99	-11.9686	11.9686	-0.71	0.71	925.1014	921.38	-3.8254	3.8254	-0.10	0.10
	1062.1445	1056.2818	1062.07	5.8627	5.8627	0.07	0.07	1050.8136	1062.18	11.3309	11.3309	-0.04	0.04
	1062.1445	1056.2820	1062.09	5.8625	5.8625	0.05	0.05	1050.8136	1062.18	11.3309	11.3309	-0.04	0.04
	1414.0177	1409.3153	1414.01	4.7024	4.7024	0.01	0.01	1402.1070	1413.98	11.9107	11.9107	0.04	0.04
	1487.5665	1472.7346	1487.60	14.8319	14.8319	-0.03	0.03	1468.8686	1487.59	18.6979	18.6979	-0.02	0.02
	1487.5665	1472.7392	1487.61	14.8273	14.8273	-0.04	0.04	1468.8686	1487.59	18.6979	18.6979	-0.02	0.02
	2298.7273	2369.7261	2298.65	-70.9988	70.9988	0.08	0.08	2288.4291	2298.80	10.2982	10.2982	-0.07	0.07
	3066.0265	3058.9543	3065.94	7.0722	7.0722	0.09	0.09	3073.2819	3066.05	-7.2554	7.2554	-0.02	0.02
	3149.9325	3132.0016	3149.84	17.9309	17.9309	0.09	0.09	3169.3111	3149.84	-19.3786	19.3786	0.09	0.09
	3149.9325	3132.0090	3149.88	17.9235	17.9235	0.05	0.05	3169.3111	3149.84	-19.3786	19.3786	0.09	0.09

	TZ/TZ	B3LYP/6-31G(2df,p) Freq	TZ/DFT CMA	Shift	Abs Shift	Diff	Abs Diff	DZ/DZ Freq	TZ/DZ MH	Shift	Abs Shift	Diff	Abs Diff
Propyne (1.47)	322.4589	342.5483	322.62	-20.0894	20.0894	-0.16	0.16	310.0179	323.16	12.4410	12.4410	-0.70	0.70
CHCCH3	322.4611	342.5486	322.63	-20.0875	20.0875	-0.17	0.17	310.0181	323.21	12.4430	12.4430	-0.75	0.75
	619.8289	644.4411	619.59	-24.6122	24.6122	0.24	0.24	594.2670	619.38	25.5619	25.5619	0.45	0.45
	619.8293	644.4418	619.60	-24.6125	24.6125	0.23	0.23	594.2671	619.39	25.5622	25.5622	0.44	0.44
	935.4985	949.7184	936.14	-14.2199	14.2199	-0.64	0.64	938.1304	935.61	-2.6319	2.6319	-0.11	0.11
	1059.9327	1056.3457	1059.90	3.5870	3.5870	0.03	0.03	1049.4823	1059.86	10.4504	10.4504	0.07	0.07
	1059.9356	1056.3461	1059.92	3.5895	3.5895	0.02	0.02	1049.4826	1059.93	10.4530	10.4530	0.01	0.01
	1417.1207	1415.2171	1417.07	1.9036	1.9036	0.05	0.05	1406.4484	1417.10	10.6723	10.6723	0.02	0.02
	1491.3598	1477.0724	1491.30	14.2874	14.2874	0.06	0.06	1473.3273	1491.32	18.0325	18.0325	0.04	0.04
	1491.3599	1477.0770	1491.31	14.2829	14.2829	0.05	0.05	1473.3286	1491.33	18.0313	18.0313	0.03	0.03
	2177.6089	2245.8810	2177.44	-68.2721	68.2721	0.17	0.17	2166.3507	2177.61	11.2582	11.2582	0.00	0.00
	3048.3465	3037.3841	3048.37	10.9624	10.9624	-0.02	0.02	3054.9350	3048.43	-6.5885	6.5885	-0.08	0.08
	3122.3319	3098.2452	3122.44	24.0867	24.0867	-0.11	0.11	3141.1305	3122.44	-18.7986	18.7986	-0.11	0.11
	3122.3323	3098.2524	3122.44	24.0799	24.0799	-0.11	0.11	3141.1314	3122.45	-18.7991	18.7991	-0.12	0.12
	3470.2533	3496.5862	3470.39	-26.3329	26.3329	-0.14	0.14	3459.2701	3470.37	10.9832	10.9832	-0.12	0.12
Trifluoroacetonitril (1.48)	189.8642	192.9748	190.69	-3.1106	3.1106	-0.83	0.83	183.4784	189.93	6.3858	6.3858	-0.07	0.07
F3CCN	189.8642	193.2945	190.71	-3.4303	3.4303	-0.85	0.85	183.4784	189.93	6.3858	6.3858	-0.07	0.07
	469.3285	465.4173	469.46	3.9112	3.9112	-0.13	0.13	463.9901	469.37	5.3384	5.3384	-0.04	0.04
	469.3285	465.4933	469.81	3.8352	3.8352	-0.48	0.48	463.9901	469.37	5.3384	5.3384	-0.04	0.04
	527.1535	520.3180	527.46	6.8355	6.8355	-0.31	0.31	524.4787	527.25	2.6748	2.6748	-0.10	0.10
	629.3020	627.6602	628.65	1.6418	1.6418	0.65	0.65	621.0402	629.24	8.2618	8.2618	0.06	0.06
	629.3020	627.6626	628.86	1.6394	1.6394	0.44	0.44	621.0402	629.24	8.2618	8.2618	0.06	0.06
	821.0873	817.1905	821.24	3.8968	3.8968	-0.15	0.15	811.1772	821.18	9.9101	9.9101	-0.09	0.09
	1258.5285	1234.8601	1258.33	23.6684	23.6684	0.20	0.20	1257.0219	1258.59	1.5066	1.5066	-0.06	0.06
	1258.5285	1237.0084	1258.59	21.5201	21.5201	-0.06	0.06	1268.9051	1258.59	-10.3766	10.3766	-0.06	0.06
	1258.8543	1237.0099	1259.57	21.8444	21.8444	-0.72	0.72	1268.9053	1258.78	-10.0510	10.0510	0.07	0.07
	2304.3951	2382.9949	2304.06	-78.5998	78.5998	0.34	0.34	2292.2212	2304.44	12.1739	12.1739	-0.04	0.04
Silicon tetrachloride (1.49)	145.3091	143.2807	145.33	2.0284	2.0284	-0.02	0.02	143.0888	145.31	2.2203	2.2203	0.00	0.00
SiCl4	145.3093	143.5456	145.34	1.7637	1.7637	-0.03	0.03	143.0888	145.31	2.2205	2.2205	0.00	0.00
	219.8806	214.8719	219.92	5.0087	5.0087	-0.04	0.04	215.7688	219.89	4.1118	4.1118	-0.01	0.01
	219.8807	215.7268	219.93	4.1539	4.1539	-0.05	0.05	215.7688	219.89	4.1119	4.1119	-0.01	0.01
	219.8807	216.9731	219.93	2.9076	2.9076	-0.05	0.05	215.7688	219.89	4.1119	4.1119	-0.01	0.01
	422.7350	408.6715	422.74	14.0635	14.0635	0.00	0.00	414.6448	422.74	8.0902	8.0902	0.00	0.00
	625.4863	606.6702	625.48	18.8161	18.8161	0.01	0.01	620.0402	625.49	5.4461	5.4461	0.00	0.00
	625.4864	606.7261	625.49	18.7603	18.7603	0.00	0.00	620.0404	625.49	5.4460	5.4460	0.00	0.00
	625.4864	606.8004	625.49	18.6860	18.6860	0.00	0.00	620.0404	625.49	5.4460	5.4460	0.00	0.00

	TZ/TZ	B3LYP/6-31G(2df,p) Freq	TZ/DFT CMA	Shift	Abs Shift	Diff	Abs Diff	DZ/DZ Freq	TZ/DZ MH	Shift	Abs Shift	Diff	Abs Diff
Silicon tetrafluoride (1.50)	259.7978	261.6713	259.80	-1.8735	1.8735	0.00	0.00	240.4524	259.80	19.3454	19.3454	0.00	0.00
SiF4	259.7980	261.7033	259.80	-1.9053	1.9053	0.00	0.00	240.4527	259.80	19.3453	19.3453	0.00	0.00
	384.3434	383.9225	384.40	0.4209	0.4209	-0.06	0.06	361.1784	384.35	23.1650	23.1650	-0.01	0.01
	384.3436	383.9226	384.40	0.4210	0.4210	-0.06	0.06	361.1790	384.35	23.1646	23.1646	-0.01	0.01
	384.3437	383.9230	384.40	0.4207	0.4207	-0.06	0.06	361.1800	384.35	23.1637	23.1637	-0.01	0.01
	794.8609	789.4532	794.87	5.4077	5.4077	-0.01	0.01	762.1291	794.87	32.7318	32.7318	-0.01	0.01
	1036.4931	1041.5328	1036.47	-5.0397	5.0397	0.02	0.02	1013.5626	1036.49	22.9305	22.9305	0.00	0.00
	1036.4931	1041.5523	1036.48	-5.0592	5.0592	0.01	0.01	1013.5626	1036.50	22.9305	22.9305	-0.01	0.01
	1036.4935	1041.5581	1036.48	-5.0646	5.0646	0.01	0.01	1013.5627	1036.50	22.9308	22.9308	-0.01	0.01
Disilane (1.51)	135.7152	126.3936	135.71	9.3216	9.3216	0.01	0.01	132.5136	135.71	3.2016	3.2016	0.01	0.01
SiH3SiH3	371.9701	373.9199	372.00	-1.9498	1.9498	-0.03	0.03	372.7169	371.99	-0.7468	0.7468	-0.02	0.02
	371.9724	374.4233	372.00	-2.4509	2.4509	-0.03	0.03	372.7170	371.99	-0.7446	0.7446	-0.02	0.02
	437.3599	424.0408	437.39	13.3191	13.3191	-0.03	0.03	432.9304	437.39	4.4295	4.4295	-0.03	0.03
	635.3149	632.1891	635.36	3.1258	3.1258	-0.05	0.05	633.0775	635.32	2.2374	2.2374	-0.01	0.01
	635.3160	632.5525	635.37	2.7635	2.7635	-0.05	0.05	633.0777	635.32	2.2383	2.2383	0.00	0.00
	857.6325	851.6260	857.63	6.0065	6.0065	0.00	0.00	855.1313	857.63	2.5012	2.5012	0.00	0.00
	932.0965	924.8903	932.09	7.2062	7.2062	0.01	0.01	926.9287	932.10	5.1678	5.1678	0.00	0.00
	950.3416	942.6533	950.33	7.6883	7.6883	0.01	0.01	944.9782	950.34	5.3634	5.3634	0.00	0.00
	950.3420	943.0078	950.33	7.3342	7.3342	0.01	0.01	944.9783	950.34	5.3637	5.3637	0.00	0.00
	964.1638	955.9918	964.16	8.1720	8.1720	0.00	0.00	958.7645	964.17	5.3993	5.3993	-0.01	0.01
	964.1645	956.2234	964.16	7.9411	7.9411	0.00	0.00	958.7667	964.17	5.3978	5.3978	-0.01	0.01
	2222.5146	2216.1666	2222.53	6.3480	6.3480	-0.02	0.02	2218.0189	2222.53	4.4957	4.4957	-0.02	0.02
	2231.2588	2224.2553	2231.24	7.0035	7.0035	0.02	0.02	2226.4002	2231.27	4.8586	4.8586	-0.01	0.01
	2232.5510	2226.1885	2232.56	6.3625	6.3625	-0.01	0.01	2230.2299	2232.56	2.3211	2.3211	-0.01	0.01
	2232.5511	2226.2215	2232.59	6.3296	6.3296	-0.04	0.04	2230.2301	2232.57	2.3210	2.3210	-0.02	0.02
	2241.0450	2236.0852	2241.06	4.9598	4.9598	-0.01	0.01	2238.0711	2241.06	2.9739	2.9739	-0.01	0.01
	2241.0459	2236.0881	2241.06	4.9578	4.9578	-0.01	0.01	2238.0713	2241.06	2.9746	2.9746	-0.01	0.01

	TZ/TZ	B3LYP/6-31G(2df,p) Freq	TZ/DFT CMA	Shift	Abs Shift	Diff	Abs Diff	DZ/DZ Freq	TZ/DZ MH	Shift	Abs Shift	Diff	Abs Diff
Methylsilane (1.52)	202.8948	197.4393	202.88	5.4555	5.4555	0.01	0.01	204.4209	202.88	-1.5261	1.5261	0.01	0.01
SiH3CH3	517.7165	522.3570	517.88	-4.6405	4.6405	-0.16	0.16	513.4146	517.85	4.3019	4.3019	-0.13	0.13
	517.7179	522.3609	517.88	-4.6430	4.6430	-0.16	0.16	513.4146	517.85	4.3033	4.3033	-0.13	0.13
	704.5834	695.1283	704.81	9.4551	9.4551	-0.23	0.23	692.1177	704.63	12.4657	12.4657	-0.05	0.05
	887.9111	889.0826	888.00	-1.1715	1.1715	-0.09	0.09	887.0313	888.00	0.8798	0.8798	-0.09	0.09
	887.9163	889.0834	888.00	-1.1671	1.1671	-0.08	0.08	887.0336	888.00	0.8827	0.8827	-0.08	0.08
	954.2528	949.4444	954.28	4.8084	4.8084	-0.03	0.03	947.8500	954.29	6.4028	6.4028	-0.04	0.04
	971.4756	961.3830	971.40	10.0926	10.0926	0.08	0.08	964.5290	971.46	6.9466	6.9466	0.02	0.02
	971.4793	961.3885	971.40	10.0908	10.0908	0.08	0.08	964.5294	971.46	6.9499	6.9499	0.02	0.02
	1293.8161	1297.7406	1293.82	-3.9245	3.9245	0.00	0.00	1284.5708	1293.80	9.2453	9.2453	0.02	0.02
	1470.1070	1470.0970	1470.08	0.0100	0.0100	0.03	0.03	1454.8009	1470.10	15.3061	15.3061	0.01	0.01
	1470.1090	1470.1016	1470.08	0.0074	0.0074	0.03	0.03	1454.8012	1470.10	15.3078	15.3078	0.01	0.01
	2235.9766	2223.2668	2235.87	12.7098	12.7098	0.11	0.11	2230.1380	2235.99	5.8386	5.8386	-0.01	0.01
	2236.8310	2224.9955	2236.86	11.8355	11.8355	-0.03	0.03	2233.8912	2236.86	2.9398	2.9398	-0.03	0.03
	2236.8325	2224.9991	2236.98	11.8334	11.8334	-0.15	0.15	2233.8913	2236.86	2.9412	2.9412	-0.03	0.03
	3038.7953	3045.3482	3038.81	-6.5529	6.5529	-0.01	0.01	3046.6504	3038.82	-7.8551	7.8551	-0.02	0.02
	3123.3908	3121.3605	3123.42	2.0303	2.0303	-0.03	0.03	3141.3849	3123.44	-17.9941	17.9941	-0.05	0.05
	3123.3914	3121.3685	3123.42	2.0229	2.0229	-0.03	0.03	3141.3850	3123.44	-17.9936	17.9936	-0.05	0.05
Phosphane (1.53)	1018.1732	1024.7790	1018.18	-6.6058	6.6058	-0.01	0.01	1033.8996	1018.16	-15.7264	15.7264	0.01	0.01
PH3	1142.1557	1143.4271	1142.16	-1.2714	1.2714	0.00	0.00	1142.6119	1142.15	-0.4562	0.4562	0.01	0.01
	1142.1563	1144.3962	1142.16	-2.2399	2.2399	0.00	0.00	1142.6122	1142.15	-0.4559	0.4559	0.01	0.01
	2412.8109	2396.6947	2412.83	16.1162	16.1162	-0.02	0.02	2412.2358	2412.83	0.5751	0.5751	-0.02	0.02
	2421.5713	2408.4828	2421.60	13.0885	13.0885	-0.03	0.03	2424.0378	2421.60	-2.4665	2.4665	-0.03	0.03
	2421.5717	2408.4931	2421.60	13.0786	13.0786	-0.03	0.03	2424.0381	2421.60	-2.4664	2.4664	-0.03	0.03
Phosphorus trifluoride (1.54)	345.4341	338.3275	345.44	7.1066	7.1066	-0.01	0.01	322.8530	345.48	22.5811	22.5811	-0.05	0.05
PF3	345.4346	339.5453	345.45	5.8893	5.8893	-0.02	0.02	322.8534	345.48	22.5812	22.5812	-0.05	0.05
	485.9895	475.3707	486.02	10.6188	10.6188	-0.03	0.03	453.7990	485.97	32.1905	32.1905	0.02	0.02
	877.8288	871.2760	877.84	6.5528	6.5528	-0.01	0.01	863.7106	877.86	14.1182	14.1182	-0.03	0.03
	877.8290	871.7448	877.84	6.0842	6.0842	-0.01	0.01	863.7113	877.86	14.1177	14.1177	-0.03	0.03
	905.6490	887.9696	905.64	17.6794	17.6794	0.01	0.01	878.9148	905.84	26.7342	26.7342	-0.19	0.19
Hypochlorous acid (1.55)	729.7070	742.1431	729.74	-12.4361	12.4361	-0.03	0.03	673.6885	730.21	56.0185	56.0185	-0.50	0.50
HOCl	1279.5272	1277.8900	1279.59	1.6372	1.6372	-0.06	0.06	1238.2379	1279.53	41.2893	41.2893	0.00	0.00
	3809.2097	3777.7663	3809.38	31.4434	31.4434	-0.17	0.17	3774.5243	3809.36	34.6854	34.6854	-0.15	0.15
Nitrosyl chloride (1.56)	343.5397	339.9619	343.58	3.5778	3.5778	-0.04	0.04	328.8382	344.09	14.7015	14.7015	-0.55	0.55
ONCl	609.8207	617.3714	609.78	-7.5507	7.5507	0.04	0.04	593.4126	610.21	16.4081	16.4081	-0.39	0.39
	1831.7386	1928.1670	1831.84	-96.4284	96.4284	-0.10	0.10	1874.5335	1831.58	-42.7949	42.7949	0.16	0.16

	TZ/TZ	B3LYP/6-31G(2df,p) Freq	TZ/DFT CMA	Shift	Abs Shift	Diff	Abs Diff	DZ/DZ Freq	TZ/DZ MH	Shift	Abs Shift	Diff	Abs Diff
Ozone (1.57)	715.6843	751.6656	716.03	-35.9813	35.9813	-0.35	0.35	704.2489	715.78	11.4354	11.4354	-0.10	0.10
O3	1054.3239	1247.8445	1054.39	-193.5206	193.5206	-0.07	0.07	976.7596	1054.39	77.5643	77.5643	-0.07	0.07
	1153.1092	1279.5940	1153.39	-126.4848	126.4848	-0.28	0.28	1117.5022	1153.18	35.6070	35.6070	-0.07	0.07
Difluorine monoxide (1.58)	469.2858	479.5276	469.47	-10.2418	10.2418	-0.18	0.18	437.1096	469.54	32.1762	32.1762	-0.25	0.25
OF2	867.4242	900.2475	867.44	-32.8233	32.8233	-0.02	0.02	758.5915	867.44	108.8327	108.8327	-0.02	0.02
	950.1065	1024.0064	950.18	-73.8999	73.8999	-0.07	0.07	857.3517	950.32	92.7548	92.7548	-0.21	0.21
Water (1.59)	1668.8743	1655.9138	1668.89	12.9605	12.9605	-0.02	0.02	1690.2999	1668.88	-21.4256	21.4256	-0.01	0.01
H2O	3840.9239	3806.5393	3841.07	34.3846	34.3846	-0.15	0.15	3821.6053	3841.02	19.3186	19.3186	-0.10	0.10
	3945.5343	3912.5203	3945.95	33.0140	33.0140	-0.42	0.42	3927.5815	3945.63	17.9528	17.9528	-0.10	0.10
Trifluoroamine (1.60)	502.4840	492.0152	502.56	10.4688	10.4688	-0.08	0.08	485.1748	502.85	17.3092	17.3092	-0.37	0.37
NF3	502.4842	492.0257	502.56	10.4585	10.4585	-0.08	0.08	485.1749	502.86	17.3093	17.3093	-0.38	0.38
	659.9066	655.1732	660.00	4.7334	4.7334	-0.09	0.09	634.8493	660.60	25.0573	25.0573	-0.69	0.69
	949.1950	929.8400	949.17	19.3550	19.3550	0.03	0.03	897.9625	949.20	51.2325	51.2325	0.00	0.00
	949.1953	929.8464	949.17	19.3489	19.3489	0.03	0.03	897.9625	949.20	51.2328	51.2328	0.00	0.00
	1058.3486	1063.5006	1058.37	-5.1520	5.1520	-0.02	0.02	1016.7530	1058.24	41.5956	41.5956	0.11	0.11
Chlorine trifluoride (1.61)	330.1323	311.2969	330.15	18.8354	18.8354	-0.02	0.02	299.8843	330.28	30.2480	30.2480	-0.15	0.15
ClF3	330.5654	323.2706	330.56	7.2948	7.2948	0.01	0.01	305.9482	330.56	24.6172	24.6172	0.01	0.01
	433.6738	413.1318	433.70	20.5420	20.5420	-0.03	0.03	387.5177	433.64	46.1561	46.1561	0.03	0.03
	539.2599	531.1495	539.40	8.1104	8.1104	-0.14	0.14	492.3425	539.40	46.9174	46.9174	-0.14	0.14
	733.0030	732.0465	733.01	0.9565	0.9565	-0.01	0.01	671.0140	733.13	61.9890	61.9890	-0.13	0.13
	758.9202	745.5494	758.92	13.3708	13.3708	0.00	0.00	727.8021	758.79	31.1181	31.1181	0.13	0.13
Hydrogen peroxide (1.62)	372.1704	397.5561	372.34	-25.3857	25.3857	-0.17	0.17	337.2663	372.48	34.9041	34.9041	-0.31	0.31
HOOH	911.7946	960.0645	911.97	-48.2699	48.2699	-0.18	0.18	861.3084	911.96	50.4862	50.4862	-0.17	0.17
	1323.6377	1343.3125	1323.67	-19.6748	19.6748	-0.03	0.03	1294.9483	1323.71	28.6894	28.6894	-0.07	0.07
	1435.9816	1448.2786	1435.95	-12.2970	12.2970	0.03	0.03	1432.3826	1435.88	3.5990	3.5990	0.10	0.10
	3807.9102	3762.4967	3807.98	45.4135	45.4135	-0.07	0.07	3781.7989	3808.02	26.1113	26.1113	-0.11	0.11
	3809.2866	3762.5769	3809.39	46.7097	46.7097	-0.10	0.10	3783.7566	3809.37	25.5300	25.5300	-0.08	0.08
Carbonyl fluoride (1.63)	588.7372	585.7574	588.76	2.9798	2.9798	-0.02	0.02	581.1912	588.77	7.5460	7.5460	-0.03	0.03
F2CO	626.1054	625.4681	626.18	0.6373	0.6373	-0.07	0.07	619.6645	626.17	6.4409	6.4409	-0.06	0.06
	786.0177	789.8695	786.02	-3.8518	3.8518	0.00	0.00	776.8374	786.02	9.1803	9.1803	0.00	0.00
	983.5280	990.6053	983.57	-7.0773	7.0773	-0.04	0.04	967.6807	983.56	15.8473	15.8473	-0.03	0.03
	1293.9935	1284.3103	1293.99	9.6832	9.6832	0.00	0.00	1295.0744	1294.06	-1.0809	1.0809	-0.07	0.07
	1978.0332	1989.4023	1978.09	-11.3691	11.3691	-0.06	0.06	1993.5730	1978.12	-15.5398	15.5398	-0.09	0.09
Carbon dioxide (1.64)	660.2964	683.0664	660.32	-22.7700	22.7700	-0.02	0.02	650.2015	660.30	10.0949	10.0949	0.00	0.00
CO2 (Linear)	660.2964	683.0665	660.32	-22.7701	22.7701	-0.02	0.02	650.2015	660.31	10.0949	10.0949	-0.01	0.01
	1346.1961	1374.6691	1346.22	-28.4730	28.4730	-0.02	0.02	1337.8677	1346.22	8.3284	8.3284	-0.02	0.02
	2396.2729	2437.9088	2396.32	-41.6359	41.6359	-0.05	0.05	2398.1836	2396.32	-1.9107	1.9107	-0.05	0.05

	TZ/TZ	B3LYP/6-31G(2df,p) Freq	TZ/DFT CMA	Shift	Abs Shift	Diff	Abs Diff	DZ/DZ Freq	TZ/DZ MH	Shift	Abs Shift	Diff	Abs Diff
Singlet silylene (1.65)	1023.1079	1023.2684	1023.14	-0.1605	0.1605	-0.03	0.03	1028.6167	1023.10	-5.5088	5.5088	0.01	0.01
SiH2 (Singlet)	2062.3730	2045.5625	2062.40	16.8105	16.8105	-0.03	0.03	2053.8296	2062.40	8.5434	8.5434	-0.03	0.03
	2063.5566	2048.4905	2063.56	15.0661	15.0661	0.00	0.00	2055.6949	2063.58	7.8617	7.8617	-0.02	0.02
Nitrous oxide (1.66)	601.1834	627.5804	601.20	-26.3970	26.3970	-0.02	0.02	579.9076	601.18	21.2758	21.2758	0.00	0.00
NNO (Linear)	601.1834	627.5804	601.20	-26.3970	26.3970	-0.02	0.02	579.9076	601.19	21.2758	21.2758	-0.01	0.01
	1297.0933	1343.2857	1297.35	-46.1924	46.1924	-0.26	0.26	1307.4248	1297.47	-10.3315	10.3315	-0.38	0.38
	2282.5663	2367.0542	2282.57	-84.4879	84.4879	0.00	0.00	2283.4510	2282.49	-0.8847	0.8847	0.08	0.08
Hydrazine (1.67)	25.6213	79.3703	29.39	-53.7490	53.7490	-3.77	3.77	203.1097	26.62	-177.4884	177.4884	-1.00	1.00
H2NNH2	943.7822	951.5262	943.93	-7.7440	7.7440	-0.15	0.15	940.2109	944.63	3.5713	3.5713	-0.85	0.85
	1068.3681	1064.0076	1068.55	4.3605	4.3605	-0.18	0.18	1096.8720	1069.01	-28.5039	28.5039	-0.64	0.64
	1108.5129	1115.7470	1108.44	-7.2341	7.2341	0.07	0.07	1118.7839	1108.50	-10.2710	10.2710	0.01	0.01
	1256.7865	1248.0153	1256.92	8.7712	8.7712	-0.13	0.13	1293.3891	1256.65	-36.6026	36.6026	0.14	0.14
	1487.9800	1491.8385	1488.03	-3.8585	3.8585	-0.05	0.05	1495.2194	1487.99	-7.2394	7.2394	-0.01	0.01
	1638.6766	1631.5364	1638.58	7.1402	7.1402	0.10	0.10	1635.2328	1638.25	3.4438	3.4438	0.43	0.43
	1690.4652	1689.9699	1690.36	0.4953	0.4953	0.11	0.11	1685.0191	1690.33	5.4461	5.4461	0.14	0.14
	3437.7729	3429.3995	3437.80	8.3734	8.3734	-0.03	0.03	3400.7946	3437.81	36.9783	36.9783	-0.04	0.04
	3455.3523	3447.8167	3455.38	7.5356	7.5356	-0.03	0.03	3416.9816	3455.35	38.3707	38.3707	0.00	0.00
	3512.9046	3499.2661	3512.92	13.6385	13.6385	-0.02	0.02	3478.9164	3512.95	33.9882	33.9882	-0.05	0.05
	3533.9699	3520.5781	3533.99	13.3918	13.3918	-0.02	0.02	3499.4968	3534.01	34.4731	34.4731	-0.04	0.04
Cyanogen (1.68)	236.2583	251.2758	236.28	-15.0175	15.0175	-0.02	0.02	232.1557	236.27	4.1026	4.1026	-0.01	0.01
NCCN	236.2583	251.2760	236.28	-15.0177	15.0177	-0.02	0.02	232.1557	236.33	4.1026	4.1026	-0.07	0.07
	498.6045	555.7806	498.67	-57.1761	57.1761	-0.07	0.07	496.7541	498.66	1.8504	1.8504	-0.06	0.06
	498.6045	555.7807	498.67	-57.1762	57.1762	-0.07	0.07	496.7541	498.68	1.8504	1.8504	-0.08	0.08
	855.8247	888.6421	855.94	-32.8174	32.8174	-0.12	0.12	855.5786	855.96	0.2461	0.2461	-0.14	0.14
	2175.8461	2263.5175	2175.89	-87.6714	87.6714	-0.04	0.04	2157.3962	2175.89	18.4499	18.4499	-0.04	0.04
	2367.7422	2435.5172	2367.74	-67.7750	67.7750	0.00	0.00	2353.0768	2367.91	14.6654	14.6654	-0.17	0.17

	TZ/TZ	B3LYP/6-31G(2df,p) Freq	TZ/DFT CMA	Shift	Abs Shift	Diff	Abs Diff	DZ/DZ Freq	TZ/DZ MH	Shift	Abs Shift	Diff	Abs Diff
Aziridine (1.69)	782.1298	771.1135	780.45	11.0163	11.0163	1.68	1.68	772.9931	779.73	9.1367	9.1367	2.40	2.40
NHCH2CH2 (Cyclic)	840.7892	869.5698	847.03	-28.7806	28.7806	-6.24	6.24	844.8012	844.12	-4.0120	4.0120	-3.33	3.33
	874.8302	878.8796	878.61	-4.0494	4.0494	-3.78	3.78	875.7922	876.02	-0.9620	0.9620	-1.19	1.19
	923.4311	913.9619	918.81	9.4692	9.4692	4.62	4.62	916.3148	921.18	7.1163	7.1163	2.25	2.25
	1022.4617	1006.0746	1024.31	16.3871	16.3871	-1.85	1.85	1015.3063	1023.09	7.1554	7.1554	-0.63	0.63
	1113.5943	1113.4481	1107.98	0.1462	0.1462	5.61	5.61	1095.5136	1109.10	18.0807	18.0807	4.49	4.49
	1120.1953	1119.3846	1122.06	0.8107	0.8107	-1.86	1.86	1116.5138	1120.58	3.6815	3.6815	-0.38	0.38
	1162.6046	1155.0579	1170.17	7.5467	7.5467	-7.57	7.57	1150.9481	1166.65	11.6565	11.6565	-4.05	4.05
	1245.9429	1246.4494	1249.80	-0.5065	0.5065	-3.86	3.86	1248.5792	1245.95	-2.6363	2.6363	-0.01	0.01
	1272.2632	1273.0152	1272.29	-0.7520	0.7520	-0.03	0.03	1272.7963	1271.80	-0.5331	0.5331	0.46	0.46
	1307.5808	1303.4727	1303.51	4.1081	4.1081	4.07	4.07	1305.2380	1308.01	2.3428	2.3428	-0.43	0.43
	1501.7625	1494.9413	1502.94	6.8212	6.8212	-1.18	1.18	1484.5158	1502.12	17.2467	17.2467	-0.36	0.36
	1532.6495	1524.4667	1533.88	8.1828	8.1828	-1.23	1.23	1523.6453	1532.79	9.0042	9.0042	-0.14	0.14
	3130.2569	3111.1498	3130.38	19.1071	19.1071	-0.12	0.12	3125.6341	3130.19	4.6228	4.6228	0.07	0.07
	3137.2686	3117.4324	3137.35	19.8362	19.8362	-0.08	0.08	3134.1360	3137.23	3.1326	3.1326	0.04	0.04
	3214.7394	3188.3822	3214.61	26.3572	26.3572	0.13	0.13	3214.6726	3214.72	0.0668	0.0668	0.02	0.02
	3228.0312	3203.7102	3227.92	24.3210	24.3210	0.11	0.11	3228.4656	3228.02	-0.4344	0.4344	0.01	0.01
	3515.0155	3511.3880	3515.27	3.6275	3.6275	-0.25	0.25	3486.6835	3515.23	28.3320	28.3320	-0.21	0.21

	TZ/TZ	B3LYP/6-31G(2df,p) Freq	TZ/DFT CMA	Shift	Abs Shift	Diff	Abs Diff	DZ/DZ Freq	TZ/DZ MH	Shift	Abs Shift	Diff	Abs Diff
Acetamide (1.70)	57.9076	39.8809	80.82	18.0267	18.0267	-22.91	22.91	81.2686	72.89	-23.3610	23.3610	-14.98	14.98
H3CCONH2	299.3755	154.8408	315.32	144.5347	144.5347	-15.94	15.94	400.9535	388.86	-101.5780	101.5780	-89.48	89.48
	416.3253	413.3406	416.81	2.9847	2.9847	-0.48	0.48	437.7553	414.95	-21.4300	21.4300	1.38	1.38
	508.2247	519.8434	511.58	-11.6187	11.6187	-3.36	3.36	507.6511	490.47	0.5736	0.5736	17.75	17.75
	553.5676	550.8134	554.23	2.7542	2.7542	-0.66	0.66	555.7573	556.56	-2.1897	2.1897	-2.99	2.99
	638.4045	643.6663	640.77	-5.2618	5.2618	-2.37	2.37	629.3840	632.78	9.0205	9.0205	5.62	5.62
	854.2037	838.4478	855.62	15.7559	15.7559	-1.42	1.42	857.0323	856.23	-2.8286	2.8286	-2.03	2.03
	981.9773	978.3329	973.13	3.6444	3.6444	8.85	8.85	974.0132	974.31	7.9641	7.9641	7.67	7.67
	1057.3076	1053.1155	1059.04	4.1921	4.1921	-1.73	1.73	1045.5692	1058.55	11.7384	11.7384	-1.24	1.24
	1134.2471	1120.3102	1133.42	13.9369	13.9369	0.83	0.83	1146.1017	1133.57	-11.8546	11.8546	0.68	0.68
	1344.1858	1339.5126	1343.52	4.6732	4.6732	0.67	0.67	1333.6613	1344.04	10.5245	10.5245	0.15	0.15
	1409.8122	1399.0184	1411.43	10.7938	10.7938	-1.62	1.62	1406.5545	1411.08	3.2577	3.2577	-1.27	1.27
	1481.0497	1476.3216	1479.70	4.7281	4.7281	1.35	1.35	1464.8123	1480.74	16.2374	16.2374	0.31	0.31
	1495.8918	1488.1108	1495.56	7.7810	7.7810	0.33	0.33	1475.4327	1494.75	20.4591	20.4591	1.14	1.14
	1628.5096	1613.2396	1626.91	15.2700	15.2700	1.60	1.60	1622.4414	1627.46	6.0682	6.0682	1.05	1.05
	1794.3290	1809.8389	1793.36	-15.5099	15.5099	0.97	0.97	1819.7193	1794.15	-25.3903	25.3903	0.18	0.18
	3050.8188	3048.1772	3051.13	2.6416	2.6416	-0.31	0.31	3053.6554	3050.89	-2.8366	2.8366	-0.07	0.07
	3122.9640	3109.1155	3123.73	13.8485	13.8485	-0.77	0.77	3134.7820	3123.32	-11.8180	11.8180	-0.36	0.36
	3165.4189	3168.8707	3165.06	-3.4518	3.4518	0.36	0.36	3185.1247	3165.58	-19.7058	19.7058	-0.16	0.16
	3604.3495	3605.8465	3604.81	-1.4970	1.4970	-0.46	0.46	3566.8716	3605.15	37.4779	37.4779	-0.80	0.80
	3738.9954	3743.1353	3739.05	-4.1399	4.1399	-0.05	0.05	3696.8746	3738.92	42.1208	42.1208	0.08	0.08

	TZ/TZ	B3LYP/6-31G(2df,p) Freq	TZ/DFT CMA	Shift	Abs Shift	Diff	Abs Diff	DZ/DZ Freq	TZ/DZ MH	Shift	Abs Shift	Diff	Abs Diff
Dimethylamine (1.71)	223.2044	232.5121	223.41	-9.3077	9.3077	-0.21	0.21	236.9244	223.34	-13.7200	13.7200	-0.14	0.14
CH3NHCH3	268.9600	259.5702	269.75	9.3898	9.3898	-0.79	0.79	282.3184	269.06	-13.3584	13.3584	-0.10	0.10
	385.5542	380.2418	385.54	5.3124	5.3124	0.01	0.01	391.3664	385.65	-5.8122	5.8122	-0.10	0.10
	812.7009	765.1911	818.43	47.5098	47.5098	-5.73	5.73	839.3328	814.63	-26.6319	26.6319	-1.93	1.93
	953.4057	950.2251	954.11	3.1806	3.1806	-0.70	0.70	959.9202	954.13	-6.5145	6.5145	-0.72	0.72
	1028.8647	1035.5448	1028.89	-6.6801	6.6801	-0.03	0.03	1023.6483	1028.99	5.2164	5.2164	-0.13	0.13
	1100.8962	1103.2226	1101.04	-2.3264	2.3264	-0.14	0.14	1092.6314	1101.12	8.2648	8.2648	-0.22	0.22
	1177.6492	1178.6492	1178.01	-1.0000	1.0000	-0.36	0.36	1186.2935	1177.79	-8.6443	8.6443	-0.14	0.14
	1198.2571	1189.3720	1198.73	8.8851	8.8851	-0.47	0.47	1194.4525	1198.61	3.8046	3.8046	-0.35	0.35
	1273.3219	1272.6756	1272.92	0.6463	0.6463	0.40	0.40	1271.4922	1273.05	1.8297	1.8297	0.27	0.27
	1438.9451	1441.9673	1438.95	-3.0222	3.0222	0.00	0.00	1431.2201	1438.99	7.7250	7.7250	-0.04	0.04
	1467.7747	1471.7987	1467.57	-4.0240	4.0240	0.20	0.20	1461.7964	1468.21	5.9783	5.9783	-0.44	0.44
	1478.4106	1479.6991	1478.39	-1.2885	1.2885	0.02	0.02	1470.0063	1482.08	8.4043	8.4043	-3.67	3.67
	1492.6738	1488.2275	1492.18	4.4463	4.4463	0.49	0.49	1477.5103	1490.63	15.1635	15.1635	2.04	2.04
	1504.3514	1498.2383	1504.62	6.1131	6.1131	-0.27	0.27	1488.2901	1504.04	16.0613	16.0613	0.31	0.31
	1522.5208	1520.3335	1523.77	2.1873	2.1873	-1.25	1.25	1507.3508	1520.87	15.1700	15.1700	1.65	1.65
	1524.8426	1520.5807	1525.05	4.2619	4.2619	-0.21	0.21	1511.7874	1524.79	13.0552	13.0552	0.05	0.05
	2958.2989	2934.0511	2958.98	24.2478	24.2478	-0.68	0.68	2956.9724	2958.32	1.3265	1.3265	-0.02	0.02
	2959.9116	2939.6181	2960.74	20.2935	20.2935	-0.83	0.83	2961.4453	2959.93	-1.5337	1.5337	-0.02	0.02
	3065.2693	3055.4424	3064.56	9.8269	9.8269	0.71	0.71	3074.8694	3065.34	-9.6001	9.6001	-0.07	0.07
	3066.3239	3055.6515	3065.72	10.6724	10.6724	0.60	0.60	3075.0852	3066.39	-8.7613	8.7613	-0.07	0.07
	3112.9000	3105.1693	3112.95	7.7307	7.7307	-0.05	0.05	3125.4997	3112.97	-12.5997	12.5997	-0.07	0.07
	3113.8072	3106.1686	3113.87	7.6386	7.6386	-0.06	0.06	3126.5378	3113.86	-12.7306	12.7306	-0.05	0.05
	3524.7204	3531.5677	3525.01	-6.8473	6.8473	-0.29	0.29	3492.1011	3525.01	32.6193	32.6193	-0.29	0.29

	TZ/TZ	B3LYP/6-31G(2df,p) Freq	TZ/DFT CMA	Shift	Abs Shift	Diff	Abs Diff	DZ/DZ Freq	TZ/DZ MH	Shift	Abs Shift	Diff	Abs Diff
Ethylamine (1.72)	254.0826	247.8684	254.44	6.2142	6.2142	-0.36	0.36	266.4912	255.66	-12.4086	12.4086	-1.58	1.58
CH3CH2NH2	288.5112	287.7487	288.28	0.7625	0.7625	0.23	0.23	326.3946	287.43	-37.8834	37.8834	1.08	1.08
	396.6063	399.3057	396.73	-2.6994	2.6994	-0.12	0.12	399.8882	396.79	-3.2819	3.2819	-0.18	0.18
	777.1142	775.9757	777.18	1.1385	1.1385	-0.07	0.07	776.1455	777.19	0.9687	0.9687	-0.08	0.08
	877.0709	859.1094	879.45	17.9615	17.9615	-2.38	2.38	890.1672	881.80	-13.0963	13.0963	-4.73	4.73
	914.8482	901.5328	914.66	13.3154	13.3154	0.19	0.19	944.6400	914.35	-29.7918	29.7918	0.50	0.50
	1008.3599	1006.5625	1008.37	1.7974	1.7974	-0.01	0.01	1010.5350	1008.42	-2.1751	2.1751	-0.06	0.06
	1081.5534	1063.9003	1081.59	17.6531	17.6531	-0.04	0.04	1090.0706	1081.30	-8.5172	8.5172	0.25	0.25
	1160.2451	1154.6845	1160.28	5.5606	5.5606	-0.03	0.03	1172.6091	1161.25	-12.3640	12.3640	-1.00	1.00
	1276.0952	1275.3684	1276.19	0.7268	0.7268	-0.09	0.09	1271.8260	1276.32	4.2692	4.2692	-0.22	0.22
	1380.2526	1380.1624	1380.69	0.0902	0.0902	-0.44	0.44	1373.2791	1380.68	6.9735	6.9735	-0.43	0.43
	1396.0987	1391.9533	1396.10	4.1454	4.1454	0.00	0.00	1397.1055	1395.75	-1.0068	1.0068	0.35	0.35
	1408.5805	1407.9041	1407.88	0.6764	0.6764	0.70	0.70	1406.4451	1407.98	2.1354	2.1354	0.60	0.60
	1493.3049	1488.5044	1493.56	4.8005	4.8005	-0.26	0.26	1477.1758	1493.23	16.1291	16.1291	0.07	0.07
	1499.4327	1496.9530	1499.42	2.4797	2.4797	0.01	0.01	1483.4967	1499.42	15.9360	15.9360	0.01	0.01
	1511.2952	1508.5776	1511.10	2.7176	2.7176	0.20	0.20	1495.9294	1511.20	15.3658	15.3658	0.10	0.10
	1663.1806	1660.4530	1663.12	2.7276	2.7276	0.06	0.06	1658.8647	1662.87	4.3159	4.3159	0.31	0.31
	3022.3720	3024.3779	3022.45	-2.0059	2.0059	-0.08	0.08	3027.0222	3022.65	-4.6502	4.6502	-0.28	0.28
	3043.4507	3033.2322	3043.48	10.2185	10.2185	-0.03	0.03	3043.8669	3043.34	-0.4162	0.4162	0.11	0.11
	3074.1126	3061.2879	3074.63	12.8247	12.8247	-0.52	0.52	3084.1110	3074.54	-9.9984	9.9984	-0.43	0.43
	3100.0856	3093.8957	3100.13	6.1899	6.1899	-0.04	0.04	3115.3293	3100.11	-15.2437	15.2437	-0.02	0.02
	3103.2408	3098.1974	3102.82	5.0434	5.0434	0.42	0.42	3115.4543	3102.91	-12.2135	12.2135	0.33	0.33
	3477.7465	3480.7015	3477.86	-2.9550	2.9550	-0.11	0.11	3444.6017	3477.92	33.1448	33.1448	-0.17	0.17
	3559.1612	3557.4114	3559.23	1.7498	1.7498	-0.07	0.07	3526.4517	3559.24	32.7095	32.7095	-0.08	0.08

	TZ/TZ	B3LYP/6-31G(2df,p) Freq	TZ/DFT CMA	Shift	Abs Shift	Diff	Abs Diff	DZ/DZ Freq	TZ/DZ MH	Shift	Abs Shift	Diff	Abs Diff
Acetone (1.73)	20.7812	57.9595	23.15	-37.1783	37.1783	-2.37	2.37	59.2064	20.93	-38.4252	38.4252	-0.15	0.15
CH3COCH3	141.0938	143.4966	141.46	-2.4028	2.4028	-0.37	0.37	153.0644	141.11	-11.9706	11.9706	-0.02	0.02
	371.5569	374.8152	371.60	-3.2583	3.2583	-0.04	0.04	371.8585	371.59	-0.3016	0.3016	-0.03	0.03
	480.4684	490.1921	480.56	-9.7237	9.7237	-0.09	0.09	480.4786	480.48	-0.0102	0.0102	-0.01	0.01
	527.5769	531.0412	527.67	-3.4643	3.4643	-0.09	0.09	526.5469	527.61	1.0300	1.0300	-0.03	0.03
	794.7257	784.4781	795.37	10.2476	10.2476	-0.64	0.64	797.3314	794.78	-2.6057	2.6057	-0.05	0.05
	887.4013	881.3239	887.44	6.0774	6.0774	-0.04	0.04	877.0182	887.50	10.3831	10.3831	-0.10	0.10
	894.5229	885.9753	895.54	8.5476	8.5476	-1.02	1.02	891.9564	894.71	2.5665	2.5665	-0.19	0.19
	1081.1723	1084.9487	1081.32	-3.7764	3.7764	-0.15	0.15	1073.1134	1081.21	8.0589	8.0589	-0.04	0.04
	1116.2690	1115.6606	1116.24	0.6084	0.6084	0.03	0.03	1105.7097	1116.38	10.5593	10.5593	-0.11	0.11
	1246.4598	1235.1018	1247.05	11.3580	11.3580	-0.59	0.59	1241.5792	1246.65	4.8806	4.8806	-0.19	0.19
	1386.9584	1385.1627	1387.25	1.7957	1.7957	-0.29	0.29	1375.9304	1386.94	11.0280	11.0280	0.02	0.02
	1395.1100	1386.1883	1394.51	8.9217	8.9217	0.60	0.60	1389.6842	1394.82	5.4258	5.4258	0.29	0.29
	1468.8005	1462.3144	1468.52	6.4861	6.4861	0.28	0.28	1451.7982	1468.78	17.0023	17.0023	0.02	0.02
	1474.2667	1467.7044	1474.21	6.5623	6.5623	0.06	0.06	1458.7914	1474.25	15.4753	15.4753	0.02	0.02
	1476.5434	1471.4881	1476.39	5.0553	5.0553	0.15	0.15	1459.3973	1476.64	17.1461	17.1461	-0.10	0.10
	1495.9267	1489.6580	1495.89	6.2687	6.2687	0.04	0.04	1479.3826	1495.90	16.5441	16.5441	0.03	0.03
	1786.2222	1820.9464	1785.91	-34.7242	34.7242	0.31	0.31	1796.2432	1786.21	-10.0210	10.0210	0.01	0.01
	3037.0772	3037.0148	3037.11	0.0624	0.0624	-0.03	0.03	3043.5989	3037.15	-6.5217	6.5217	-0.07	0.07
	3042.4111	3043.7002	3042.42	-1.2891	1.2891	-0.01	0.01	3048.6310	3042.49	-6.2199	6.2199	-0.08	0.08
	3104.0252	3094.4545	3104.03	9.5707	9.5707	0.00	0.00	3122.2647	3104.03	-18.2395	18.2395	0.00	0.00
	3110.2790	3101.7709	3110.30	8.5081	8.5081	-0.02	0.02	3127.9895	3110.30	-17.7105	17.7105	-0.02	0.02
	3157.8092	3155.2115	3157.81	2.5977	2.5977	0.00	0.00	3172.1298	3157.77	-14.3206	14.3206	0.04	0.04
	3159.2593	3156.5805	3159.27	2.6788	2.6788	-0.01	0.01	3173.4784	3159.22	-14.2191	14.2191	0.04	0.04

	TZ/TZ	B3LYP/6-31G(2df,p) Freq	TZ/DFT CMA	Shift	Abs Shift	Diff	Abs Diff	DZ/DZ Freq	TZ/DZ MH	Shift	Abs Shift	Diff	Abs Diff
1-Chloropropane (1.74)	117.3622	116.4422	117.56	0.9200	0.9200	-0.20	0.20	122.9829	117.47	-5.6207	5.6207	-0.11	0.11
CH3CH2CH2Cl	231.6062	232.2267	231.73	-0.6205	0.6205	-0.12	0.12	235.0060	231.73	-3.3998	3.3998	-0.12	0.12
	232.8045	233.9149	232.87	-1.1104	1.1104	-0.07	0.07	242.3977	232.84	-9.5932	9.5932	-0.04	0.04
	363.4392	359.4349	363.80	4.0043	4.0043	-0.36	0.36	364.9558	363.47	-1.5166	1.5166	-0.03	0.03
	751.0778	732.2780	751.24	18.7998	18.7998	-0.16	0.16	749.9607	751.22	1.1171	1.1171	-0.14	0.14
	755.9308	751.9184	756.69	4.0124	4.0124	-0.76	0.76	754.7417	755.99	1.1891	1.1891	-0.06	0.06
	870.1284	870.5563	870.25	-0.4279	0.4279	-0.12	0.12	865.1879	870.21	4.9405	4.9405	-0.08	0.08
	915.2620	908.0465	915.35	7.2155	7.2155	-0.09	0.09	916.5963	915.37	-1.3343	1.3343	-0.11	0.11
	1055.3799	1039.2846	1056.23	16.0953	16.0953	-0.85	0.85	1064.5815	1055.84	-9.2016	9.2016	-0.46	0.46
	1096.5624	1092.1551	1096.68	4.4073	4.4073	-0.12	0.12	1090.7779	1096.55	5.7845	5.7845	0.01	0.01
	1126.3378	1120.1057	1126.09	6.2321	6.2321	0.25	0.25	1123.8396	1126.38	2.4982	2.4982	-0.04	0.04
	1251.0625	1249.2400	1251.10	1.8225	1.8225	-0.04	0.04	1242.8263	1251.15	8.2362	8.2362	-0.09	0.09
	1284.0421	1283.9506	1284.29	0.0915	0.0915	-0.25	0.25	1275.4093	1284.16	8.6328	8.6328	-0.12	0.12
	1322.9336	1322.8198	1322.90	0.1138	0.1138	0.03	0.03	1311.9999	1322.96	10.9337	10.9337	-0.03	0.03
	1375.0037	1372.2988	1374.89	2.7049	2.7049	0.11	0.11	1374.2118	1375.76	0.7919	0.7919	-0.76	0.76
	1414.5849	1416.3638	1413.98	-1.7789	1.7789	0.60	0.60	1408.9308	1413.58	5.6541	5.6541	1.00	1.00
	1493.2405	1488.2890	1493.57	4.9515	4.9515	-0.33	0.33	1480.3763	1493.71	12.8642	12.8642	-0.47	0.47
	1499.5745	1496.7535	1499.82	2.8210	2.8210	-0.25	0.25	1483.8980	1498.96	15.6765	15.6765	0.61	0.61
	1506.4356	1503.0392	1506.43	3.3964	3.3964	0.01	0.01	1487.8637	1506.45	18.5719	18.5719	-0.01	0.01
	1514.4896	1514.3784	1514.45	0.1112	0.1112	0.04	0.04	1497.7164	1514.51	16.7732	16.7732	-0.02	0.02
	3033.8168	3039.1065	3033.94	-5.2897	5.2897	-0.12	0.12	3040.1567	3034.02	-6.3399	6.3399	-0.20	0.20
	3054.4908	3052.3267	3054.41	2.1641	2.1641	0.08	0.08	3059.8540	3054.42	-5.3632	5.3632	0.07	0.07
	3081.2753	3082.2120	3081.31	-0.9367	0.9367	-0.03	0.03	3081.6507	3081.29	-0.3754	0.3754	-0.01	0.01
	3087.1008	3084.3360	3087.32	2.7648	2.7648	-0.22	0.22	3101.4434	3087.50	-14.3426	14.3426	-0.40	0.40
	3108.5804	3107.4892	3108.45	1.0912	1.0912	0.13	0.13	3123.5535	3108.33	-14.9731	14.9731	0.25	0.25
	3116.7479	3114.4390	3116.77	2.3089	2.3089	-0.02	0.02	3132.1947	3116.73	-15.4468	15.4468	0.02	0.02
	3141.3203	3143.6443	3141.32	-2.3240	2.3240	0.00	0.00	3147.9649	3141.28	-6.6446	6.6446	0.04	0.04

	TZ/TZ	B3LYP/6-31G(2df,p) Freq	TZ/DFT CMA	Shift	Abs Shift	Diff	Abs Diff	DZ/DZ Freq	TZ/DZ MH	Shift	Abs Shift	Diff	Abs Diff
Methoxyethane (1.75)	112.8670	114.1915	113.81	-1.3245	1.3245	-0.94	0.94	112.1994	112.94	0.6676	0.6676	-0.07	0.07
CH3CH2OCH3	209.7436	207.1717	209.89	2.5719	2.5719	-0.15	0.15	215.3830	210.21	-5.6394	5.6394	-0.47	0.47
	259.0979	257.8950	259.29	1.2029	1.2029	-0.19	0.19	270.3363	259.21	-11.2384	11.2384	-0.11	0.11
	288.7881	285.4081	288.87	3.3800	3.3800	-0.08	0.08	289.0254	288.87	-0.2373	0.2373	-0.08	0.08
	468.2177	465.6531	468.31	2.5646	2.5646	-0.09	0.09	470.1423	468.26	-1.9246	1.9246	-0.04	0.04
	820.7155	823.3105	820.86	-2.5950	2.5950	-0.14	0.14	818.7312	820.77	1.9843	1.9843	-0.05	0.05
	874.8839	870.1434	875.04	4.7405	4.7405	-0.16	0.16	877.4508	875.01	-2.5669	2.5669	-0.13	0.13
	1048.4326	1037.0420	1049.07	11.3906	11.3906	-0.64	0.64	1052.9934	1048.71	-4.5608	4.5608	-0.28	0.28
	1119.0906	1117.3075	1119.17	1.7831	1.7831	-0.08	0.08	1113.5009	1119.18	5.5897	5.5897	-0.09	0.09
	1171.7367	1168.0290	1171.94	3.7077	3.7077	-0.20	0.20	1163.3473	1171.95	8.3894	8.3894	-0.21	0.21
	1174.1722	1169.4818	1174.22	4.6904	4.6904	-0.05	0.05	1178.4911	1174.32	-4.3189	4.3189	-0.15	0.15
	1204.6518	1201.2815	1204.67	3.3703	3.3703	-0.02	0.02	1199.3613	1204.44	5.2905	5.2905	0.21	0.21
	1244.7197	1238.6860	1244.69	6.0337	6.0337	0.03	0.03	1240.1921	1244.87	4.5276	4.5276	-0.15	0.15
	1301.1912	1298.7572	1301.10	2.4340	2.4340	0.09	0.09	1289.5995	1301.20	11.5917	11.5917	-0.01	0.01
	1396.6609	1400.0909	1396.78	-3.4300	3.4300	-0.12	0.12	1384.4352	1396.72	12.2257	12.2257	-0.06	0.06
	1431.7367	1426.2426	1431.43	5.4941	5.4941	0.31	0.31	1429.1847	1431.58	2.5520	2.5520	0.16	0.16
	1480.9589	1478.7190	1480.67	2.2399	2.2399	0.29	0.29	1471.2704	1481.71	9.6885	9.6885	-0.75	0.75
	1490.2941	1486.8067	1490.29	3.4874	3.4874	0.00	0.00	1472.1678	1490.28	18.1263	18.1263	0.01	0.01
	1495.3733	1489.9454	1495.36	5.4279	5.4279	0.01	0.01	1475.7794	1495.42	19.5939	19.5939	-0.05	0.05
	1506.8994	1502.4356	1507.17	4.4638	4.4638	-0.27	0.27	1492.0714	1506.75	14.8280	14.8280	0.15	0.15
	1515.6392	1510.2326	1515.68	5.4066	5.4066	-0.04	0.04	1498.7750	1515.34	16.8642	16.8642	0.30	0.30
	1538.2903	1534.2771	1538.65	4.0132	4.0132	-0.36	0.36	1526.4835	1537.81	11.8068	11.8068	0.48	0.48
	2971.3904	2952.8736	2971.34	18.5168	18.5168	0.05	0.05	2966.2130	2971.36	5.1774	5.1774	0.03	0.03
	2985.2507	2974.7120	2985.26	10.5387	10.5387	-0.01	0.01	2985.0939	2985.14	0.1568	0.1568	0.11	0.11
	3001.9979	2975.1080	3002.02	26.8899	26.8899	-0.02	0.02	3002.5381	3002.05	-0.5402	0.5402	-0.05	0.05
	3034.7200	3013.6848	3034.66	21.0352	21.0352	0.06	0.06	3038.9840	3034.67	-4.2640	4.2640	0.05	0.05
	3045.7576	3049.2931	3045.69	-3.5355	3.5355	0.07	0.07	3052.8709	3045.66	-7.1133	7.1133	0.10	0.10
	3123.7397	3119.7878	3123.61	3.9519	3.9519	0.13	0.13	3139.9997	3123.61	-16.2600	16.2600	0.13	0.13
	3128.0490	3121.1926	3128.42	6.8564	6.8564	-0.37	0.37	3142.0171	3128.54	-13.9681	13.9681	-0.49	0.49
	3128.6745	3124.8500	3128.71	3.8245	3.8245	-0.04	0.04	3147.0341	3128.67	-18.3596	18.3596	0.00	0.00

	TZ/TZ	B3LYP/6-31G(2df,p) Freq	TZ/DFT CMA	Shift	Abs Shift	Diff	Abs Diff	DZ/DZ Freq	TZ/DZ MH	Shift	Abs Shift	Diff	Abs Diff
Isopropyl alcohol (1.76)	224.4278	224.4041	224.71	0.0237	0.0237	-0.28	0.28	239.4181	226.59	-14.9903	14.9903	-2.16	2.16
CH3CHOHCH3	270.9295	261.6180	271.02	9.3115	9.3115	-0.09	0.09	279.3217	271.02	-8.3922	8.3922	-0.09	0.09
	273.0341	267.4779	272.75	5.5562	5.5562	0.28	0.28	314.5494	273.26	-41.5153	41.5153	-0.23	0.23
	357.7359	356.1780	357.29	1.5579	1.5579	0.45	0.45	357.0547	357.43	0.6812	0.6812	0.31	0.31
	425.5037	423.5631	425.12	1.9406	1.9406	0.38	0.38	428.6035	423.96	-3.0998	3.0998	1.54	1.54
	464.6360	469.2301	465.17	-4.5941	4.5941	-0.53	0.53	467.7831	465.12	-3.1471	3.1471	-0.48	0.48
	825.9970	818.1263	826.86	7.8707	7.8707	-0.86	0.86	829.1491	826.28	-3.1521	3.1521	-0.28	0.28
	922.1123	922.2268	925.16	-0.1145	0.1145	-3.05	3.05	915.5941	923.52	6.5182	6.5182	-1.41	1.41
	939.5329	937.5907	937.84	1.9422	1.9422	1.69	1.69	937.1109	938.69	2.4220	2.4220	0.84	0.84
	983.0284	973.5444	982.32	9.4840	9.4840	0.71	0.71	985.1035	982.70	-2.0751	2.0751	0.33	0.33
	1092.2460	1089.2233	1092.92	3.0227	3.0227	-0.67	0.67	1095.7220	1093.46	-3.4760	3.4760	-1.21	1.21
	1159.9352	1148.3048	1159.98	11.6304	11.6304	-0.04	0.04	1159.2402	1160.15	0.6950	0.6950	-0.21	0.21
	1196.6390	1192.3670	1196.53	4.2720	4.2720	0.11	0.11	1196.1850	1196.80	0.4540	0.4540	-0.16	0.16
	1315.3774	1310.7641	1315.52	4.6133	4.6133	-0.14	0.14	1323.1543	1315.32	-7.7769	7.7769	0.06	0.06
	1367.1906	1365.9103	1368.25	1.2803	1.2803	-1.06	1.06	1356.2944	1367.34	10.8962	10.8962	-0.15	0.15
	1403.3362	1399.2112	1401.62	4.1250	4.1250	1.72	1.72	1401.2254	1402.68	2.1108	2.1108	0.66	0.66
	1410.6403	1412.1491	1410.52	-1.5088	1.5088	0.12	0.12	1403.3220	1410.28	7.3183	7.3183	0.36	0.36
	1426.6428	1419.6544	1426.37	6.9884	6.9884	0.27	0.27	1434.7515	1427.08	-8.1087	8.1087	-0.44	0.44
	1488.0270	1485.6842	1488.65	2.3428	2.3428	-0.62	0.62	1471.8401	1488.69	16.1869	16.1869	-0.66	0.66
	1490.9858	1487.4473	1490.79	3.5385	3.5385	0.20	0.20	1475.3217	1490.40	15.6641	15.6641	0.59	0.59
	1504.0119	1500.1389	1503.60	3.8730	3.8730	0.41	0.41	1489.1572	1502.61	14.8547	14.8547	1.40	1.40
	1511.4722	1509.0800	1512.24	2.3922	2.3922	-0.77	0.77	1494.9942	1511.86	16.4780	16.4780	-0.39	0.39
	3024.6568	3025.4653	3026.27	-0.8085	0.8085	-1.61	1.61	3030.7313	3024.72	-6.0745	6.0745	-0.06	0.06
	3028.6304	3028.9784	3032.48	-0.3480	0.3480	-3.85	3.85	3034.9764	3028.87	-6.3460	6.3460	-0.24	0.24
	3060.7586	3043.7102	3058.50	17.0484	17.0484	2.26	2.26	3061.2329	3061.21	-0.4743	0.4743	-0.45	0.45
	3092.7660	3090.0752	3092.24	2.6908	2.6908	0.53	0.53	3108.8056	3092.79	-16.0396	16.0396	-0.02	0.02
	3103.9089	3101.1797	3104.09	2.7292	2.7292	-0.18	0.18	3117.9455	3103.47	-14.0366	14.0366	0.44	0.44
	3121.5357	3118.8214	3120.43	2.7143	2.7143	1.11	1.11	3136.6660	3121.52	-15.1303	15.1303	0.02	0.02
	3124.1880	3121.2213	3122.73	2.9667	2.9667	1.46	1.46	3139.2154	3124.13	-15.0274	15.0274	0.06	0.06
	3819.4900	3799.3343	3819.69	20.1557	20.1557	-0.20	0.20	3795.9247	3819.71	23.5653	23.5653	-0.22	0.22

	TZ/TZ	B3LYP/6-31G(2df,p) Freq	TZ/DFT CMA	Shift	Abs Shift	Diff	Abs Diff	DZ/DZ Freq	TZ/DZ MH	Shift	Abs Shift	Diff	Abs Diff
Propane (1.77)	215.5589	221.2903	215.66	-5.7314	5.7314	-0.10	0.10	228.2347	215.60	-12.6758	12.6758	-0.04	0.04
CH3CH2CH3	273.4113	269.1842	273.45	4.2271	4.2271	-0.04	0.04	284.6291	273.46	-11.2178	11.2178	-0.05	0.05
	362.5331	364.6701	362.60	-2.1370	2.1370	-0.07	0.07	363.7282	362.54	-1.1951	1.1951	-0.01	0.01
	748.6296	750.1212	748.67	-1.4916	1.4916	-0.04	0.04	747.2450	748.64	1.3846	1.3846	-0.01	0.01
	885.7767	876.9343	885.97	8.8424	8.8424	-0.19	0.19	891.1136	885.91	-5.3369	5.3369	-0.13	0.13
	906.6088	910.5149	906.66	-3.9061	3.9061	-0.05	0.05	900.8174	906.63	5.7914	5.7914	-0.02	0.02
	928.9806	931.9432	929.31	-2.9626	2.9626	-0.33	0.33	924.0462	929.01	4.9344	4.9344	-0.03	0.03
	1074.0408	1064.3754	1074.36	9.6654	9.6654	-0.32	0.32	1083.4274	1074.38	-9.3866	9.3866	-0.34	0.34
	1181.2937	1180.7227	1181.24	0.5710	0.5710	0.05	0.05	1175.5523	1181.34	5.7414	5.7414	-0.05	0.05
	1217.5441	1219.8787	1217.62	-2.3346	2.3346	-0.08	0.08	1210.7020	1217.58	6.8421	6.8421	-0.04	0.04
	1319.3177	1321.2966	1319.33	-1.9789	1.9789	-0.01	0.01	1309.1615	1319.33	10.1562	10.1562	-0.01	0.01
	1367.1457	1372.1567	1367.74	-5.0110	5.0110	-0.59	0.59	1358.6737	1368.02	8.4720	8.4720	-0.87	0.87
	1407.5228	1408.2773	1406.85	-0.7545	0.7545	0.67	0.67	1407.3384	1406.55	0.1844	0.1844	0.97	0.97
	1420.8105	1425.3868	1420.86	-4.5763	4.5763	-0.05	0.05	1413.8513	1420.89	6.9592	6.9592	-0.08	0.08
	1496.3255	1493.3427	1496.36	2.9828	2.9828	-0.03	0.03	1478.7422	1496.23	17.5833	17.5833	0.10	0.10
	1496.5877	1494.2824	1496.56	2.3053	2.3053	0.03	0.03	1479.0326	1496.60	17.5551	17.5551	-0.01	0.01
	1503.8731	1501.8533	1503.99	2.0198	2.0198	-0.12	0.12	1487.2722	1503.70	16.6009	16.6009	0.17	0.17
	1513.8053	1511.4213	1513.80	2.3840	2.3840	0.01	0.01	1495.7827	1513.82	18.0226	18.0226	-0.01	0.01
	1518.5767	1518.2579	1518.48	0.3188	0.3188	0.10	0.10	1501.3824	1518.53	17.1943	17.1943	0.05	0.05
	3026.7003	3025.8487	3026.72	0.8516	0.8516	-0.02	0.02	3032.7146	3026.40	-6.0143	6.0143	0.30	0.30
	3028.7666	3030.4663	3028.83	-1.6997	1.6997	-0.06	0.06	3033.3874	3030.52	-4.6208	4.6208	-1.75	1.75
	3033.7366	3033.8451	3033.79	-0.1085	0.1085	-0.05	0.05	3039.0154	3032.44	-5.2788	5.2788	1.30	1.30
	3061.4591	3049.1130	3061.74	12.3461	12.3461	-0.28	0.28	3073.8152	3061.80	-12.3561	12.3561	-0.34	0.34
	3093.7065	3091.3578	3093.74	2.3487	2.3487	-0.03	0.03	3110.9919	3093.74	-17.2854	17.2854	-0.03	0.03
	3104.6800	3100.1699	3104.42	4.5101	4.5101	0.26	0.26	3120.0331	3104.43	-15.3531	15.3531	0.25	0.25
	3105.0342	3101.9714	3105.06	3.0628	3.0628	-0.03	0.03	3120.5919	3105.04	-15.5577	15.5577	-0.01	0.01
	3107.7478	3103.1793	3107.82	4.5685	4.5685	-0.07	0.07	3123.1731	3107.71	-15.4253	15.4253	0.04	0.04

	TZ/TZ	B3LYP/6-31G(2df,p) Freq	TZ/DFT CMA	Shift	Abs Shift	Diff	Abs Diff	DZ/DZ Freq	TZ/DZ MH	Shift	Abs Shift	Diff	Abs Diff
Acrylonitrile (1.78)	227.1279	236.7661	227.67	-9.6382	9.6382	-0.54	0.54	224.1510	227.16	2.9769	2.9769	-0.03	0.03
CH2CHCN	336.2510	351.3908	338.38	-15.1398	15.1398	-2.13	2.13	330.4789	338.34	5.7721	5.7721	-2.09	2.09
	559.5088	576.0787	559.55	-16.5699	16.5699	-0.04	0.04	551.4880	559.62	8.0208	8.0208	-0.11	0.11
	688.7316	718.2249	687.99	-29.4933	29.4933	0.74	0.74	671.5995	689.55	17.1321	17.1321	-0.82	0.82
	873.0854	885.5269	873.52	-12.4415	12.4415	-0.43	0.43	873.2604	873.07	-0.1750	0.1750	0.02	0.02
	969.0900	990.0490	969.47	-20.9590	20.9590	-0.38	0.38	939.3968	969.19	29.6932	29.6932	-0.10	0.10
	993.5090	1011.5578	993.65	-18.0488	18.0488	-0.14	0.14	975.2459	993.34	18.2631	18.2631	0.17	0.17
	1104.1445	1109.6238	1104.23	-5.4793	5.4793	-0.09	0.09	1094.4328	1104.15	9.7117	9.7117	-0.01	0.01
	1314.4132	1320.4857	1315.31	-6.0725	6.0725	-0.90	0.90	1299.9711	1314.31	14.4421	14.4421	0.10	0.10
	1447.1308	1448.0713	1447.99	-0.9405	0.9405	-0.86	0.86	1430.7091	1447.11	16.4217	16.4217	0.02	0.02
	1659.6430	1683.8928	1658.33	-24.2498	24.2498	1.31	1.31	1657.8620	1659.90	1.7810	1.7810	-0.26	0.26
	2271.9161	2341.0013	2271.79	-69.0852	69.0852	0.13	0.13	2260.2677	2271.98	11.6484	11.6484	-0.06	0.06
	3164.3239	3166.7539	3165.14	-2.4300	2.4300	-0.82	0.82	3168.9899	3164.38	-4.6660	4.6660	-0.06	0.06
	3202.5790	3181.7768	3201.93	20.8022	20.8022	0.65	0.65	3207.4184	3202.68	-4.8394	4.8394	-0.10	0.10
	3262.5757	3261.5830	3262.58	0.9927	0.9927	0.00	0.00	3275.0028	3262.62	-12.4271	12.4271	-0.04	0.04

	TZ/TZ	B3LYP/6-31G(2df,p) Freq	TZ/DFT CMA	Shift	Abs Shift	Diff	Abs Diff	DZ/DZ Freq	TZ/DZ MH	Shift	Abs Shift	Diff	Abs Diff
Trimethylamine (1.79)	240.7264	249.3147	241.21	-8.5883	8.5883	-0.48	0.48	242.6066	241.13	-1.8802	1.8802	-0.40	0.40
N(CH3)3	279.9505	260.8706	280.45	19.0799	19.0799	-0.50	0.50	283.5337	280.25	-3.5832	3.5832	-0.30	0.30
	279.9617	260.8977	280.45	19.0640	19.0640	-0.49	0.49	283.5345	280.25	-3.5728	3.5728	-0.29	0.29
	373.1138	340.0495	374.27	33.0643	33.0643	-1.16	1.16	376.2248	373.16	-3.1110	3.1110	-0.05	0.05
	417.2562	420.9051	417.14	-3.6489	3.6489	0.12	0.12	419.7725	417.29	-2.5163	2.5163	-0.03	0.03
	417.2564	420.9117	417.15	-3.6553	3.6553	0.11	0.11	419.7727	417.29	-2.5163	2.5163	-0.03	0.03
	847.5262	837.6285	847.67	9.8977	9.8977	-0.14	0.14	851.8825	847.62	-4.3563	4.3563	-0.09	0.09
	1063.5611	1066.6836	1063.54	-3.1225	3.1225	0.02	0.02	1054.6823	1063.58	8.8788	8.8788	-0.02	0.02
	1065.0033	1066.6954	1065.26	-1.6921	1.6921	-0.26	0.26	1066.1751	1065.27	-1.1718	1.1718	-0.27	0.27
	1065.0059	1071.0765	1065.32	-6.0706	6.0706	-0.31	0.31	1066.1756	1065.27	-1.1697	1.1697	-0.26	0.26
	1120.5595	1121.3912	1120.53	-0.8317	0.8317	0.03	0.03	1112.2200	1120.66	8.3395	8.3395	-0.10	0.10
	1120.5621	1121.4010	1120.53	-0.8389	0.8389	0.03	0.03	1112.2201	1120.66	8.3420	8.3420	-0.10	0.10
	1215.4903	1209.0984	1217.45	6.3919	6.3919	-1.96	1.96	1207.2288	1215.56	8.2615	8.2615	-0.07	0.07
	1309.8597	1313.3960	1310.12	-3.5363	3.5363	-0.26	0.26	1309.9241	1309.96	-0.0644	0.0644	-0.10	0.10
	1309.8619	1313.4009	1310.12	-3.5390	3.5390	-0.26	0.26	1309.9251	1309.96	-0.0632	0.0632	-0.10	0.10
	1436.7396	1440.9596	1436.61	-4.2200	4.2200	0.13	0.13	1429.2740	1436.41	7.4656	7.4656	0.33	0.33
	1436.7437	1440.9658	1436.61	-4.2221	4.2221	0.13	0.13	1429.2749	1436.41	7.4688	7.4688	0.33	0.33
	1478.5792	1483.2950	1479.09	-4.7158	4.7158	-0.51	0.51	1470.4142	1479.13	8.1650	8.1650	-0.55	0.55
	1488.6843	1483.2996	1488.92	5.3847	5.3847	-0.24	0.24	1470.4150	1488.86	18.2693	18.2693	-0.18	0.18
	1488.6877	1485.1241	1488.92	3.5636	3.5636	-0.23	0.23	1471.7171	1488.86	16.9706	16.9706	-0.17	0.17
	1496.4830	1493.6705	1496.58	2.8125	2.8125	-0.10	0.10	1479.5472	1496.54	16.9358	16.9358	-0.06	0.06
	1508.1921	1503.4744	1508.19	4.7177	4.7177	0.00	0.00	1491.0256	1507.77	17.1665	17.1665	0.42	0.42
	1517.1193	1515.2046	1517.16	1.9147	1.9147	-0.04	0.04	1499.6986	1517.11	17.4207	17.4207	0.01	0.01
	1517.1258	1515.2091	1517.16	1.9167	1.9167	-0.03	0.03	1499.7007	1517.11	17.4251	17.4251	0.02	0.02
	2925.2966	2910.9983	2925.78	14.2983	14.2983	-0.48	0.48	2932.3775	2925.61	-7.0809	7.0809	-0.31	0.31
	2925.2981	2911.0165	2925.78	14.2816	14.2816	-0.48	0.48	2932.3779	2925.61	-7.0798	7.0798	-0.31	0.31
	2934.8011	2926.0594	2935.48	8.7417	8.7417	-0.68	0.68	2945.1706	2935.04	-10.3695	10.3695	-0.24	0.24
	3068.4877	3060.8125	3068.08	7.6752	7.6752	0.41	0.41	3078.4943	3068.29	-10.0066	10.0066	0.20	0.20
	3068.4891	3060.8157	3068.08	7.6734	7.6734	0.41	0.41	3078.4948	3068.29	-10.0057	10.0057	0.20	0.20
	3071.9263	3064.8352	3071.35	7.0911	7.0911	0.58	0.58	3082.2622	3071.75	-10.3359	10.3359	0.18	0.18
	3112.2611	3103.9280	3112.19	8.3331	8.3331	0.07	0.07	3126.0206	3112.18	-13.7595	13.7595	0.08	0.08
	3116.4361	3108.6536	3116.37	7.7825	7.7825	0.07	0.07	3130.5750	3116.39	-14.1389	14.1389	0.05	0.05
	3116.4377	3108.6548	3116.37	7.7829	7.7829	0.07	0.07	3130.5759	3116.39	-14.1382	14.1382	0.05	0.05

	TZ/TZ	B3LYP/6-31G(2df,p) Freq	TZ/DFT CMA	Shift	Abs Shift	Diff	Abs Diff	DZ/DZ Freq	TZ/DZ MH	Shift	Abs Shift	Diff	Abs Diff
Isobutane (1.80)	200.4526	212.4678	200.96	-12.0152	12.0152	-0.51	0.51	215.0630	200.92	-14.6104	14.6104	-0.47	0.47
CH(CH3)3	258.8640	254.7270	259.47	4.1370	4.1370	-0.61	0.61	267.7921	259.78	-8.9281	8.9281	-0.92	0.92
	258.8769	254.9428	259.48	3.9341	3.9341	-0.60	0.60	267.8012	259.78	-8.9243	8.9243	-0.90	0.90
	359.1617	362.0880	357.95	-2.9263	2.9263	1.21	1.21	362.8290	357.71	-3.6673	3.6673	1.45	1.45
	359.1659	362.1032	357.95	-2.9373	2.9373	1.22	1.22	362.8410	357.74	-3.6751	3.6751	1.43	1.43
	423.3531	428.8812	424.85	-5.5281	5.5281	-1.50	1.50	425.9952	424.80	-2.6421	2.6421	-1.45	1.45
	808.9308	799.7103	809.29	9.2205	9.2205	-0.36	0.36	812.7620	809.17	-3.8312	3.8312	-0.24	0.24
	921.2070	925.1928	923.03	-3.9858	3.9858	-1.82	1.82	916.6647	922.37	4.5423	4.5423	-1.16	1.16
	921.2099	925.2730	923.04	-4.0631	4.0631	-1.83	1.83	916.6651	922.37	4.5448	4.5448	-1.16	1.16
	953.5855	957.3707	952.08	-3.7852	3.7852	1.51	1.51	947.5574	952.08	6.0281	6.0281	1.51	1.51
	984.8376	976.9663	984.43	7.8713	7.8713	0.41	0.41	987.6405	984.44	-2.8029	2.8029	0.40	0.40
	984.8394	976.9903	984.43	7.8491	7.8491	0.41	0.41	987.6462	984.44	-2.8068	2.8068	0.40	0.40
	1199.4679	1196.7082	1199.52	2.7597	2.7597	-0.05	0.05	1197.5775	1199.65	1.8904	1.8904	-0.18	0.18
	1199.4710	1196.7222	1199.52	2.7488	2.7488	-0.05	0.05	1197.5804	1199.65	1.8906	1.8906	-0.18	0.18
	1214.0592	1215.0388	1214.56	-0.9796	0.9796	-0.50	0.50	1207.1293	1214.58	6.9299	6.9299	-0.52	0.52
	1361.6229	1364.4715	1361.61	-2.8486	2.8486	0.01	0.01	1355.1681	1362.05	6.4548	6.4548	-0.43	0.43
	1361.6229	1364.4819	1361.61	-2.8590	2.8590	0.01	0.01	1355.1815	1362.05	6.4414	6.4414	-0.43	0.43
	1401.3973	1404.1937	1401.08	-2.7964	2.7964	0.32	0.32	1398.7281	1400.84	2.6692	2.6692	0.56	0.56
	1401.4033	1404.2013	1401.09	-2.7980	2.7980	0.31	0.31	1398.7292	1400.84	2.6741	2.6741	0.56	0.56
	1425.6763	1431.9316	1425.71	-6.2553	6.2553	-0.03	0.03	1419.2298	1425.68	6.4465	6.4465	0.00	0.00
	1487.4569	1485.6272	1488.56	1.8297	1.8297	-1.10	1.10	1470.0971	1488.66	17.3598	17.3598	-1.20	1.20
	1494.1921	1492.1867	1493.24	2.0054	2.0054	0.95	0.95	1476.6147	1493.24	17.5774	17.5774	0.95	0.95
	1494.1932	1492.2157	1493.32	1.9775	1.9775	0.87	0.87	1476.6176	1493.24	17.5756	17.5756	0.95	0.95
	1511.8990	1510.7672	1512.75	1.1318	1.1318	-0.85	0.85	1495.0679	1512.55	16.8311	16.8311	-0.65	0.65
	1511.9030	1510.8018	1512.75	1.1012	1.1012	-0.85	0.85	1495.0712	1512.55	16.8318	16.8318	-0.65	0.65
	1519.4487	1517.0925	1518.43	2.3562	2.3562	1.02	1.02	1501.6052	1518.40	17.8435	17.8435	1.05	1.05
	3019.9795	3003.5400	3020.47	16.4395	16.4395	-0.49	0.49	3021.2516	3020.00	-1.2721	1.2721	-0.02	0.02
	3019.9813	3025.1898	3020.75	-5.2085	5.2085	-0.77	0.77	3026.3948	3020.00	-6.4135	6.4135	-0.02	0.02
	3020.6378	3025.2159	3020.89	-4.5781	4.5781	-0.25	0.25	3026.3968	3020.95	-5.7590	5.7590	-0.31	0.31
	3024.9940	3032.0335	3025.69	-7.0395	7.0395	-0.70	0.70	3032.6509	3024.99	-7.6569	7.6569	0.00	0.00
	3092.8561	3088.0155	3091.51	4.8406	4.8406	1.35	1.35	3108.2468	3092.91	-15.3907	15.3907	-0.05	0.05
	3092.8562	3088.0436	3092.10	4.8126	4.8126	0.76	0.76	3110.1934	3092.95	-17.3372	17.3372	-0.09	0.09
	3092.8901	3095.9267	3093.21	-3.0366	3.0366	-0.32	0.32	3110.1942	3092.95	-17.3041	17.3041	-0.06	0.06
	3096.8514	3097.7110	3096.84	-0.8596	0.8596	0.01	0.01	3112.7398	3096.80	-15.8884	15.8884	0.05	0.05
	3096.8515	3100.3921	3097.20	-3.5406	3.5406	-0.35	0.35	3112.7412	3096.80	-15.8897	15.8897	0.05	0.05
	3102.0156	3100.4015	3101.52	1.6141	1.6141	0.50	0.50	3118.4170	3101.82	-16.4014	16.4014	0.20	0.20

	TZ/TZ	B3LYP/6-31G(2df,p) Freq	TZ/DFT CMA	Shift	Abs Shift	Diff	Abs Diff	DZ/DZ Freq	TZ/DZ MH	Shift	Abs Shift	Diff	Abs Diff
n-Butane (1.81)	115.6852	120.0265	115.92	-4.3413	4.3413	-0.23	0.23	121.6872	115.77	-6.0020	6.0020	-0.08	0.08
CH3CH2CH2CH3	221.7700	221.1775	221.84	0.5925	0.5925	-0.07	0.07	231.4793	221.84	-9.7093	9.7093	-0.07	0.07
	253.4263	257.2453	253.46	-3.8190	3.8190	-0.03	0.03	255.1962	253.44	-1.7699	1.7699	-0.01	0.01
	257.3255	258.8989	257.40	-1.5734	1.5734	-0.07	0.07	269.4916	257.40	-12.1661	12.1661	-0.07	0.07
	422.7139	424.1500	422.88	-1.4361	1.4361	-0.17	0.17	424.2050	422.76	-1.4911	1.4911	-0.05	0.05
	733.7216	735.7220	733.78	-2.0004	2.0004	-0.06	0.06	734.1523	733.78	-0.4307	0.4307	-0.06	0.06
	807.4415	811.1893	807.47	-3.7478	3.7478	-0.03	0.03	804.8750	807.47	2.5665	2.5665	-0.03	0.03
	848.7133	843.2933	848.95	5.4200	5.4200	-0.24	0.24	851.6047	848.80	-2.8914	2.8914	-0.09	0.09
	957.8470	963.7415	957.90	-5.8945	5.8945	-0.05	0.05	951.4837	957.86	6.3633	6.3633	-0.01	0.01
	977.8662	982.8122	978.56	-4.9460	4.9460	-0.69	0.69	973.3951	978.12	4.4711	4.4711	-0.25	0.25
	1032.2758	1021.3470	1031.95	10.9288	10.9288	0.33	0.33	1040.0966	1032.26	-7.8208	7.8208	0.02	0.02
	1082.9821	1070.9704	1083.81	12.0117	12.0117	-0.83	0.83	1090.8223	1083.38	-7.8402	7.8402	-0.40	0.40
	1175.1150	1172.2913	1175.06	2.8237	2.8237	0.06	0.06	1170.1706	1175.20	4.9444	4.9444	-0.09	0.09
	1213.0021	1216.2134	1213.07	-3.2113	3.2113	-0.07	0.07	1206.5370	1213.01	6.4651	6.4651	-0.01	0.01
	1290.4231	1294.4410	1290.46	-4.0179	4.0179	-0.04	0.04	1282.2854	1290.44	8.1377	8.1377	-0.02	0.02
	1318.7659	1328.5278	1318.83	-9.7619	9.7619	-0.06	0.06	1309.2730	1318.88	9.4929	9.4929	-0.11	0.11
	1332.5922	1337.2801	1332.61	-4.6879	4.6879	-0.02	0.02	1322.3653	1332.62	10.2269	10.2269	-0.03	0.03
	1398.2297	1400.3743	1399.52	-2.1446	2.1446	-1.29	1.29	1394.7378	1400.67	3.4919	3.4919	-2.44	2.44
	1412.5505	1415.6084	1410.92	-3.0579	3.0579	1.63	1.63	1408.8156	1410.03	3.7349	3.7349	2.52	2.52
	1414.0256	1416.9861	1413.95	-2.9605	2.9605	0.08	0.08	1414.2103	1413.87	-0.1847	0.1847	0.16	0.16
	1490.6537	1489.6015	1490.74	1.0522	1.0522	-0.09	0.09	1475.4793	1490.56	15.1744	15.1744	0.09	0.09
	1496.9149	1494.6945	1497.05	2.2204	2.2204	-0.14	0.14	1480.0024	1496.78	16.9125	16.9125	0.13	0.13
	1505.1297	1502.7642	1505.10	2.3655	2.3655	0.03	0.03	1487.0859	1505.14	18.0438	18.0438	-0.01	0.01
	1506.7030	1504.2298	1506.69	2.4732	2.4732	0.01	0.01	1488.4555	1506.71	18.2475	18.2475	-0.01	0.01
	1511.2706	1509.4265	1511.29	1.8441	1.8441	-0.02	0.02	1494.8137	1511.02	16.4569	16.4569	0.25	0.25
	1515.9871	1517.7394	1515.87	-1.7523	1.7523	0.12	0.12	1498.7171	1516.05	17.2700	17.2700	-0.06	0.06
	3016.7718	3011.7202	3016.84	5.0516	5.0516	-0.07	0.07	3021.7207	3016.99	-4.9489	4.9489	-0.22	0.22
	3023.9134	3019.7285	3023.97	4.1849	4.1849	-0.06	0.06	3026.6818	3024.42	-2.7684	2.7684	-0.51	0.51
	3028.0486	3031.6221	3028.05	-3.5735	3.5735	0.00	0.00	3034.2034	3027.63	-6.1548	6.1548	0.42	0.42
	3028.9068	3032.6854	3028.87	-3.7786	3.7786	0.04	0.04	3036.2464	3028.75	-7.3396	7.3396	0.16	0.16
	3042.4215	3033.4456	3042.46	8.9759	8.9759	-0.04	0.04	3054.9165	3042.52	-12.4950	12.4950	-0.10	0.10
	3064.0335	3055.0267	3064.11	9.0068	9.0068	-0.08	0.08	3075.6017	3064.30	-11.5682	11.5682	-0.27	0.27
	3097.4201	3095.5514	3097.43	1.8687	1.8687	-0.01	0.01	3114.7135	3097.39	-17.2934	17.2934	0.03	0.03
	3101.2327	3099.2482	3101.19	1.9845	1.9845	0.04	0.04	3117.6975	3101.02	-16.4648	16.4648	0.21	0.21
	3105.5065	3101.4544	3105.53	4.0521	4.0521	-0.02	0.02	3121.2604	3105.50	-15.7539	15.7539	0.01	0.01
	3106.1890	3102.3787	3106.19	3.8103	3.8103	0.00	0.00	3121.9381	3106.17	-15.7491	15.7491	0.02	0.02

	TZ/TZ	B3LYP/6-31G(2df,p) Freq	TZ/DFT CMA	Shift	Abs Shift	Diff	Abs Diff	DZ/DZ Freq	TZ/DZ MH	Shift	Abs Shift	Diff	Abs Diff
Furan (1.82)	603.1714	618.0495	603.49	-14.8781	14.8781	-0.32	0.32	587.0320	604.20	16.1394	16.1394	-1.03	1.03
CHCHCHCHO (Cyclic)	612.4352	627.6320	612.50	-15.1968	15.1968	-0.06	0.06	607.1527	612.74	5.2825	5.2825	-0.30	0.30
	731.4082	741.7684	731.45	-10.3602	10.3602	-0.04	0.04	720.1789	731.40	11.2293	11.2293	0.01	0.01
	759.6477	768.0817	760.09	-8.4340	8.4340	-0.44	0.44	748.8956	759.33	10.7521	10.7521	0.32	0.32
	844.4109	849.0110	844.02	-4.6001	4.6001	0.39	0.39	822.4301	844.80	21.9808	21.9808	-0.39	0.39
	860.4270	883.4246	860.18	-22.9976	22.9976	0.25	0.25	828.6066	859.75	31.8204	31.8204	0.68	0.68
	877.5232	885.9407	877.65	-8.4175	8.4175	-0.13	0.13	872.1191	877.73	5.4041	5.4041	-0.21	0.21
	882.4964	892.7466	882.71	-10.2502	10.2502	-0.21	0.21	873.6468	882.53	8.8496	8.8496	-0.03	0.03
	1012.3121	1021.2233	1012.56	-8.9112	8.9112	-0.25	0.25	1004.3184	1012.47	7.9937	7.9937	-0.16	0.16
	1061.1427	1067.9960	1061.51	-6.8533	6.8533	-0.37	0.37	1051.4177	1061.28	9.7250	9.7250	-0.14	0.14
	1090.4921	1097.6986	1090.92	-7.2065	7.2065	-0.43	0.43	1090.4547	1091.02	0.0374	0.0374	-0.53	0.53
	1160.7062	1168.6858	1160.69	-7.9796	7.9796	0.02	0.02	1152.6346	1160.56	8.0716	8.0716	0.15	0.15
	1217.7734	1220.4574	1217.69	-2.6840	2.6840	0.08	0.08	1215.1038	1218.09	2.6696	2.6696	-0.32	0.32
	1289.5888	1284.9245	1289.66	4.6643	4.6643	-0.07	0.07	1273.2268	1289.44	16.3620	16.3620	0.15	0.15
	1416.4694	1417.9253	1416.47	-1.4559	1.4559	0.00	0.00	1418.1769	1416.49	-1.7075	1.7075	-0.02	0.02
	1524.3465	1517.4496	1524.05	6.8969	6.8969	0.30	0.30	1529.0414	1524.13	-4.6949	4.6949	0.22	0.22
	1591.8173	1600.9976	1591.54	-9.1803	9.1803	0.28	0.28	1594.5854	1591.74	-2.7681	2.7681	0.08	0.08
	3257.6003	3253.1527	3257.72	4.4476	4.4476	-0.12	0.12	3258.6646	3257.65	-1.0643	1.0643	-0.05	0.05
	3268.3909	3264.2219	3268.57	4.1690	4.1690	-0.18	0.18	3270.4916	3268.43	-2.1007	2.1007	-0.04	0.04
	3287.5903	3287.1328	3287.53	0.4575	0.4575	0.06	0.06	3291.6065	3287.62	-4.0162	4.0162	-0.03	0.03
	3295.0467	3294.2160	3294.93	0.8307	0.8307	0.12	0.12	3298.8916	3295.06	-3.8449	3.8449	-0.01	0.01

	TZ/TZ	B3LYP/6-31G(2df,p) Freq	TZ/DFT CMA	Shift	Abs Shift	Diff	Abs Diff	DZ/DZ Freq	TZ/DZ MH	Shift	Abs Shift	Diff	Abs Diff
1,3-Butadiene (1.83)	164.7826	161.8059	165.51	2.9767	2.9767	-0.73	0.73	157.5517	165.13	7.2309	7.2309	-0.35	0.35
CH2CHCHCH2	271.8715	272.1884	271.50	-0.3169	0.3169	0.37	0.37	270.5521	271.71	1.3194	1.3194	0.16	0.16
	466.8378	476.2280	466.96	-9.3902	9.3902	-0.12	0.12	460.4956	467.04	6.3422	6.3422	-0.20	0.20
	610.0523	615.4159	610.37	-5.3636	5.3636	-0.32	0.32	601.4838	610.02	8.5685	8.5685	0.03	0.03
	742.4089	762.6935	743.05	-20.2846	20.2846	-0.64	0.64	727.4536	742.73	14.9553	14.9553	-0.32	0.32
	886.4107	887.1143	886.48	-0.7036	0.7036	-0.07	0.07	886.8867	886.72	-0.4760	0.4760	-0.31	0.31
	927.6933	945.9522	927.62	-18.2589	18.2589	0.07	0.07	901.8875	927.62	25.8058	25.8058	0.07	0.07
	929.5434	946.8367	929.73	-17.2933	17.2933	-0.19	0.19	904.0781	929.61	25.4653	25.4653	-0.07	0.07
	998.5563	1025.9159	999.12	-27.3596	27.3596	-0.56	0.56	983.1892	998.40	15.3671	15.3671	0.16	0.16
	1017.1973	1036.9931	1017.14	-19.7958	19.7958	0.06	0.06	1001.1948	1017.14	16.0025	16.0025	0.06	0.06
	1058.5548	1067.5674	1058.19	-9.0126	9.0126	0.36	0.36	1052.9753	1058.48	5.5795	5.5795	0.07	0.07
	1098.9175	1106.9021	1099.53	-7.9846	7.9846	-0.61	0.61	1091.0016	1098.92	7.9159	7.9159	0.00	0.00
	1301.4395	1313.6695	1301.80	-12.2300	12.2300	-0.36	0.36	1288.7872	1301.35	12.6523	12.6523	0.09	0.09
	1333.3421	1346.1192	1334.20	-12.7771	12.7771	-0.86	0.86	1322.0395	1333.27	11.3026	11.3026	0.07	0.07
	1437.3054	1439.5353	1437.98	-2.2299	2.2299	-0.67	0.67	1421.9200	1437.26	15.3854	15.3854	0.05	0.05
	1468.4464	1468.5317	1468.51	-0.0853	0.0853	-0.06	0.06	1457.7992	1468.38	10.6472	10.6472	0.07	0.07
	1666.7514	1684.9055	1666.06	-18.1541	18.1541	0.69	0.69	1670.6310	1666.91	-3.8796	3.8796	-0.16	0.16
	1674.8273	1703.9464	1673.73	-29.1191	29.1191	1.10	1.10	1672.9207	1675.07	1.9066	1.9066	-0.24	0.24
	3143.0650	3130.1083	3147.18	12.9567	12.9567	-4.11	4.11	3146.7524	3143.33	-3.6874	3.6874	-0.26	0.26
	3145.5952	3142.2601	3148.05	3.3351	3.3351	-2.45	2.45	3150.7745	3145.70	-5.1793	5.1793	-0.10	0.10
	3152.0588	3149.0742	3151.32	2.9846	2.9846	0.74	0.74	3156.5754	3151.88	-4.5166	4.5166	0.18	0.18
	3164.7304	3154.4882	3159.03	10.2422	10.2422	5.70	5.70	3168.8024	3164.73	-4.0720	4.0720	0.00	0.00
	3237.2179	3233.9424	3237.24	3.2755	3.2755	-0.02	0.02	3249.5157	3237.18	-12.2978	12.2978	0.04	0.04
	3238.8770	3235.8105	3238.89	3.0665	3.0665	-0.01	0.01	3251.3995	3238.83	-12.5225	12.5225	0.05	0.05

	TZ/TZ	B3LYP/6-31G(2df,p) Freq	TZ/DFT CMA	Shift	Abs Shift	Diff	Abs Diff	DZ/DZ Freq	TZ/DZ MH	Shift	Abs Shift	Diff	Abs Diff
2-Butyne (1.84)	19.8455	20.6158	18.80	-0.7703	0.7703	1.05	1.05	18.9030	18.79	0.9425	0.9425	1.06	1.06
CH3CCCH3	197.5041	203.1357	197.38	-5.6316	5.6316	0.12	0.12	193.3862	197.52	4.1179	4.1179	-0.02	0.02
	197.5129	203.1495	197.38	-5.6366	5.6366	0.13	0.13	193.3994	197.70	4.1135	4.1135	-0.19	0.19
	348.3257	383.4579	349.18	-35.1322	35.1322	-0.85	0.85	324.3274	348.23	23.9983	23.9983	0.10	0.10
	348.3274	383.4600	349.18	-35.1326	35.1326	-0.85	0.85	324.3306	350.24	23.9968	23.9968	-1.91	1.91
	716.4513	729.3444	716.72	-12.8931	12.8931	-0.27	0.27	718.9099	716.52	-2.4586	2.4586	-0.07	0.07
	1046.0548	1043.1150	1045.86	2.9398	2.9398	0.19	0.19	1034.9912	1045.64	11.0636	11.0636	0.41	0.41
	1046.0576	1043.1157	1045.86	2.9419	2.9419	0.20	0.20	1035.0045	1045.81	11.0531	11.0531	0.25	0.25
	1067.9806	1066.2778	1067.92	1.7028	1.7028	0.06	0.06	1061.0591	1067.52	6.9215	6.9215	0.46	0.46
	1067.9833	1066.2815	1067.92	1.7018	1.7018	0.06	0.06	1061.0830	1067.53	6.9003	6.9003	0.45	0.45
	1167.2795	1173.9251	1167.34	-6.6456	6.6456	-0.06	0.06	1173.6168	1167.38	-6.3373	6.3373	-0.10	0.10
	1415.8922	1413.9298	1415.90	1.9624	1.9624	-0.01	0.01	1406.3872	1415.81	9.5050	9.5050	0.08	0.08
	1420.5995	1419.7730	1420.68	0.8265	0.8265	-0.08	0.08	1410.6397	1420.64	9.9598	9.9598	-0.04	0.04
	1492.1434	1479.6882	1492.13	12.4552	12.4552	0.01	0.01	1474.2058	1492.11	17.9376	17.9376	0.03	0.03
	1492.1470	1479.6889	1492.13	12.4581	12.4581	0.02	0.02	1474.2168	1492.13	17.9302	17.9302	0.02	0.02
	1493.1842	1479.9776	1493.18	13.2066	13.2066	0.00	0.00	1474.7125	1493.21	18.4717	18.4717	-0.03	0.03
	1493.1868	1479.9789	1493.18	13.2079	13.2079	0.01	0.01	1474.7210	1493.21	18.4658	18.4658	-0.02	0.02
	2324.0484	2380.1375	2324.24	-56.0891	56.0891	-0.19	0.19	2309.8725	2324.34	14.1759	14.1759	-0.29	0.29
	3042.1401	3030.5622	3042.03	11.5779	11.5779	0.11	0.11	3048.5194	3042.17	-6.3793	6.3793	-0.03	0.03
	3042.5143	3030.6811	3042.59	11.8332	11.8332	-0.08	0.08	3048.5619	3042.55	-6.0476	6.0476	-0.04	0.04
	3113.2516	3087.9861	3113.30	25.2655	25.2655	-0.05	0.05	3131.3876	3113.32	-18.1360	18.1360	-0.07	0.07
	3113.2534	3087.9924	3113.31	25.2610	25.2610	-0.06	0.06	3131.3922	3113.32	-18.1388	18.1388	-0.07	0.07
	3113.8097	3088.5955	3113.86	25.2142	25.2142	-0.05	0.05	3131.8126	3113.87	-18.0029	18.0029	-0.06	0.06
	3113.8117	3088.6023	3113.86	25.2094	25.2094	-0.05	0.05	3131.8281	3113.87	-18.0164	18.0164	-0.06	0.06

	TZ/TZ	B3LYP/6-31G(2df,p) Freq	TZ/DFT CMA	Shift	Abs Shift	Diff	Abs Diff	DZ/DZ Freq	TZ/DZ MH	Shift	Abs Shift	Diff	Abs Diff
Bicyclo[1.1.0]butane (1.85)	413.1788	428.4155	415.24	-15.2367	15.2367	-2.06	2.06	400.8110	413.59	12.3678	12.3678	-0.41	0.41
CH2CHCHCH2 (Bicyclic)	664.9378	711.1552	666.57	-46.2174	46.2174	-1.63	1.63	640.4588	664.72	24.4790	24.4790	0.22	0.22
	751.5357	755.3009	751.80	-3.7652	3.7652	-0.26	0.26	749.5935	751.85	1.9422	1.9422	-0.31	0.31
	865.4970	846.6903	861.27	18.8067	18.8067	4.23	4.23	851.4053	866.25	14.0917	14.0917	-0.75	0.75
	867.0025	879.9034	866.34	-12.9009	12.9009	0.66	0.66	868.0463	867.84	-1.0438	1.0438	-0.84	0.84
	925.7429	931.8010	925.44	-6.0581	6.0581	0.30	0.30	919.2592	925.08	6.4837	6.4837	0.66	0.66
	948.5392	952.2095	946.79	-3.6703	3.6703	1.75	1.75	936.7615	948.58	11.7777	11.7777	-0.04	0.04
	1003.9079	1012.9451	1003.75	-9.0372	9.0372	0.16	0.16	986.9454	1003.88	16.9625	16.9625	0.03	0.03
	1091.1138	1083.8306	1091.39	7.2832	7.2832	-0.28	0.28	1082.1805	1091.42	8.9333	8.9333	-0.31	0.31
	1106.7915	1105.3041	1108.31	1.4874	1.4874	-1.52	1.52	1100.1136	1106.76	6.6779	6.6779	0.03	0.03
	1109.2572	1114.2946	1109.33	-5.0374	5.0374	-0.07	0.07	1101.2459	1109.22	8.0113	8.0113	0.04	0.04
	1145.1109	1138.1891	1145.10	6.9218	6.9218	0.01	0.01	1135.8215	1146.28	9.2894	9.2894	-1.17	1.17
	1172.1998	1173.1311	1172.20	-0.9313	0.9313	0.00	0.00	1170.7703	1170.87	1.4295	1.4295	1.33	1.33
	1185.3951	1179.0482	1196.93	6.3469	6.3469	-11.53	11.53	1182.6528	1184.83	2.7423	2.7423	0.57	0.57
	1290.3693	1305.3817	1289.94	-15.0124	15.0124	0.43	0.43	1284.6421	1290.60	5.7272	5.7272	-0.23	0.23
	1320.7524	1318.2022	1323.56	2.5502	2.5502	-2.81	2.81	1326.6753	1321.67	-5.9229	5.9229	-0.92	0.92
	1498.4492	1491.0038	1498.75	7.4454	7.4454	-0.30	0.30	1483.6230	1497.83	14.8262	14.8262	0.62	0.62
	1533.5388	1533.3241	1533.22	0.2147	0.2147	0.32	0.32	1521.6906	1533.27	11.8482	11.8482	0.27	0.27
	3076.3915	3060.5974	3076.59	15.7941	15.7941	-0.20	0.20	3078.3476	3076.45	-1.9561	1.9561	-0.06	0.06
	3082.3487	3063.6416	3082.66	18.7071	18.7071	-0.31	0.31	3082.3913	3082.39	-0.0426	0.0426	-0.04	0.04
	3182.3877	3165.8954	3182.28	16.4923	16.4923	0.11	0.11	3186.9766	3182.44	-4.5889	4.5889	-0.05	0.05
	3184.1773	3167.7624	3183.95	16.4149	16.4149	0.23	0.23	3188.4137	3184.20	-4.2364	4.2364	-0.02	0.02
	3259.4877	3241.5442	3259.55	17.9435	17.9435	-0.06	0.06	3253.3114	3259.55	6.1763	6.1763	-0.06	0.06
	3272.0093	3255.2518	3272.07	16.7575	16.7575	-0.06	0.06	3265.9210	3272.02	6.0883	6.0883	-0.01	0.01

	TZ/TZ	B3LYP/6-31G(2df,p) Freq	TZ/DFT CMA	Shift	Abs Shift	Diff	Abs Diff	DZ/DZ Freq	TZ/DZ MH	Shift	Abs Shift	Diff	Abs Diff
Cyclobutene (1.86)	302.2926	322.6514	302.70	-20.3588	20.3588	-0.41	0.41	289.7757	302.40	12.5169	12.5169	-0.11	0.11
CHCHCH2CH2 (Cyclic)	644.4517	656.2459	644.89	-11.7942	11.7942	-0.44	0.44	636.3493	644.62	8.1024	8.1024	-0.17	0.17
	856.4343	863.8663	856.53	-7.4320	7.4320	-0.10	0.10	853.0506	856.47	3.3837	3.3837	-0.04	0.04
	864.9637	873.3669	864.93	-8.4032	8.4032	0.03	0.03	858.6219	864.87	6.3418	6.3418	0.09	0.09
	895.5756	895.1112	895.67	0.4644	0.4644	-0.09	0.09	894.8861	895.75	0.6895	0.6895	-0.17	0.17
	901.8736	905.4858	901.82	-3.6122	3.6122	0.05	0.05	898.3125	902.06	3.5611	3.5611	-0.19	0.19
	916.3538	942.9255	916.71	-26.5717	26.5717	-0.36	0.36	899.5688	916.54	16.7850	16.7850	-0.19	0.19
	1002.3503	1008.3599	1002.55	-6.0096	6.0096	-0.20	0.20	993.4911	1003.12	8.8592	8.8592	-0.77	0.77
	1029.8447	1042.9123	1029.60	-13.0676	13.0676	0.24	0.24	1019.1667	1029.69	10.6780	10.6780	0.15	0.15
	1099.8997	1102.0217	1099.77	-2.1220	2.1220	0.13	0.13	1088.5835	1099.92	11.3162	11.3162	-0.02	0.02
	1134.8117	1138.1964	1136.08	-3.3847	3.3847	-1.27	1.27	1129.2352	1134.18	5.5765	5.5765	0.63	0.63
	1176.5353	1174.3417	1176.26	2.1936	2.1936	0.28	0.28	1164.8827	1176.51	11.6526	11.6526	0.03	0.03
	1219.1729	1221.4662	1218.79	-2.2933	2.2933	0.38	0.38	1218.9930	1218.98	0.1799	0.1799	0.19	0.19
	1232.8040	1238.3928	1232.89	-5.5888	5.5888	-0.09	0.09	1219.1744	1233.09	13.6296	13.6296	-0.29	0.29
	1323.4804	1326.3903	1323.50	-2.9099	2.9099	-0.02	0.02	1318.5042	1323.08	4.9762	4.9762	0.40	0.40
	1470.9466	1470.3063	1470.97	0.6403	0.6403	-0.02	0.02	1455.5270	1470.84	15.4196	15.4196	0.11	0.11
	1493.8843	1489.2960	1493.81	4.5883	4.5883	0.07	0.07	1481.1813	1493.82	12.7030	12.7030	0.06	0.06
	1604.9213	1645.8145	1604.36	-40.8932	40.8932	0.56	0.56	1604.5559	1605.16	0.3654	0.3654	-0.24	0.24
	3052.1798	3038.8644	3052.21	13.3154	13.3154	-0.03	0.03	3051.0294	3052.21	1.1504	1.1504	-0.03	0.03
	3058.2093	3044.9892	3058.23	13.2201	13.2201	-0.02	0.02	3059.0274	3058.22	-0.8181	0.8181	-0.01	0.01
	3097.0040	3074.9832	3097.03	22.0208	22.0208	-0.03	0.03	3103.2135	3097.04	-6.2095	6.2095	-0.04	0.04
	3111.4235	3090.3210	3111.45	21.1025	21.1025	-0.03	0.03	3117.7985	3111.45	-6.3750	6.3750	-0.03	0.03
	3181.9351	3176.5618	3181.98	5.3733	5.3733	-0.04	0.04	3183.2466	3181.99	-1.3115	1.3115	-0.05	0.05
	3213.6590	3210.2729	3213.68	3.3861	3.3861	-0.02	0.02	3214.5069	3213.72	-0.8479	0.8479	-0.06	0.06

	TZ/TZ	B3LYP/6-31G(2df,p) Freq	TZ/DFT CMA	Shift	Abs Shift	Diff	Abs Diff	DZ/DZ Freq	TZ/DZ MH	Shift	Abs Shift	Diff	Abs Diff
Methylenecyclopropane (1.87)	277.6483	302.6634	278.72	-25.0151	25.0151	-1.07	1.07	269.5401	278.02	8.1082	8.1082	-0.37	0.37
CH2CH2CCH2 (Cyclic)	349.2756	361.1818	349.36	-11.9062	11.9062	-0.08	0.08	343.5684	349.30	5.7072	5.7072	-0.02	0.02
	615.7428	619.5238	615.95	-3.7810	3.7810	-0.21	0.21	604.2107	615.82	11.5321	11.5321	-0.08	0.08
	737.6736	748.4049	738.21	-10.7313	10.7313	-0.54	0.54	735.8782	737.95	1.7954	1.7954	-0.28	0.28
	753.1345	751.0040	753.02	2.1305	2.1305	0.11	0.11	748.2175	753.21	4.9170	4.9170	-0.08	0.08
	907.6930	906.8153	907.76	0.8777	0.8777	-0.07	0.07	882.7415	907.80	24.9515	24.9515	-0.11	0.11
	908.2640	923.8090	908.20	-15.5450	15.5450	0.06	0.06	907.6077	908.48	0.6563	0.6563	-0.22	0.22
	953.9918	962.9308	953.88	-8.9390	8.9390	0.11	0.11	941.2511	954.04	12.7407	12.7407	-0.05	0.05
	1041.0052	1045.1166	1040.92	-4.1114	4.1114	0.09	0.09	1037.6738	1041.12	3.3314	3.3314	-0.11	0.11
	1055.3223	1072.8487	1055.46	-17.5264	17.5264	-0.14	0.14	1059.1887	1055.65	-3.8664	3.8664	-0.33	0.33
	1072.8437	1076.1784	1073.02	-3.3347	3.3347	-0.18	0.18	1061.5287	1073.16	11.3150	11.3150	-0.32	0.32
	1097.5068	1099.8235	1097.19	-2.3167	2.3167	0.32	0.32	1084.5930	1097.48	12.9138	12.9138	0.03	0.03
	1147.3835	1148.6466	1147.49	-1.2631	1.2631	-0.11	0.11	1143.3046	1146.97	4.0789	4.0789	0.41	0.41
	1171.6524	1168.9192	1171.73	2.7332	2.7332	-0.08	0.08	1159.3098	1171.63	12.3426	12.3426	0.02	0.02
	1450.5254	1445.0342	1450.99	5.4912	5.4912	-0.46	0.46	1435.0285	1450.47	15.4969	15.4969	0.06	0.06
	1455.6456	1449.3190	1455.83	6.3266	6.3266	-0.18	0.18	1437.0715	1455.63	18.5741	18.5741	0.02	0.02
	1493.0304	1484.7330	1493.10	8.2974	8.2974	-0.07	0.07	1481.0017	1492.86	12.0287	12.0287	0.17	0.17
	1819.3464	1854.3790	1818.91	-35.0326	35.0326	0.44	0.44	1824.0112	1819.42	-4.6648	4.6648	-0.07	0.07
	3126.9170	3112.2535	3126.94	14.6635	14.6635	-0.02	0.02	3125.0717	3126.91	1.8453	1.8453	0.01	0.01
	3130.3312	3113.9211	3130.37	16.4101	16.4101	-0.04	0.04	3129.1548	3130.31	1.1764	1.1764	0.02	0.02
	3139.9098	3133.8068	3139.92	6.1030	6.1030	-0.01	0.01	3143.3298	3139.96	-3.4200	3.4200	-0.05	0.05
	3207.2961	3182.8167	3207.32	24.4794	24.4794	-0.02	0.02	3212.0961	3207.32	-4.8000	4.8000	-0.02	0.02
	3219.3989	3196.8012	3219.42	22.5977	22.5977	-0.02	0.02	3224.4245	3219.42	-5.0256	5.0256	-0.02	0.02
	3225.9493	3214.4523	3226.00	11.4970	11.4970	-0.05	0.05	3238.7370	3226.00	-12.7877	12.7877	-0.05	0.05

	TZ/TZ	B3LYP/6-31G(2df,p) Freq	TZ/DFT CMA	Shift	Abs Shift	Diff	Abs Diff	DZ/DZ Freq	TZ/DZ MH	Shift	Abs Shift	Diff	Abs Diff
Cyclobutane (1.88)	230.6367	186.3189	230.89	44.3178	44.3178	-0.25	0.25	236.6182	230.66	-5.9815	5.9815	-0.02	0.02
CH2CH2CH2CH2 (Cyclic)	620.2623	636.4988	620.35	-16.2365	16.2365	-0.09	0.09	619.6946	620.30	0.5677	0.5677	-0.04	0.04
	755.0600	751.2876	755.34	3.7724	3.7724	-0.28	0.28	750.9127	755.16	4.1473	4.1473	-0.10	0.10
	755.0606	751.2934	755.34	3.7672	3.7672	-0.28	0.28	750.9136	755.16	4.1470	4.1470	-0.10	0.10
	909.3955	886.3276	909.25	23.0679	23.0679	0.15	0.15	910.0794	909.41	-0.6839	0.6839	-0.01	0.01
	916.8986	919.0213	917.45	-2.1227	2.1227	-0.55	0.55	916.8948	917.20	0.0038	0.0038	-0.30	0.30
	916.8987	919.0343	917.45	-2.1356	2.1356	-0.55	0.55	916.8950	917.20	0.0037	0.0037	-0.30	0.30
	942.9410	948.0337	943.17	-5.0927	5.0927	-0.23	0.23	945.0676	943.43	-2.1266	2.1266	-0.49	0.49
	958.2561	961.7927	958.59	-3.5366	3.5366	-0.33	0.33	950.9769	958.30	7.2792	7.2792	-0.04	0.04
	1025.3451	1019.9411	1025.42	5.4040	5.4040	-0.07	0.07	1031.6205	1025.56	-6.2754	6.2754	-0.21	0.21
	1167.6985	1175.2009	1167.47	-7.5024	7.5024	0.23	0.23	1158.9633	1167.92	8.7352	8.7352	-0.22	0.22
	1180.5523	1179.5744	1179.94	0.9779	0.9779	0.61	0.61	1171.6334	1180.49	8.9189	8.9189	0.06	0.06
	1253.5044	1253.8428	1253.10	-0.3384	0.3384	0.40	0.40	1240.4074	1253.63	13.0970	13.0970	-0.13	0.13
	1253.5046	1253.8560	1253.10	-0.3514	0.3514	0.40	0.40	1242.2732	1253.63	11.2314	11.2314	-0.13	0.13
	1254.8371	1262.5417	1254.53	-7.7046	7.7046	0.31	0.31	1242.2734	1254.85	12.5637	12.5637	-0.01	0.01
	1259.2477	1263.0319	1259.37	-3.7842	3.7842	-0.12	0.12	1258.2913	1258.56	0.9564	0.9564	0.69	0.69
	1288.3730	1294.6618	1288.42	-6.2888	6.2888	-0.05	0.05	1287.6070	1288.24	0.7660	0.7660	0.13	0.13
	1288.3731	1294.6807	1288.42	-6.3076	6.3076	-0.05	0.05	1287.6070	1288.24	0.7661	0.7661	0.13	0.13
	1486.5227	1485.6267	1487.21	0.8960	0.8960	-0.69	0.69	1467.5642	1486.27	18.9585	18.9585	0.25	0.25
	1486.5227	1485.6275	1487.21	0.8952	0.8952	-0.69	0.69	1467.5642	1486.27	18.9585	18.9585	0.25	0.25
	1493.4782	1492.7526	1493.83	0.7256	0.7256	-0.35	0.35	1473.5503	1493.47	19.9279	19.9279	0.01	0.01
	1526.1873	1522.0276	1527.88	4.1597	4.1597	-1.69	1.69	1511.5859	1526.09	14.6014	14.6014	0.10	0.10
	3058.0833	3054.4243	3058.29	3.6590	3.6590	-0.21	0.21	3057.3651	3058.10	0.7182	0.7182	-0.02	0.02
	3058.7875	3055.5527	3059.00	3.2348	3.2348	-0.21	0.21	3059.6061	3058.84	-0.8186	0.8186	-0.05	0.05
	3058.7875	3055.5710	3059.00	3.2165	3.2165	-0.21	0.21	3059.6061	3058.84	-0.8186	0.8186	-0.05	0.05
	3063.3759	3062.2391	3063.41	1.1368	1.1368	-0.03	0.03	3067.8910	3063.49	-4.5151	4.5151	-0.11	0.11
	3104.8409	3089.9936	3104.86	14.8473	14.8473	-0.02	0.02	3110.4492	3104.75	-5.6083	5.6083	0.09	0.09
	3115.6310	3103.7612	3115.47	11.8698	11.8698	0.16	0.16	3121.2165	3115.63	-5.5855	5.5855	0.00	0.00
	3115.6310	3103.7680	3115.47	11.8630	11.8630	0.16	0.16	3121.2165	3115.63	-5.5855	5.5855	0.00	0.00
	3131.2779	3122.2999	3131.07	8.9780	8.9780	0.21	0.21	3136.6652	3131.29	-5.3873	5.3873	-0.01	0.01

	TZ/TZ	B3LYP/6-31G(2df,p) Freq	TZ/DFT CMA	Shift	Abs Shift	Diff	Abs Diff	DZ/DZ Freq	TZ/DZ MH	Shift	Abs Shift	Diff	Abs Diff
Isobutene (1.89)	161.0187	172.3646	161.23	-11.3459	11.3459	-0.21	0.21	165.6036	161.12	-4.5849	4.5849	-0.10	0.10
CH2C(CH3)2	206.0329	209.8207	206.31	-3.7878	3.7878	-0.28	0.28	204.8264	206.38	1.2065	1.2065	-0.35	0.35
	368.4878	376.7558	368.53	-8.2680	8.2680	-0.04	0.04	368.3276	368.54	0.1602	0.1602	-0.05	0.05
	424.3609	437.5445	424.56	-13.1836	13.1836	-0.20	0.20	418.5744	424.42	5.7865	5.7865	-0.06	0.06
	426.3734	442.2924	426.42	-15.9190	15.9190	-0.05	0.05	423.9352	426.43	2.4382	2.4382	-0.06	0.06
	702.9675	706.5140	703.08	-3.5465	3.5465	-0.11	0.11	691.7757	702.95	11.1918	11.1918	0.02	0.02
	818.6925	819.2101	819.18	-0.5176	0.5176	-0.49	0.49	821.0212	818.76	-2.3287	2.3287	-0.07	0.07
	905.2569	923.6376	905.22	-18.3807	18.3807	0.04	0.04	886.2784	905.41	18.9785	18.9785	-0.15	0.15
	963.5695	962.9720	965.47	0.5975	0.5975	-1.90	1.90	957.3684	963.97	6.2011	6.2011	-0.40	0.40
	988.2504	985.2189	987.06	3.0315	3.0315	1.19	1.19	986.6507	988.10	1.5997	1.5997	0.15	0.15
	1019.7544	1023.0037	1019.67	-3.2493	3.2493	0.08	0.08	1008.6662	1019.76	11.0882	11.0882	-0.01	0.01
	1081.3886	1086.4434	1081.62	-5.0548	5.0548	-0.23	0.23	1072.6219	1081.43	8.7667	8.7667	-0.04	0.04
	1103.2561	1107.0368	1103.08	-3.7807	3.7807	0.18	0.18	1090.6066	1103.12	12.6495	12.6495	0.14	0.14
	1305.9900	1297.7801	1306.69	8.2099	8.2099	-0.70	0.70	1302.7027	1306.09	3.2873	3.2873	-0.10	0.10
	1410.4303	1409.9935	1410.56	0.4368	0.4368	-0.13	0.13	1400.9854	1410.53	9.4449	9.4449	-0.10	0.10
	1414.3378	1414.1218	1413.78	0.2160	0.2160	0.56	0.56	1410.7036	1414.03	3.6342	3.6342	0.31	0.31
	1447.5296	1447.4179	1448.00	0.1117	0.1117	-0.47	0.47	1437.1716	1447.45	10.3580	10.3580	0.08	0.08
	1478.4082	1473.7188	1478.38	4.6894	4.6894	0.03	0.03	1460.9882	1478.42	17.4200	17.4200	-0.01	0.01
	1491.2593	1486.3114	1491.05	4.9479	4.9479	0.21	0.21	1473.6227	1491.28	17.6366	17.6366	-0.02	0.02
	1495.1002	1490.7922	1495.08	4.3080	4.3080	0.02	0.02	1477.6526	1495.11	17.4476	17.4476	-0.01	0.01
	1506.8685	1503.1806	1506.82	3.6879	3.6879	0.05	0.05	1489.4304	1506.87	17.4381	17.4381	0.00	0.00
	1710.5788	1732.8655	1709.95	-22.2867	22.2867	0.63	0.63	1712.0976	1710.65	-1.5188	1.5188	-0.07	0.07
	3020.5212	3018.3559	3020.78	2.1653	2.1653	-0.26	0.26	3027.0245	3020.57	-6.5033	6.5033	-0.05	0.05
	3024.2149	3024.0164	3024.44	0.1985	0.1985	-0.23	0.23	3031.0474	3024.27	-6.8325	6.8325	-0.06	0.06
	3077.6552	3063.5978	3077.69	14.0574	14.0574	-0.03	0.03	3095.3596	3077.69	-17.7044	17.7044	-0.03	0.03
	3079.7512	3066.8078	3079.78	12.9434	12.9434	-0.03	0.03	3097.5500	3079.79	-17.7988	17.7988	-0.04	0.04
	3119.4625	3117.9252	3119.25	1.5373	1.5373	0.21	0.21	3135.1110	3119.46	-15.6485	15.6485	0.00	0.00
	3121.4582	3120.0887	3121.30	1.3695	1.3695	0.16	0.16	3136.8253	3121.58	-15.3671	15.3671	-0.12	0.12
	3140.7792	3140.4689	3140.80	0.3103	0.3103	-0.02	0.02	3145.1497	3140.68	-4.3705	4.3705	0.10	0.10
	3226.1165	3220.8892	3226.17	5.2273	5.2273	-0.05	0.05	3238.3047	3226.17	-12.1882	12.1882	-0.05	0.05

	TZ/TZ	B3LYP/6-31G(2df,p) Freq	TZ/DFT CMA	Shift	Abs Shift	Diff	Abs Diff	DZ/DZ Freq	TZ/DZ MH	Shift	Abs Shift	Diff	Abs Diff
Pyrrole (1.90)	441.8788	475.3152	442.13	-33.4364	33.4364	-0.25	0.25	420.8481	442.58	21.0307	21.0307	-0.70	0.70
CHCHCHCHNH (Cyclic)	615.6180	629.6844	615.84	-14.0664	14.0664	-0.22	0.22	598.5572	616.77	17.0608	17.0608	-1.15	1.15
	634.2271	641.4414	634.39	-7.2143	7.2143	-0.16	0.16	627.6788	634.58	6.5483	6.5483	-0.35	0.35
	689.5055	695.3804	689.55	-5.8749	5.8749	-0.04	0.04	671.4882	689.59	18.0173	18.0173	-0.08	0.08
	732.1688	740.4211	732.16	-8.2523	8.2523	0.01	0.01	718.5772	732.31	13.5916	13.5916	-0.14	0.14
	825.1862	830.7004	824.96	-5.5142	5.5142	0.23	0.23	802.0837	824.50	23.1025	23.1025	0.69	0.69
	854.7997	872.4760	854.55	-17.6763	17.6763	0.25	0.25	826.2479	853.93	28.5518	28.5518	0.87	0.87
	868.6913	883.6783	869.04	-14.9870	14.9870	-0.35	0.35	860.2530	868.76	8.4383	8.4383	-0.07	0.07
	889.6008	899.0801	889.69	-9.4793	9.4793	-0.09	0.09	881.6754	889.67	7.9254	7.9254	-0.07	0.07
	1032.9620	1039.6418	1033.26	-6.6798	6.6798	-0.30	0.30	1026.2046	1033.32	6.7574	6.7574	-0.36	0.36
	1065.9845	1075.3006	1066.62	-9.3161	9.3161	-0.64	0.64	1057.5542	1066.28	8.4303	8.4303	-0.30	0.30
	1094.8443	1099.8743	1094.60	-5.0300	5.0300	0.24	0.24	1089.3919	1095.44	5.4524	5.4524	-0.60	0.60
	1159.5080	1159.3746	1159.16	0.1334	0.1334	0.35	0.35	1154.2937	1159.42	5.2143	5.2143	0.09	0.09
	1167.2271	1177.8770	1167.49	-10.6499	10.6499	-0.26	0.26	1168.3222	1166.71	-1.0951	1.0951	0.52	0.52
	1310.4238	1311.1468	1310.49	-0.7230	0.7230	-0.07	0.07	1296.5215	1310.52	13.9023	13.9023	-0.10	0.10
	1423.1596	1423.4837	1423.15	-0.3241	0.3241	0.01	0.01	1431.4438	1422.99	-8.2842	8.2842	0.17	0.17
	1465.5992	1456.3081	1465.48	9.2911	9.2911	0.12	0.12	1483.7982	1465.34	-18.1990	18.1990	0.26	0.26
	1508.8805	1507.0326	1508.68	1.8479	1.8479	0.20	0.20	1513.0090	1508.62	-4.1285	4.1285	0.26	0.26
	1572.7590	1583.7323	1572.54	-10.9733	10.9733	0.22	0.22	1574.4082	1572.74	-1.6492	1.6492	0.02	0.02
	3246.8762	3241.0403	3247.00	5.8359	5.8359	-0.12	0.12	3246.2058	3246.93	0.6704	0.6704	-0.05	0.05
	3257.7451	3252.9594	3257.92	4.7857	4.7857	-0.17	0.17	3257.9768	3257.79	-0.2317	0.2317	-0.04	0.04
	3272.1271	3269.2941	3272.10	2.8330	2.8330	0.03	0.03	3273.7450	3272.16	-1.6179	1.6179	-0.03	0.03
	3279.0959	3275.7738	3278.99	3.3221	3.3221	0.11	0.11	3280.8522	3279.12	-1.7563	1.7563	-0.02	0.02
	3700.4415	3696.0145	3700.60	4.4270	4.4270	-0.16	0.16	3685.5783	3700.59	14.8632	14.8632	-0.15	0.15

	TZ/TZ	B3LYP/6-31G(2df,p) Freq	TZ/DFT CMA	Shift	Abs Shift	Diff	Abs Diff	DZ/DZ Freq	TZ/DZ MH	Shift	Abs Shift	Diff	Abs Diff
Pyridine (1.91)	378.4400	384.5327	378.60	-6.0927	6.0927	-0.16	0.16	373.9092	378.51	4.5308	4.5308	-0.07	0.07
CHCHCHCHCHN (Cyclic)	409.2152	420.9439	409.30	-11.7287	11.7287	-0.08	0.08	400.6872	409.57	8.5280	8.5280	-0.35	0.35
	603.3113	612.0139	603.42	-8.7026	8.7026	-0.11	0.11	598.3191	603.33	4.9922	4.9922	-0.02	0.02
	656.9786	655.7459	657.09	1.2327	1.2327	-0.11	0.11	651.3723	657.00	5.6063	5.6063	-0.02	0.02
	711.8862	723.8082	712.36	-11.9220	11.9220	-0.47	0.47	695.0196	714.88	16.8666	16.8666	-2.99	2.99
	753.1688	772.2585	753.04	-19.0897	19.0897	0.13	0.13	733.6714	751.76	19.4974	19.4974	1.41	1.41
	890.7844	904.3853	890.87	-13.6009	13.6009	-0.09	0.09	879.6937	890.91	11.0907	11.0907	-0.13	0.13
	953.6411	966.1007	953.58	-12.4596	12.4596	0.06	0.06	936.7951	953.75	16.8460	16.8460	-0.11	0.11
	995.1066	1009.7248	995.01	-14.6182	14.6182	0.10	0.10	969.2549	995.07	25.8517	25.8517	0.04	0.04
	996.8655	1010.0982	996.64	-13.2327	13.2327	0.23	0.23	975.5726	995.72	21.2929	21.2929	1.15	1.15
	1001.2398	1017.7565	1002.44	-16.5167	16.5167	-1.20	1.20	994.3371	1001.65	6.9027	6.9027	-0.41	0.41
	1043.1401	1050.6245	1042.20	-7.4844	7.4844	0.94	0.94	1035.6004	1043.01	7.5397	7.5397	0.13	0.13
	1071.3501	1080.0382	1071.43	-8.6881	8.6881	-0.08	0.08	1066.4153	1071.38	4.9348	4.9348	-0.03	0.03
	1087.8556	1095.4755	1087.88	-7.6199	7.6199	-0.02	0.02	1081.1547	1087.60	6.7009	6.7009	0.26	0.26
	1158.8194	1171.6074	1161.07	-12.7880	12.7880	-2.25	2.25	1150.3421	1159.09	8.4773	8.4773	-0.27	0.27
	1236.7241	1246.7768	1236.81	-10.0527	10.0527	-0.09	0.09	1229.6720	1236.63	7.0521	7.0521	0.09	0.09
	1266.9456	1300.7264	1265.53	-33.7808	33.7808	1.42	1.42	1275.8520	1266.90	-8.9064	8.9064	0.05	0.05
	1379.1987	1384.1787	1379.13	-4.9800	4.9800	0.07	0.07	1365.4744	1379.14	13.7243	13.7243	0.06	0.06
	1464.6584	1472.7824	1464.32	-8.1240	8.1240	0.34	0.34	1456.0916	1464.50	8.5668	8.5668	0.16	0.16
	1510.1155	1516.1755	1510.07	-6.0600	6.0600	0.05	0.05	1503.5946	1510.15	6.5209	6.5209	-0.03	0.03
	1618.4276	1625.9531	1618.33	-7.5255	7.5255	0.10	0.10	1619.8724	1618.51	-1.4448	1.4448	-0.08	0.08
	1630.2948	1629.9487	1630.27	0.3461	0.3461	0.02	0.02	1633.9628	1630.41	-3.6680	3.6680	-0.12	0.12
	3168.4220	3153.4863	3168.50	14.9357	14.9357	-0.08	0.08	3170.6237	3168.48	-2.2017	2.2017	-0.06	0.06
	3169.8341	3155.9584	3170.04	13.8757	13.8757	-0.21	0.21	3171.7019	3169.88	-1.8678	1.8678	-0.05	0.05
	3187.5657	3179.2780	3187.53	8.2877	8.2877	0.04	0.04	3189.9820	3187.63	-2.4163	2.4163	-0.06	0.06
	3204.4892	3194.7810	3204.47	9.7082	9.7082	0.02	0.02	3206.4280	3204.53	-1.9388	1.9388	-0.04	0.04
	3212.8541	3204.3355	3212.83	8.5186	8.5186	0.02	0.02	3215.5116	3212.87	-2.6575	2.6575	-0.02	0.02

	TZ/TZ	B3LYP/6-31G(2df,p) Freq	TZ/DFT CMA	Shift	Abs Shift	Diff	Abs Diff	DZ/DZ Freq	TZ/DZ MH	Shift	Abs Shift	Diff	Abs Diff
Sulfur dioxide (1.92)	519.2534	517.3857	519.26	1.8677	1.8677	-0.01	0.01	509.5071	519.29	9.7463	9.7463	-0.04	0.04
SO2 (Need tight-d functions)	1169.0969	1177.0649	1169.12	-7.9680	7.9680	-0.02	0.02	1105.2890	1169.14	63.8079	63.8079	-0.04	0.04
	1388.9138	1385.5396	1388.94	3.3742	3.3742	-0.03	0.03	1326.4760	1388.94	62.4378	62.4378	-0.03	0.03
Hydrogen sulfide (1.93)	1209.6486	1210.5783	1209.55	-0.9297	0.9297	0.10	0.10	1216.2951	1209.55	-6.6465	6.6465	0.10	0.10
H2S	2722.0751	2697.2007	2722.13	24.8744	24.8744	-0.05	0.05	2738.3166	2722.12	-16.2415	16.2415	-0.04	0.04
	2736.7529	2713.0301	2736.80	23.7228	23.7228	-0.05	0.05	2759.3918	2736.80	-22.6389	22.6389	-0.05	0.05
Carbon disulfide (1.94)	401.6980	411.3792	401.72	-9.6812	9.6812	-0.02	0.02	392.3358	401.70	9.3622	9.3622	0.00	0.00
CS2 (Linear)	401.6980	411.3793	401.72	-9.6813	9.6813	-0.02	0.02	392.3358	401.70	9.3622	9.3622	0.00	0.00
	667.8809	675.2407	667.89	-7.3598	7.3598	-0.01	0.01	669.3365	667.89	-1.4556	1.4556	-0.01	0.01
	1558.5649	1575.3433	1558.59	-16.7784	16.7784	-0.03	0.03	1568.0807	1558.59	-9.5158	9.5158	-0.03	0.03
Carbonyl sulfide (1.95)	523.0944	536.0389	523.12	-12.9445	12.9445	-0.03	0.03	511.8895	523.10	11.2049	11.2049	-0.01	0.01
SCO (Linear)	523.0944	536.0390	523.12	-12.9446	12.9446	-0.03	0.03	511.8895	523.10	11.2049	11.2049	-0.01	0.01
	869.0879	877.5212	869.18	-8.4333	8.4333	-0.09	0.09	870.9267	869.15	-1.8388	1.8388	-0.06	0.06
	2091.6800	2140.2245	2091.72	-48.5445	48.5445	-0.04	0.04	2088.6065	2091.73	3.0735	3.0735	-0.05	0.05
Thiirane (1.96)	640.9521	632.7605	641.18	8.1916	8.1916	-0.23	0.23	649.8704	641.21	-8.9183	8.9183	-0.26	0.26
H2CSCH2	679.8203	668.9505	679.80	10.8698	10.8698	0.02	0.02	676.5623	679.85	3.2580	3.2580	-0.03	0.03
	833.2681	832.3146	833.24	0.9535	0.9535	0.03	0.03	830.6251	833.30	2.6430	2.6430	-0.03	0.03
	904.3662	896.3749	904.38	7.9913	7.9913	-0.01	0.01	895.7295	904.42	8.6367	8.6367	-0.05	0.05
	962.6964	953.4370	962.80	9.2594	9.2594	-0.10	0.10	959.7989	962.74	2.8975	2.8975	-0.04	0.04
	1048.5302	1047.6950	1048.64	0.8352	0.8352	-0.11	0.11	1042.9382	1048.48	5.5920	5.5920	0.05	0.05
	1073.8287	1076.6911	1074.22	-2.8624	2.8624	-0.39	0.39	1062.7445	1073.93	11.0842	11.0842	-0.10	0.10
	1139.9255	1149.9421	1139.99	-10.0166	10.0166	-0.06	0.06	1145.1403	1140.26	-5.2148	5.2148	-0.33	0.33
	1198.5964	1196.4335	1198.66	2.1629	2.1629	-0.06	0.06	1185.2123	1198.62	13.3841	13.3841	-0.02	0.02
	1477.3143	1472.3162	1477.38	4.9981	4.9981	-0.07	0.07	1460.6149	1477.39	16.6994	16.6994	-0.08	0.08
	1502.5713	1493.1935	1502.64	9.3778	9.3778	-0.07	0.07	1492.5333	1502.48	10.0380	10.0380	0.09	0.09
	3139.0426	3134.4053	3139.06	4.6373	4.6373	-0.02	0.02	3132.7566	3139.06	6.2860	6.2860	-0.02	0.02
	3142.6865	3136.0438	3142.68	6.6427	6.6427	0.01	0.01	3137.8888	3142.69	4.7977	4.7977	0.00	0.00
	3224.3404	3214.9747	3224.36	9.3657	9.3657	-0.02	0.02	3222.5005	3224.37	1.8399	1.8399	-0.03	0.03
	3238.0148	3231.0324	3238.04	6.9824	6.9824	-0.03	0.03	3236.0993	3238.04	1.9155	1.9155	-0.03	0.03

	TZ/TZ	B3LYP/6-31G(2df,p) Freq	TZ/DFT CMA	Shift	Abs Shift	Diff	Abs Diff	DZ/DZ Freq	TZ/DZ MH	Shift	Abs Shift	Diff	Abs Diff
Dimethyl sulfide (1.97)	174.7014	177.6159	175.12	-2.9145	2.9145	-0.42	0.42	179.0143	174.91	-4.3129	4.3129	-0.21	0.21
H3CSCH3	186.0106	180.8875	186.31	5.1231	5.1231	-0.30	0.30	189.2853	186.16	-3.2747	3.2747	-0.15	0.15
	262.3297	259.6129	262.41	2.7168	2.7168	-0.08	0.08	267.5770	262.37	-5.2473	5.2473	-0.04	0.04
	708.4500	689.0021	708.61	19.4479	19.4479	-0.16	0.16	707.7717	708.51	0.6783	0.6783	-0.06	0.06
	762.1322	741.9541	762.33	20.1781	20.1781	-0.20	0.20	761.5135	762.18	0.6187	0.6187	-0.05	0.05
	911.6026	911.0838	911.70	0.5188	0.5188	-0.10	0.10	907.8142	911.66	3.7884	3.7884	-0.06	0.06
	953.9442	951.0008	954.09	2.9434	2.9434	-0.15	0.15	951.1946	954.01	2.7496	2.7496	-0.07	0.07
	990.2304	986.6445	990.40	3.5859	3.5859	-0.17	0.17	989.0418	990.29	1.1886	1.1886	-0.06	0.06
	1050.4941	1051.3126	1050.55	-0.8185	0.8185	-0.06	0.06	1045.6088	1050.55	4.8853	4.8853	-0.06	0.06
	1343.7396	1342.2574	1343.74	1.4822	1.4822	0.00	0.00	1337.0618	1343.77	6.6778	6.6778	-0.03	0.03
	1368.1265	1366.7822	1368.16	1.3443	1.3443	-0.03	0.03	1364.4980	1368.16	3.6285	3.6285	-0.03	0.03
	1469.6065	1466.3415	1469.58	3.2650	3.2650	0.03	0.03	1453.2689	1469.61	16.3376	16.3376	0.00	0.00
	1478.6221	1475.5576	1478.60	3.0645	3.0645	0.02	0.02	1462.7047	1478.63	15.9174	15.9174	-0.01	0.01
	1486.4787	1482.6123	1486.55	3.8664	3.8664	-0.07	0.07	1471.7536	1486.55	14.7251	14.7251	-0.07	0.07
	1494.0269	1489.5796	1494.12	4.4473	4.4473	-0.09	0.09	1479.1320	1494.08	14.8949	14.8949	-0.05	0.05
	3034.8989	3041.9647	3034.87	-7.0658	7.0658	0.03	0.03	3036.2886	3034.87	-1.3897	1.3897	0.03	0.03
	3038.7176	3044.7146	3038.69	-5.9970	5.9970	0.03	0.03	3039.0530	3038.69	-0.3354	0.3354	0.03	0.03
	3113.4486	3117.5891	3113.46	-4.1405	4.1405	-0.01	0.01	3122.1189	3113.47	-8.6703	8.6703	-0.02	0.02
	3120.9327	3124.1522	3120.95	-3.2195	3.2195	-0.02	0.02	3128.9709	3120.95	-8.0382	8.0382	-0.02	0.02
	3138.7129	3142.7431	3138.71	-4.0302	4.0302	0.00	0.00	3149.6339	3138.73	-10.9210	10.9210	-0.02	0.02
	3139.3766	3143.3739	3139.36	-3.9973	3.9973	0.02	0.02	3150.0562	3139.39	-10.6796	10.6796	-0.01	0.01

	TZ/TZ	B3LYP/6-31G(2df,p) Freq	TZ/DFT CMA	Shift	Abs Shift	Diff	Abs Diff	DZ/DZ Freq	TZ/DZ MH	Shift	Abs Shift	Diff	Abs Diff
Thioethanol (1.98)	177.3867	176.3090	177.50	1.0777	1.0777	-0.11	0.11	182.8061	177.86	-5.4194	5.4194	-0.47	0.47
H3CCH2SH	252.9522	247.4006	252.92	5.5516	5.5516	0.03	0.03	262.5979	252.74	-9.6457	9.6457	0.21	0.21
	301.9438	300.2982	302.09	1.6456	1.6456	-0.15	0.15	304.5091	301.97	-2.5653	2.5653	-0.03	0.03
	687.0828	665.7418	687.45	21.3410	21.3410	-0.37	0.37	685.9024	687.11	1.1804	1.1804	-0.03	0.03
	789.8805	789.6991	790.12	0.1814	0.1814	-0.24	0.24	786.7630	790.02	3.1175	3.1175	-0.14	0.14
	863.9462	857.5241	864.18	6.4221	6.4221	-0.23	0.23	871.2698	863.98	-7.3236	7.3236	-0.03	0.03
	1001.7738	995.1454	1002.08	6.6284	6.6284	-0.31	0.31	1006.1983	1002.02	-4.4245	4.4245	-0.25	0.25
	1046.6329	1043.3597	1046.65	3.2732	3.2732	-0.02	0.02	1043.6220	1046.67	3.0109	3.0109	-0.04	0.04
	1116.0852	1112.9699	1115.90	3.1153	3.1153	0.19	0.19	1116.3771	1116.08	-0.2919	0.2919	0.01	0.01
	1271.8612	1271.2141	1271.87	0.6471	0.6471	-0.01	0.01	1264.2704	1271.91	7.5908	7.5908	-0.05	0.05
	1302.2037	1299.2550	1302.26	2.9487	2.9487	-0.06	0.06	1300.3295	1302.35	1.8742	1.8742	-0.15	0.15
	1413.6137	1417.1493	1413.50	-3.5356	3.5356	0.11	0.11	1404.9435	1413.31	8.6702	8.6702	0.30	0.30
	1496.3979	1492.1000	1496.58	4.2979	4.2979	-0.18	0.18	1482.5443	1496.37	13.8536	13.8536	0.03	0.03
	1500.2015	1496.1436	1500.17	4.0579	4.0579	0.03	0.03	1483.3756	1500.19	16.8259	16.8259	0.01	0.01
	1510.0123	1507.4441	1510.05	2.5682	2.5682	-0.04	0.04	1493.8505	1510.03	16.1618	16.1618	-0.02	0.02
	2709.3301	2685.7093	2709.40	23.6208	23.6208	-0.07	0.07	2726.2319	2709.41	-16.9018	16.9018	-0.08	0.08
	3040.5841	3045.7274	3040.84	-5.1433	5.1433	-0.26	0.26	3047.2841	3040.95	-6.7000	6.7000	-0.37	0.37
	3068.1612	3066.3368	3068.20	1.8244	1.8244	-0.04	0.04	3064.3789	3068.02	3.7823	3.7823	0.14	0.14
	3107.0593	3105.4619	3107.24	1.5974	1.5974	-0.18	0.18	3114.0538	3110.20	-6.9945	6.9945	-3.14	3.14
	3118.1519	3114.3396	3118.02	3.8123	3.8123	0.13	0.13	3135.1840	3118.12	-17.0321	17.0321	0.03	0.03
	3129.7588	3129.9204	3129.66	-0.1616	0.1616	0.10	0.10	3140.9314	3126.75	-11.1726	11.1726	3.01	3.01

	TZ/TZ	B3LYP/6-31G(2df,p) Freq	TZ/DFT CMA	Shift	Abs Shift	Diff	Abs Diff	DZ/DZ Freq	TZ/DZ MH	Shift	Abs Shift	Diff	Abs Diff
Thiophene (1.100)	453.2529	458.0544	453.30	-4.8015	4.8015	-0.05	0.05	442.4466	453.48	10.8063	10.8063	-0.23	0.23
CHCHCHCHS (Cyclic)	565.5249	578.5135	565.74	-12.9886	12.9886	-0.22	0.22	549.4212	566.12	16.1037	16.1037	-0.60	0.60
	609.9358	613.4307	610.17	-3.4949	3.4949	-0.23	0.23	608.4860	609.97	1.4498	1.4498	-0.03	0.03
	688.0406	695.0116	688.16	-6.9710	6.9710	-0.12	0.12	676.2139	688.06	11.8267	11.8267	-0.02	0.02
	725.7584	733.8368	725.94	-8.0784	8.0784	-0.18	0.18	716.1720	725.71	9.5864	9.5864	0.05	0.05
	758.8766	755.4577	759.99	3.4189	3.4189	-1.11	1.11	756.4881	758.98	2.3885	2.3885	-0.10	0.10
	845.4944	839.8370	845.55	5.6574	5.6574	-0.06	0.06	844.1407	845.75	1.3537	1.3537	-0.26	0.26
	875.5068	875.7876	875.51	-0.2808	0.2808	0.00	0.00	856.1675	875.60	19.3393	19.3393	-0.09	0.09
	878.2804	886.5196	877.76	-8.2392	8.2392	0.52	0.52	874.1227	878.25	4.1577	4.1577	0.03	0.03
	902.5891	923.8767	902.62	-21.2876	21.2876	-0.03	0.03	875.5396	902.23	27.0495	27.0495	0.36	0.36
	1051.5976	1058.6232	1051.98	-7.0256	7.0256	-0.38	0.38	1047.9524	1051.93	3.6452	3.6452	-0.33	0.33
	1098.2603	1104.8743	1098.61	-6.6140	6.6140	-0.35	0.35	1087.6574	1098.23	10.6029	10.6029	0.03	0.03
	1100.8536	1108.0280	1101.43	-7.1744	7.1744	-0.58	0.58	1091.5370	1100.97	9.3166	9.3166	-0.12	0.12
	1278.8925	1274.0830	1278.68	4.8095	4.8095	0.21	0.21	1267.9082	1279.07	10.9843	10.9843	-0.18	0.18
	1396.0792	1396.4020	1396.03	-0.3228	0.3228	0.05	0.05	1397.6122	1396.65	-1.5330	1.5330	-0.57	0.57
	1442.5942	1453.0228	1442.17	-10.4286	10.4286	0.42	0.42	1454.7657	1442.02	-12.1715	12.1715	0.57	0.57
	1545.3954	1560.5239	1545.17	-15.1285	15.1285	0.23	0.23	1551.6227	1545.31	-6.2273	6.2273	0.09	0.09
	3213.8195	3205.8925	3213.97	7.9270	7.9270	-0.15	0.15	3217.6264	3213.93	-3.8069	3.8069	-0.11	0.11
	3227.8067	3220.6545	3228.08	7.1522	7.1522	-0.27	0.27	3231.4530	3228.02	-3.6463	3.6463	-0.21	0.21
	3256.0539	3258.6742	3255.99	-2.6203	2.6203	0.06	0.06	3255.3121	3256.04	0.7418	0.7418	0.01	0.01
	3259.2923	3261.2042	3259.08	-1.9119	1.9119	0.21	0.21	3259.1489	3259.15	0.1434	0.1434	0.14	0.14
Methanol (1.101)	304.1109	307.9492	304.25	-3.8383	3.8383	-0.14	0.14	347.1988	304.10	-43.0879	43.0879	0.01	0.01
CH3OH	1065.0202	1056.4050	1065.61	8.6152	8.6152	-0.59	0.59	1073.4534	1066.57	-8.4332	8.4332	-1.55	1.55
	1095.5355	1096.1018	1095.26	-0.5663	0.5663	0.28	0.28	1099.7619	1094.68	-4.2264	4.2264	0.86	0.86
	1179.6132	1170.7586	1179.71	8.8546	8.8546	-0.10	0.10	1171.2769	1179.64	8.3363	8.3363	-0.03	0.03
	1393.8677	1385.3506	1393.91	8.5171	8.5171	-0.04	0.04	1405.1042	1393.90	-11.2365	11.2365	-0.03	0.03
	1487.6428	1481.5629	1487.44	6.0799	6.0799	0.20	0.20	1483.2613	1487.32	4.3815	4.3815	0.32	0.32
	1507.6636	1499.3966	1507.62	8.2670	8.2670	0.04	0.04	1489.2928	1507.69	18.3708	18.3708	-0.03	0.03
	1523.2346	1514.9107	1523.45	8.3239	8.3239	-0.22	0.22	1507.3130	1523.27	15.9216	15.9216	-0.04	0.04
	3009.2876	2989.0771	3009.69	20.2105	20.2105	-0.40	0.40	2998.8858	3009.39	10.4018	10.4018	-0.10	0.10
	3064.4862	3031.8984	3064.54	32.5878	32.5878	-0.05	0.05	3054.7629	3064.55	9.7233	9.7233	-0.06	0.06
	3128.1077	3115.5862	3127.91	12.5215	12.5215	0.20	0.20	3134.7933	3128.21	-6.6856	6.6856	-0.10	0.10
	3864.9772	3838.0099	3865.17	26.9673	26.9673	-0.19	0.19	3837.8498	3865.18	27.1274	27.1274	-0.20	0.20

	TZ/TZ	B3LYP/6-31G(2df,p) Freq	TZ/DFT CMA	Shift	Abs Shift	Diff	Abs Diff	DZ/DZ Freq	TZ/DZ MH	Shift	Abs Shift	Diff	Abs Diff
Methanol (1.101)	304.1109	307.9492	304.25	-3.8383	3.8383	-0.14	0.14	347.1988	304.10	-43.0879	43.0879	0.01	0.01
CH3OH	1065.0202	1056.4050	1065.61	8.6152	8.6152	-0.59	0.59	1073.4534	1066.57	-8.4332	8.4332	-1.55	1.55
	1095.5355	1096.1018	1095.26	-0.5663	0.5663	0.28	0.28	1099.7619	1094.68	-4.2264	4.2264	0.86	0.86
	1179.6132	1170.7586	1179.71	8.8546	8.8546	-0.10	0.10	1171.2769	1179.64	8.3363	8.3363	-0.03	0.03
	1393.8677	1385.3506	1393.91	8.5171	8.5171	-0.04	0.04	1405.1042	1393.90	-11.2365	11.2365	-0.03	0.03
	1487.6428	1481.5629	1487.44	6.0799	6.0799	0.20	0.20	1483.2613	1487.32	4.3815	4.3815	0.32	0.32
	1507.6636	1499.3966	1507.62	8.2670	8.2670	0.04	0.04	1489.2928	1507.69	18.3708	18.3708	-0.03	0.03
	1523.2346	1514.9107	1523.45	8.3239	8.3239	-0.22	0.22	1507.3130	1523.27	15.9216	15.9216	-0.04	0.04
	3009.2876	2989.0771	3009.69	20.2105	20.2105	-0.40	0.40	2998.8858	3009.39	10.4018	10.4018	-0.10	0.10
	3064.4862	3031.8984	3064.54	32.5878	32.5878	-0.05	0.05	3054.7629	3064.55	9.7233	9.7233	-0.06	0.06
	3128.1077	3115.5862	3127.91	12.5215	12.5215	0.20	0.20	3134.7933	3128.21	-6.6856	6.6856	-0.10	0.10
	3864.9772	3838.0099	3865.17	26.9673	26.9673	-0.19	0.19	3837.8498	3865.18	27.1274	27.1274	-0.20	0.20
Propene	199.4306	206.1504	199.58	-6.7198	6.7198	-0.15	0.15	214.2714	199.63	-14.8408	14.8408	-0.20	0.20
CH3CHCH2	418.0731	421.3172	418.11	-3.2441	3.2441	-0.04	0.04	419.6814	418.18	-1.6083	1.6083	-0.11	0.11
	582.6462	591.8854	583.01	-9.2392	9.2392	-0.36	0.36	579.2287	582.75	3.4175	3.4175	-0.10	0.10
	925.2372	928.8305	925.43	-3.5933	3.5933	-0.19	0.19	908.9799	925.49	16.2573	16.2573	-0.25	0.25
	930.9398	944.0239	931.17	-13.0841	13.0841	-0.23	0.23	933.6709	930.57	-2.7311	2.7311	0.37	0.37
	942.3826	945.8311	942.72	-3.4485	3.4485	-0.34	0.34	938.8442	942.90	3.5384	3.5384	-0.52	0.52
	1014.2579	1033.5551	1015.18	-19.2972	19.2972	-0.92	0.92	1005.0224	1014.18	9.2355	9.2355	0.08	0.08
	1067.9936	1073.2037	1066.92	-5.2101	5.2101	1.07	1.07	1058.8010	1067.86	9.1926	9.1926	0.13	0.13
	1191.6409	1192.0434	1191.87	-0.4025	0.4025	-0.23	0.23	1185.2512	1191.73	6.3897	6.3897	-0.09	0.09
	1320.2872	1330.2267	1321.16	-9.9395	9.9395	-0.87	0.87	1308.0120	1320.22	12.2752	12.2752	0.07	0.07
	1408.0992	1408.7444	1408.67	-0.6452	0.6452	-0.57	0.57	1400.3199	1408.36	7.7793	7.7793	-0.26	0.26
	1455.8330	1452.4047	1455.86	3.4283	3.4283	-0.03	0.03	1446.8319	1455.54	9.0011	9.0011	0.29	0.29
	1488.1420	1482.1878	1488.07	5.9542	5.9542	0.07	0.07	1473.3595	1488.15	14.7825	14.7825	-0.01	0.01
	1501.6555	1495.6817	1501.52	5.9738	5.9738	0.14	0.14	1486.6055	1501.63	15.0500	15.0500	0.03	0.03
	1696.3873	1724.5643	1695.19	-28.1770	28.1770	1.20	1.20	1698.7843	1696.59	-2.3970	2.3970	-0.20	0.20
	3029.4803	3024.9320	3029.99	4.5483	4.5483	-0.51	0.51	3031.9340	3029.52	-2.4537	2.4537	-0.04	0.04
	3089.8001	3070.8190	3089.85	18.9811	18.9811	-0.05	0.05	3103.8512	3089.86	-14.0511	14.0511	-0.06	0.06
	3113.1739	3108.3692	3113.34	4.8047	4.8047	-0.17	0.17	3125.7347	3114.06	-12.5608	12.5608	-0.89	0.89
	3138.1863	3133.7063	3140.93	4.4800	4.4800	-2.74	2.74	3140.1528	3137.68	-1.9665	1.9665	0.51	0.51
	3151.6563	3142.4129	3148.39	9.2434	9.2434	3.27	3.27	3152.6935	3151.42	-1.0372	1.0372	0.24	0.24
	3230.2716	3223.6202	3230.33	6.6514	6.6514	-0.06	0.06	3239.6224	3230.28	-9.3508	9.3508	-0.01	0.01

	TZ/TZ	B3LYP/6-31G(2df,p) Freq	TZ/DFT CMA	Shift	Abs Shift	Diff	Abs Diff	DZ/DZ Freq	TZ/DZ MH	Shift	Abs Shift	Diff	Abs Diff
Oxirane	816.2603	814.7705	816.29	1.4898	1.4898	-0.03	0.03	812.5166	816.32	3.7437	3.7437	-0.06	0.06
H2COCH2 (Oxirane)	849.9257	861.7361	850.15	-11.8104	11.8104	-0.22	0.22	846.2905	849.94	3.6352	3.6352	-0.01	0.01
	899.6776	905.1501	899.99	-5.4725	5.4725	-0.31	0.31	896.3386	900.05	3.3390	3.3390	-0.37	0.37
	1052.0025	1042.5656	1051.96	9.4369	9.4369	0.04	0.04	1036.7035	1052.29	15.2990	15.2990	-0.29	0.29
	1156.6660	1150.0725	1156.72	6.5935	6.5935	-0.05	0.05	1137.5043	1156.70	19.1617	19.1617	-0.03	0.03
	1157.9222	1154.1327	1158.34	3.7895	3.7895	-0.42	0.42	1153.4692	1157.82	4.4530	4.4530	0.10	0.10
	1175.0671	1165.1270	1175.06	9.9401	9.9401	0.01	0.01	1162.8074	1175.06	12.2597	12.2597	0.01	0.01
	1176.5738	1172.6829	1176.63	3.8909	3.8909	-0.06	0.06	1166.3494	1176.33	10.2244	10.2244	0.24	0.24
	1300.1357	1309.2378	1299.71	-9.1021	9.1021	0.43	0.43	1298.5264	1300.35	1.6093	1.6093	-0.21	0.21
	1513.2637	1501.6778	1513.34	11.5859	11.5859	-0.08	0.08	1496.7101	1513.33	16.5536	16.5536	-0.07	0.07
	1549.9581	1540.3219	1549.94	9.6362	9.6362	0.02	0.02	1543.6585	1549.64	6.2996	6.2996	0.32	0.32
	3109.1368	3087.5105	3109.16	21.6263	21.6263	-0.02	0.02	3103.1958	3109.15	5.9410	5.9410	-0.01	0.01
	3117.4164	3096.2234	3117.45	21.1930	21.1930	-0.03	0.03	3113.6501	3117.42	3.7663	3.7663	0.00	0.00
	3196.1096	3167.5283	3196.14	28.5813	28.5813	-0.03	0.03	3193.7442	3196.14	2.3654	2.3654	-0.03	0.03
	3210.7653	3184.7323	3210.79	26.0330	26.0330	-0.02	0.02	3209.4598	3210.79	1.3055	1.3055	-0.02	0.02
Hydrogen cyanide	716.0093	784.2195	716.00	-68.2102	68.2102	0.01	0.01	707.5381	716.02	8.4712	8.4712	-0.01	0.01
HCN	716.0093	784.2195	716.00	-68.2102	68.2102	0.01	0.01	707.5381	716.02	8.4712	8.4712	-0.01	0.01
	2111.3807	2199.7485	2111.88	-88.3678	88.3678	-0.50	0.50	2097.9900	2111.51	13.3907	13.3907	-0.13	0.13
	3443.4280	3472.7744	3443.29	-29.3464	29.3464	0.14	0.14	3446.5556	3443.51	-3.1276	3.1276	-0.08	0.08

	TZ/TZ	B3LYP/6-31G(2df,p) Freq	TZ/DFT CMA	Shift	Abs Shift	Diff	Abs Diff	DZ/DZ Freq	TZ/DZ MH	Shift	Abs Shift	Diff	Abs Diff
Methyl radical (2.1)	496.1334	475.5092	496.11	20.6242	20.6242	0.02	0.02	400.9736	496.16	95.1598	95.1598	-0.03	0.03
CH3 (Doublet)	1426.6652	1411.9611	1426.68	14.7041	14.7041	-0.01	0.01	1410.6507	1426.67	16.0145	16.0145	0.00	0.00
	1426.6652	1411.9659	1426.68	14.6993	14.6993	-0.01	0.01	1410.6507	1426.67	16.0145	16.0145	0.00	0.00
	3119.4985	3121.7678	3119.54	-2.2693	2.2693	-0.04	0.04	3120.6177	3119.54	-1.1192	1.1192	-0.04	0.04
	3300.4738	3307.5690	3300.53	-7.0952	7.0952	-0.06	0.06	3313.8399	3300.53	-13.3661	13.3661	-0.06	0.06
	3300.4738	3307.5795	3300.53	-7.1057	7.1057	-0.06	0.06	3313.8399	3300.53	-13.3661	13.3661	-0.06	0.06
Triplet carbene (2.2)	1105.6696	1082.1806	1105.88	23.4890	23.489	-0.21	0.21	1126.9396	1105.68	-21.2700	21.27	-0.01	0.01
CH2 (Triplet)	3139.2662	3131.7501	3139.25	7.5161	7.5161	0.02	0.02	3139.0977	3139.32	0.1685	0.1685	-0.05	0.05
	3365.4434	3372.8856	3365.52	-7.4422	7.4422	-0.08	0.08	3364.9500	3365.52	0.4934	0.4934	-0.08	0.08
Ethynyl radical (2.3)	320.8589	91.1552	316.29	229.7037	229.7037	4.57	4.57	136.1009	316.38	184.7580	184.758	4.48	4.48
HCC (Doublet)	320.8589	91.1555	316.29	229.7034	229.7034	4.57	4.57	136.1009	316.45	184.7580	184.758	4.41	4.41
	2009.6408	2096.9522	2010.05	-87.3114	87.3114	-0.41	0.41	1987.6803	2009.76	21.9605	21.9605	-0.12	0.12
	3454.2969	3486.5239	3454.22	-32.2270	32.227	0.08	0.08	3444.8708	3454.39	9.4261	9.4261	-0.09	0.09
Formyl radical (2.4)	1122.6777	1104.3918	1122.72	18.2859	18.2859	-0.04	0.04	1117.0933	1122.78	5.5844	5.5844	-0.10	0.10
CHO (Doublet)	1888.3910	1944.8900	1888.50	-56.4990	56.499	-0.11	0.11	1885.3517	1888.65	3.0393	3.0393	-0.26	0.26
	2691.4822	2645.1026	2691.57	46.3796	46.3796	-0.09	0.09	2645.9595	2691.45	45.5227	45.5227	0.03	0.03
Vinyl radical (2.5)	725.9930	711.1893	726.62	14.8037	14.8037	-0.63	0.63	731.3856	726.46	-5.3926	5.3926	-0.47	0.47
H2CCH (Doublet)	806.0611	820.0588	806.20	-13.9977	13.9977	-0.14	0.14	779.2793	807.06	26.7818	26.7818	-1.00	1.00
	914.7673	930.4084	914.96	-15.6411	15.6411	-0.19	0.19	893.2267	914.38	21.5406	21.5406	0.39	0.39
	1070.8985	1052.9431	1070.83	17.9554	17.9554	0.07	0.07	1073.2463	1070.69	-2.3478	2.3478	0.21	0.21
	1396.0025	1396.7806	1398.92	-0.7781	0.7781	-2.92	2.92	1378.5993	1395.75	17.4032	17.4032	0.25	0.25
	1614.0524	1662.1138	1611.49	-48.0614	48.0614	2.56	2.56	1609.4200	1614.43	4.6324	4.6324	-0.38	0.38
	3074.4951	3057.6316	3074.76	16.8635	16.8635	-0.26	0.26	3085.8176	3074.68	-11.3225	11.3225	-0.18	0.18
	3178.9039	3153.8862	3178.82	25.0177	25.0177	0.08	0.08	3197.7800	3178.88	-18.8761	18.8761	0.02	0.02
	3246.6118	3253.1351	3246.55	-6.5233	6.5233	0.06	0.06	3242.0706	3246.71	4.5412	4.5412	-0.10	0.10
Carbonyl methane (2.6)	97.7359	118.3161	98.63	-20.5802	20.5802	-0.89	0.89	105.1383	94.39	-7.4024	7.4024	3.35	3.35
H3CCO (Doublet)	466.4589	460.0306	466.71	6.4283	6.4283	-0.25	0.25	459.6427	466.50	6.8162	6.8162	-0.04	0.04
	861.0317	849.8131	861.45	11.2186	11.2186	-0.42	0.42	860.0598	861.18	0.9719	0.9719	-0.15	0.15
	950.4771	946.9542	954.72	3.5229	3.5229	-4.24	4.24	942.2256	953.94	8.2515	8.2515	-3.46	3.46
	1050.3962	1049.0410	1050.43	1.3552	1.3552	-0.03	0.03	1036.8256	1050.50	13.5706	13.5706	-0.10	0.10
	1355.8505	1353.3131	1355.87	2.5374	2.5374	-0.02	0.02	1343.0591	1355.80	12.7914	12.7914	0.05	0.05
	1463.5530	1457.6837	1467.44	5.8693	5.8693	-3.89	3.89	1451.1213	1466.87	12.4317	12.4317	-3.32	3.32
	1468.6869	1459.7938	1468.77	8.8931	8.8931	-0.08	0.08	1452.9638	1468.66	15.7231	15.7231	0.03	0.03
	1899.3242	1938.4643	1899.37	-39.1401	39.1401	-0.05	0.05	1895.7315	1899.39	3.5927	3.5927	-0.07	0.07
	3039.3823	3031.4414	3039.71	7.9409	7.9409	-0.33	0.33	3046.0995	3039.56	-6.7172	6.7172	-0.18	0.18
	3137.4025	3125.1979	3137.11	12.2046	12.2046	0.29	0.29	3154.5581	3137.40	-17.1556	17.1556	0.00	0.00
	3145.5180	3128.8871	3143.14	16.6309	16.6309	2.38	2.38	3161.6033	3142.83	-16.0853	16.0853	2.69	2.69

	TZ/TZ	B3LYP/6-31G(2df,p) Freq	TZ/DFT CMA	Shift	Abs Shift	Diff	Abs Diff	DZ/DZ Freq	TZ/DZ MH	Shift	Abs Shift	Diff	Abs Diff
Hydroxymethyl radical (2.7)	432.0276	429.4348	432.12	2.5928	2.5928	-0.09	0.09	457.5822	433.51	-25.5546	25.5546	-1.48	1.48
CH2OH (Doublet)	620.0192	603.4129	620.06	16.6063	16.6063	-0.04	0.04	704.9704	619.50	-84.9512	84.9512	0.52	0.52
	1064.7913	1052.8559	1064.87	11.9354	11.9354	-0.08	0.08	1063.7381	1065.09	1.0532	1.0532	-0.30	0.30
	1209.2145	1218.9796	1209.45	-9.7651	9.7651	-0.24	0.24	1213.5858	1209.54	-4.3713	4.3713	-0.33	0.33
	1383.7557	1366.1060	1383.63	17.6497	17.6497	0.13	0.13	1388.6230	1383.67	-4.8673	4.8673	0.09	0.09
	1498.8008	1481.7489	1498.72	17.0519	17.0519	0.08	0.08	1489.6112	1498.74	9.1896	9.1896	0.06	0.06
	3139.5374	3122.5370	3139.62	17.0004	17.0004	-0.08	0.08	3122.1331	3139.86	17.4043	17.4043	-0.32	0.32
	3280.0241	3265.8293	3280.05	14.1948	14.1948	-0.03	0.03	3265.0216	3279.89	15.0025	15.0025	0.13	0.13
	3861.9725	3840.8954	3862.17	21.0771	21.0771	-0.20	0.20	3840.9133	3862.18	21.0592	21.0592	-0.21	0.21
Triplet silylene (2.9)	886.4052	888.7570	886.43	-2.3518	2.3518	-0.02	0.02	882.7068	886.42	3.6984	3.6984	-0.01	0.01
SiH2 (Triplet)	2189.3334	2164.6086	2189.35	24.7248	24.7248	-0.02	0.02	2182.8811	2189.36	6.4523	6.4523	-0.03	0.03
	2251.4008	2236.0268	2251.41	15.3740	15.374	-0.01	0.01	2244.6809	2251.42	6.7199	6.7199	-0.02	0.02
Silyl radical (1.5) (2.10)	778.7210	761.0802	778.84	17.6408	17.6408	-0.12	0.12	787.3448	778.75	-8.6238	8.6238	-0.03	0.03
SiH3 (Doublet)	943.1821	934.7184	943.22	8.4637	8.4637	-0.04	0.04	941.5637	943.22	1.6184	1.6184	-0.04	0.04
	943.1821	934.7187	943.22	8.4634	8.4634	-0.04	0.04	941.5637	943.22	1.6184	1.6184	-0.04	0.04
	2217.2497	2201.4555	2217.23	15.7942	15.7942	0.02	0.02	2219.1498	2217.26	-1.9001	1.9001	-0.01	0.01
	2250.3945	2242.6519	2250.40	7.7426	7.7426	-0.01	0.01	2254.2942	2250.41	-3.8997	3.8997	-0.02	0.02
	2250.3945	2242.6548	2250.40	7.7397	7.7397	-0.01	0.01	2254.2942	2250.41	-3.8997	3.8997	-0.02	0.02
Phosphino radical (2.11)	1124.5215	1128.0295	1124.53	-3.5080	3.508	-0.01	0.01	1128.9951	1124.52	-4.4736	4.4736	0.00	0.00
PH2 (Doublet)	2386.6727	2375.3419	2386.70	11.3308	11.3308	-0.03	0.03	2381.3999	2386.71	5.2728	5.2728	-0.04	0.04
	2395.5510	2386.1289	2395.58	9.4221	9.4221	-0.03	0.03	2391.5473	2395.58	4.0037	4.0037	-0.03	0.03
Nitrogen dioxide (2.14)	758.3753	759.1480	758.50	-0.7727	0.7727	-0.12	0.12	741.6315	759.08	16.7438	16.7438	-0.70	0.70
NO2 (Doublet)	1349.1871	1400.4676	1351.00	-51.2805	51.2805	-1.81	1.81	1305.2332	1350.97	43.9539	43.9539	-1.78	1.78
	1681.3859	1726.4445	1681.29	-45.0586	45.0586	0.10	0.10	1614.7038	1679.47	66.6821	66.6821	1.92	1.92
Amino radical (1.4) (2.15)	1557.7447	1552.8072	1557.74	4.9375	4.9375	0.00	0.00	1564.0090	1557.74	-6.2643	6.2643	0.00	0.00
NH2 (Doublet)	3364.8094	3347.0048	3364.88	17.8046	17.8046	-0.07	0.07	3318.2021	3364.90	46.6073	46.6073	-0.09	0.09
	3457.6509	3435.5002	3457.73	22.1507	22.1507	-0.08	0.08	3414.9394	3457.73	42.7115	42.7115	-0.08	0.08

	TZ/TZ	B3LYP/6-31G(2df,p) Freq	TZ/DFT CMA	Shift	Abs Shift	Diff	Abs Diff	DZ/DZ Freq	TZ/DZ MH	Shift	Abs Shift	Diff	Abs Diff
Ethyl radical (2.16)	128.2650	114.3143	128.72	13.9507	13.9507	-0.46	0.46	150.4930	128.38	-22.2280	22.228	-0.12	0.12
H3CCH2 (Doublet)	469.5154	469.1901	469.51	0.3253	0.3253	0.01	0.01	446.4529	469.65	23.0625	23.0625	-0.13	0.13
	809.1368	808.1640	809.18	0.9728	0.9728	-0.04	0.04	800.4288	809.14	8.7080	8.708	0.00	0.00
	987.4301	984.7612	987.51	2.6689	2.6689	-0.08	0.08	979.6953	987.46	7.7348	7.7348	-0.03	0.03
	1069.9056	1069.3451	1070.11	0.5605	0.5605	-0.20	0.20	1075.7699	1070.29	-5.8643	5.8643	-0.38	0.38
	1200.8975	1197.0999	1200.90	3.7976	3.7976	0.00	0.00	1189.7290	1200.92	11.1685	11.1685	-0.02	0.02
	1403.4295	1403.3107	1403.61	0.1188	0.1188	-0.18	0.18	1392.0291	1403.74	11.4004	11.4004	-0.31	0.31
	1480.0023	1469.3720	1480.75	10.6303	10.6303	-0.75	0.75	1462.8561	1479.60	17.1462	17.1462	0.40	0.40
	1492.2998	1483.6270	1492.26	8.6728	8.6728	0.04	0.04	1473.6216	1492.30	18.6782	18.6782	0.00	0.00
	1493.3992	1485.4338	1492.57	7.9654	7.9654	0.83	0.83	1478.7392	1493.32	14.6600	14.66	0.08	0.08
	2983.4447	2959.4718	2984.78	23.9729	23.9729	-1.34	1.34	2992.8937	2983.88	-9.4490	9.449	-0.44	0.44
	3064.9310	3050.7577	3063.74	14.1733	14.1733	1.19	1.19	3079.0911	3064.62	-14.1601	14.1601	0.31	0.31
	3108.8073	3095.4210	3108.85	13.3863	13.3863	-0.04	0.04	3125.5478	3108.85	-16.7405	16.7405	-0.04	0.04
	3157.2304	3153.2980	3157.28	3.9324	3.9324	-0.05	0.05	3154.4335	3157.30	2.7969	2.7969	-0.07	0.07
	3260.3276	3255.7819	3260.39	4.5457	4.5457	-0.06	0.06	3261.7923	3260.38	-1.4647	1.4647	-0.05	0.05

	TZ/TZ	B3LYP/6-31G(2df,p) Freq	TZ/DFT CMA	Shift	Abs Shift	Diff	Abs Diff	DZ/DZ Freq	TZ/DZ MH	Shift	Abs Shift	Diff	Abs Diff
tert-Butyl radical (2.18)	135.0389	123.9933	132.58	11.0456	11.0456	2.46	2.46	140.3829	132.39	-5.3440	5.344	2.65	2.65
C(CH3)3 (doublet)	148.3060	124.0462	147.92	24.2598	24.2598	0.39	0.39	149.5236	147.84	-1.2176	1.2176	0.47	0.47
	148.3060	129.0979	147.97	19.2081	19.2081	0.34	0.34	149.5236	147.84	-1.2176	1.2176	0.47	0.47
	261.1598	254.1061	262.91	7.0537	7.0537	-1.75	1.75	265.4776	261.20	-4.3178	4.3178	-0.04	0.04
	367.5114	377.1976	367.03	-9.6862	9.6862	0.48	0.48	370.2740	367.07	-2.7626	2.7626	0.44	0.44
	367.5114	377.2109	367.03	-9.6995	9.6995	0.48	0.48	370.2740	367.07	-2.7626	2.7626	0.44	0.44
	767.8509	759.5070	768.00	8.3439	8.3439	-0.15	0.15	771.9500	767.91	-4.0991	4.0991	-0.06	0.06
	941.4632	941.7542	933.80	-0.2910	0.291	7.66	7.66	926.3988	933.90	15.0644	15.0644	7.56	7.56
	941.4632	941.7681	933.80	-0.3049	0.3049	7.66	7.66	926.3988	933.90	15.0644	15.0644	7.56	7.56
	975.0530	971.4270	964.12	3.6260	3.626	10.93	10.93	956.1290	964.08	18.9240	18.924	10.97	10.97
	1016.1541	1010.3030	1014.26	5.8511	5.8511	1.89	1.89	1009.9491	1014.06	6.2050	6.205	2.09	2.09
	1016.1541	1010.3126	1014.26	5.8415	5.8415	1.89	1.89	1009.9491	1014.06	6.2050	6.205	2.09	2.09
	1105.3827	1094.9459	1106.68	10.4368	10.4368	-1.30	1.30	1096.3516	1105.31	9.0311	9.0311	0.07	0.07
	1308.1077	1300.4483	1304.73	7.6594	7.6594	3.38	3.38	1302.2183	1303.90	5.8894	5.8894	4.21	4.21
	1308.1077	1300.4537	1304.73	7.6540	7.654	3.38	3.38	1302.2183	1303.90	5.8894	5.8894	4.21	4.21
	1400.7396	1398.5596	1397.20	2.1800	2.18	3.54	3.54	1395.7452	1397.77	4.9944	4.9944	2.97	2.97
	1400.7396	1398.5659	1397.20	2.1737	2.1737	3.54	3.54	1395.7452	1397.77	4.9944	4.9944	2.97	2.97
	1419.8303	1427.3085	1420.11	-7.4782	7.4782	-0.28	0.28	1411.3401	1419.92	8.4902	8.4902	-0.09	0.09
	1471.7449	1472.4694	1474.32	-0.7245	0.7245	-2.58	2.58	1456.7225	1474.28	15.0224	15.0224	-2.54	2.54
	1478.1055	1472.4997	1477.67	5.6058	5.6058	0.44	0.44	1461.5678	1477.74	16.5377	16.5377	0.37	0.37
	1478.1055	1472.6029	1477.71	5.5026	5.5026	0.40	0.40	1461.5678	1477.74	16.5377	16.5377	0.37	0.37
	1496.4079	1488.6930	1496.22	7.7149	7.7149	0.19	0.19	1478.5884	1496.33	17.8195	17.8195	0.08	0.08
	1497.3434	1496.2074	1497.68	1.1360	1.136	-0.34	0.34	1478.5884	1497.54	18.7550	18.755	-0.20	0.20
	1497.3434	1496.2196	1497.69	1.1238	1.1238	-0.35	0.35	1479.6192	1497.54	17.7242	17.7242	-0.20	0.20
	2946.0227	2936.0304	2948.38	9.9923	9.9923	-2.36	2.36	2959.9663	2948.31	-13.9436	13.9436	-2.29	2.29
	2946.0227	2936.0431	2948.40	9.9796	9.9796	-2.38	2.38	2959.9663	2948.31	-13.9436	13.9436	-2.29	2.29
	2954.0487	2945.0664	2954.78	8.9823	8.9823	-0.73	0.73	2971.5773	2954.85	-17.5286	17.5286	-0.80	0.80
	3052.4005	3041.3411	3052.39	11.0594	11.0594	0.01	0.01	3066.4128	3052.49	-14.0123	14.0123	-0.09	0.09
	3052.4005	3041.3673	3052.40	11.0332	11.0332	0.00	0.00	3066.4128	3052.49	-14.0123	14.0123	-0.09	0.09
	3054.3386	3044.1995	3053.63	10.1391	10.1391	0.71	0.71	3069.2498	3053.57	-14.9112	14.9112	0.77	0.77
	3096.0569	3085.7936	3097.56	10.2633	10.2633	-1.50	1.50	3113.9137	3098.03	-17.8568	17.8568	-1.97	1.97
	3098.6861	3090.7907	3102.31	7.8954	7.8954	-3.62	3.62	3118.5269	3102.37	-19.8408	19.8408	-3.68	3.68
	3098.6861	3090.8062	3102.79	7.8799	7.8799	-4.10	4.10	3118.5269	3102.37	-19.8408	19.8408	-3.68	3.68

Table 6.7: Tables containing CMA0 frequency information (in cm^{-1}) for the filtered G2 Test set.